

The impact of heterogeneity in
stomatal anatomical characters
on stomatal function and physiology in wheat

Shellie Wall

A thesis submitted for the degree of Doctor of Philosophy

School of Life Sciences

University of Essex

October 2020

Abstract

Factors affecting food insecurity include the effects of climate change, losses of agricultural land to urbanization and increasing competition for non-food uses of crops. Stomatal anatomical characteristics including stomatal density (SD), size (SS) and pore aperture determine stomatal conductance (g_s) where changes in anatomy impact g_s and photosynthetic assimilation (A) which is known to be linked with crop yield.

This study presents heterogeneity of SD and SS between elite MAGIC wheat cultivars (EW) and wheat wild relatives (WWR), and the affect these changes had on stomatal kinetics. Results propose that WWR may be better-able to deal with elevated temperatures and dynamic light environments due to faster stomatal kinetics and higher g_s facilitating greater evaporative cooling in well-watered condition, however, where water is less available, higher g_s would have deleterious effects; the 'slow and steady' approach found in EW is more beneficial.

To explore differences in stomatal anatomy between the two leaf surfaces a novel gas chamber was constructed to measure separate but simultaneous leaf gas exchange of each leaf surface in real time. The adaxial leaf surface boasted higher SD, higher g_s and A compared with the abaxial leaf surface and when the abaxial leaf surface g_s was blocked, the leaf could not compensate for the loss, suggesting that both leaf surfaces are crucial to overall leaf g_s and A , albeit with unequal contributions. Differences in wheat species with varying ploidy grown at differing CO_2 concentrations revealed that diploid species have a reduced SD and increased SS in plants grown at elevated CO_2 concentrations whereas tetraploid species showed the opposite. Furthermore, although g_s changed between ploidy, it did not affect the overall A . The interest in understanding plant adaptations and natural variants with interesting anatomical features are to assist in targeting traits for enhanced water-use efficiency and, moreover, crop productivity.

Acknowledgements

First and foremost, I would like to thank Professor Tracy Lawson for her continual guidance, encouragement, and patience. I sincerely appreciate the time you have invested in me and am acutely aware that I would not be finishing my PhD without your support. I truly wanted to thank you for sharing your passion of plant science and being the strong female role model that I have looked-up to from my undergrad degree through to the completion of my PhD.

Secondly, I would like to thank all the past and present members of the Plant Physiology Lab at Essex - Dr Silvere Vialet-Chabrand, Dr James Stevens, Dr Jack Matthews, Dr John Stamford, Dr Martin Battle, Dr. Michele Faralli, Dr. Duncan Sweeny, Amnah Alamri, Robyn Emmerson, and Joe Chadwick for the camaraderie. Phil Davey, your expertise is an asset to the lab and I am grateful for your patience, help and technical advice.

Furthermore, I am indebted to all my friends who have supported me over the last few years and for all the wine! So many people have been so kind and so many of their children have brought me joy - Carla & James, my godson *Dylan*, Rocco, Charlie & Robbie, Aubin, Claire, Chris, Emma, Tabitha, Fionnuala, Gemma & Matt, Charlie, Isobel, Freya, Jacob, *Jareth & Sarah*, Kirsty, Lauren, Louise & James, Freddie, Lorna, Mother Mary, Natalie & Barry, Luther, Reginald, Oscar, Patricia, Phil, Sam & Roxy, Rhona, Martha, Tom & Emily, Sophie and finally little Thomas. Furthermore, to my Siblings and extended family for their patience and support - Craig, my darling Logan, Jake & Kayleigh, Solomon, Debbie & Terry, Rickie & Dionne, Gillian, Liz & Kev, Nick, Frankie, Sidney and Albert.

Jon, this would not have come into fruition without your continued belief in my abilities, your love, constant attention and our shared taste in excellent music, films, food, rum and scrabble.

Lastly, I would like to thank my parents for everything.
For their love, moral support, altruism,
and the amazing chances they have given me over the years.
I hope I have made you both proud.

I am Grateful to the Biotechnology and Biological Sciences Research Council (BBSRC) and BASF for their financial support throughout this PhD and to NIAB.

I would also like to thank Jeroen Van Rie, Alexader Galle, James Cockram, Karel Vercruysse, Sander Coussement and Brecht Van Reusel for all their help and advice.

Table of Contents

Abstract	1
Acknowledgements page	2
List of Figures	8
List of Abbreviations	15
Publications	17
CHAPTER 1	18
1.1 Introduction	19
1.1.1 Climate change and food security	19
1.1.2 Wheat	21
1.1.3 Multi-parent Advanced Generation Inter-Cross (MAGIC) wheat.....	25
1.1.4 Introduction to stomata	27
1.1.5 Stomatal Development and Patterning	31
1.1.6 Stomatal Anatomy: Intra-inter-specific variation	34
1.1.7 Stomatal Density and Size	43
1.1.8 Factors influencing stomatal responses	46
1.1.9 Steady state and kinetic stomatal responses	47
1.2 Aims and Objectives.....	48
CHAPTER 2	50
2.1 Plant Material and Growth Conditions	51
2.2 Leaf and stomatal characteristics	53
2.2.1 Leaf epidermal impressions	53
2.2.2. Measurements of stomatal density.....	53
2.2.2.1 Measurements of stomatal density using Light Microscopy	53
2.2.2.2 Snapshot measurements of stomatal density.....	54
2.2.3 Measurements of Stomatal size	54
2.2.4 Potential anatomical maximum stomatal conductance	55
2.2.5 Leaf optical properties	56
2.2.6 Leaf thickness	57

2.2.7 Leaf anatomical measurements	57
2.3 Leaf gas exchange	59
2.3.1 PPFD-step measurements	59
2.3.2 Intracellular CO ₂ response curves (<i>A/C_i</i>).....	60
2.4 Gas exchange measurements using split leaf chamber	61
2.4.1 Design of split leaf chamber for measuring each surface individually and simultaneously.	61
2.4.2 Individual leaf surface response of <i>A</i> and <i>g_s</i> to a step change in PPFD.....	65
2.4.3 Greased intracellular CO ₂ (<i>A/C_i</i>) response curves	67
2.5 Modelling gas exchange parameters.....	69
2.5.1 Estimating photosynthetic capacities.....	69
2.5.2 Determining the rapidity of <i>g_s</i> response	69
2.5.3 Determining the rapidity of <i>A</i> response	70
2.6 Statistical analysis	71
2.7 Split chamber modelling of gas exchange parameters	72
CHAPTER 3	73
3.1. Introduction	74
3.2 Materials and Methods	79
3.2.1 Plant material and growth conditions.....	79
3.2.2 Leaf and stomatal characteristics	79
3.2.2.1 Leaf epidermal impressions	79
3.2.2.2 Stomatal anatomical measurements	80
3.2.3 Leaf gas exchange	81
3.2.3.1 PPFD-step measurements	81
3.2.3.2 Intracellular CO ₂ response curves (<i>A/C_i</i>).....	81
3.2.4 Modelling gas exchange parameters.....	81
3.2.4.1. Estimating photosynthetic capacities.....	81
3.2.4.2. Determining the rapidity of <i>A</i> and <i>g_s</i> response	81
3.2.5 Statistical analysis	81
3.3. Results	82
3.3.1 Stomatal anatomy	82
3.3.1.1 Stomatal Density	82
3.3.1.2 Guard Cell Length	89

3.3.1.3 Maximum potential stomatal conductance (g_{smax})	94
3.3.2 Leaf gas exchange	100
3.3.2.1 Response of g_s and A to a step change in PPFD	100
3.3.2.2. Speed of g_s response to a step change in light intensity	103
3.3.2.3. A/C_i response analysis	107
3.4. Discussion	110
 CHAPTER 4	 117
4.1 Introduction	118
4.2 Materials and Methods	121
4.2.1 Plant material and growth conditions.....	121
4.2.2 Leaf and stomatal characteristics	121
4.2.2.1 Leaf epidermal impressions	121
4.2.2.2 Stomatal anatomical measurements	121
4.2.3 IRGA measurements using split leaf chamber	122
4.2.3.1 Single leaf surface response of g_s and A to a step change in PPFD	122
4.2.3.2 Greased intracellular CO_2 (A/C_i) response curves	122
4.2.4 Modelling gas exchange parameters.....	122
4.2.4.1. Determining the rapidity of stomatal conductance response	122
4.2.5 Statistical analysis	122
4.3 Results	123
4.3.1 Stomatal anatomy	123
4.3.2 Leaf gas exchange	128
4.3.2.1 Response of g_s and A to a step change in PPFD.....	128
4.3.2.2. Speed of g_s response to a step change in light intensity	131
4.3.2.4. intracellular CO_2 (A/C_i) response curves	135
4.4 Discussion	137
 CHAPTER 5	 144
5.1. Introduction	145
5.2 Materials and Methods	150
5.2.1 Plant material and growth conditions.....	150

5.2.2 Leaf and stomatal characteristics	151
5.2.2.1 Leaf epidermal impressions	151
5.2.2.2 Stomatal anatomical measurements	151
5.2.3 Leaf gas exchange	152
5.2.3.1 PPFD-step measurements	152
5.2.3.2 Intracellular CO ₂ response curves (A/Ci).....	152
5.2.4 Modelling gas exchange parameters.....	152
5.2.4.1. Estimating photosynthetic capacities.....	152
5.2.4.2. Determining the rapidity of stomatal conductance response	152
5.2.4.3. Determining the rapidity of net CO ₂ assimilation response.....	153
5.2.5 Statistical analysis	153
5.3. Results	154
5.3.1 Stomatal anatomy	154
5.3.1.1 Stomatal Density	154
5.3.1.2 Guard Cell Length	157
5.3.1.3 Maximum potential stomatal conductance (g_{smax})	161
5.3.2 Leaf gas exchange	164
5.3.2.1 Response of g_s and A to a step change in PPFD.....	164
5.3.2.2. Speed of g_s response to a step change in light intensity.....	167
5.3.2.2. A/C_i response analysis.....	172
5.4. Discussion.....	175
CHAPTER 6	181
6.1. Introduction	182
6.2 Materials and Methods	185
6.2.1 Plant material and growth conditions.....	185
6.2.2 Leaf and stomatal characteristics	186
6.2.2.1 Leaf epidermal impressions	186
6.2.2.2 Stomatal anatomical measurements	186
6.2.2.2 Leaf thickness	187
6.2.2.3 Leaf anatomical measurements	187
6.2.3 Leaf gas exchange	187
6.2.3.1 PPFD-step measurements	187
6.2.3.2 Intracellular CO ₂ response curves (A/Ci).....	187

6.2.4 Modelling gas exchange parameters.....	188
6.2.4.1. Estimating photosynthetic capacities.....	188
6.2.4.1 Determining the rapidity of A and g_s response	188
6.2.5 Statistical analysis	188
6.3. Results	189
6.3.1 Leaf and stomatal anatomy	189
6.3.1.1 Stomatal Density	191
6.3.1.2 Guard Cell Length	193
6.3.1.3 potential maximum rate of g_s	197
6.3.1.4 Leaf area, leaf dry weight, and leaf thickness	200
6.3.2 Leaf gas exchange	205
6.3.2.1 Response of g_s and A to a step change in PPFD	205
6.3.2.2. Speed of g_s response to a step change in light intensity	207
6.3.2.3. A/C_i response analysis.....	214
6.4. Discussion.....	217
 CHAPTER 7	 224
7.1 Main Discussion	225
7.1.1 Spatial heterogeneity of stomata.....	225
7.1.2 Intra specific variation of anatomical traits leading to functional differences .	227
7.1.3 Amphistomaty in leaves and its effect on function.....	230
7.1.4 The effect of high CO_2 on wheat species	233
 CHAPTER 8	 236
8.1 References.....	237

List of Figures

Figure 1.1. The evolutionary lineages involving <i>Triticum</i> wheat species with sub-genome lettering	23
Figure 1.2. Diversity of Stomata across Land Plant Taxa.....	28
Figure 1.3. Stomatal development in <i>A. thaliana</i>	32
Figure 1.4. Comparison of the molecular and morphological features of stomatal development in <i>Arabidopsis</i> and representatives of the grasses and mosses for which molecular data exist	33
Figure 1.5. Examples of stomatal complex types composed of guard cells and surrounding subsidiary cells.	37
Figure 1.6. Schematised leaf cross-sections indicating lengths of pathways for water and CO ₂ across hypostomatous and amphistomatous leaves.....	39
Figure 1.7. Impact of stomatal characteristics on response to environmental cues.....	43
Figure 2.1. Diagram representing the anatomy of the stomatal complex highlighting the dimensions of guard cell length and pore length	53
Figure 2.2. Lab-made chamber for direct measurement of simultaneous but separate leaf surface gas exchange.	61
Figure 3.1. Diagram of single wheat tiller	75
Figure 3.2. Variation of flag leaf stomatal density and second leaf stomatal density for eight MAGIC wheat cultivars	79
Figure 3.3. Variation of flag leaf stomatal density calculated for the abaxial and adaxial leaf surfaces at the tip middle and base leaf locations for eight MAGIC wheat cultivars.	80
Figure 3.4. Variation of second leaf stomatal density calculated for the abaxial and adaxial leaf surfaces at the tip middle and base leaf locations for eight MAGIC wheat cultivars.	81
Figure 3.5. Percentage of stomatal density for flag leaf and second leaf	82
Figure 3.6. Variation of flag leaf and second leaf guard cell length for eight MAGIC wheat cultivars.	85

Figure 3.7. Variation of flag leaf guard cell length calculated for the abaxial and adaxial leaf surfaces at the tip middle and base leaf locations for eight MAGIC wheat cultivars	86
Figure 3.8. Variation of second leaf guard cell length calculated for the abaxial and adaxial leaf surfaces at the tip middle and base leaf locations for eight MAGIC wheat cultivars	87
Figure 3.9 Correlation between total cultivar stomatal density and total guard cell length	88
Figure 3.10. Variation of flag leaf g_{smax} calculated for the abaxial and adaxial leaf surfaces at the tip middle and base leaf locations for eight MAGIC wheat cultivars.....	91
Figure 3.11. Flag leaf g_{smax} as percentage for the abaxial and adaxial leaf surfaces	92
Figure 3.12. Variation of second leaf g_{smax} calculated for the abaxial and adaxial leaf surfaces at the tip middle and base leaf locations for eight MAGIC wheat cultivars.....	94
Figure 3.13. Temporal response of stomatal conductance, net CO ₂ assimilation and intrinsic water use efficiency to a step increase in light intensity for eight MAGIC wheat cultivars	97
Figure 3.14. Stomatal kinetics from a step increase in light intensity for eight MAGIC wheat cultivars.	100
Figure 3.15. Correlations between time constant for stomatal opening and difference in g_s following the step increase in light intensity, for eight MAGIC wheat cultivars	101
Figure 3.16. Variation of g_s at 1000 μ mol and g_{smax} for eight MAGIC wheat cultivars.	102
Figure 3.17. The response of CO ₂ assimilation as a function of intercellular [CO ₂]	103
Figure 3.18. Variation of the measured CO ₂ -saturated rate of photosynthesis, the maximum rate of carboxylation and maximum rate of electron transport from eight MAGIC wheat cultivars.....	104
Figure 4.1. Variation of flag leaf stomatal density, guard cell length representing stomatal size and potential maximum stomatal conductance for eight MAGIC wheat cultivars	120
Figure 4.2. Variation of flag leaf stomatal density, guard cell length representing stomatal size and potential maximum stomatal conductance for the abaxial and adaxial leaf surfaces of eight MAGIC wheat cultivars	121

Figure 4.3. Variation of flag leaf area, leaf thickness and leaf absorbance of eight MAGIC wheat cultivars.....	123
Figure 4.4. Temporal response of stomatal conductance and net CO ₂ assimilation to a step increase in light intensity for eight MAGIC wheat cultivars using the split leaf chamber	125
Figure 4.5. Variation of Stomatal conductance, net CO ₂ assimilation, Lag time in stomatal opening and the time constant for stomatal opening using the split leaf chamber for the abaxial and adaxial leaf surfaces of eight MAGIC wheat cultivars to a single step change in PPFD.	128
Figure 4.6. Stomatal conductance and net CO ₂ assimilation for two selected MAGIC wheat cultivars; Brompton and XI19 using the split leaf chamber for the adaxial leaf surface with the abaxial leaf surface greased to prevent gaseous flux from the abaxial surface	130
Figure 4.7. The response of net CO ₂ assimilation to intercellular [CO ₂] cultivar Brompton. Using the split chamber with an alternating leaf surface grease regime	132
Figure 5.1. The evolutionary lineages involving Triticum wheat species with sub-genome lettering.	143
Figure 5.2. Wheat spikes showing a brittle rachis, non-brittle rachis, hulled grain and naked grain of Wild emmer wheat, domesticated emmer, durum and common wheat	145
Figure 5.3. Variation of flag leaf stomatal density for 17 wheat species	151
Figure 5.4. Variation of flag leaf stomatal density for the adaxial and abaxial leaf surfaces for 17 wheat species.....	152
Figure 5.5. Variation of flag leaf guard cell length for 17 wheat species.....	153
Figure 5.6. Variation of the adaxial and abaxial leaf surfaces for 17 wheat species	154
Figure 5.7. Correlation between stomatal density and guard cell length for 17 wheat species.	156
Figure 5.8. Variation of flag leaf g_{smax} for 17 wheat species.	158
Figure 5.9. Variation of flag leaf g_{smax} for the adaxial and abaxial leaf surfaces for 17 wheat species.	159
Figure 5.10. Temporal response of stomatal conductance and net CO ₂ assimilation to a step increase in light intensity for 17 wheat species.....	162

Figure 5.11. Stomatal kinetics from a step increase in light intensity for 17 wheat species.....	165
Figure 5.12. Stomatal kinetics correlations for g_s and A for 17 wheat species.	167
Figure 5.13. The response of CO_2 assimilation to intercellular $[CO_2]$ for 17 wheat species.....	168
Figure 5.14. Variation of the measured CO_2 -saturated rate of photosynthesis, the maximum rate of carboxylation and maximum rate of electron transport for 17 wheat species.....	170
Figure 6.1. Variation of flag leaf stomatal density for 11 wheat species at both atmospheric CO_2 and elevated CO_2	188
Figure 6.2. Variation of flag leaf stomatal density for the adaxial and abaxial leaf surfaces for 11 wheat species at both atmospheric CO_2 and elevated CO_2	189
Figure 6.3 Variation of flag leaf guard cell length for 11 wheat species at both atmospheric CO_2 and elevated CO_2	190
Figure 6.4 Variation of flag leaf guard cell length calculated for the adaxial and abaxial leaf surfaces for 11 wheat species at both atmospheric CO_2 and elevated CO_2	191
Figure 6.5 Correlation between stomatal density and guard cell length for 11 wheat species at both atmospheric CO_2 and elevated CO_2	192
Figure 6.6 Variation of flag leaf g_{smax} for 11 wheat species at both atmospheric CO_2 and elevated CO_2	194
Figure 6.7 Variation of flag leaf g_{smax} of the adaxial and abaxial for 11 wheat species at both atmospheric CO_2 and elevated CO_2	195
Figure 6.8 Variation of flag leaf area for 11 wheat species at both atmospheric CO_2 and elevated CO_2	198
Figure 6.9 Variation of flag dry weight for 11 wheat species at both atmospheric CO_2 and elevated CO_2	199
Figure 6.10 Variation of flag leaf thickness for 11 wheat species at both atmospheric CO_2 and elevated CO_2	200
Figure 6.11 Temporal response of stomatal conductance, net $[CO_2]$ assimilation and water use efficiency for 11 wheat species at both atmospheric CO_2 and elevated CO_2	202
Figure 6.12 Time constant for stomatal conductance kinetics for 11 wheat species at both atmospheric CO_2 and elevated CO_2	204

Figure 6.13 Time constant for light saturated carbon assimilation for 11 wheat species at both atmospheric CO₂ and elevated CO₂ 206

Figure 6.14 Stomatal kinetics correlations for g_s for 11 wheat species at both atmospheric CO₂ and elevated CO₂ 208

Figure 6.15 Stomatal kinetics correlations for A for 11 wheat species at both atmospheric CO₂ and elevated CO₂ 209

Figure 6.16 The response of CO₂ assimilation to intercellular [CO₂] for 11 wheat species at both atmospheric CO₂ and elevated CO₂ 210

Figure 6.17 Variation of light and CO₂ maximum photosynthesis, the maximum rate of carboxylation and maximum rate of electron transport for 11 wheat species at both atmospheric CO₂ and elevated CO₂ 212

List of Tables

Table 1.1 Founder cultivars of the eight-parent MAGIC wheat population selected in partnership with UK wheat breeders highlighting year listing and trait attributes.....	26
Table 2.1 Species selected for this study including ploidy and common name.....	52
Table 2.2 Stomatal responses to a step increase in PPFD protocols for combined chamber for individual leaf surface infra-red gas exchange.	66
Table 3.1: Analysis of variance results between flag leaf cultivars, surfaces and leaf locations and second leaf cultivars, surfaces and leaf locations for stomatal density, guard cell length and g_{smax} of eight MAGIC wheat cultivars	78
Table 3.2: Tukey post-hoc test comparisons of group means between surfaces and locations of flag and second leaf for eight MAGIC wheat cultivars.....	88
Table 3.3: Tukey post-hoc test comparisons of group g_{smax} means between flag leaf opposing leaf surfaces (abaxial vs adaxial) for eight MAGIC wheat cultivars.....	98
Table 5.1 Species selected for this chapter including ploidy and common name ..	150
Table 5.2: Two-way analysis of variance (ANOVA) results between flag leaf species and surfaces for stomatal density, guard cell length and g_{smax} of 17 wheat species	154
Table 6.1 Species selected for this chapter including ploidy and common name ..	185
Table 6.2: Two-way analysis of variance (ANOVA) results between species, leaf surfaces (abaxial and adaxial) and CO ₂ growth concentrations (atmospheric at ~ 408 ppm and elevated ~ 800 ppm) for stomatal density, guard cell length and g_{smax} of 11 wheat species	187
Table 6.3. Tukey results following a two-way ANOVA between CO ₂ growth concentrations (atmospheric at ~ 408 ppm and elevated ~ 800 ppm) of the same species for stomatal density, guard cell length and g_{smax} of 11 wheat species....	190
Table 6.4: Two-way analysis of variance (ANOVA) results between flag leaf species and CO ₂ growth concentrations (atmospheric at ~ 408 ppm and elevated ~ 800 ppm) for Leaf dry weight, leaf area and leaf thickness of 11 wheat species.....	196

Table 6.5. Tukey results following a two-way ANOVA between CO₂ growth concentrations (atmospheric at ~ 408 ppm and elevated ~ 800 ppm) of the same species for Leaf dry weight, leaf area and leaf thickness of 11 wheat species..... 197

List of Abbreviations

A	Net CO ₂ assimilation rate per unit leaf area ($\mu\text{mol m}^{-2} \text{s}^{-1}$)
A/C_i	Net CO ₂ assimilation rate (A) as a function of [CO ₂]
A_F	Final A value (average of final five A values; $\mu\text{mol m}^{-2} \text{s}^{-1}$)
A/Q	Net CO ₂ assimilation rate (A) as a function of light intensity (Q)
A_{max}	Light and CO ₂ saturated rate of CO ₂ assimilation ($\mu\text{mol m}^{-2} \text{s}^{-1}$)
a_{max}	Mean maximum stomatal pore area (μm^2)
Ca	Extracellular CO ₂ concentration ($\mu\text{mol mol}^{-1}$)
CO₂	Carbon dioxide
[CO₂]	Atmospheric CO ₂ concentration ($\mu\text{mol mol}^{-1}$)
C_i	Intercellular CO ₂ concentration ($\mu\text{mol mol}^{-1}$)
d	Diffusivity of water in air ($\text{m}^2 \text{s}^{-1}$, at 22°C)
ΔA	Difference between two steady state A values ($\mu\text{mol m}^{-2} \text{s}^{-1}$)
Δg_s	Difference between two steady state g _s values ($\text{mol m}^{-2} \text{s}^{-1}$)
DW	Dry weight of leaf (g)
E	Evapotranspiration rate ($\text{mol m}^{-2} \text{s}^{-1}$)
es	Water vapour pressure (kPa)
e(T_i)	Water vapour pressure (kPa) at temperature (°C)
EW	Elite wheat species
g_o	Initial value of g _s ($\text{mol m}^{-2} \text{s}^{-1}$)
gb	One- sided boundary layer conductance ($\text{mol m}^{-2} \text{s}^{-1}$)
GCL	Guard cell length (μm)
GS	Growth stage
g_s	Stomatal conductance to water vapour ($\text{mol m}^{-2} \text{s}^{-1}$)
g_{sF}	Final A value (average of final five A values; $\text{mol m}^{-2} \text{s}^{-1}$)
g_{smax}	Theoretical anatomical maximum stomatal conductance ($\text{mol m}^{-2} \text{s}^{-1}$)
IRGA	Infra-red gas analysis
J_{max}	Maximum rate of electron transport demand for RuBP regeneration
KNO₃	Potassium nitrate
l	Pore depth (μm)
LA	Leaf area (cm^2)
LA_b	Leaf absorbance (%)
LT	Leaf thickness (μm)

NH₄NO₃	Ammonium nitrate
NPK	Nitrogen – Phosphate – Potassium mix
P	Atmospheric pressure (kPa)
π	Mathematical constant approximated to 3.142
PL	Pore length (μm)
PPFD	Photosynthetic photon flux density
SD	Stomatal density (mm ²)
S_i	Slope of the slow linear increase of G
SS	Stomatal size (measured as guard cell length; μm)
T_{gs}	Time constant to reach 63% of final projected <i>g_s</i>
T_A	Time constant to reach 63% of final projected <i>A</i>
<i>t</i>	Time (minutes)
T_i	Leaf temperature (°C)
<i>v</i>	Molar volume of air (m ³ mol ⁻¹ , at 22°C)
V_{Cmax}	Maximum rate of carboxylation by Rubisco (μmol m ⁻² s ⁻¹)
VPD	Vapour pressure deficit (kPa)
W_i	Intrinsic water use efficiency (<i>A/g_s</i> ; μmol mol ⁻¹)
WWR	Wild wheat relative species

Publications

All publications listed below were produced using data and/or ideas associated with this thesis.

- S Wall, S Violet-Chabrand, P Davey, J Van-Rie, J Cockram, T Lawson (In Preparation) "The dark side of stomatal conductance: does photosynthesis on the abaxial and adaxial leaf surface contribute independently to overall gas exchange in wheat?" (Journal Article)
- J Stevens, M Faralli, S Wall, J D Stamford, T Lawson (In Press) *Stomatal Responses to Climate Change* (Book Chapter)
- M Faralli, J Cockram, E Ober, S Wall, A Galle, J Van-Rie, C Raines, T Lawson (2019) "Genotypic, Developmental and Environmental Effects on the Rapidity of g_s in Wheat: Impacts on Carbon Gain and Water-Use Efficiency" *Frontiers in Plant Science*, **10**, 492

CHAPTER 1

Introduction

1.1 Introduction

1.1.1 climate change and food security

The current global population is over 7.2 billion, and is projected to increase to 9.6 billion by 2050 (McGuire, 2013), which means that crop yields need to double in the next 30 years to meet increased demand for plant based products (Ray *et al.*, 2013). Increasing economic growth in this growing population will boost urbanisation, using more land to accommodate city dwellings and reducing that available for agriculture (Maggio *et al.*, 2015). In addition to population growth, changing diets and bio-fuel use are further drivers of the need to increase biomass and yield (Hannon *et al.*, 2010). The increased demands for food and fuel cannot be met by using more land use for crop production and will have to be delivered by greater crop productivity (Ray *et al.*, 2013). Food insecurity is rapidly increasing globally, in 2016, 815 million people globally were food insecure, with 108 million of those in food crisis, a 35% increase from 80 million in 2015. (FSIN, 2017; FAO, *et al.*, 2017). Between 2015 and 2016 famine was declared in South Sudan and crisis-level food insecurity situations were identified in several other countries (FAO, *et al.*, 2017). Factors affecting food shortages include increasing world population, climate change, losses of agricultural land to urbanization and increasing competition for non-food uses of crops for example biofuels and increased meat consumption (Zhu *et al.*, 2010; Ray *et al.*, 2013; Long *et al.*, 2015).

Increases in the demand for our primary foodstuffs is already surpassing increases in yields and if rates of crop yield improvement per hectare are only maintained rather than increased in the future, supply will not keep up with demand by 2050 (Ray *et al.*, 2013; Long *et al.*, 2015). In the past decades breeding efforts

have increased yields by focusing on a combination of genetic improvement resulting in high-yielding varieties, most notably the semi-dwarf wheat cultivars, better management of pest and diseases and higher applications of fertilisers (Semenov *et al.*, 2012). The traits that drove yield increases during the Green Revolution appear to have little remaining potential for further increases. With the climate changing and population growing one sustainable protocol is to improve crop mechanisms to match actual yield performance with potential performance (Ray *et al.*, 2013).

World food production is heavily reliant on a small number of crops. Rice, wheat and maize are staple foods for 80 % of the world population and rice is consumed by almost 50 % of the global population (FAO, *et al.*, 2017). Against the backdrop of the requirement for increasing productivity with less available land, the changing climate presents additional challenges. The current IPCC 5th assessment (IPCC, 2014) predicts higher concentrations of greenhouse gases leading to higher global mean surface temperatures. Atmospheric carbon dioxide concentration [CO₂] has nearly doubled in the last 100 years from 220 $\mu\text{mol mol}^{-1}$ to 400 $\mu\text{mol mol}^{-1}$, due primarily to emitted anthropogenic greenhouse gases (GHG) from industrial process, and is set to increase further to 700 $\mu\text{mol mol}^{-1}$ by 2100 (Zhu *et al.*, 2004; Long *et al.*, 2015).

This increase in atmospheric [CO₂] by emitted GHG's is raising global mean climate temperature, which has an adverse effect on the growing regime of crop plants (Schlenker *et al.*, 2006; Schlenker & Roberts, 2009; Parry *et al.*, 1999). Higher temperatures often shorten the growing periods of crop plants destabilising those specific combinations of temperature and photoperiod ranges that plants have adapted to over millions of years, affecting grain filling stages and overall grain yield (Parry *et al.*, 1999). Global mean surface temperature is likely to exceed 1.5°C by the end of the century under most climate change projections (IPCC, 2014) and rising

temperatures will be detrimental to productivity of C3 crops which face higher rates of photorespiration and a decrease in photosynthesis (Teskey *et al.*, 2015), with further impacts from greater evapotranspiration, leading to reduced soil moisture content, particularly where night temperatures are high (Hatfield & Prueger, 2015). Higher temperatures are also closely associated with water availability through the impact on transpiration. Transpiration accounts for over 90% of land-based water losses, and therefore, a major goal of crop science is to manage water use more-effectively (Morison *et al.*, 2008; Food and Agriculture Organization of the United Nations (FOA), 2014; Vialet-Chabrand *et al.*, 2016; Faralli *et al.*, 2019a; Hatfield & Dold, 2019). In addition, heat waves, drought, heavy and sporadic rain are expected to occur with greater frequency or duration, putting further pressure on crop productivity (IPCC, 2014). Higher temperatures raise evaporative demand, thus decreasing water availability, driving the need for crops that can tolerate water stress conditions (Stevens *et al.*, 2020).

1.1.2 Wheat

In recent years, increases in global wheat yields have slowed, averaging between 0 and 1.1% annually, while an increase of 1.6 and 2.4% per annum over the next 50 years is needed to keep up with demand (Dixon *et al.*, 2009). If rates of crop yield improvement per hectare are only maintained rather than increased in the future, supply will not keep up with demand (Brisson *et al.*, 2010; Ray *et al.*, 2013; Long *et al.*, 2015). Not only do crop yields need to increase, they need to increase without encumbering land and water resources and without overloading the environment with an excess of herbicides or nitrogen-rich fertilizer (Janssen *et al.*, 2014; Nair, 2014).

In the mid-1960s the 'Green Revolution' was the technological response to a world-wide food shortage, where modern or high-yielding crop varieties of rice and wheat

were subjected to intensive breeding and subsequently released to farmers in Latin America and Asia (Evenson & Gollin, 2003; Hedden, 2003). The varieties of rice and wheat delivered large increases in crop production by incorporating the dwarfing genes Reduced Height 1 (Rht1) and/or Rht2 genes. Dwarfing allowed the development of shorter, stiff-strawed varieties which devoted more of their energy to grain production rather than producing straw and leaf material, also responding better to fertilisers and pesticides (Evenson & Gollin, 2003; Hedden, 2003).

Wheat (*Triticum aestivum L.*) is a principle global food grain source, grown on more land area than any other commercial crop. In addition, it is one of the largest traded primary crop commodities, along with maize and rice (FOA, 2014). It is globally the most vital crop, providing over 20 % of the calories consumed by the world's population, and directly or indirectly (via livestock) the bulk of protein in many regions (Braun *et al.*, 2010; Lobell *et al.*, 2011). Wheat is adaptable to a wide range of climatic conditions due to its allohexaploid genome structure the result of two polyploidisation events (Petersen *et al.*, 2006). Domestication of founder western crops originated in the 'Fertile Crescent' (situated between south-eastern Turkey and northern Syria) approximately 10,000 years ago, after the last ice age, lasting several centuries (Heun *et al.*, 1997; Lev-Yadun *et al.*, 2000; Salamini *et al.*, 2002; Riehl *et al.*, 2013; Faris, 2014). The understanding of the evolution and domestication of wheat has come from

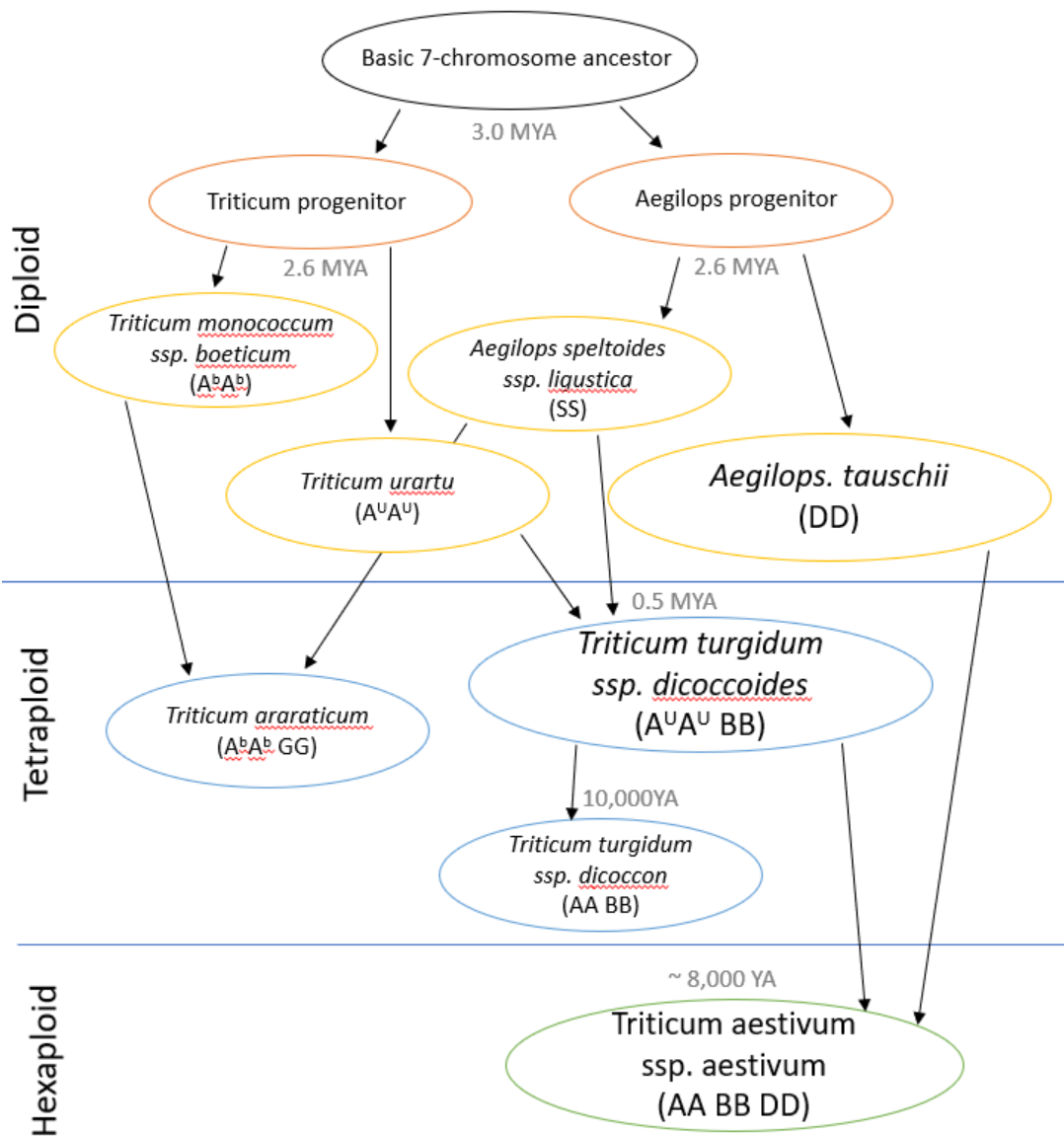


Figure 1.1 The evolutionary lineages involved in Triticum wheat species with sub-genome lettering Including Triticum monococcum ssp. boeoticum - AbAb, Triticum urartu - AuAu (GG ancestor), Aegilops speltoides ssp. ligustica - SS (BB ancestor), Aegilops tauschii – DD, Triticum araraticum - AbAb GG, Triticum turgidum ssp. dicoccoides – AuAu BB, Triticum turgidum ssp. dicoccon – AA BB, Triticum aestivum ssp. aestivum – AA BB DD. Diploid, tetraploid, and hexaploid species are separated by blue lines. Arrows indicate genomes leading to new species through polyploidization. Grey wording indicates time passed since event YA = years ago, MYA = million years ago (reproduced from Faris, 2014)

the assembly of evidence from botany, genetics, archaeology, and a knowledge of the present distribution of grass species. Modern wheat domestication resulted from polyploidization, referring to the multiplication of a complete chromosome set, resulting in multi-copy genes that exist as paralogs to each other, useful to establishing agronomic traits (Hancock, 2005; Renny-Byfield & Wendel, 2014; Zhang *et al.*, 2019). Wheat species of the genus *Triticum* have chromosome numbers organised in sevens ($1x = 7$) consisting of diploids ($2n = 2x = 14$), tetraploids ($2n = 4x = 28$), and hexaploids ($2n = 6x = 42$) (Sax, 1922; Kimber & Sears, 2015). The allohexaploid bread wheat *Triticum aestivum* L. ($2n = 6x = 42$; genomic code AABBDD), is a product of polyploidization, produced from two separate hybridisation events followed by spontaneous chromosome doubling, see fig. 1.1 (Kerber & Rowland, 1974; Faris, 2014; Marcussen *et al.*, 2014). Modern wheat species sub-genomes A, B and D derived from three diploid species, *Triticum urartu* (AA), an unknown close relative of *Aegilops speltoides* ssp. *ligustica* (SS), and *Aegilops. tauschii* (DD) converging in two steps (Johnson & Dhaliwal, 1976; Salamini *et al.*, 2002; Petersen *et al.*, 2006; Charmet, 2011; Faris, 2014). Wild diploid wheat *Triticum urartu* ($2n = 2x = 14$, sub genome AA) hybridized with the B genome ancestor *Aegilops speltoides* ssp. *ligustica*, ($2n = 2x = 14$, genome SS) (Huang *et al.*, 2002; Dvorak & Akhunov, 2005; Peng *et al.*, 2011) to produce wild emmer wheat *Triticum turgidum* ssp. *dicoccoides*, ($2n = 4x = 28$, genome AA BB). The second amphiploidization event saw *Triticum turgidum* ssp. *dicoccoides*, ($2n = 4x = 28$, genome AA BB) hybridise with *Aegilops tuschii* to produce *Triticum aestivum* ssp. *Aestivum* ($2n = 6x = 42$, genome AA BB DD; Huang *et al.*, 2002; Charmet, 2011; Faris, 2014). The evolution of wheat from the primitive to the cultivated forms saw the acquisition of valuable agronomic traits such as non-brittle rachis, which limited the natural seed dispersal mechanisms, glume tenacity for free-

threshing, spikelet articulation, awn development and an increase in grain size, which allowed for mechanised cultivation on a large scale (Kerber & Rowland, 1974).

1.1.3 Multi-parent Advanced Generation Inter-Cross (MAGIC) wheat

When developing novel wheat varieties, targeting key qualities and attributes can be troublesome as they are often controlled by multiple genes. Traditional wheat genetic studies (which only involve two parent varieties), have limited ability to define the genes determining key traits (Ladejobi *et al.*, 2016). A novel approach to overcome these inherent constraints included crossing different combinations of multiple parents, generating plants that have a genome that is a mosaic of their multiple parents (Scott *et al.*, 2020). The Multi-parent Advanced Generation Inter-Cross (MAGIC) breeding technique represents a new generation of plant mapping resources which allows the identification of genes controlling quantitative traits by crossing different combinations of multiple parents, facilitating a more-precise identification of genes that are responsible for desirable plant traits. The NIAB MAGIC population was developed in partnership with UK breeders and represents 80% of the SNP variation in North–West European bread wheat (Mackay *et al.*, 2014) which included eight founder varieties: *Triticum aestivum* L. Sp. Alchemy, Brompton, Claire, Hereward, Rialto, Robigus, Soissons and Xi19 (Table 1.1) (Gardner *et al.*, 2016). This genetic diversity gives a wide phenotypic variation facilitating QTL mapping analysis and offering the chance to further explore the extent of variation in traits such as stomatal anatomy and the impact of variation on morphological and physiological characteristics.

Table 1.1 Founder cultivars of the eight-parent MAGIC wheat population selected in partnership with UK wheat breeders highlighting year listing and trait attributes. (OWBM = orange wheat blossom midge).

Cultivar	Year listing	Trait attributes
Alchemy	2006	Yield, disease resistance, breeding use, soft
Brompton	2005	Hard feed, 1BL/1RS, OWBM-resistance
Claire	1999	Soft biscuit/distilling, slow apical development
Hereward	1991	High-quality benchmark 1 bread-making
Rialto	1994	Moderate bread-making, 1BL/1RS
Robigus	2003	Exotic introgression, disease resistance, breeding use, OWBM-resistance, <i>Rht-B1</i>
Soissons	1995	Bread-making quality, early flowering, <i>Rht-B1</i>
XI19	2002	Bread-making quality, facultative type, breeding use

Screening germplasm for differences in stomatal anatomy and behaviour under specific environmental conditions could identify genotypes with desirable characteristics. Advances in crop genotyping has resulted in genetic marker density not being a limiting factor for quantitative trait loci (QTL) studies in plants. Identifying QTLs is an approach for locating gene regions which contain the gene of interest, underlying naturally occurring variation in phenotypes, for example those which affect stomatal density (SD). It allows the use of statistical methods to identify chromosomal regions containing genetic factors contributing to variation in a polygenic trait (Lynch & Walsh, 1998). MAGIC wheat populations are a new generation of genetic mapping resources which are multi-founder equivalents of the advanced intercross introduced by Darvasi & Soller (1995). MAGIC populations are created by several generations of intercrossing among multiple founder lines conveying more allelic diversity than typical

bi-parental mapping populations. Furthermore, multiple cycles of intercrossing provide greater precision in QTL location (Mackay *et al.*, 2014).

1.1.4 Introduction to stomata

Stomata are microscopic structures found over the predominantly waterproof and CO₂-impermeable leaf cuticle. Stomata comprise two specialized guard cells (GC) flanking a central pore which facilitate diffusional gaseous flux between the interior of the leaf and the atmosphere (Weyers & Lawson, 1997; Lawson *et al.*, 1998a; Hetherington & Woodward, 2003). Stomata first appeared in terrestrial land plants over 400 million years ago (Mya) (Edwards, 1998), which marked a pivotal point in maintaining constant cell internal water content by compensating for temporary fluctuations resulting from transpiration; homoiohydry. This allowed plants to colonise the land, surviving desiccation in the dry atmosphere and facilitating gas exchange for respiration, closing the aperture to create a waterproof barrier when required (Raven, 1977, 2002; Hetherington & Woodward, 2003; Peterson *et al.*, 2010). Looking back further (Figure 1.2), stomatal evolution appears to predate that of flowers, leaves, roots and even a vascular system (Peterson *et al.*, 2010).

Astomatous land plants of the Silurian and Devonian eras had reduced water loss to the atmosphere due to well-developed cuticles around their aerial organs but also had significantly reduced [CO₂] diffusion rates to the underlying chlorenchymatous tissues (Edwards *et al.*, 1996; Woodward, 1998). Between 430 and 415 Mya, 'prestomatal state' pores in the epidermis of plant organs, at least three cell layers thick, increased in sufficient frequency to be detectable in the fossil record, and permitted higher photosynthetic rates per unit ground area. The number of pores increased monotonically to reach a peak in the Upper Carboniferous era about 300 Mya. They were strikingly similar to those of extant land plants, a demonstrable insight

to their significance and effectiveness to terrestrial plant forms, being one of the most-conserved embryophyte vegetative characters (McElwain & Chaloner, 1995; Edwards *et al.*, 1996; Edwards, 1998; Woodward, 1998; Raven, 2002; Franks *et al.*, 2012a).

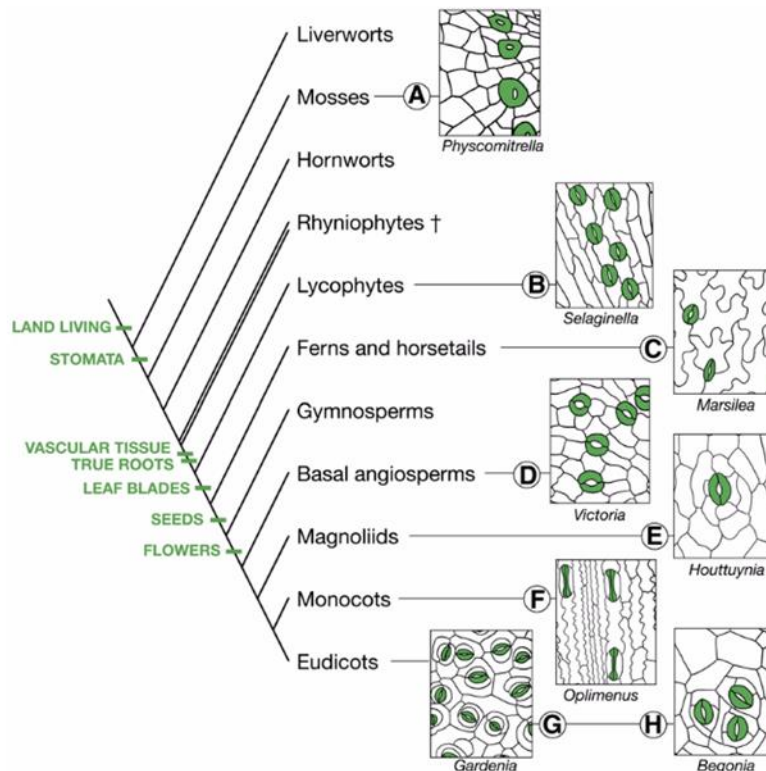


Figure 1.2 Diversity of Stomata across Land Plant Taxa. A phylogenetic tree of extant and extinct (†) land plants includes evolutionary represented traits supporting success on land. The wide diversity of stomatal complexes among these groups is shown from stomatal pictures of *P. patens* ([A]; nonvascular), *Selaginella kraussiana* ([B]; lycophyte, vascular), *Marsilea macropoda* ([C]; fern, vascular), *Victoria amazonica* ([D]; Nymphaeaceae, basal angiosperm), *Houttuynia cordata* ([E]; Piperales, magnoliid), *Oplismenus hirtellus* ([F]; Poales, monocot grass), *Gardenia taitensis* ([G]; Gentianales, eudicot angiosperm), and *Begonia rex-cultorum* 'Roberta' ([H]; Cucurbitales, eudicot angiosperm). Stomata are coloured green. Image from (Peterson *et al.*, 2010)

During the last 400 million years of the Phanerozoic era, atmospheric [CO₂] has changed considerably, and stomata have adapted to cope with these changes. The established stomatal pores have changed markedly in stomatal size (SS) and SD on plant surfaces (Hetherington & Woodward, 2003). Low concentration of atmospheric CO₂ are associated with high SD, and, the emergence of novel plant lineages such as the ferns, pteridosperms and angiosperms, although this relationship is correlative not causal (Woodward, 1998). Differences also in stomatal location would have delivered differing capabilities for the range and survival of species in differing environments (Hetherington & Woodward, 2003). The changes in stomatal heterogeneity could influence global ecology and has therefore attracted considerable attention, due to the 'recent' increase in atmospheric greenhouse gases, an effect of the Industrial Revolution (Pagani *et al.*, 1999; Pearson & Palmer, 2000; NOAA, 2020). The active control of stomatal aperture, conclusively established over 150 years ago, has guard cell turgor changing independently of leaf and epidermal cell turgor, permitting stomatal responses to environmental cues (Darwin, 1898). Following these early investigations, the mechanisms of guard cell turgor and stomatal opening regimes captured the interest of many scientists (Lloyd, 1908; Laidlaw & Knight, 1916; Wiggans, 1921). Their work demonstrated that opening and closing of the stomata was due to variations in guard cell osmotic pressure that were higher than that of surrounding epidermal cells.

Osmotic pressure was mediated by membrane ion transporters, which maintained turgor even in times of water stress and wilted leaves (Franks, 2004; Roelfsema & Hedrich, 2005; Chen *et al.*, 2017). Guard cell turgor was shown to correspond with stomatal opening and was dependent on effective osmotic potential within the cell. Also the osmotic potential of the guard cells increased in the mornings,

when stomata opened and decreased in the night when closing; a driver of stomatal responses had been found (Matthews *et al.*, 2020).

When stomatal pores open to maintain CO₂ supply to mesophyll cells for photosynthetic carbon assimilation (A), water is lost through transpiration as a consequence (Lawson *et al.*, 1998b; Morison *et al.*, 2008). Transpirational water loss plays a key role in nutrient uptake from the plant roots as well as evaporative cooling of the leaf tissue (Raven, 1977, 2002; Hetherington & Woodward, 2003; Peterson *et al.*, 2010; McAusland *et al.*, 2016; Murray *et al.*, 2016; Lawson & Vialet-Chabrand, 2019). Dynamic stomatal movement, often referred to as stomatal behaviour, acts in response to environmental cues and internal signals in an attempt to optimise the trade-off between A and the maintenance of plant water status (Farquhar & Sharkey, 1982; Mansfield *et al.*, 1990; Lawson *et al.*, 2010; Buckley & Mott, 2013; Lawson & Blatt, 2014; Buckley, 2017; Vialet-Chabrand *et al.*, 2017a; Matthews *et al.*, 2018; Yamori *et al.*, 2020). Stomatal behaviour is typically inferred from stomatal conductance (g_s), the capacity for the gaseous exchange of water vapour from the leaf to atmosphere, in mole of flux per unit area per second ($\text{mol m}^{-2} \text{s}^{-1}$) (Vialet-Chabrand *et al.*, 2017b). Stomatal conductance is a function of both SD and behaviour (Lawson & Vialet-Chabrand, 2019). Wong *et al.* (1979) described the relationship of A and g_s as proportional, although the rate of water leaving the leaf through stomata is an order of magnitude greater than CO₂ entering the leaf for A (Drake *et al.*, 2013; Lawson & Vialet-Chabrand, 2019; Vialet-Chabrand & Lawson, 2019a). While photosynthesis is occurring, there is an ongoing demand for CO₂ influx into the leaf as chloroplast [CO₂] declines. Carbon dioxide entering the leaf encounters a series of resistance points *en route* to the chloroplast, at the boundary layer, stomata and mesophyll. Of these,

stomatal resistance can create the largest impediment to CO₂ influx, with g_s being the inverse of stomatal resistance (Harrison *et al.*, 2020).

1.1.5 Stomatal Development and Patterning

Stomatal initiation is a complex series of events which pattern the developing epidermal tissues, crucial to the success of plants' exploitation of the environment (Croxdale, 2000). Angiosperm leaves exhibit two fundamentally different modes of growth and development. Eudicotyledons leaves grow from multiple points, with clones of new cells forming throughout growth and development. This addition of new cells to the leaf and their subsequent expansion complicates understanding of stomatal patterning (Croxdale, 2000). In the eudicotyledon model for *Arabidopsis thaliana* by Vatén & Bergmann (2012), new forming cells are initiated from various sites on the leaf (Fig. 1.3). A committed protodermal cell, the meristemoid mother cell (MMC), divides asymmetrically producing a larger stomatal lineage ground cell (SLGC) and smaller meristemoid. The meristemoid undergoes one to three asymmetric divisions (amplifying divisions) before it differentiates into a guard mother cell (GMC). A meristemoid has many unique cellular properties, but its most distinctive feature is that it can act like a stem cell. Therefore, they have an innate ability to both propagate and limit stomatal development (Vatén and Bergmann, 2012; Pillitteri *et al.*, 2011; Dow & Bergmann, 2014; Han & Torii, 2016). The GMC divides symmetrically to create two guard cells, and in some species the GMCs recruit neighbouring subsidiary cells. Amplifying and spacing divisions and subsidiary recruitment all require cell to cell communication and together they contribute to patterning. The frequency with which cells participate in these division types can be tuned to yield the diversity of stomatal patterns seen in nature (Peterson *et al.*, 2010; Vatén & Bergmann, 2012; Dow & Bergmann, 2014).

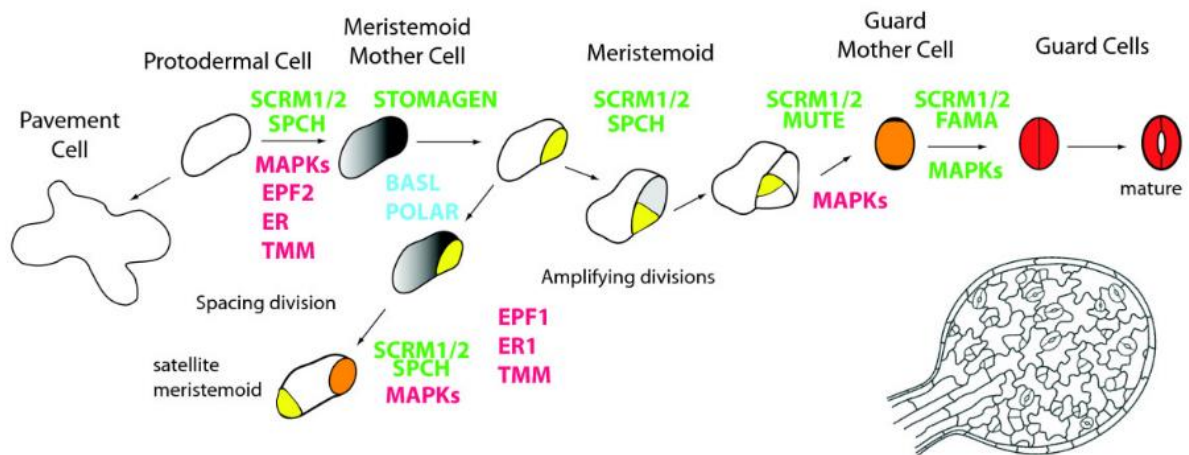


Figure 1.3 Stomatal development in *A. thaliana*

Major stages in stomatal development of *A. thaliana*; positive regulators (written in green), negative regulators (in red) and polarity regulators (in blue). Picture colour code: yellow, meristemoid; orange, guard mother cell; red, guard cell; grey, meristemoid mother cell (MMC) (Image from Vatén & Bergmann, 2012).

Shiu & Bleecker, (2001) posit the use of peptide ligands, and cell surface receptor-based signalling mediated by leucine-rich repeat, single transmembrane pass receptor-like kinases (LRR-RLKs), to ascertain cell fate and patterning (Abrash *et al.*, 2011). A family of secreted peptide signals, for example, the Epidermal Patterning Factors-Like (EPFL) proteins or Epidermal Patterning Factors (EPF) compete for cell surface receptors to compromise the receptor like protein ‘too many mouths’ (TMM) together with the ERECTA (ER) family receptors (Hara *et al.*, 2007, 2009; Hunt & Gray, 2009; Hunt *et al.*, 2010; Lee *et al.*, 2012). This competition produces altered patterning of stomata on leaves in *A. thaliana* species, specifically abnormal clustering (increased occurrence of two or more stomata in contact with each other) and increased density (Rowe & Bergmann, 2010; Franks & Casson, 2014) see figure 1.7; E. The binding of these ligands activates an intracellular cascade, phosphorylating and thus disrupting basic helix-loop-helix transcription factors required for cells to enter the stomatal lineage in early leaf development (Peterson *et al.*, 2010; Chater *et al.*, 2016; Raissig *et al.*, 2016). The expression of the peptides

specifically inhibits or activates stomatal development, determining the SD in leaves. Due to this development in genetics the EPF mutants provide a versatile model to alter stomatal patterning whilst maintaining other leaf traits, enabling researchers to explore the role of stomatal development in the optimisation of leaf gas exchange (Franks & Casson, 2014).

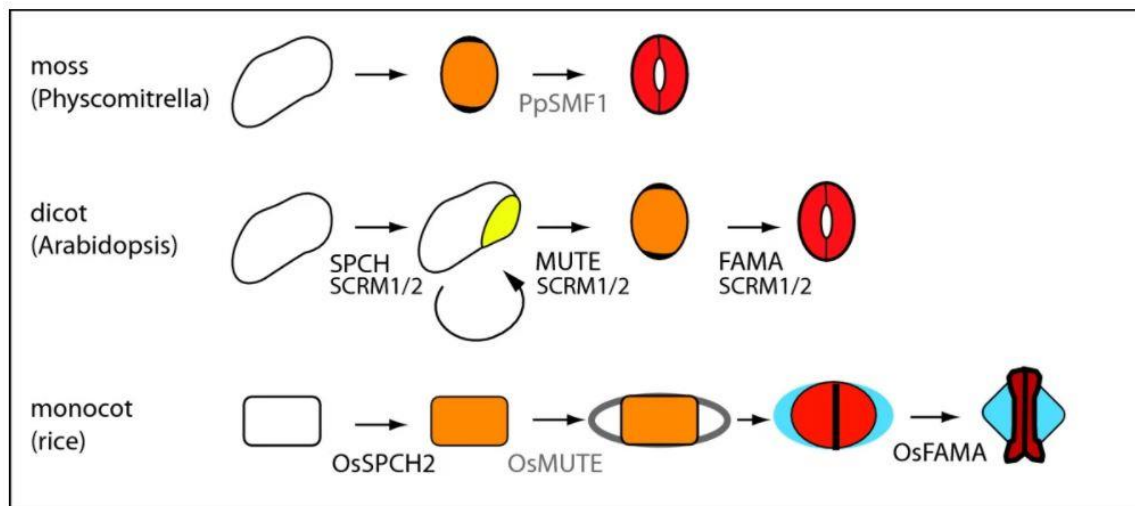


Figure 1.4 Comparison of the molecular and morphological features of stomatal development in *Arabidopsis* and representatives of the grasses and mosses for which molecular data exist. Presentation of a simplified stomatal lineage displaying only cell identities (in the same colour codes as Figure 1.3), with the addition of blue to mark the subsidiary cells in monocots. Text indicates genetic regulators of the processes, included at their points of action. The curved arrow in the dicot lineage represents the continued asymmetric amplifying divisions made by meristemoids (Image from Vatén & Bergmann, 2012).

Monocotyledon leaves, on the other hand, have polarized growth from a single point source of cells at or near the leaf base, creating a leaf blade with the oldest cells at the tip. The epidermis consists of regular longitudinal files of cells, whose cells differentiate basipetally, providing a continuum of stages along the blade length (Croxdale, 2000). Polarized growth makes monocotyledon leaves well suited for stomatal patterning studies as developmental histories can be traced down its length. New blade cells and stomatal precursors originate in polarized fashion at the leaf base and are present in a continuum of stages from the leaf tip (mature) to the leaf base

(immature) (Croxdale, 2000; Dow and Bergmann, 2014). Asymmetric cell divisions produce GMCs without a meristemoid stage, then files of protodermal cells flanking the GMC polarize towards the GMC and divide asymmetrically producing subsidiary cells. The GMC divides to produce guard cells that exhibit the dumbbell-shaped morphology (Fig. 1.4). In monocotyledons, for example the genus *Tradescantia*, the overall stomatal pattern can be refined when GMCs change fate and differentiate into epidermal cells (Vatén and Bergmann, 2012; Boetsch *et al.*, 1995). This fate change is dependent on distance from neighbouring stomata, suggesting an inhibitory communication mechanism. Approximately 20 % of undifferentiated epidermal cells become stomatal initials and around 10 % of the initials arrest early in development. Arrest of the developing stomata is a common phenomenon in monocotyledons and can be known to yield more regularly ordered stomata adhering to the one cell spacing rule (Croxdale, 1998; Vatén & Bergmann, 2012; Matthews & Lawson, 2019). Full stomatal development has not completed at the time initials arrest. And selection does not occur based on functional fitness, but on position, reflected in increasing stomatal order (Croxdale, 1998; Vatén and Bergmann, 2012).

1.1.6 Stomatal Anatomy: Intra-inter-specific variation

Guard cells (GC) together with the stomatal pore, and if relevant, subsidiary cells make up the stomatal complex (Fig. 1.5), with stomatal pores ranging in SS (10 to 80 μm in length) and SD (between 5 and 1,000 mm^{-2}), depending on the species and the environmental growth conditions (Knapp *et al.*, 1993; Willmer & Fricker, 1996; Hetherington & Woodward, 2003). Guard cells are responsible for determining stomatal aperture although the signalling pathways are complex, and many remain contentious and are not fully understood (Lawson *et al.*, 2014; Sack & Buckley, 2016).

By adjusting vacuolar volume through the movement of osmotica including malate, sucrose, and K^+ , and water, total GC volume is changed (Brearley *et al.*, 1997; Assmann & Shimazaki, 1999; Negi *et al.*, 2008, 2014; Vahisalu *et al.*, 2008; Laanemets *et al.*, 2013; Xu *et al.*, 2016; Yamamoto *et al.*, 2016). The change in GC volume and therefore turgor pressure alters stomatal aperture. When the pressure potential becomes positive, microfibrils preventing a change in GC width cause curvature of the cell (Willmer & Fricker, 1996; Blatt, 2000).

Osmoregulation in guard cells is supported by two main hypothesis, the starch-sugar hypothesis which suggested the main osmolyte in stomatal opening was sucrose, produced from the breakdown of starch (Lloyd, 1908) and the more recent K^+ -malate hypothesis (Imamura S., 1943; Raschke, 1975), which correlated stomatal opening with K^+ uptake and the counterions malate and/or Cl^- (Schnabl & Raschke, 1980; Outlaw, 1983). Talbott & Zeiger (1996) offered evidence with a new theory: that both osmoregulatory pathways operate in guard cells at different times of the day. K^+ was proposed to be important for stomatal opening early in the day, and sucrose later in the diel period to maintain stomatal aperture (Amodeo *et al.*, 1996; Talbott & Zeiger, 1996; Schroeder *et al.*, 2001; Kim *et al.*, 2010; Lawson & Matthews, 2020).

Changes in turgor result from a change in water potential (Ψ) of the guard cells by active changes in osmotic (or solute) potential ($\Psi\pi$) termed 'hydroactive' movement of water into or out of the guard cells (Aasamaa *et al.*, 2001). Water potential or the amount of potential energy in water, measured in pressure (MPa) and is the difference between the potential in a water sample and pure water. Osmotic potential decreases with increasing solute concentration whereas a decrease in $\Psi\pi$ causes a decrease in the total water potential and is negative in a plant cell and measures zero in distilled

water (Jones, 2014). The water potential in plant solutions is influenced by solute concentration, pressure, gravity, and factors called matrix effects:

$$\Psi_{\text{system}} = \Psi_{\text{total}} = \Psi_p + \Psi_{\pi} + \Psi_g$$

Where Ψ_p is the pressure potential and Ψ_g is the gravity potential (Jones, 2014). The 'System' can refer to the water potential of the soil water (Ψ_{soil}), root water (Ψ_{root}), stem water (Ψ_{stem}), leaf water (Ψ_{leaf}), or the water in the atmosphere ($\Psi_{\text{atmosphere}}$). As the single components alter, they raise or lower the Ψ_{total} of the system which initiates the movement of water to equilibrate, moving water through the plant (transpiration) from soil to atmosphere (Jones, 2014).

Buckley (2019) describes the most intuitive conceptual model of the mechanisms by which stomata respond to environmental factors that influence leaf water status, such as humidity and soil moisture and that water status controls g_s passively, by solely inflating and deflating stomatal guard cells in relation to the current water potential of the leaf is fundamentally incorrect due to the opposing effect of 'push-back' on adjacent epidermal cells causing stomata to close rather than open. Buckley (2019) suggests that in order for high Ψ to open stomata this 'push-back' epidermal effect must be overcome, and one likely mechanism is 'hydroactive feedback': the active regulation of guard cell osmotic pressure in relation to leaf water status, activated by a feedback response to changes in cell turgor or water content in the leaf. Buckley's (2019) feedback hypothesis combines stomatal responses to any factor that influences leaf water potential, including changes in humidity, soil moisture and plant water transport, under the umbrella of a single mechanism (Buckley, 2005), although the signalling mechanism(s) involved are a subject of ongoing debate.

Early stomata were anomocytic, i.e. had no distinct subsidiary cells (specialised epidermal cells that surround GCs and assist the process of opening and closing stomata (Fig. 1.5)), whereas modern species of terrestrial plants can have many subsidiary cells of varying shapes and sizes (Fig. 1.5) which surround a pair of morphologically and mechanistically diverse guard cells (Edwards et al., 1998, Franks and Farquhar, 2007). Subsidiary cells differ from epidermal cells due to their ability to shuttle ions (particularly K^+) and water rapidly between themselves and guard cells, modulated by the activity of aquaporins and ion channels, facilitating a mechanistic advantage and increased responsiveness of stomatal movement through rapid changes in turgor pressure (Franks & Farquhar, 2007; Hachez *et al.*, 2017; Raissig *et al.*, 2017; Lawson & Matthews, 2020). The number of subsidiary cells that surround a pair of guard cells differs between species although it is conserved *within* species, and ranges from zero (anomocytic - for example sporophytes of some extant hornworts and mosses) to six (hexacytic - for example *Commelina communis*) (Weyers & Paterson, 1987; Rudall & Knowles, 2013). The significance of subsidiary cells in the efficiency of stomatal functioning in grasses is supported by a recent study by Raissig *et al.* (2017) who manipulated the levels of a transcription factor (BdMUTE) necessary for subsidiary cell formation in *Brachypodium distachyon*. Plants lacking subsidiary cells, (known as subsidiary cell identity defective (*sid*)) had reduced stomatal kinetics, lower g_s and impaired growth (Hughes et al., 2017, Raissig et al., 2017, Hepworth et al., 2018). The evolutionary conservation of the stomatal complex suggests that the pairing of GC and subsidiary cells is integral for the efficiency of stomatal aperture control, highlighting the importance of further studying how the heterogeneity of stomatal complex morphologies affects plant physiology (Raissig et al., 2017; Hepworth et al., 2018; Bertolino et al., 2019).

Two main types of GC distinguished by shape are found in terrestrial plants; graminaceous or dumbbell-shaped (often paired with two main subsidiary cells); and elliptical or kidney-shaped (Hetherington and Woodward, 2003) (Fig. 1.7; E). Dumbbell-shaped GC are typical of grasses and other monocots such as palms, while kidney-shaped GC are found in all dicots, in several monocots as well as mosses, ferns, and gymnosperms (Hetherington and Woodward, 2003). Dumbbell-shaped GC evolved later than kidney shaped GC, between 70 and 50 million years ago, roughly 350 million years after the first perforation that evolved into their kidney-shaped counterparts (Kellogg, 2001; Hetherington & Woodward, 2003). It has been proposed (Hetherington and Woodward, 2003, Franks and Farquhar, 2007) that species such as wheat (*Triticum aestivum*) which possess the characteristic dumbbell-shaped GC have a faster movement of water across their semi-permeable guard-cell-membranes, facilitating superior dynamic performance. The mechanism is thought to be due to the high surface area to volume ratio of the dumbbell-shaped GC's and the close relationship with the adjacent subsidiary cells (Hetherington and Woodward, 2003), with less water needed in order for dumbbell-shaped GCs to increase turgor relative to kidney-shaped GC.

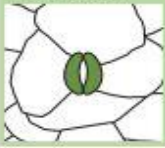
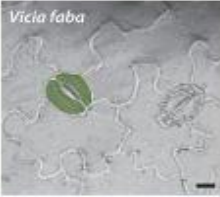
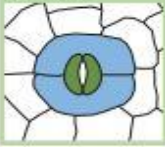
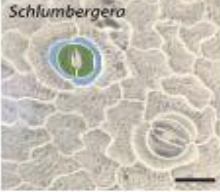
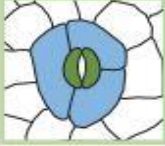

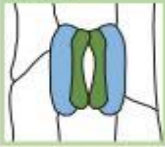
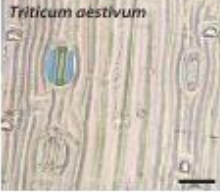
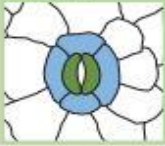
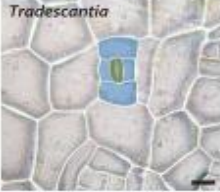
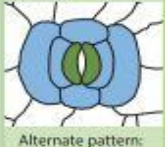
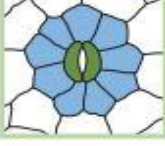

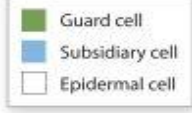
Type of stomatal complex	Description	Example families	Examples
Anomocytic (irregular celled) 	Guard cells surrounded by cells no different from epidermal cells in size and shape, and may lack true subsidiary cell function. Metcalfe & Chalk (1950) reported these occur in 142 families. Sometimes called ranunculaceous.	Chenopodiaceae Cucurbitaceae Apocynaceae Boraginaceae	<i>Vicia faba</i> 
Diacytic/Paracytic (two celled) 	Guard cells surrounded by two perpendicular (diacytic) or parallel (paracytic) subsidiary cells. Illustration is diacytic, example given is paracytic.	Caryophyllaceae Acanthaceae Cactaceae	<i>Schlumbergera</i> 
Anisocytic (unequal celled) 	Guard cells surrounded by three unequal sized subsidiary cells, one of which is distinctly smaller than the other two. Metcalfe & Chalk (1950) reported these occur in 37 families.	Crassulaceae Solanaceae Brassicaceae	<i>Nicotiana benthamiana</i> 
Graminaceous (grass-like) 	Dumbbell-shaped guard cells surrounded by subsidiary cells that lie parallel to the long axis. Metcalfe & Chalk (1950) described different types.	Cyperaceae Poaceae	<i>Triticum aestivum</i> 
Tetracytic (four celled) 	Guard cells are surrounded by four subsidiary cells—two lateral and two polar. Found mostly in monocots but can occur in dicots such as <i>Tilia</i> .	Poaceae Asclepiadaceae Asphodelaceae Commelinaceae	<i>Tradescantia</i> 
Actinocytic (star-celled) Typical pattern:  Alternate pattern: 	Typical pattern for <i>Commelina communis</i> (monocotyledon with kidney-shaped guard cells). A great deal of early stomatal work was conducted on this species due to the ease with which the epidermis peels. Alternate pattern: Guard cells surrounded by four or more subsidiary cells, elongated radially to the stomata.	Typical pattern: Ebenaceae Commelinaceae Araceae Alternate pattern: Araceae Musaceae	<i>Monstera deliciosa</i>  

Figure 1.5 Examples of stomatal complex types composed of guard cells (green) and surrounding subsidiary cells. In all illustrations and photographs, guard cells are shaded dark green and subsidiary cells are shaded blue. Included are anatomical descriptions and example families. Complex types and nomenclature follow information from (Cotthem, 1970; Melis & Zeiger, 1982). Scale bars represent 20 μm . (Image from (Lawson & Matthews, 2020).

As a result, more-rapid opening and closing is facilitated, reducing stomatal response time and supporting higher rates of photosynthetic gas exchange and higher W_i in fluctuating environments (Johnson & Dhaliwal, 1976; Willmer & Fricker, 1996; Hetherington and Woodward, 2003, Roelfsema and Hedrich, 2005, Taiz et al., 2018). Two recent reports by McAusland *et al.* (2016) and Lawson & Vialet-Chabrand (2019) supported this contention by demonstrating that longer stomatal responses reduced photosynthesis by ca. 10% as well as leading to greater unnecessary water loss during stomatal closure in plants which have kidney-shaped GC's compared with those that exhibit dumbbell-shaped GCs.

Stomatal distribution can either be confined to one leaf surface, the abaxial surface (hypostomatous), or much less commonly, only on the adaxial surface (hyperstomatous), or they can be present on both leaf surfaces (amphistomatous; Parkhurst, 1978; Morison & Lawson, 2007; Fig. 1.6). Amphistomatous leaves can also differ in SD on each leaf surfaces (Willmer & Fricker, 1996; Taylor *et al.*, 2012), but typically SD in most species is often much greater on the abaxial surface compared with adaxial (Driscoll *et al.*, 2006). This distribution is referred to as the stomatal ratio (R or SR), which can be referred to in two different ways, either R_{propAD} or R_{even} (Muir, 2015, 2018). R_{propAD} describes the proportion of stomatal density on the adaxial leaf surface by dividing the adaxial SD with the total SD, which distinguishes between hypostomatous ($R_{propAd} = 0$), amphistomatous ($0 < R_{propAd} < 1$) and hyperstomatous species ($R_{propAd} = 1$). R_{even} indicates how evenly stomatal densities are distributed across both leaf surfaces used in several studies as a hypothesis that a more even distribution should optimize leaf CO₂ diffusion, following the equation of Muir (2015):

$$R_{even} = \frac{\min \{abaxial\ SD, adaxial\ SD\}}{\max \{abaxial\ SD, adaxial\ SD\}}$$

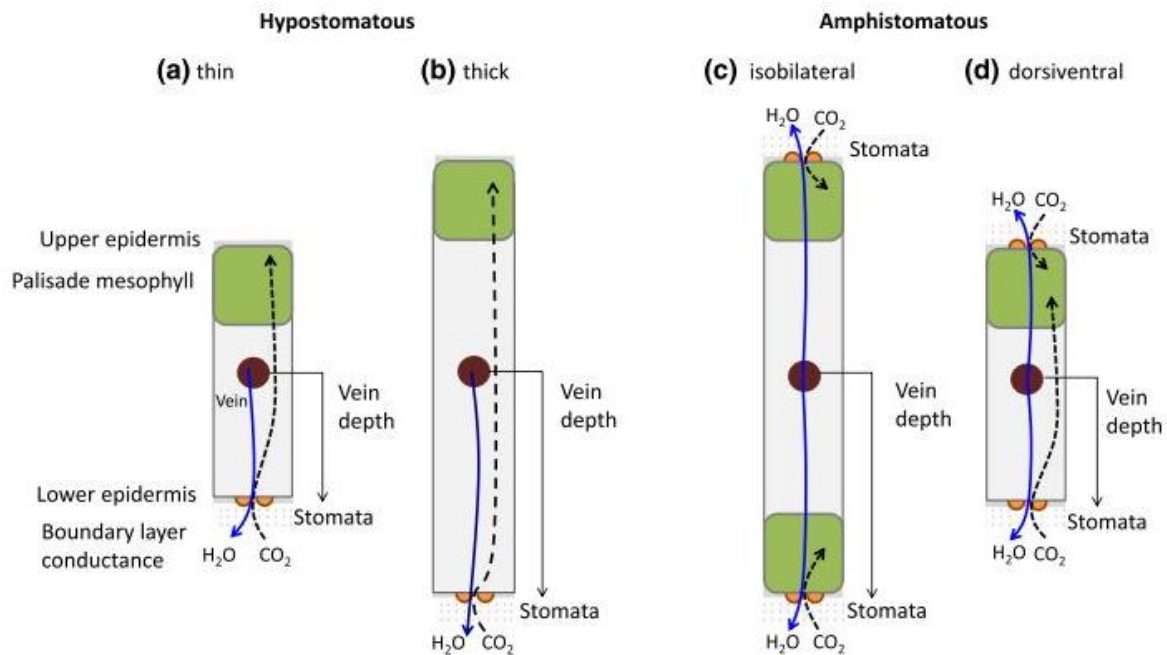


Figure 1.6 Schematised leaf cross-sections indicating lengths of pathways for water and CO₂ across hypostomatous and amphistomatous leaves. (a) Thin hypostomatous and dorsiventral leaf. (b) Thick hypostomatous and dorsiventral leaf with a long diffusion pathway for CO₂. (c) Thick amphistomatous and isobilateral leaf, enabling a short diffusion pathway for CO₂. (d) In this scheme the difference between dorsiventral and isobilateral leaves is based on the position of the tissue performing most of the CO₂ uptake (typically palisade mesophyll). The scheme focusses on C₃ species. Note the potential for vein depth, the distance from the vein to the lower epidermis, to vary (a, b, d). (Figure from Drake *et al.*, 2019)

Amphistomatous leaves can be further subdivided into dorsiventral or isobilateral species, where dorsoventrality presents palisade mesophyll cells, the tissue performing most of the CO₂ uptake, positioned nearest to the upper epidermis (for example, *Rhododendron catawbiense*) and the term Isobilateral describes species with palisade mesophyll cells at both the upper and lower epidermis (for example, *Triticum aestivum L.*; Rudall, 1980; Brodribb *et al.*, 2007; Drake *et al.*, 2019). Isobilateral amphistomatous species have been suggested to have operational independence, whereby abaxial and adaxial leaf surfaces can respond separately to

external stimuli such as differences in evaporative demand and sensitivity to light (Wong *et al.*, 1985; Lu *et al.*, 1993; Richardson *et al.*, 2017). Characteristically, dorsiventral leaves are found in fast-growing dicotyledonous herbaceous crops whereas isobilateral leaves are typically adapted to arid conditions, usually with a near-vertical leaf orientation to enable the capture of light on both leaf surfaces (Drake *et al.*, 2019; Richardson *et al.*, 2020).

In general, amphistomatous species tend to have higher gas exchange capacity compared with hypostomatous species (Mott & O'Leary, 1984; Beerling & Kelly, 1996), which could be due to shorter diffusion pathways, and differences in the boundary layer (de Boer *et al.*, 2012; Drake *et al.*, 2019; Xiong & Flexas, 2020). Several studies have suggested that stomata on each surface responded to changes in evaporative demand (Mott & Parkhurst, 1991; Richardson *et al.*, 2017) and light and [CO₂] (Mott & Peak, 2018) independently of each other. The higher functionality of amphistomatous species creates a greater risk of desiccation and therefore these plants must invest in higher vein density to increase hydraulic efficiency (Brodribb *et al.*, 2007; Buckley *et al.*, 2015). Richardson *et al.* (2020) observed a lack of asymmetry in vein position in *Helianthus annuus*, with minor veins closer to the abaxial compared with the adaxial leaf surface. The same authors also reported a decrease of coordination between stomata on the two leaf surfaces that were driven by leaf hydraulics, demonstrating the tight coupling between stomatal behaviour and leaf water supply. Amphistomaty has therefore adapted to cope with greater irradiance, temperature and evaporative demand to avoid desiccation.

1.1.7 Stomatal Density and Size

Stomatal anatomical characteristics including the number of stomata per unit area (i.e. density), stomatal SS and pore aperture together determine g_s (Lawson and Blatt, 2014) and therefore changes in any one of these variables has a direct influence on g_s (Fig. 1.7). Developmentally, SD differs between and within species and is influenced by a number of environmental variables including light intensity, $[CO_2]$ and water availability (Gay and Hurd, 1975, Woodward, 1987, Gray et al., 2000, Hetherington and Woodward, 2003, Doheny-Adams et al., 2012). Stomata are morphologically diverse (Willmer and Fricker, 1996) and species with high densities, often have smaller stomata and *vice-versa* (Franks and Beerling, 2009, Hetherington and Woodward, 2003, Lawson and Blatt, 2014). Hetherington and Woodward (2003) suggested that smaller stomata have a more-rapid opening and closing time (speed of response) partly due to less water and solute movement between GC and subsidiary cells (osmotic shuttling) (Franks and Farquhar, 2007) and shorter diffusional pathways of water and solutes from between guard cells and subsidiary cells (Franks and Beerling, 2009) both owing to the greater surface area to volume ratio of smaller cells. Smaller stomata therefore provide the capacity for rapid increases in g_s , allowing faster diffusion of CO_2 into the leaf for photosynthesis during favourable conditions (Aasamaa *et al.*, 2001; Drake *et al.*, 2013; Raven, 2014). However, species with different stomatal features may have distinct mechanisms influencing the speed of response independently of SS (Franks and Farquhar, 2007). Although smaller stomata are not always faster to respond to changing environmental conditions, this relationship typically holds within closely-related species although it is less strong across taxa (Drake *et al.*, 2013; Elliott-Kingston *et al.*, 2016; Lawson & Vialet-Chabrand, 2019).

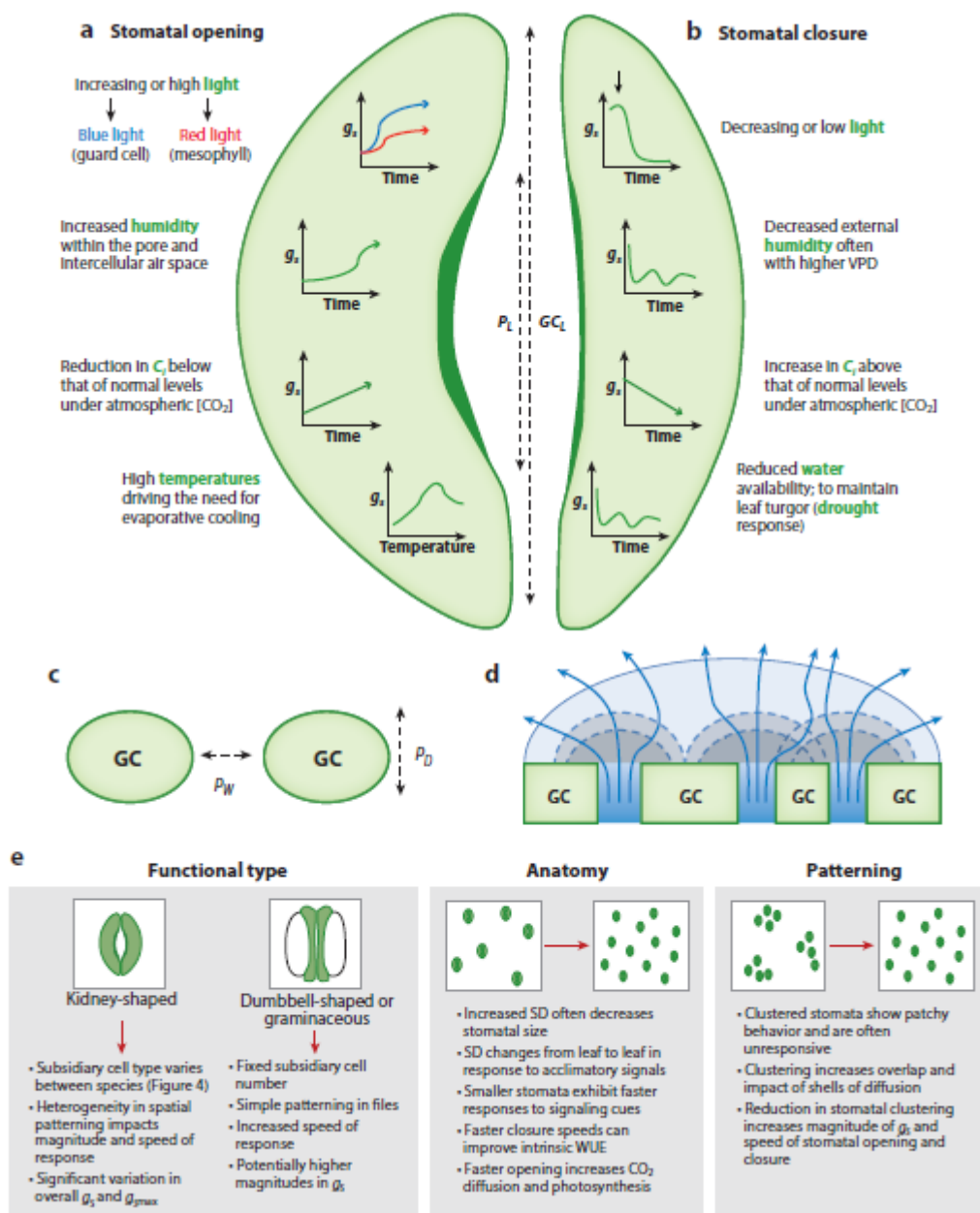


Figure 1.7 Impact of stomatal characteristics on response to environmental cues. (a, b) Key environmental factors contributing to stomatal opening and closure, (a–c) Stomatal dimensions contributing to the calculation of g_{smax} , including pore depth (PD), pore width (PW), pore length (PL), and guard cell length (GCL). (d) Shells of diffusion: semi-circular pattern of gaseous flux from the stomatal pore. (e) Key anatomical features of stomata and the impact these have on behaviour, g_s , and stomatal response kinetics. Abbreviations: g_s , stomatal conductance; C_i , internal CO_2 concentration; GC, guard cell; SD, stomatal density; VPD, vapor pressure deficit; WUE, water use efficiency. Figure from (Lawson & Matthews, 2020)

Manipulating gene expression of key components in the stomatal developmental pathway has proven to be a powerful tool in modifying SD, SS and stomatal patterning (Franks *et al.*, 2015). For example, the epidermal patterning factors (EPF) are a family of 11 related small, secreted peptides, some of which are found to regulate SD in *Arabidopsis thaliana* (Franks *et al.*, 2015). Reducing the expression of EPF1 and EPF2 results in higher stomatal densities while the constitutive overexpression produced a similar phenotype to wild type but with reduced numbers of stomata (Hara *et al.*, 2007; Hara *et al.*, 2009; Hunt and Gray, 2009; Franks *et al.*, 2015). Differences in the spacing of cells or the number of stomatal clusters were also demonstrated. A lack of EPF1, which is expressed in GCs of young stomata and their precursors led to high clustering, whereas plants with EPF2 expressed at slightly earlier stages of stomatal development showed almost no clustering (Hara *et al.*, 2007; Hara *et al.*, 2009; Hunt and Gray, 2009; Franks *et al.*, 2015). These studies also indicated that a strong negative correlation between SD and SS was maintained within these plants and the changes in these parameters have the potential to influence A , g_s , and W_i (Doheny-Adams *et al.*, 2012). Both Doheny-Adams *et al.* (2012) and Mohammed *et al.* (2019) found that plants with reduced SD and larger SS also had reduced g_s yet greater plant biomass. The increase in biomass could be attributed to improved water use and lower metabolic costs associated with GC development, and Lawson and Blatt (2014) suggested that CO₂ influx was not a limiting factor and growth was dominated by leaf water status.

1.1.8 Factors influencing stomatal responses

Abiotic variables such as light intensity and spectral quality, $[\text{CO}_2]$ and temperature are considered to have the greatest direct and indirect impacts on stomatal behaviour (Blatt, 2000), although there is disparity in stomatal sensitivity and responsiveness among different species (Lawson *et al.*, 2003; Lawson *et al.*, 2012; Lawson and Vialet-Chabrand, 2019). Typically, stomata in C3 and C4 species open in response to increasing or high light intensity, low internal $[\text{CO}_2]$, high temperatures and low VPD. Conversely, stomatal closure is driven by low or decreasing light, high internal $[\text{CO}_2]$ and high VPD as well as hormones such as ABA (Woodward, 1987; Poole *et al.*, 2000; Franks & Farquhar, 2001; Outlaw, 2003; Wang *et al.*, 2008; Berry *et al.*, 2010; Mott & Peak, 2013; Elliott-Kingston *et al.*, 2016; Inoue & Kinoshita, 2017; Vialet-chabrand *et al.*, 2017; Vialet-Chabrand *et al.*, 2017b).

The close positive relationship between A and g_s has been well documented in the laboratory (Wong *et al.*, 1979) and a positive correlation between steady state g_s and yield reported by Fischer *et al.* (1998) in the field. In contrast, in the short term (minutes) stomata can be 'sluggish' in their response to environmental factors and internal stimuli leading to nonsynchronous behaviour between A and g_s , which under dynamic conditions can lead to either a limit in A or an unnecessary loss of water (Farquhar and Sharkey, 1982, Hetherington and Woodward, 2003, Franks and Farquhar, 2007, Brodribb *et al.*, 2010, Brodribb *et al.*, 2009, Lawson and von Caemmerer, 2010, Lawson *et al.*, 2012, McAusland *et al.*, 2016, Lawson and Vialet-Chabrand, 2019) leading to sub-optimal water use efficiencies ($W_u = A/g_s$; (Lawson and Vialet-Chabrand, 2019)). For instance, Vialet-Chabrand *et al.* (2017b) reported 18.8% lower than expected A under fluctuating light during the course of a day, which was attributed to stomatal limitation.

1.1.9 Steady state and kinetic stomatal responses

Steady state measurements of g_s have remained the core technique for understanding stomatal physiology, (see Ainsworth & Rogers, 2007). Fischer (1998) for example, made point measurements in the early afternoon over the course of a season, and showed a strong correlation between yield and g_s , underlining the value of steady state g_s as a measure of breeding success. Successive rounds of breeding had produced wheat cultivars with increased g_s which reduced diffusional constraints, reducing leaf temperature and increasing A (Fischer et al., 1998). Not only is steady state g_s important in determining yield, but also the kinetics and magnitude of change. To explore stomatal responses in more detail, the rate at which stomata open and close under changing environmental conditions has recently been investigated as a novel target for manipulation (Lawson and Blatt, 2014, Lawson and Vialet-Chabrand, 2019, Raven, 2014), with light induced changes in g_s the main focus of this work, but with water availability as well as temperature and VPD also being variables whose manipulation might be of interest. Stomata open and close much more slowly than the rate at which environmental inputs vary and an order of magnitude slower than photosynthetic responses (Lawson & Blatt, 2014; McAusland *et al.*, 2016; Qu *et al.*, 2017), and these response rates can be parameterised and modelled (Vialet-Chabrand et al., 2013; Vialet-Chabrand et al., 2016; Vialet-Chabrand et al., 2017a; Vialet-Chabrand et al., 2017c). Environmental conditions are expected to become more-variable under climate change (IPCC, 2014) introducing longer dryer, hotter periods, among others weather patterns, driving the need to develop new breeding targets under climate change constraints. Latterly, there have been attempts to understand the impact not just of simple step changes to changing environmental parameters, but of naturalistic fluctuations in them as in the future enhancing stomatal

speed could improve W_i in dry fluctuating environments (Matthews et al., 2018, Vialet-Chabrand et al., 2017b), although this work remains in its infancy.

1.2 Aims and Objectives

The factors affecting food insecurity include the effects of a changing climate, losses of agricultural land to urbanization and increasing competition for non-food uses of crops. Stomatal anatomical characteristics including stomatal density (SD), size (SS) and pore aperture which together determine stomatal conductance (g_s). Therefore, any changes in stomatal anatomy will impact stomatal conductance and moreover photosynthetic assimilation which is known to be linked with crop yield.

There has been a considerable amount of research into understanding the anatomical and physiological response of stomata to environmental stimuli and the relationship between these two characteristics for different species under steady state conditions. In this study, the aim of chapters 3 and 5 is to assess the extent of phenotypic variation in morphological traits. The key aim was to determine variation of SD and SS between elite MAGIC wheat parental cultivars (EW) and wheat wild relatives (WWR). Stomatal density and size data was collected from the flag leaves and lower leaves in the canopy over three specific areas of the leaf from both leaf surfaces. This data was used to calculate and determine variation in potential anatomical maximum stomatal conductance (g_{smax} , calculated from SD and SS measurements) between areas of the leaf lamina, leaf surfaces and differences between flag leaves and lower leaves in the canopy leaves of the EW and WWR. Furthermore, infra-red gas analysers were utilised to evaluate the impact of any phenotypic variation had on the rapidity of stomatal responses, and if this influenced CO₂ assimilation, and photosynthetic capacity.

Chapter 4 will evaluate the functional impact of any differing SD and SS between the two leaf surfaces of the EW using a self-built chamber which measured the simultaneous yet independent gas exchange from the two individual leaf surfaces. Chapter 6 will utilise the same experiments as in chapters 3 and 5 using two sets of wheat that have been grown in differing CO₂ conditions (atmospheric at 408 ppm ([CO₂]) and elevated at 800 ppm (e[CO₂])). This highlighted the impact of phenotypic variation at differing growth CO₂ concentrations and how this influenced stomatal functionality, specifically the rapidity of stomatal responses, CO₂ assimilation, and photosynthetic capacity.

CHAPTER 2

Materials and Methods

This section outlines methods generic to all experimental chapters. Modifications made to protocols outlined here and protocols specific to a chapter can be found in the methods section of each experimental chapter.

2.1 Plant Material and Growth Conditions

All wheat (for species see Table 2.1) seeds were germinated on wet tissue paper in sealed Petri dishes in a controlled environment growth chamber (ADAPTIS A1000; Conviron Ltd., USA) at 22 °C, photosynthetically active photon flux density (PPFD) of $200 \pm 10 \mu\text{mol m}^{-2} \text{s}^{-1}$, 9/15-hour light/dark photo period, 1.1 kPa vapor pressure deficit (VPD) at $\text{CO}_2 \sim 400 \text{ mmol mol}^{-1}$. After ~8 days, germinated seeds were transplanted into modular seed trays containing Levingtons soil (universal extra compost, horticulture Ltd, Ipswich, UK) in the same controlled environment, plants were well watered. After ~12 days, when two small wheat leaves were produced, plants were vernalised at 2 °C, PPFD of $80 \pm 10 \mu\text{mol m}^{-2} \text{s}^{-1}$ light, $[\text{CO}_2] \sim 400 \mu\text{mol mol}^{-1}$ for eight weeks. Ten replicates of each cultivar were transferred into 4 l pots and grown in glasshouse conditions at various times throughout the year. In the glasshouse, supplementary lighting provided $300 \mu\text{mol m}^{-2} \text{s}^{-1}$ PPFD from sodium vapour lamps (600W; Hortilux Schröder, The Netherlands) when external solar radiation fell below a PPFD of $500 \mu\text{mol m}^{-2} \text{s}^{-1}$, over a 10-hour photo-period, air temperature was maintained at $25 \text{ °C} \pm 5 \text{ °C}$ during the day and $17 \text{ °C} \pm 5 \text{ °C}$ at night. Wheat pots were separated by reps into individual trays (1-10) which were moved once a week to avoid any block effects. Wheat was watered everyday including a once weekly Hoagland's nutrient solution (1 mmol/L KNO_3 and 0.5 mmol/L NH_4NO_3 (Hoagland & Arnon, 1950).

Table 2.1 Genotypes selected for this study including species name, common name and ploidy. The list includes a variety diploid, Tetraploid and Hexaploid species. Referred to in text by their genotypic name.

Genotype	Species	Common Name	Ploidy
Alchemy-1A	<i>Triticum aestivum</i>	Common or Bread Wheat	Hexaploid
Brompton-1B	<i>Triticum aestivum</i>	Common or Bread Wheat	Hexaploid
Claire-4	<i>Triticum aestivum</i>	Common or Bread Wheat	Hexaploid
Hereward-1A	<i>Triticum aestivum</i>	Common or Bread Wheat	Hexaploid
RIALTO	<i>Triticum aestivum</i>	Common or Bread Wheat	Hexaploid
Robigus	<i>Triticum aestivum</i>	Common or Bread Wheat	Hexaploid
SOISSONS	<i>Triticum aestivum</i>	Common or Bread Wheat	Hexaploid
Xi19	<i>Triticum aestivum</i>	Common or Bread Wheat	Hexaploid
AE 146	<i>Aegilops tauschii</i>	Goatgrass or rough-Spike Hard Grass	Diploid
AE 472/87	<i>Aegilops tauschii</i>	Goatgrass or rough-Spike Hard Grass	Diploid
IG 48509	<i>Aegilops tauschii</i>	Goatgrass or rough-Spike Hard Grass	Diploid
IG 48514	<i>Aegilops tauschii</i>	Goatgrass or rough-Spike Hard Grass	Diploid
IG 48556	<i>Aegilops tauschii</i>	Goatgrass or rough-Spike Hard Grass	Diploid
KU 2010	<i>Aegilops tauschii</i>	Goatgrass or rough-Spike Hard Grass	Diploid
KU 2018	<i>Aegilops tauschii</i>	Goatgrass or rough-Spike Hard Grass	Diploid
KU 2036	<i>Aegilops tauschii</i>	Goatgrass or rough-Spike Hard Grass	Diploid
KU 2043	<i>Aegilops tauschii</i>	Goatgrass or rough-Spike Hard Grass	Diploid
KU 2056	<i>Aegilops tauschii</i>	Goatgrass or rough-Spike Hard Grass	Diploid
KU 2636	<i>Aegilops tauschii</i>	Goatgrass or rough-Spike Hard Grass	Diploid
TRI 11502	<i>Triticum dicoccoides</i>	Wild Emmer	Tetraploid
TRI 17123	<i>Triticum urartu</i>	Red Wild Einkorn	Diploid
TRI 17137	<i>Triticum urartu</i>	Red Wild Einkorn	Diploid
TRI 17162	<i>Triticum urartu</i>	Red Wild Einkorn	Diploid
TRI 18510	<i>Triticum araraticum</i>	Araratian or Armenian Wild Emmer	Tetraploid
TRI 3432	<i>Triticum dicoccon</i>	Emmer	Tetraploid

2.2 Leaf and stomatal characteristics

2.2.1 Leaf epidermal impressions

Analysis of stomatal characteristics was achieved by creating negative impressions of the leaf surface using dental precision moulding material. Polysiloxane precision material, mix of 0.1ml liquid activator to 1cm³ blue polymer (Xantopren, Heraeus, Hanau, Germany) was mixed for approx. 10 seconds and spread directly onto the leaf area. All species impressions were taken from fully expanded single leaves of similar position at the midpoint of both the abaxial and adaxial leaf surfaces avoiding major veins and leaf edges before anthesis (GS 49-59) (Zadok *et al.*, 1974; Weyers & Johansen, 1985; Weyers *et al.*, 1997). Dry impressions were removed from the leaf. A positive impression was made by covering the blue polymer impression surface with a thin layer of acrylic polymer (clear nail varnish, Rimmel, London, UK) which was left to dry for at least 30 min. The dry acrylic polymer was then lifted off with clear adhesive tape (Sello-Tape, Henkel Limited, Cheshire, UK) and mounted onto labelled microscope slides.

2.2.2. Measurements of stomatal density

2.2.2.1 Measurements of stomatal density using Light Microscopy

Stomatal density, guard cell length and pore length were measured via light microscopy (Olympus BX60, Southend-on-Sea, Essex, UK) set to x10 magnification for density measurements and x40 magnification for length measurements using a Digi-Pad viewer (5 mega-pixel digital camera with 9 LCD screen mounted to the microscope eyepiece), calibrated with a 1 mm graticule slide. For stomatal density, all

pores within the images were counted with the exception of those that touched the top or right hand side of the image following the protocol of Weyers *et al.* (1997).

2.2.2.2 Snapshot measurements of stomatal density

For a stomatal density “snapshot” a handheld microscope (0.3m CMOS sensor x1000 magnification handheld digital microscope, Beijing, China) and laptop, calibrated with a 1 mm graticule slide, to view, image, and count stomata. All species impressions were taken from fully expanded single leaves of similar position at the midpoint of both the abaxial and adaxial leaf surfaces avoiding major veins and leaf edges (as above), following the protocol of Weyers & Johansen (1985; Weyers *et al.*, 1997).

2.2.3 Measurements of Stomatal size

When measuring wheat guard cell length and pore length, an ellipse shape was assumed. Guard cells were measured from end to end through the mid-section of the longest axis of symmetry; this was called the guard cell length (Fig. 2.1). The ellipse shape was again measured from pore end to end through the mid-section of the longest axis of symmetry; this was called the pore length (Fig. 2.1). Guard cell length and pore length measurements were adapted from Sack & Buckley (2016).

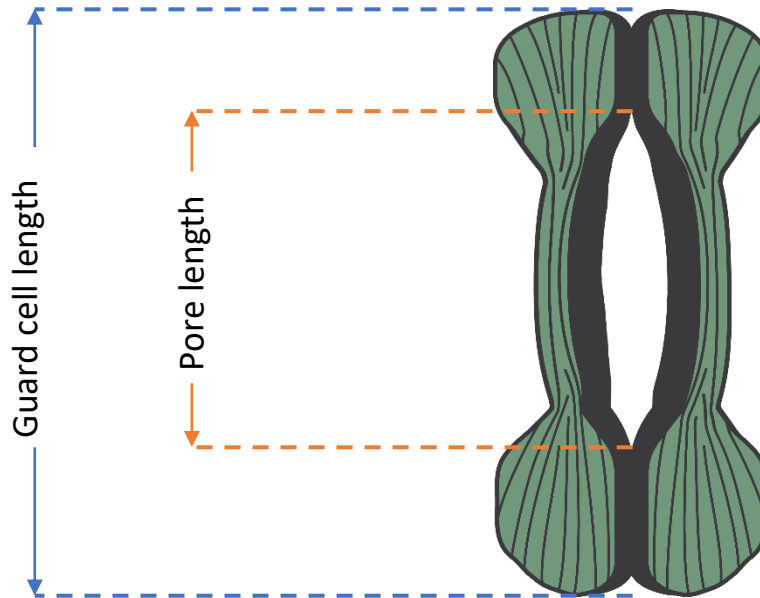


Figure 2.1. Diagram representing the anatomy of a dumbbell shaped stomata highlighting the dimensions measured for guard cell length and pore length.

2.2.4 Potential anatomical maximum stomatal conductance

Potential anatomical maximum stomatal conductance (Anatomical g_{smax} mol m⁻² s⁻¹) was calculated from the measurements of guard cell dimensions following the equations of Franks & Farquhar (2001):

$$(d \cdot S_D \cdot a_{max}) / (v \cdot (1 + (\pi / 2)) \cdot \sqrt{(a_{max} / \pi)})$$

Where d is the diffusivity of water in air (m² s⁻¹, at 22°C), v is the molar volume of air (m³ mol⁻¹, at 22°C) and π is the mathematical constant, approximated to 3.142. Stomata shape was defined as an ellipse. For stomatal size (μm^2), guard cells were measured from end to end through the mid-section of the longest axis of symmetry equalling the major axis measurement and the minor axis being equal to the width of the entire stomata, represented as half the guard cell length. Pore depth (l ; μm) was assumed to be equal to guard cell width at the centre of the stoma represented as half the guard cell length. The mean maximum stomatal pore area (a_{max} ; μm^2) was calculated as an ellipse with major axis equal to pore length and minor axis equal to

half pore length. Stomatal density (SD) and stomatal size (SS) measurements were determined independently for each leaf with values of pore depth and mean maximum stomatal pore area calculated from measurements of guard cell and pore lengths. Total leaf anatomical g_{smax} for each cultivar was calculated as the sum of abaxial anatomical g_{smax} and adaxial anatomical g_{smax} data using empirical values of stomatal density, pore length, and mean maximum stomatal pore area.

2.2.5 Leaf optical properties

Leaf absorbance (LA_b) was measured using an Ulbricht integrating sphere (built at The University of Essex) and a light meter (Skye instruments, Powys, UK). Six measurements of transmittance and reflectance of light, using the External Method were taken per species and for each of the eight parental MAGIC wheat cultivars. Using the External Method, LA_b was estimated from reflectance and transmittance as:

$$LA_b = 1 - R_H - T_H$$

Where R_H and T_H are the leaf hemispherical reflectance and transmittance factors, respectively. R_H was obtained by comparing the PPFD in the sphere when a leaf or a highly reflective reference panel is placed in the sphere's measuring port opposite to the light source. Similarly, T_H is obtained by placing the leaf between the light source and the sphere, and by comparing the PPFD with and without the leaf. The estimation of R_H and T_H , and by extension of LA_b , is that the area of the measurement surface (either leaf or reference panel) needs to be equal (Taylor, 1920; Olascoaga *et al.*, 2016). The transmittance and reflectance for each leaf was used to calculate absorbance (as above) with the mean absorbance for each treatment determined from six combined measurements. All species measurements were taken from fully

expanded single leaves of similar position, at the mid-point of the leaf, before anthesis, between GS 49-59 on the Zadok's growth scale (Zadok *et al.*, 1974)

2.2.6 Leaf thickness

All species leaf thickness (LT) measurements were taken from fully expanded single leaves of similar position as above using a MultispeQ v1.0 (Michigan State University, East Lansing, MI, USA), an updated version of the MultispeQ Beta (Kuhlgert *et al.*, 2016). The device contains a Hall Effect sensor, in which the variable magnetic strength between two magnets due to a difference in distance between them, generates a variable voltage. The device was calibrated to actual thickness by using multiple layers of Whatman 1001-110 filter paper (Whatman, Maidstone, Kent, UK), which has a thickness of 0.18mm per filter. The device was attached on the same anatomical region of the leaf as that inside the chamber, but on a part of the leaf outside of the chamber. An average leaf thickness was calculated from 3 measurements of a one-time leaf thickness protocol. All species measurements were taken from fully expanded single leaves of similar position, at the mid-point of the leaf, before anthesis, between GS 49-59 on the Zadok's growth scale (Zadok *et al.*, 1974)

2.2.7 Leaf anatomical measurements

Dry weight (g), and leaf area (cm²) were measured using fully expanded single leaves of similar position, at the mid-point of the leaf, before anthesis, between GS 49-59 on the Zadok's growth scale (Zadok *et al.*, 1974). For dry weight, leaves were placed individually in labelled paper bags and set in an oven at 60°C for three days until completely dry, then weighed using electronic precision scales (Kern,

Northamptonshire, UK). Leaf area was calculated (unless stated) by passing leaves through a bench-top LI-3100C area meter (Li-Cor, Lincoln, Nebraska, USA). An average leaf area was calculated from 3 leaf area replicate measurements.

2.3 Leaf gas exchange

All gas exchange measurements (unless stated), specifically stomatal conductance (g_s) and the net rate assimilation of CO_2 (A) were recorded using a Li-Cor 6400XT portable gas exchange system, with light delivered via a Li-Cor 6400-40 fluorometer head unit (Li-Cor, Lincoln, Nebraska, USA), with blue and red LEDs. Gas exchange measurements had a constant flow rate set at $300 \mu\text{mol s}^{-1}$, with cuvette conditions maintained at a CO_2 concentration of $400 \mu\text{mol mol}^{-1}$ and a leaf temperature of 22°C . When needed, to maintain a leaf to air water vapour pressure deficit of 1 ± 0.2 kPa, the system was connected to a Li-Cor 610 portable dew point generator. All measurements were made between 8am and 3pm to guarantee a high level of stomatal opening and photosynthetic activation, and to reduce diurnal effects. All measurements were taken from fully expanded single leaves from the mid-point of an similar leaf position, before anthesis (GS 49-59) (Zadok *et al.*, 1974). Intrinsic water use efficiency was calculated as $W_i = A/g_s$.

2.3.1 PPFD-step measurements

To measure the response of A and g_s to step changes in photosynthetically active photon flux density (PPFD), leaves were placed in the Li-Cor cuvette and equilibrated at a PPFD of $100 \mu\text{mol m}^{-2} \text{s}^{-1}$ until both A and g_s were at steady state, defined as less than a 2 % change of parameters during a 5-minute period. To reach steady state could take between 10 and 30 minutes. Plants were then measured at steady state, at regular 30 second intervals, for 20 minutes then PPFD was increased in a single step to $1000 \mu\text{mol m}^{-2} \text{s}^{-1}$ until A and g_s again reached a steady state (60 minutes). Leaf temperature (T_i), VPD and CO_2 concentration were all maintained at

22 °C, 1 ± 0.2 kPa and $400 \mu\text{mol mol}^{-1}$ respectively throughout the measurement. The data from this experiment was used to model the response of A , g_s and W_i to changes in PPFD.

2.3.2 Intracellular CO₂ response curves (A/C_i)

A/C_i response curves (net CO₂ assimilation rate (A) to intercellular CO₂ concentration (C_i)) were measured at a saturating light intensity of $1500 \mu\text{mol m}^{-2} \text{s}^{-1}$. Leaves were stabilized for a minimum of 15 minutes at ambient CO₂ concentration of $400 \mu\text{mol mol}^{-1}$, upon reaching a stable signal the first measurement was taken. Ambient CO₂ was decreased and measured at 250, 150, 100, 50 $\mu\text{mol mol}^{-1}$ before returning to the initial value of 400, and increased to 550, 700, 900, 1100, 1300, 1500 $\mu\text{mol mol}^{-1}$. Recordings were taken at each new CO₂ level when A had reached a new steady state (approx. 1-3 min), and before stomatal conductance (g_s) changed to the new CO₂ levels to reduce the possibility of stomatal limitation of A .

2.4 Gas exchange measurements using split leaf chamber

2.4.1 Design of split leaf chamber for measuring each surface individually and simultaneously.

A cuvette was specifically designed (Fig. 2.2; University of Essex, UK) to simultaneously measure independent photosynthetic gas exchange from the adaxial and abaxial leaf surfaces. In brief, the cuvette used a neoprene gasket to enclose and sample a projected leaf area of 23.87mm². Discrete gas flow to the adaxial and abaxial leaf surfaces was achieved by having separate gas flows to each side of the cuvette. An integral water jacket provided temperature control via a recirculating water chiller (BC20, Fisher Scientific, UK). The two Infra-red gas analysers (Li-6400, Li-Cor) were cross-calibrated with two dewpoint generators (Li-610, Li-Cor) and supplied with CO₂ using certified 1000 ppm CO₂ in air canisters (BOC, UK) to provide a known flow of CO₂ and H₂O concentration to each leaf surface. Additionally, the two IRGAs attached to the split chamber measured the photosynthetic CO₂ and H₂O sample gas concentrations in the cuvette used to calculate photosynthesis. Air and leaf temperature were recorded using E type thermocouples (Omega engineering, Manchester, UK) independently for both the adaxial and abaxial leaf surfaces. PPFD was provided to each leaf surface by independently controlled white LED arrays (Isolight 400, Technologica, Essex, UK). Any leaks out of the cuvette were detected by in-line flow sensors (FLR1005-D, Omega) ensuring that flows out of the cuvette were identical to the flows in. To detect any leaks within the cuvette, i.e. between the two leaf surfaces, a CO₂ concentration differential of 400 µmol mol⁻¹ was temporarily generated between the two leaf surfaces. If unilluminated, any [CO₂] differential >2 µmol mol⁻¹ across a leaf surface, could indicate gas flow between the two halves of

the cuvette. This was checked with a leaf in the cuvette before each measurement. Prior to each day's measurements, any pressure differential between both sides of the cuvette was detected with a manometer, using plastic film acting as a non-porous 'artificial leaf' (Para-Film, WI, USA) with an equal flow of $600 \mu\text{mol s}^{-1}$. These checks confirmed gas isolation of each surface, whilst avoiding any pressure differentials that could have potentially occurred, generating artefactual errors in the calculation of photosynthesis. As the air in the 'standard' leaf cuvette (Li6400, Li-Cor) was actively mixed, combined leaf surface gas exchange was calculated assuming that the leaf boundary layer conductance was similar on both leaf surfaces, using the factory estimated value (Li-Cor). As convention, photosynthesis was expressed as per unit projected leaf area. In contrast, individual surface leaf photosynthetic gas exchange was calculated independently for the adaxial and abaxial surfaces. Leaf boundary layer conductance was estimated separately for each surface using a water saturated filter paper to simulate a leaf. If fully saturated, it can be assumed that the only resistance to evapotranspiration is the boundary layer, using the following equation from Licor (2011), derived from (Ehleringer, 1989).

$$gb = EP/2 (e(TI) - es)$$

$$gb = \text{one-sided boundary layer conductance (mol m}^{-2}\text{s}^{-1}\text{)}$$

$$e(TI) = \text{water vapour pressure (kPa) at the temperature of the filter paper (}^{\circ}\text{C)}$$

$$P = \text{atmospheric pressure (kPa)}$$

$$E = \text{evapotranspiration rate (mol m}^{-2}\text{s}^{-1}\text{)}$$

$$es = \text{water vapour pressure (kPa)}$$

As the cuvette was unstirred, it was critical that the gas flow across the filter paper was identical to that used for leaf photosynthetic gas exchange ($600 \mu\text{mol s}^{-1}$). The air and filter paper temperature for each surface were measured individually using E type

thermocouples (Omega engineering, Manchester, UK). Following this method, leaf boundary conductance was calculated as $0.582 \text{ mol m}^{-2}\text{s}^{-1}$ for each individual leaf surface.

Photosynthetic parameters were calculated following the equations of (von Caemmerer & Farquhar, 1981), using spreadsheet software (Li6400XT, v6.0, Licor) independently for the adaxial and abaxial surfaces. Corrections to the output data were made for leaf temperature, measured in real time with a thermocouple on the back plate (fig. 1 i:B2) where one sided light-regimes were lit onto the front plate (fig. 1 i:B2), boundary layer conductance (summarised above) and leaf area. In wheat, as both leaf surfaces contribute the overall rate of photosynthesis, when comparing against conventional 'combined leaf surface' gas exchange to allow a comparison in rates with a control, independent leaf surface gas exchange measurements were summed.

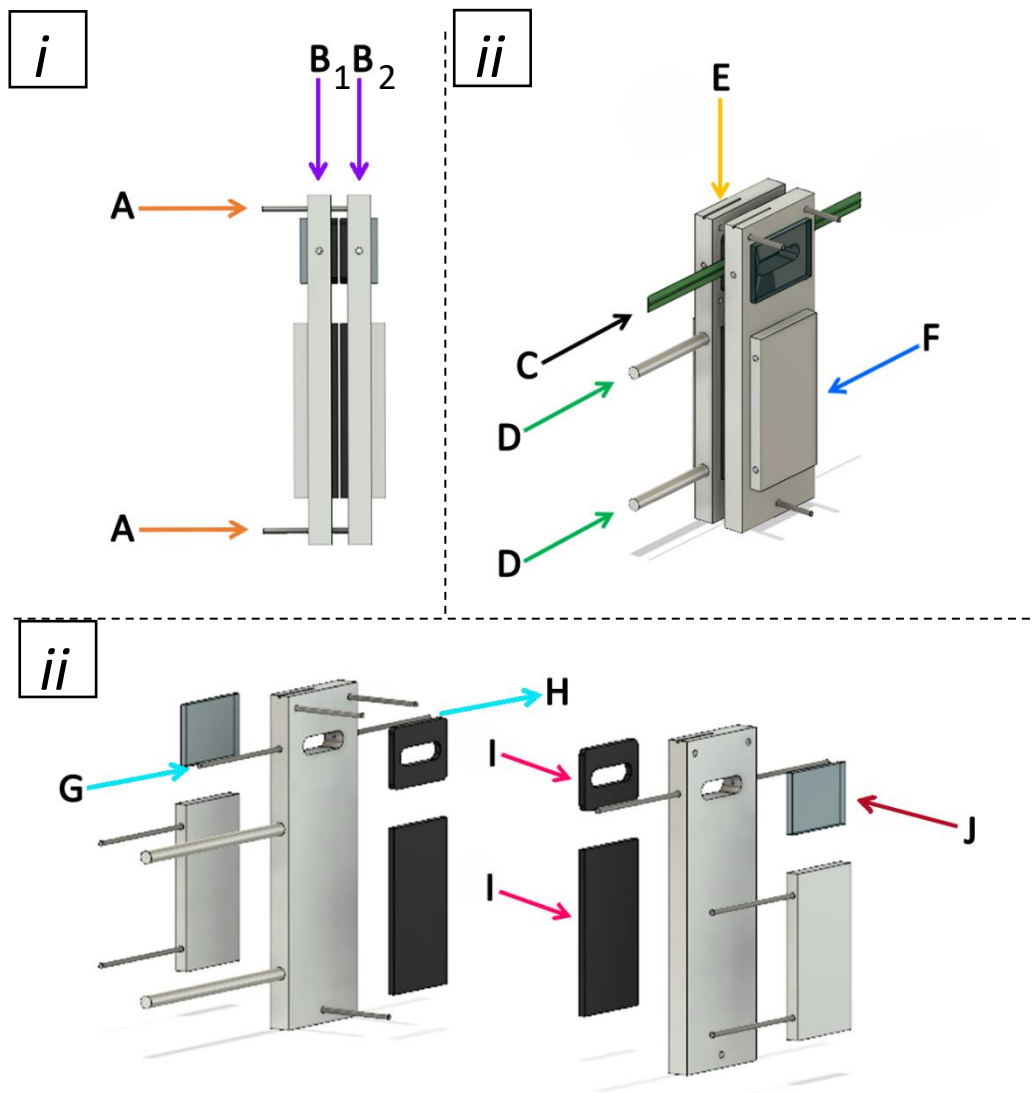


Figure 2.2 Lab-made chamber for direct measurement of simultaneous but separate leaf surface gas exchange. View from (i) side-on and (ii) front side with leaf clamped (C), and (iii) exploded computer aided design image of the chamber. The aluminium chamber was designed to fit with any infra-red gas analyser, this experiment used two Li-Cor LI-6400XT open gas-exchange systems. The two constituent parts of the chamber (B_1 and B_2) are identical with the addition of three threaded metal bars (A) which, using wing nuts, secure the chamber together tightly. When the leaf (C) is clamped between the chamber windows (23.87 mm^2), it creates a tight seal, forming two separate compartments for gas exchange. The leaf-clamp seal is fortified by neoprene gaskets (I). The chamber is fixed into place, between two light sources, using two metal rods (D) and a clamp. The light source enters the chamber window through fixed non-reflective glass (J). Leaf temperature was maintained using cooled water recirculating from a water bath to metal plates attached to the chamber (F) and measured by three leaf-temperature thermocouples (front air, back air and back leaf temperature) inserted into the chamber via a groove and hole (E). The mixing air passes through the compartment (in the direction of G to H) allowing the leaf surface to exchange gasses.

2.4.2 Individual leaf surface response of A and g_s to a step change in PPFD.

This procedure followed that of the combined leaf surface gas exchange. Carbon dioxide concentration, leaf temperature and VPD were controlled to $400 \mu\text{mol mol}^{-1}$, 22°C and $1 \pm 0.3 \text{ kPa}$ respectively, the latter maintained by a dewpoint generator (Li-610, Li-Cor). Measurements were made on the flag leaf of wheat plants, before anthesis, at GS 49-59 (Zadok *et al.*, 1974). Steady state A and g_s , (defined as $< 2\%$ change in rate over 5 min) was measured every 30 seconds at PPFD $100 \mu\text{mol m}^{-2} \text{ s}^{-1}$. After 20 minutes, the PPFD was increased in a single step to $1000 \mu\text{mol m}^{-2} \text{ s}^{-1}$ and photosynthesis continued to be recorded for a further 60 minutes or until steady state A and g_s had been achieved.

Three initial experiments (Table 2.2 – protocol 1, 2 and 3) were conducted to measure the separate surface responses of A and g_s to a single step change in PPFD. Both protocols 1 and 2 (Table 2.2) demonstrated a step increase in PPFD from $100 \mu\text{mol m}^{-2} \text{ s}^{-1}$ to $1000 \mu\text{mol m}^{-2} \text{ s}^{-1}$ with the light source either illuminating the adaxial leaf surface (protocol 1) or the abaxial leaf surface (protocol 2). The leaf surface, which was not illuminated during protocol 1 and 2 (Table 2.2), were covered to prevent any light entering the chamber. Protocol 3 (Table 2.2) demonstrated a step increase in PPFD from $50 \mu\text{mol m}^{-2} \text{ s}^{-1}$ to $500 \mu\text{mol m}^{-2} \text{ s}^{-1}$ with the light source illuminating both the adaxial and abaxial leaf surfaces simultaneously. A further two experiments (Table 2.2 – protocol 4 and 5) were conducted to measure the adaxial surface responses of A and g_s to a single step change in PPFD with the abaxial surface coated in silicone grease to prevent gas exchange on the abaxial leaf surface. Experiment 4 (Table 2.2) demonstrated a step increase in PPFD from $100 \mu\text{mol m}^{-2} \text{ s}^{-1}$ to $1000 \mu\text{mol m}^{-2} \text{ s}^{-1}$ with the light source illuminating the adaxial leaf surface with the adaxial leaf surface chamber window covered, allowing no light to enter. Experiment 5 (Table 2.2)

demonstrated a step increase in PPFD from $50 \mu\text{mol m}^{-2} \text{s}^{-1}$ to $500 \mu\text{mol m}^{-2} \text{s}^{-1}$ with the light source illuminating both the adaxial and abaxial leaf surfaces simultaneously. When completing experiment 4 and 5 (Table 2.2), experiment 1 was repeated as a control measure.

Table 2.2 Stomatal responses to a step increase in PPFD protocols for combined chamber for individual leaf surface infra-red gas exchange.

Protocol	Start light and duration of protocol	Step increase light and duration of protocol	Surface in light	Surface in dark	Surface with grease
1	$100 \mu\text{mol m}^{-2} \text{s}^{-1}$ for 10 min	$1000 \mu\text{mol m}^{-2} \text{s}^{-1}$ for 60 min	Adaxial	Abaxial	None
2	$100 \mu\text{mol m}^{-2} \text{s}^{-1}$ for 10 min	$1000 \mu\text{mol m}^{-2} \text{s}^{-1}$ for 60 min	Abaxial	Adaxial	None
3	$50 \mu\text{mol m}^{-2} \text{s}^{-1}$ for 10 min	$500 \mu\text{mol m}^{-2} \text{s}^{-1}$ for 60 min	Both	None	None
4	$100 \mu\text{mol m}^{-2} \text{s}^{-1}$ for 10 min	$1000 \mu\text{mol m}^{-2} \text{s}^{-1}$ for 60 min	Adaxial	Abaxial	Abaxial
5	$50 \mu\text{mol m}^{-2} \text{s}^{-1}$ for 10 min	$500 \mu\text{mol m}^{-2} \text{s}^{-1}$ for 60 min	Both	None	Abaxial

2.4.3 Greased intracellular CO₂ (A/C_i) response curves

A/C_i response curves (net CO₂ assimilation rate (A) to intercellular CO₂ concentration (C_i)) were measured at 2000 $\mu\text{mol m}^{-2} \text{s}^{-1}$ using an infra-red gas exchange system (Li6800, Licor) with an integrated light source (Li-Cor 6800-01A; Li-Cor, Lincoln, Nebraska, USA). Gas exchange measurements had a constant flow rate set at 600 $\mu\text{mol s}^{-1}$, with cuvette conditions maintained at a leaf temperature of 22°C and VPD 1.2 kPa. All measurements were made between 8am and 3pm to guarantee a high level of stomatal opening and photosynthetic activation, and to reduce diurnal effects. All species measurements were taken from fully expanded single leaves of similar position, in wheat before anthesis (GS 49-59) (Zadok *et al.*, 1974). Leaves were coated on either the adaxial or abaxial leaf surface with silicone grease to prevent gas exchange, using an ungreased leaf as a control. Leaves were stabilized for a minimum of 15 minutes at ambient CO₂ concentration of 400 $\mu\text{mol mol}^{-1}$, upon reaching a stable signal the first measurement was taken. Ambient CO₂ was decreased and measured at 250, 150, 100, 50 $\mu\text{mol mol}^{-1}$ before returning to the initial value of 400, and increased to 550, 700, 900, 1100, 1300, 1500 $\mu\text{mol mol}^{-1}$. Recordings were taken at each new CO₂ level when A had reached a new steady state (approx. 1-3 min), and before stomatal conductance (g_s) changed to the new CO₂ levels to reduce the possibility of stomatal limitation of A . The A/C_i curves were conducted on the cultivar Brompton at two differing light treatments (1000 $\mu\text{mol m}^{-2} \text{s}^{-1}$ PPFD and 2000 $\mu\text{mol m}^{-2} \text{s}^{-1}$ PPFD). At each light treatment three separate protocols were completed, the first protocol had grease applied to the adaxial leaf surface allowing gas exchange from the abaxial leaf surface only, the second possessed grease on the abaxial leaf surface allowing gas exchange from the adaxial leaf surface only and the third protocol remained ungreased as a control. The term 'greased' refers to the covering with

silicone grease to prevent gaseous flux by blocking stomata. When recording standard combined measurements using a Li6800 Licor leaves were clamped into the chamber with the adaxial leaf surface pressed against the upper gasket in the path of direct light.

2.5 Modelling gas exchange parameters

2.5.1 Estimating photosynthetic capacities

The maximum rate of electron transport for RuBP regeneration (J_{\max} ; $\mu\text{mol m}^{-1} \text{s}^{-1}$) and the maximum velocity of Rubisco for carboxylation (V_{cmax} ; $\mu\text{mol m}^{-1} \text{s}^{-1}$) were estimated using the curve fitting method described by Sharkey *et al.*, (2007). Maximum rates of CO_2 assimilation (A_{\max}) were determined from recorded values at $1500 \mu\text{mol mol}^{-1} \text{CO}_2$ concentration and $1500 \mu\text{mol m}^{-2} \text{s}^{-1}$ PPFD.

2.5.2 Determining the rapidity of g_s response

The rapidity of the stomatal response following a step change in PPFD was assessed as a function of time (t) using a custom exponential equation (Violet-Chabrand *et al.*, 2013) including a slow linear increase of the steady state target (G):

$$g_s = (G + S_l t + (g_0 - (G + S_l t)) e^{-t/\tau})$$

where S_l is the slope of the slow linear increase of G observed during the response, g_0 the initial value of g_s , and τ the time constant to reach 63 % of G (following the equation of Violet-Chabrand *et al.*, 2013):

$$\left(\text{when } \tau = t, \frac{g_s - g_0}{((G + S_l t) - g_0)} = 1 - e^{-1} \sim 0.63\right)$$

Due to the asymmetry of response observed after a step increase in PPFD, a different value of τ was used in each condition (τ_i and τ_d). If g_s did not reach a plateau within the time duration, the model was able to predict the final asymptotic response and

thus, the time constant (τ_i and τ_d). Parameter G , g_0 and S_l were assumed to vary at individual level (random effects) and τ was assumed to vary only at treatment level (fixed effect). R and the nlme package were used to perform the analysis. Confidence interval at 95% were reported at treatment level.

2.5.3 Determining the rapidity of A response

The rapidity of the photosynthesis response following a step change in PPFD was assessed as a function of time (t):

$$A_t = (A_s + S_l t + (A_0 - (A_s + S_l t))e^{-t/\tau})$$

where A_t is A at time t , A_s is the plateau of A reached in steady state, S_l is the slope of the slow linear increase of A , A_0 the initial value of A , and τ the time constant to reach 63% of A_s (following the equation of Vialet-Chabrand *et al.*, 2013). Parameter A_0 and S_l were assumed to vary at individual level (random effects) and τ was assumed to vary only at treatment level (fixed effect). R and the nlme package were used to perform the analysis. Confidence interval at 95% were reported at treatment level.

2.6 Statistical analysis

Statistics were conducted using R software (www.r-project.org; version 3.5.3). A Shapiro-Wilk test was used to test for normality and a Levene's test of homogeneity was used to determine if samples had equal variance. A log transformation was applied if data was not normally distributed to meet modelling assumptions of an ANOVA. Single factor differences were analysed using a one-way ANOVA. When more than one factor existed, a two-way ANOVA was applied with an interaction between the two factors, if a significant difference was found, a Tukey post-hoc test was performed.

2.7 Split chamber modelling of gas exchange parameters

The curve fitting method used in this thesis to describe the temporal response of g_s was detailed in (McAusland *et al.*, 2016) and completed by Silvere Vialet-Chabrand. In short, a model representing g_s as a function of time (t) was applied on each curve:

$$g_s = (G_{smax} - r_0)e^{-e\left(\frac{\lambda-\tau}{\kappa}+1\right)} + r_0$$

The model used an initial time lag describing the time before g_s started to rise (λ , min), a time constant representing the time to reach 63 % of the variation (κ , min), and a steady-state target (g_{smax} , mol m⁻² s⁻¹). The time was defined at 0 when PPFD was increased from 100 to 1000 $\mu\text{mol m}^{-2} \text{s}^{-1}$; and r_0 (mol m⁻² s⁻¹) represented the predicted initial value of g_s at time point zero.

CHAPTER 3

**Heterogeneity in anatomical features
and functional traits in NIAB MAGIC
wheat parental cultivars**

3.1. Introduction

Stomata facilitate the diffusional gaseous flux between the interior of the leaf and the atmosphere and provide mesophyll cells access to atmospheric CO₂ ([CO₂]) (Zeiger *et al.*, 1987; Lawson & Weyers, 1999; Hetherington & Woodward, 2003). Stomata adjust their pore aperture in response to abiotic and biotic stimuli by actively adjust guard cell turgor pressure, altering stomatal pore width, which alters CO₂ supply to mesophyll cells for photosynthetic carbon assimilation (A) and relinquish water through transpiration (Willmer & Fricker, 1996; Shimazaki *et al.*, 2007; Morison *et al.*, 2008; Lawson & Blatt, 2014). Stomatal conductance (g_s), the capacity for the gaseous exchange of water vapor from the leaf to atmosphere, in mole of flux per unit area per second ($\text{mol m}^{-2} \text{s}^{-1}$; (Violet-Chabrand *et al.*, 2017b) is frequently used a measurement of stomatal behaviour and is determined by anatomical features, including both stomatal density and size, as well as and the speed of stomatal response (Lawson & Violet-Chabrand, 2019).

Stomata first appeared in terrestrial land plants over 400-million-years ago, and due to altering atmospheric [CO₂] and changes in prevailing hydrologic cycles, stomata have had to change some of their characteristics to adapt to new environments (Raven, 2002; Franks & Farquhar, 2007). Stomatal anatomical characteristics including the number of stomata per unit area (i.e. density), stomatal size and pore aperture together determine g_s (Weyers & Lawson, 1997; Lawson & Blatt, 2014) and therefore changes in any one of these variables has a direct influence on g_s . Moreover, the maximum potential anatomical stomatal conductance (g_{smax}), assuming all stomata are fully open, is calculated using empirical measurements of stomatal density, pore area and pore depth which can consequently dictate the

theoretical capacity for gas exchange with infinite combinations of either of the two parameters achieving the same g_{smax} (Franks & Farquhar, 2001; Dow *et al.*, 2014a).

For steady state values over the long term, a close positive relationship between A and g_s is well documented (Wong *et al.*, 1979; Farquhar & Sharkey, 1982; Mansfield *et al.*, 1990; Buckley & Mott, 2013) and a positive correlation between steady state g_s and yield reported by Fischer *et al.*, (1998) in the field. In contrast, over the short term (minutes) stomata can be 'sluggish' in their response to changing environmental factors and internal stimuli compared with the faster responses of A , leading to nonsynchronous behaviour between A and g_s , which under dynamic conditions can lead to either a limit in A or an unnecessary loss of water (Farquhar & Sharkey, 1982; Hetherington & Woodward, 2003; Franks & Farquhar, 2007; Brodribb & Feild, 2010; Lawson *et al.*, 2010, 2012; McAusland *et al.*, 2016; Vialet-Chabrand & Lawson, 2019b) and sub-optimal intrinsic water use efficiency ($W_i = A/g_s$) that can ultimately reduce plant growth and biomass (Lawson & Vialet-Chabrand, 2019). For instance, Vialet-Chabrand *et al.* (2017) reported 18.8% lower than expected A under fluctuating light during the course of a day, which was attributed to stomatal limitation. Stomata range in size from approx. 10 - 80 μm in length and occur at densities between 5 and 1,000 mm^{-2} of leaf depending on the species and the environmental growth conditions (Ticha, 1982; Knapp *et al.*, 1993; Willmer & Fricker, 1996; Hetherington & Woodward, 2003). In many plants (such as *Arabidopsis thaliana*) the majority of stomata found on the lower surface, termed hypostomatous, whilst some aquatic plants (such as water lilies) have stomata only on the upper surface, termed epistomatous (Ticha, 1982; Morison, 2003; Lawson & Morison, 2004; Lawson, 2009). *Triticum aestivum* (wheat) are amphistomatous meaning that stomata can be found

on both the upper surface (adaxial) and lower surface (abaxial) with a near 50/50 ratio between the two (Mohammady, 2002; Khazaei *et al.*, 2010).

Although values for stomata density and size can be determined for different leaves, it is well known that stomatal anatomical features are not uniform over the leaf and can vary considerably depending on the species and growth condition (Ticha, 1982; Smith *et al.*, 1989a; Willmer & Fricker, 1996; Weyers & Lawson, 1997; Weyers *et al.*, 1997; Croxdale, 2000). The patterning of stomata over the leaf surface is not random, although it may appear this way, particularly in dicotyledonous species (Croxdale, 2000). Stomatal patterning generally obeys the one-cell spacing rule, whereby any stoma is separated from any surrounding stomata by at least one epidermal cell (Nadeau & Sack, 2002) and breaking this rule can have major implications for gas exchange (Dow *et al.*, 2014a), leaf energetics and cost (de Boer *et al.*, 2016). Heterogeneity in stomatal characteristics occur between and within species, from the scale of plant community down to the individual leaf and cell (Ticha, 1982; Poole *et al.*, 1996; Weyers & Lawson, 1997; Lawson *et al.*, 1998b; Mott & Buckley, 1998), and is influenced by a number of environmental variables including light intensity, [CO₂] and water availability (Gay & Hurd, 1975; Woodward, 1987; Gray *et al.*, 2000; Doheny-Adams *et al.*, 2012; Hepworth *et al.*, 2015; Fiorin *et al.*, 2016; Hughes *et al.*, 2017). What is not well understood is the advantages or disadvantages of heterogeneity in stomatal characteristic and the impact on leaf and canopy level gas exchange (Weyers & Lawson, 1997).

Stomatal conductance is determined by both anatomical characteristics detailed above as well as functional responses that alter pore aperture (Willmer & Fricker, 1996; Weyers & Lawson, 1997; Hetherington & Woodward, 2003; Casson & Hetherington, 2010; Lawson & Blatt, 2014). Whilst anatomical characters determine

the g_{smax} (McElwain et al., 2016), dynamic changes in g_s are driven completely by changes in function (aperture). In this way, changes in stomatal behaviour across the leaf, when environmental conditions alter (for example water availability), can cause other types of stomatal heterogeneity known as “patchy stomatal behaviour” (Weyers & Lawson, 1997; Mott & Buckley, 1998; Lawson & Morison, 2004). This functional patchiness may or may not be influenced by anatomical features (Cardon *et al.*, 1994; Vialet-Chabrand & Lawson, 2019b) but are the key driver of significant differences in stomatal aperture in adjacent groups of stomata (Mott & Buckley, 1998). In 1997, Weyers & Lawson reviewed the ‘micro’ and ‘macro’ heterogeneity of stomatal behaviour (function), where groups of stomata have differing pore apertures to neighbouring groups, or areoles, resulting in compartmentalised stomatal behaviour across the leaf (Mott & Buckley, 1998). Two possible forms of macro behavioural variation were explained: patches and trends. Patches were explained to be distinct areoles of the leaf which have behavioural borders that stop abruptly and trends are areas differing from others with a continuous and smooth transition between zones (Weyers & Lawson, 1997). The phenomenon of patchy stomatal behaviour received a great deal of attention in the 1990’s, due to the impact non-uniform stomatal behaviour had on the calculation of internal $[CO_2]$ (C_i) which assumes uniformity in g_s over the surface for correct calculation (Mott & Parkhurst, 1991)

The work here focuses on spatial variation of stomatal characteristics across the flag and second leaf of wheat. The flag leaf is the most photosynthetically active during the grain filling stages and the last leaf to senesce after anthesis, and during the grain filling stages of growth it is at the top of the canopy to intercept more light than lower leaves and is closest to the ear to pass assimilates (Gooding *et al.*, 2000). The importance of the flag leaf was described by Evans & Rawson (1970) as one of

the major source of assimilates for the grain filling, indicating that 45 % comes from the flag leaf, while only approximately 5 % comes from the second leaf and 25 % comes from the ear themselves, although the proportion can differ between species and the environmental conditions (Buttrose & May, 1959).

The first aim of this chapter is to identify whether there is variation in stomatal anatomical characteristics, specifically size, density and therefore g_{smax} between the eight wheat MAGIC parental cultivars, and between different areas of the leaf and between differing leaves. Secondly, to ascertain whether any variation in these characteristics translates to differences in gas exchange responses between cultivars. The hypothesis being that although the eight cultivars will be grown in a similar environment, there will be variation within the stomatal size, density and distribution over and between leaves and this will influence g_{smax} and stomatal behaviour and therefore g_s and A in the different cultivars.

3.2 Materials and Methods

This section outlines methods specific to this chapter and modifications made to protocols outlined in Chapter 2 – “Materials and Methods”.

3.2.1 Plant material and growth conditions

Wheat cultivars Alchemy, Brompton, Claire, Hereward, Rialto, Robigus, Soissons and Xi19 were grown as outlined in Chapter 2 – “Materials and Methods” – 2.2.1.

3.2.2 Leaf and stomatal characteristics

3.2.2.1 Leaf epidermal impressions

Leaf epidermal impressions were generated following the method 2.2.1. All impressions were taken before anthesis (growth stage 49-59), from fully expanded single leaves in similar positions on the leaf lamina avoiding major veins and leaf edges. Impressions were taken from three distinct areas (base middle and tip, see Fig. 3.1b) on both the abaxial and adaxial leaf surfaces, from both the flag leaf and the second leaf (Fig. 3.1a). These 12 impressions were taken from the same lead tillers of six wheat plant replicates equalling 72 impressions per cultivar.

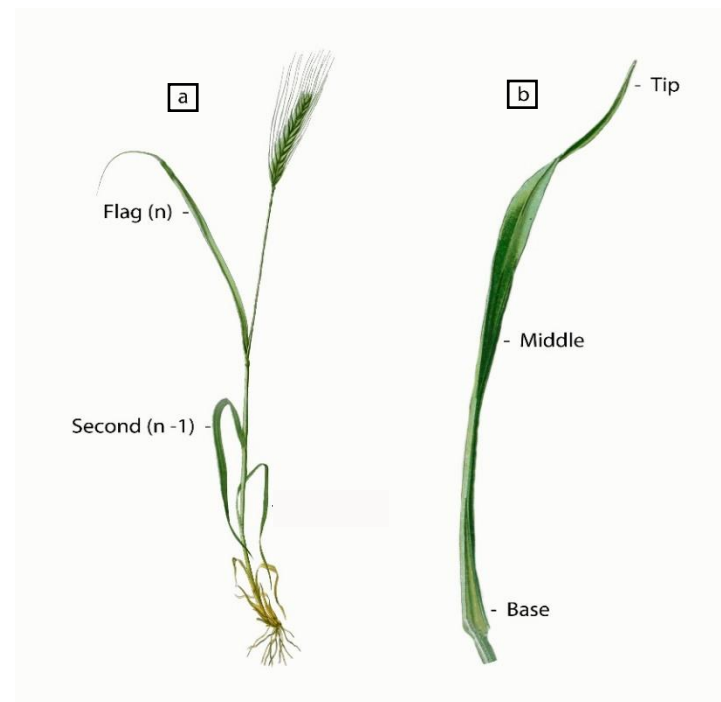


Figure 3.1. Diagram of single wheat tiller highlighting [a] the location of the flag (n) and second leaf (n-1), and [b] the three positions of the leaf where impressions were taken (base, middle and tip).

3.2.2.2 Stomatal anatomical measurements

Stomatal density, guard cell length and pore length were measured via light microscopy (Olympus BX60, Southend-on-Sea, Essex, UK) following the method 2.2.2 and 2.2.3 respectively. Guard cell length and pore length measurements were used to generate potential anatomical maximum stomatal conductance (g_{smax} mol m⁻² s⁻¹) following the calculation in method 2.2.4.

3.2.3 Leaf gas exchange

All gas exchange parameters were recorded using a Li-Cor 6400XT portable gas exchange system (Li-Cor, Lincoln, Nebraska, USA) following the method 2.3.

3.2.3.1 PPFD-step measurements

The response of net CO₂ assimilation rate (A) and stomatal conductance (g_s) to a step change in photosynthetic photon flux density ($PPFD$) was carried out as described in method 2.3.1.

3.2.3.2 Intracellular CO₂ response curves (A/C_i)

A/C_i response curves (net CO₂ assimilation rate (A) to intercellular CO₂ concentration (C_i)) were measured as described in method 2.3.2.

3.2.4 Modelling gas exchange parameters

3.2.4.1. Estimating photosynthetic capacities

Photosynthetic capacities ($V_{C_{max}}$ and J_{max}) were estimated from the A/C_i response curves using method 2.5.1.

3.2.4.2. Determining the rapidity of A and g_s response

The rapidity of the photosynthesis response following a step change in light intensity was assessed using method 2.5.3, whilst method 2.5.2 was used to determine the rapidity of the stomatal response following a step change in light intensity.

3.2.5 Statistical analysis

Statistics were conducted using R software (www.r-project.org; version 3.5.3) following the methods in section 2.6.

3.3. Results

3.3.1 Stomatal anatomy

Stomatal impressions for each MAGIC parental wheat cultivar were used to measure stomatal density (SD; mm^{-2} ; Fig. 3.2), guard cell length (GCL; μm) as a proxy for stomatal size (SS; Fig. 3.6), and pore length (PL; μm) and calculate the maximum potential anatomical g_s (g_{smax} ; $\text{mol m}^{-2} \text{s}^{-1}$) for each species. Stomatal densities (flag leaf: Fig. 3.3, second leaf; Fig. 3.4), SS (flag leaf: Fig. 3.7, second leaf; Fig. 3.8) and g_{smax} (flag leaf: Fig. 3.10, second leaf; Fig. 3.12) were compared between cultivars, surfaces and location on the leaf (Table 1).

3.3.1.1 Stomatal Density

Significant differences ($P < 0.0001$) in SD were observed (Table 1) between cultivars, surfaces, and locations in both the flag, and second leaf (Fig. 3.2). There was also a significant interaction ($P < 0.0001$) of SD between surfaces and locations for the flag and second leaf. A cultivar and location interaction ($P < 0.05$) of SD was also observed on the second leaf. SD was significantly different ($p < 0.0001$) between cultivars of the flag leaf and second leaf (Fig. 3.2). Also, SD was generally higher in the flag leaf than the second leaf for all cultivars, with the flag leaf of cultivar Brompton having highest SD and Robigus having the lowest SD (Fig. 3.2). On the second leaf, SD was greatest in Alchemy and Xi19 had the lowest SD ($p < 0.05$) (Fig. 3.2).

Table 3.1: Analysis of variance results between flag leaf cultivars, surfaces and leaf locations and second leaf cultivars, surfaces and leaf locations for stomatal density, guard cell length and g_{smax} of eight MAGIC wheat cultivars (Alchemy, Brompton, Claire, Hereward, Rialto, Robigus, Soissons and Xi19), indicating F values and P values, highlighting where significant differences have been observed. Significance codes: 0 '***' 0.001 '**' 0.01 '*' 0.05 '.'

Flag Leaf	Stomatal Density			Guard Cell Length			g_{smax}		
	F value	Pr(>F)	Sig	F value	Pr(>F)	Sig	F value	Pr(>F)	Sig
Line	20.723	2.00E-16	***	20.783	2.00E-16	***	8.753	1.4E-09	***
Surface	114.396	2.00E-16	***	3.479	6.34E-02		141.823	2E-16	***
Location	29.888	2.57E-12	***	40.623	6.38E-16	***	4.097	0.0178	*
Line: Surface	7.04	1.21E-07	***	0.402	9.00E-01		4.683	6.1E-05	***
Line: Location	0.999	0.455		1.168	0.30067		1.065	0.39	
Surface: Location	44.176	2.00E-16	***	5.749	3.64E-03	**	25.823	7E-11	***
Line: Surface: Location	0.887	0.573		0.989	0.46538		0.831	0.6346	
Second Leaf	Stomatal Density			Guard Cell Length			g_{smax}		
	F value	Pr(>F)	Sig	F value	Pr(>F)	Sig	F value	Pr(>F)	Sig
Line	21.7	2E-16	***	15.577	2E-16	***	0.868	0.532	
Surface	107.739	2E-16	***	6.237	0.0132	*	0.015	0.901	
Location	16.883	1.4E-07	***	12.072	1E-05	***	1.948	0.145	
Line: Surface	0.665	0.701		0.587	0.7662		1.138	0.34	
Line: Location	3.367	5.7E-05	***	5.242	1.2E-08	***	0.861	0.602	
Surface: Location	21.549	2.5E-09	***	1.07	0.3446		0.033	0.968	
Line: Surface: Location	1.024	0.43		1.086	0.3708		1.14	0.323	

The highest flag leaf SDs ($P < 0.05$) were found in Brompton and Hereward on the abaxial leaf surface and Brompton and Xi19 on the adaxial leaf surface (Fig. 3.3) and similarly, the highest second leaf SD ($P < 0.05$) were observed in cultivars Alchemy, Brompton, Claire and Hereward on the abaxial and adaxial leaf surface (Fig. 3.4). Whereas the lowest flag leaf SD ($P < 0.05$) were found in Rialto, Robigus and Soissons on the abaxial leaf surface and Robigus on the adaxial leaf surface with the lowest second leaf SD ($P < 0.05$) were found in Xi19 on both the abaxial and adaxial leaf surface.

Stomatal densities were assessed on the abaxial and adaxial leaf surfaces of both the flag and second leaf as wheat is known to be amphistomatous. Overall a significant ($P < 0.05$) differences on SD between the flag leaf abaxial and the adaxial

leaf surface and the second leaf abaxial and the adaxial leaf surface was observed (Table 2).

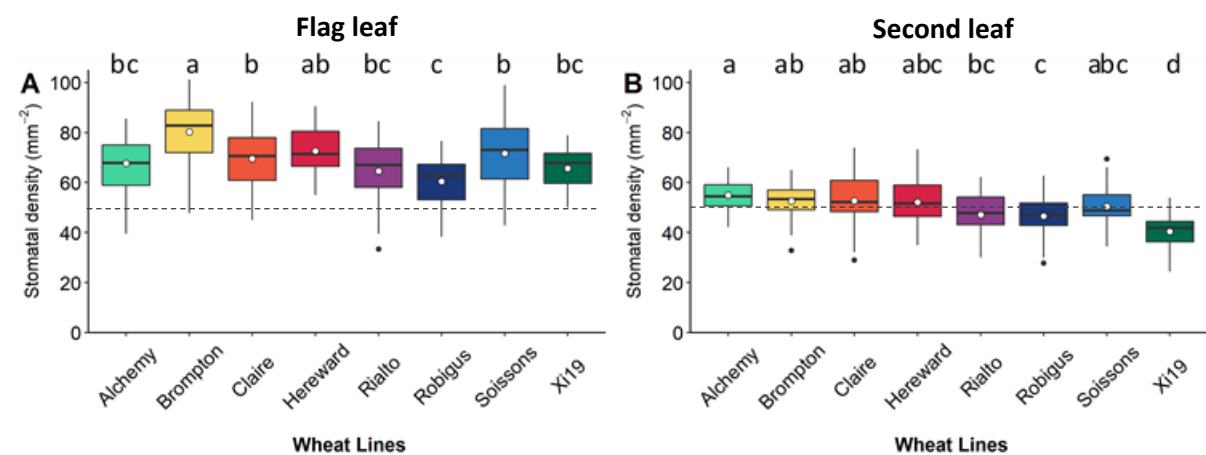


Figure 3.2. Variation (box and whisker plots displaying distribution of biological replicates) and mean (white dot) of flag leaf stomatal density (mm²; A) and second leaf stomatal density (mm²; B) from a culmination of the leaf surfaces and leaf location stomatal densities for eight MAGIC wheat cultivars (Alchemy, Brompton, Claire, Hereward, Rialto, Robigus, Soissons and Xi19). Different letters represent statistically significant differences ($P < 0.05$) between means of different cultivars. Dotted line represents 50 mm² ($n = 36$).

When separating abaxial and adaxial SD by specific regions of the leaf (tip, middle and base), significant differences ($P < 0.001$) was observed between SD on the adaxial and abaxial leaf surface at the middle and tip leaf location on both the flag leaf and the second leaf, although no significant differences in SD between the abaxial and adaxial leaf surface were observed at the base location for either the flag leaf or the second leaf (table 2). When SD was viewed as a percentage of the total number stomatal density (sum of abaxial and adaxial density = 100%), it was obvious that the greater number of stomata occupy the adaxial leaf surface of the flag leaf (Fig. 3.5), except for the cultivar Robigus.

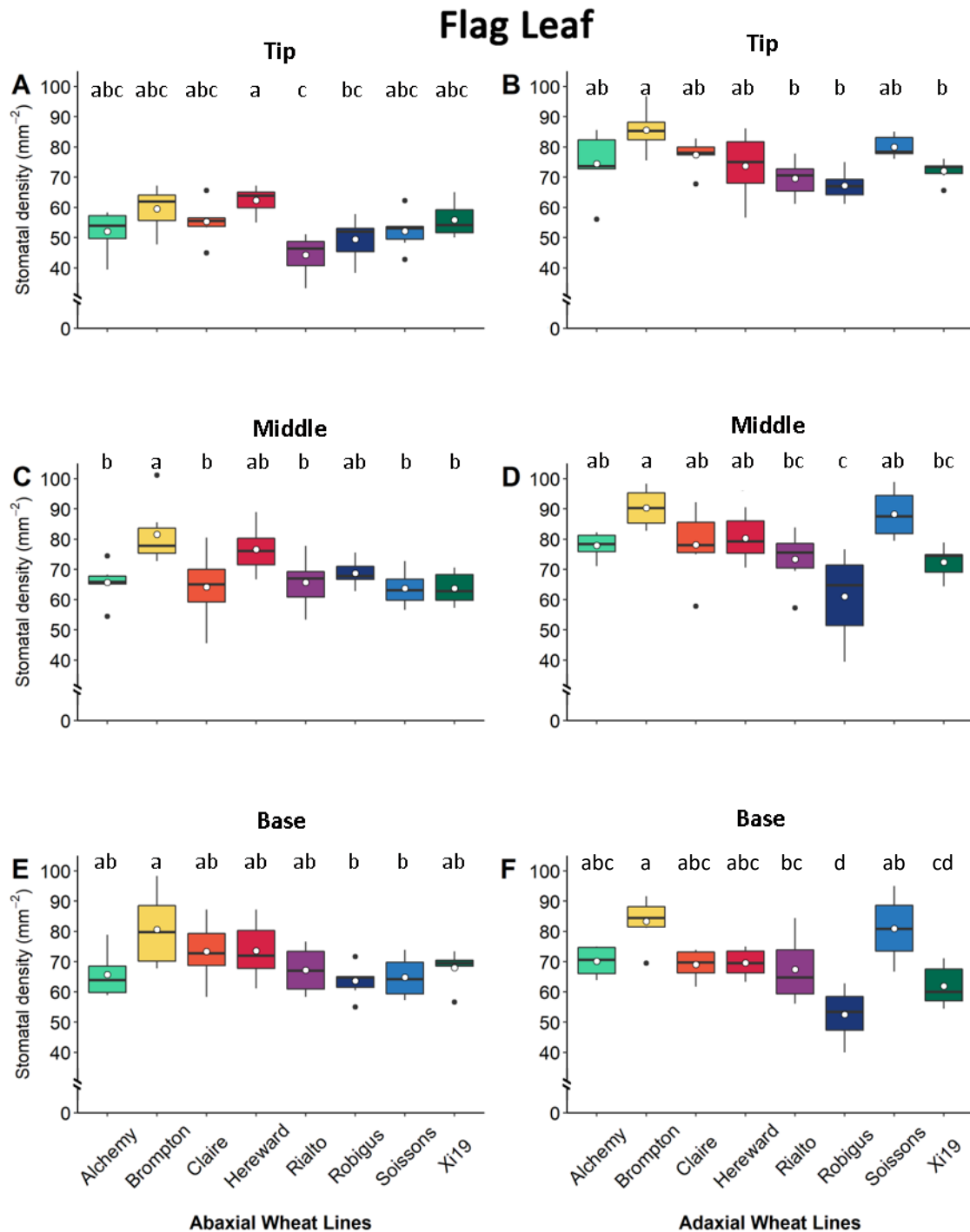


Figure 3.3. Variation (box and whisker plots displaying distribution of biological replicates) and mean (white dot) of flag leaf stomatal density (mm^{-2}), calculated for the abaxial (A, C, E) and adaxial (B, D, F) leaf surfaces at the tip (A, B) middle (C, D) and base (E, F) leaf locations for eight MAGIC wheat cultivars (Alchemy, Brompton, Claire, Hereward, Rialto, Robigus, Soissons and Xi19). Different letters represent statistically significant differences ($P < 0.05$) between means of different cultivars ($n = 6$).

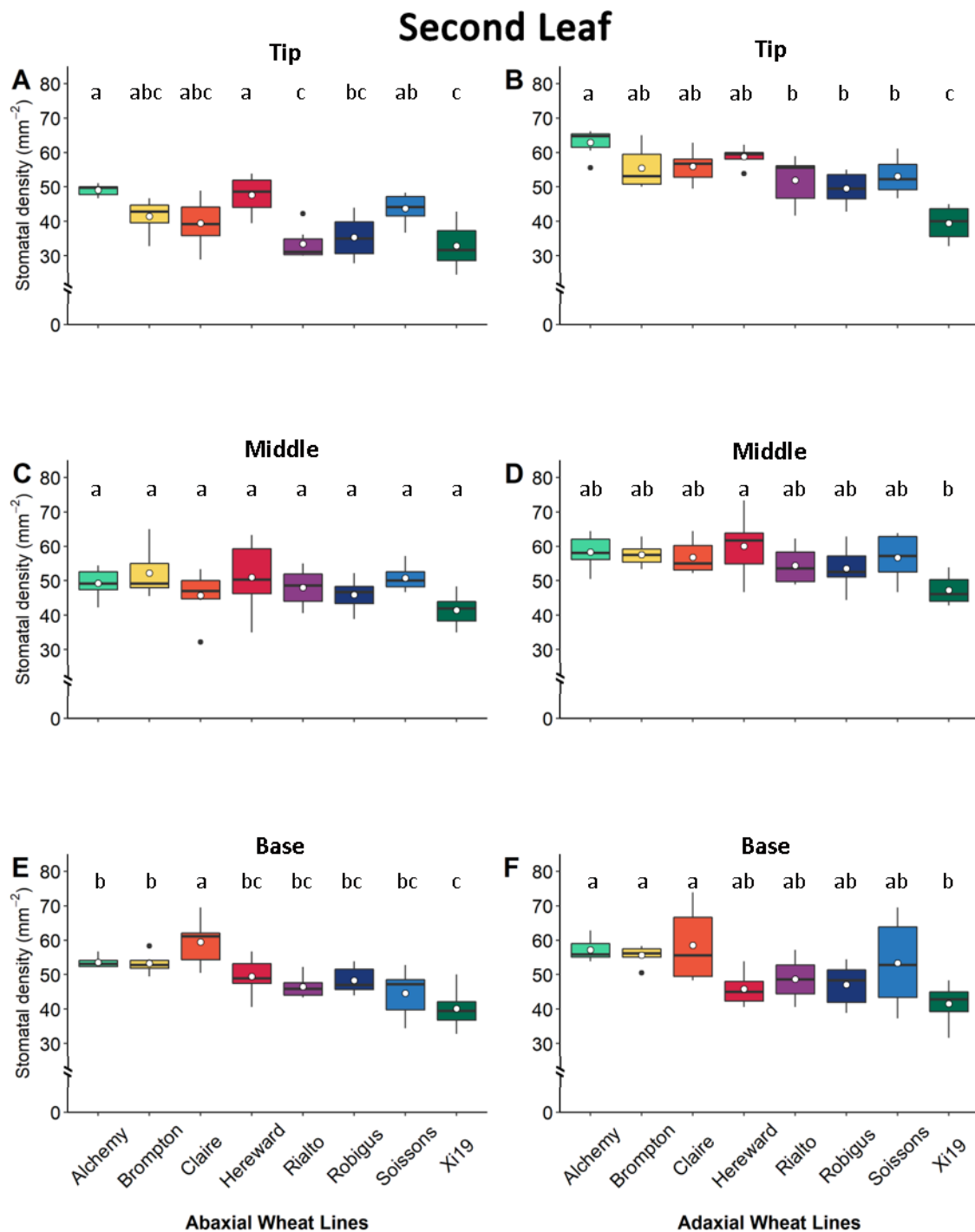


Figure 3.4. Variation (box and whisker plots displaying distribution of biological replicates) and mean (white dot) of second leaf stomatal density (mm²), calculated for the abaxial (A, C, E) and adaxial (B, D, F) leaf surfaces at the tip (A, B), middle (C, D) and base (E, F) leaf locations for eight MAGIC wheat cultivars (Alchemy, Brompton, Claire, Hereward, Rialto, Robigus, Soissons and Xi19). Different letters represent statistically significant differences ($P < 0.05$) between means of different cultivars ($n = 6$).

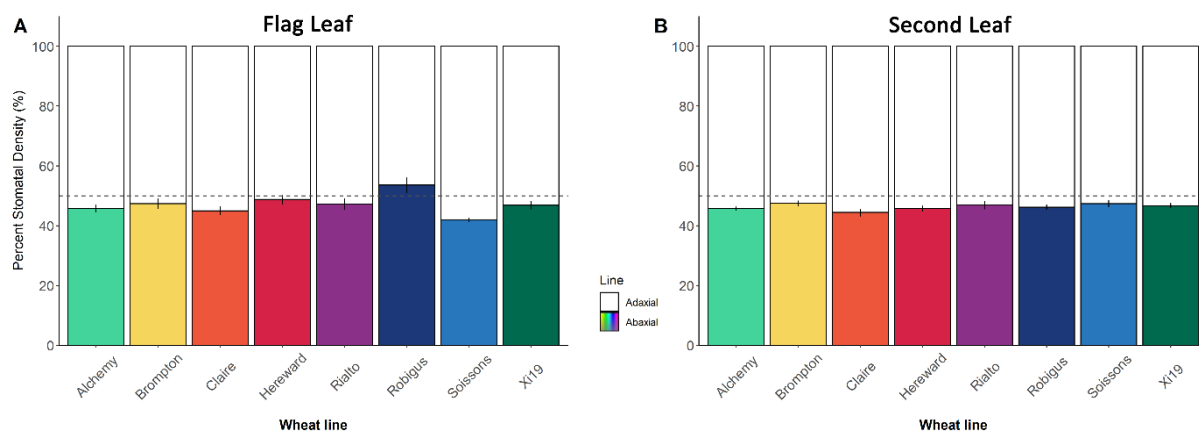


Figure 3.5. Percentage (%) of stomatal density (mm^2) for flag leaf (A) and second leaf (B), calculated as a percentage of the total stomata per leaf (sum of abaxial and adaxial density = 100%). Abaxial percentage represented by coloured bars and adaxial white bars. Measurements taken from the middle leaf location for eight MAGIC wheat cultivars (Alchemy, Brompton, Claire, Hereward, Rialto, Robigus, Soissons and Xi19). Grey dashed line represents 50 % mark. Error bars represent mean \pm SE (n = 6).

Table 3.2: Tukey post-hoc test comparisons of group means between surfaces and locations of flag and second leaf for eight MAGIC wheat cultivars (Alchemy, Brompton, Claire, Hereward, Rialto, Robigus, Soissons and Xi19) for stomatal density, guard cell length and g_{smax} , indicating F values and P values, highlighting where significant differences have been observed. Significance codes: 0 '****' 0.001 '**' 0.01 '*' 0.05 '.'

Flag Leaf		Stomatal Density		Guard Cell Length		g_{smax}	
		P Value	Sig	P Value	Sig	P Value	Sig
Abaxial-Adaxial		0.00E+00	***	1.32E-01		0.00E+00	***
Abaxial	Middle-Base	8.39E-01		4.51E-01		8.84E-01	
Abaxial	Tip-Base	0.00E+00	***	1.30E-02	.	1.40E-03	*
Abaxial	Tip-Middle	0.00E+00	***	2.25E-04	**	6.50E-03	*
Adaxial	Middle-Base	4.00E-06	***	9.28E-01		3.37E-04	**
Adaxial	Tip-Base	2.36E-03	*	0.00E+00	***	0.00E+00	***
Adaxial	Tip-Middle	2.25E-01		0.00E+00	***	2.10E-02	.
Second Leaf		Stomatal Density		Guard Cell Length		g_{smax}	
		P Value	Sig	P Value	Sig	P Value	Sig
Abaxial-Adaxial		0.00E+00	***	2.40E-02	.	8.49E-03	*
Abaxial	Middle-Base	4.85E-01		8.94E-01		5.51E-01	
Abaxial	Tip-Base	0.00E+00	***	1.11E-01		2.35E-01	
Abaxial	Tip-Middle	0.00E+00	***	2.62E-01		8.25E-01	
Adaxial	Middle-Base	1.37E-03	*	7.76E-01		3.96E-01	
Adaxial	Tip-Base	1.56E-01		1.75E-04	**	1.89E-03	*
Adaxial	Tip-Middle	1.94E-01		1.98E-03	*	7.63E-02	

Table 2 highlights the significant differences in SD between abaxial and adaxial surfaces and between leaf locations for both leaf surfaces of the flag leaf and second leaf. SD differences ($p < 0.05$) were observed (Table 2) between flag leaf abaxial tip - base, and tip - middle leaf location, additionally for the adaxial leaf surface differences were observed between middle - base, and the tip - base leaf locations. SD differences ($p < 0.05$) were observed (Table 2) between second leaf abaxial tip - base, and tip - middle leaf location, additionally for the adaxial leaf surface differences were observed between middle and base leaf locations.

3.3.1.2 Guard Cell Length

Significant differences ($P < 0.0001$) in stomatal size (SS; measured as guard cell length; μm^2) was observed (Table 1) in both flag and second leaf between cultivars and locations. SS was different ($P < 0.05$) between leaf surfaces on the second leaf but not the flag leaf ($P = 0.063$). A significant interaction ($P < 0.05$) between surface and location effected flag leaf SS (Table 1) but not the second leaf, and an interaction ($P < 0.05$) between cultivar and location effected second leaf SS (Table 1) but this did not affect the flag leaf SS, although no further test was completed to examine these interactions. SS was different ($p < 0.0001$) between cultivars (Fig. 3.6), and in general the largest stomata were observed in the second leaf. On the flag leaf, Soissons had the largest SS (Fig. 3.6) and on the second leaf, SS were found to be largest on Xi19 and smallest in the cultivar Brompton for both the flag and the second leaf.

The largest ($P < 0.05$) flag leaf abaxial SS were found in Soissons and Xi19 with the largest adaxial SS on Hereward, Soissons and Xi19 (Fig. 3.7), and similarly, the largest ($P < 0.05$) second leaf SS were observed in cultivar Hereward, Soissons and Xi19 on the abaxial and adaxial leaf surfaces (Fig. 3.8). The smallest ($P < 0.05$) SS in the flag leaf found in Brompton and Rialto in both the abaxial and adaxial leaf surface (Fig. 3.7), whilst the smallest (sig. $P < 0.05$) second leaf SS were in Brompton and Claire on the abaxial leaf surface and Alchemy, Brompton, Claire and Hereward on the adaxial leaf surfaces (Fig. 3.8).

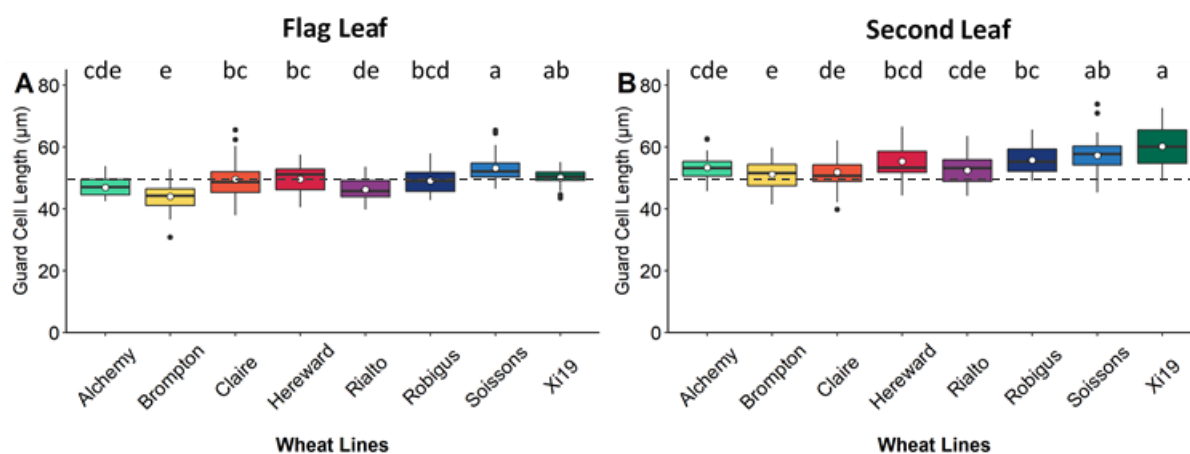


Figure 3.6. Variation (box and whisker plots displaying distribution of biological replicates) and mean (white dot) of guard cell length (μm ; A) and second leaf guard cell length (μm ; B) from a culmination of the leaf surfaces and leaf location guard cell lengths for eight MAGIC wheat cultivars (Alchemy, Brompton, Claire, Hereward, Rialto, Robigus, Soissons and Xi19). Different letters represent statistically significant differences ($P < 0.05$) between means of different cultivars. Dotted line represents $50 \mu\text{m}$ ($n = 36$).

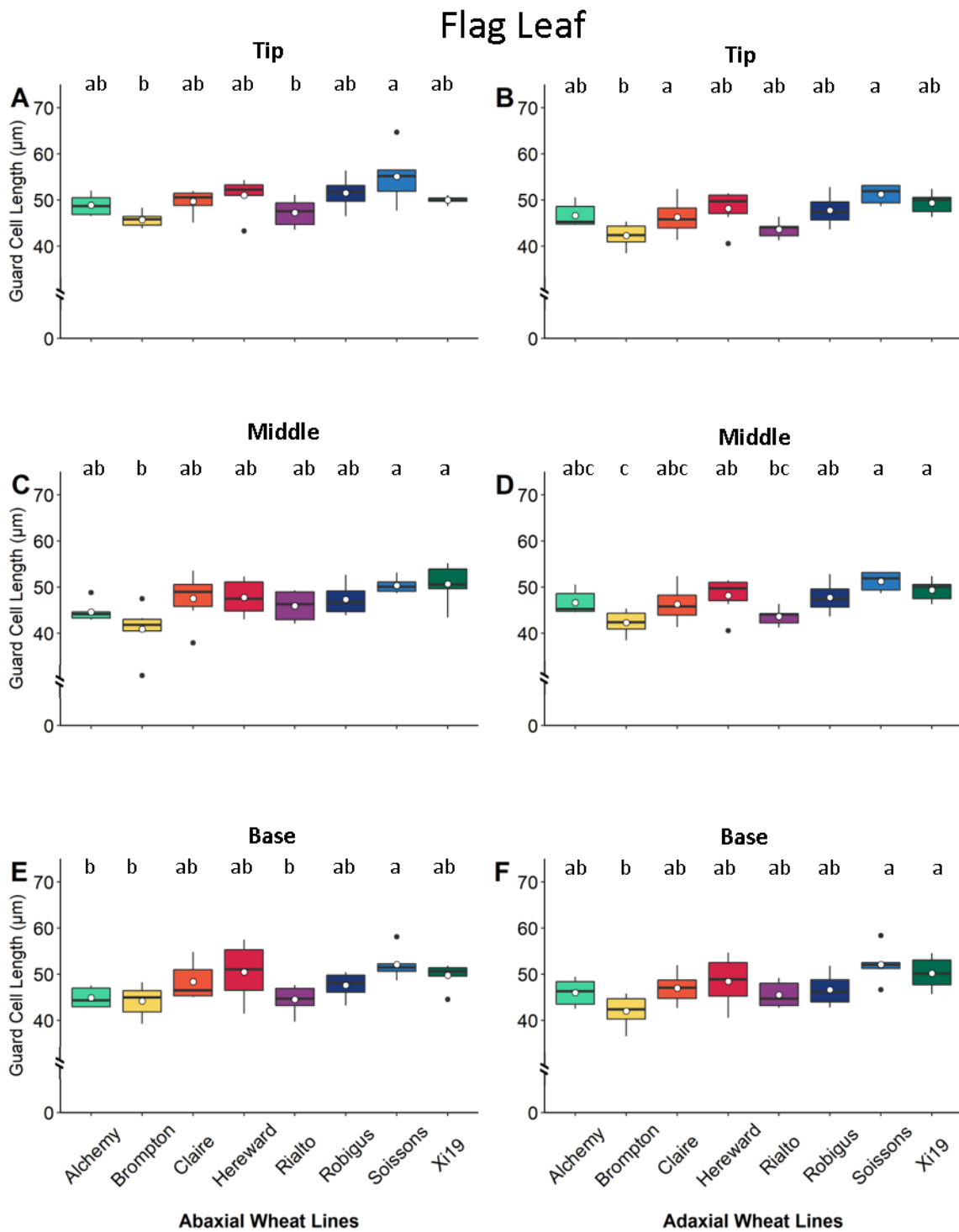


Figure 3.7. Variation (box and whisker plots displaying distribution of biological replicates) and mean (white dot) of flag leaf guard cell length (μm), calculated for the abaxial (A, C, E) and adaxial (B, D, F) leaf surfaces at the tip (A, B), middle (C, D) and base (E, F) leaf locations for eight MAGIC wheat cultivars. Different letters represent statistically significant differences ($P < 0.05$) between means of different cultivars ($n = 6$).

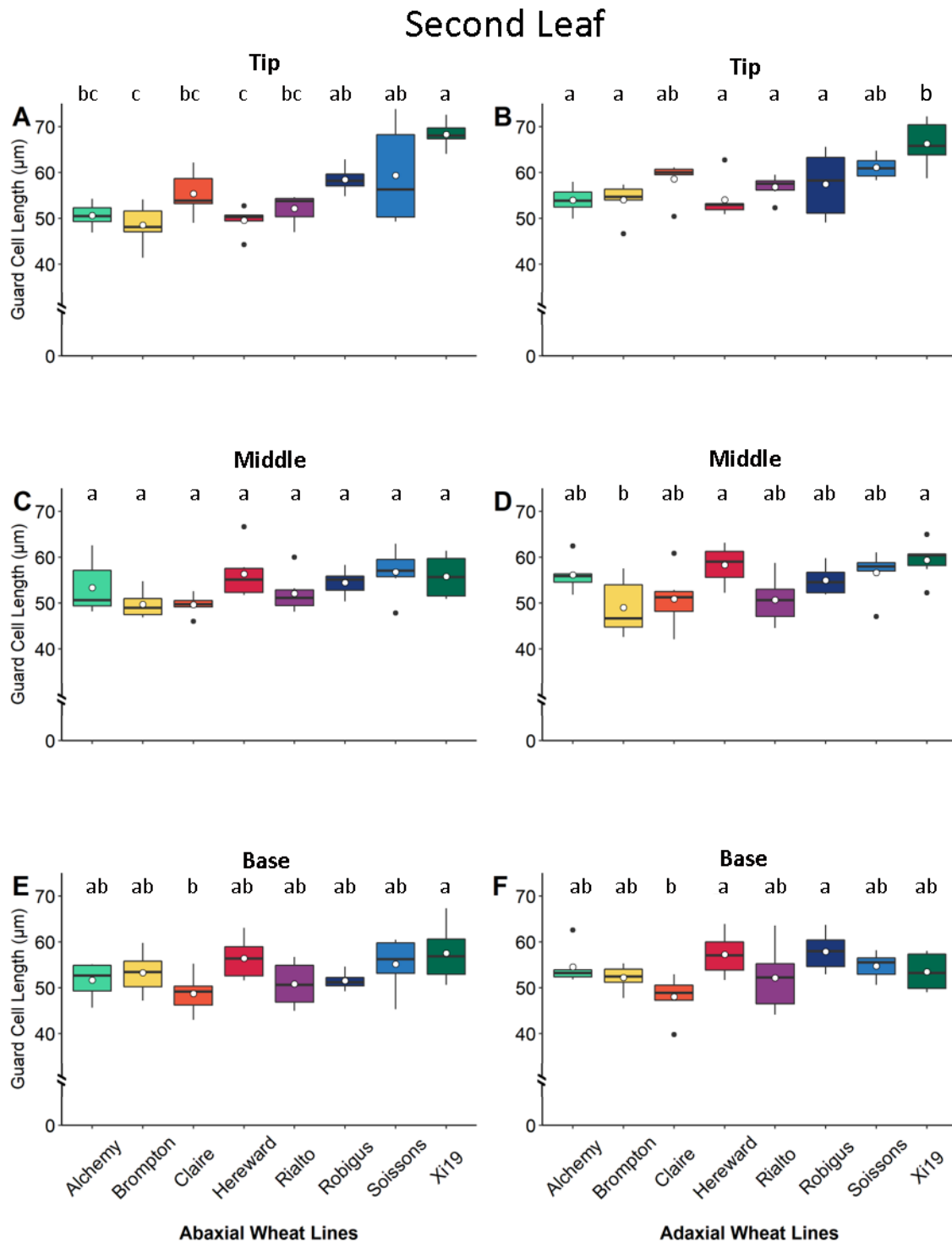


Figure 3.8. Variation (box and whisker plots displaying distribution of biological replicates) and mean (white dot) of second leaf guard cell length (μm), calculated for the abaxial (A, C, E) and adaxial (B, D, F) leaf surfaces at the tip (A, B), middle (C, D) and base (E, F) leaf locations for eight MAGIC wheat cultivars. Different letters represent statistically significant differences ($P < 0.05$) between means of different cultivars ($n = 6$).

No differences (Table 2) in flag leaf SS were found between abaxial and the adaxial leaf surface ($P=0.132$), whereas SS in the second leaf was significantly different between leaf surfaces ($P<0.05$) however, a Tukey post-hoc test revealed no significant differences between abaxial and adaxial leaf surfaces of the same cultivars (for example - Alchemy abaxial was not significantly different to Alchemy adaxial) for either flag leaf or second leaf.

Table 2 highlights the significant differences in SS between abaxial and adaxial surfaces and between leaf locations for both leaf surfaces of the flag leaf and second leaf. SS differences ($p<0.05$) were observed (Table 2) between flag leaf abaxial and adaxial tip - base, and tip - middle leaf location. SD differences ($p<0.05$) were observed (Table 2) between second leaf adaxial tip - base, and tip - middle leaf location only, no differences between leaf location were observed on the second leaf abaxial leaf surface.

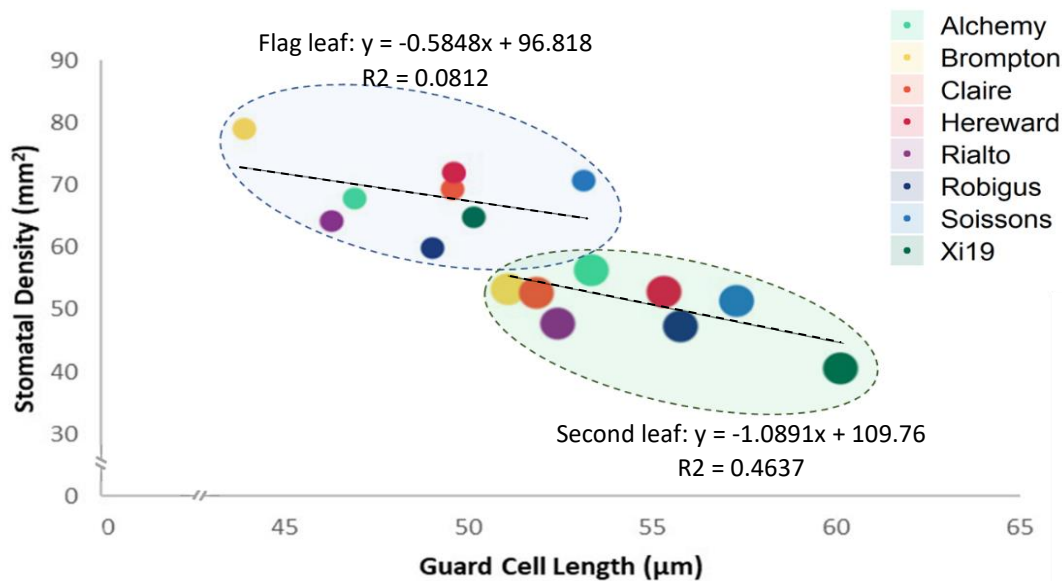


Figure 3.9 Correlation between mean leaf stomatal density (mm^2) and guard cell length (μm). Filled areas highlight flag leaf measurements (blue) and second leaf measurements (green), whilst black dotted lines represent the trend in the data for all individuals of that leaf. A negative correlation was observed between SD and SS in both the flag leaf and the second leaf (Fig. 3.9). The cultivar with the highest flag leaf SD, Brompton also displayed the smallest SS, however, the cultivar with the lowest flag leaf SD, Robigus did not have the largest stomatal size, it was observed in the cultivar Soissons (Fig. 3.9). The cultivar with the highest second leaf SD, Alchemy does not follow the same trend by not displaying the smallest SS, although the cultivar XI19 had the lowest second leaf SD and largest SS (Fig. 3.9).

3.3.1.3 Maximum potential stomatal conductance (g_{smax})

Significant differences ($P < 0.05$) in flag leaf anatomical maximum g_s (g_{smax} ; $\text{mol m}^{-2} \text{s}^{-1}$) was observed (Table 1) between cultivars, surfaces, and locations. A significant interaction ($P < 0.05$) between cultivar and surface, and surface and location effected flag leaf g_{smax} (Table 1) although no further test was completed to examine these interactions.

Flag leaf g_{smax} on the adaxial surface showed (Fig. 3.10) cultivar Soissons had the highest values at all three leaf locations and lowest in Robigus for the middle and base locations, and Hereward for the tip, all differences were statistically significant

($P < 0.05$) between the highest and lowest g_{smax} values. No differences between the flag leaf abaxial g_{smax} values (Fig. 3.10) were observed. Second leaf g_{smax} on the adaxial surface showed cultivar Claire and Hereward (Fig. 3.12) had the highest values at the tip and middle leaf location respectively, and cultivar Xi19 had the lowest values at all three leaf locations, with no differences in g_{smax} values observed at the base leaf location. Second leaf g_{smax} on the abaxial leaf surface (Fig. 3.12) showed the cultivar Soissons had the highest values at the middle and tip leaf location and cultivars Rialto and Xi19 with the lowest g_{smax} values at the tip and middle leaf location respectively. No differences of g_{smax} (Fig. 3.12) were observed between cultivars at the base leaf location for either leaf surface. All differences were statistically significant ($P < 0.05$) between the highest and lowest g_{smax} values. Both the flag (Fig. 3.10) and second leaf (Fig. 3.12) displayed a difference ($P < 0.05$) in *anatomical* g_{smax} between the abaxial and adaxial leaf surface (Table 2). The flag leaf g_{smax} were plotted as a percentage, of the total sum of g_{smax} of both surfaces, it is clear that the flag leaf adaxial leaf surface has the higher g_{smax} (Fig. 3.11) at all leaf locations.

In all cultivars, the flag leaf g_{smax} at the tip and the middle (except Robigus) leaf location is higher on the adaxial leaf surface (Fig. 3.11), although only the g_{smax} at the tip leaf location and one cultivar (Soissons) of the middle leaf location showed significant differences. A difference ($P < 0.001$) of flag leaf g_{smax} was observed between leaf locations for both the abaxial and adaxial leaf surfaces between middle and tip, tip and base, and base and middle (Table 2), although no difference of flag leaf abaxial g_{smax} between the middle and base leaf locations were observed. On the second leaf g_{smax} differences ($P < 0.001$) were observed between leaf locations of the adaxial leaf surface, specifically between the tip and base leaf locations (Table 2). No second leaf abaxial leaf location differences of g_{smax} were observed.

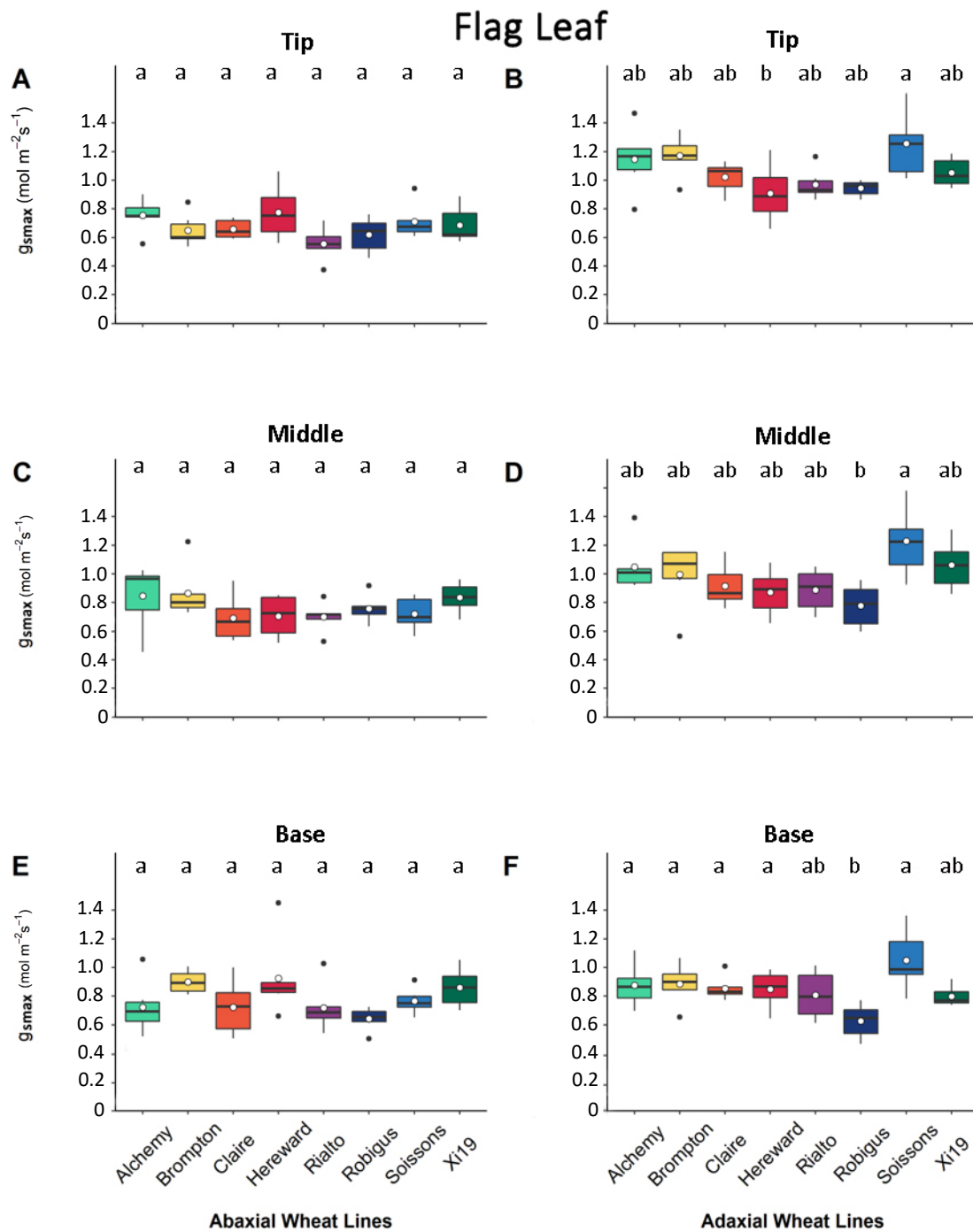


Figure 3.10. Variation (box and whisker plots displaying distribution of biological replicates) and mean (white dot) of flag leaf g_{smax} (mol m⁻¹ s⁻¹), calculated from stomatal density and dimensions, for the abaxial (A, C, E) and adaxial (B, D, F) leaf surfaces at the tip (A, B), middle (C, D) and base (E, F) leaf locations for eight MAGIC wheat cultivars. Different letters represent statistically significant differences ($P < 0.05$) between means of different cultivars ($n = 6$).

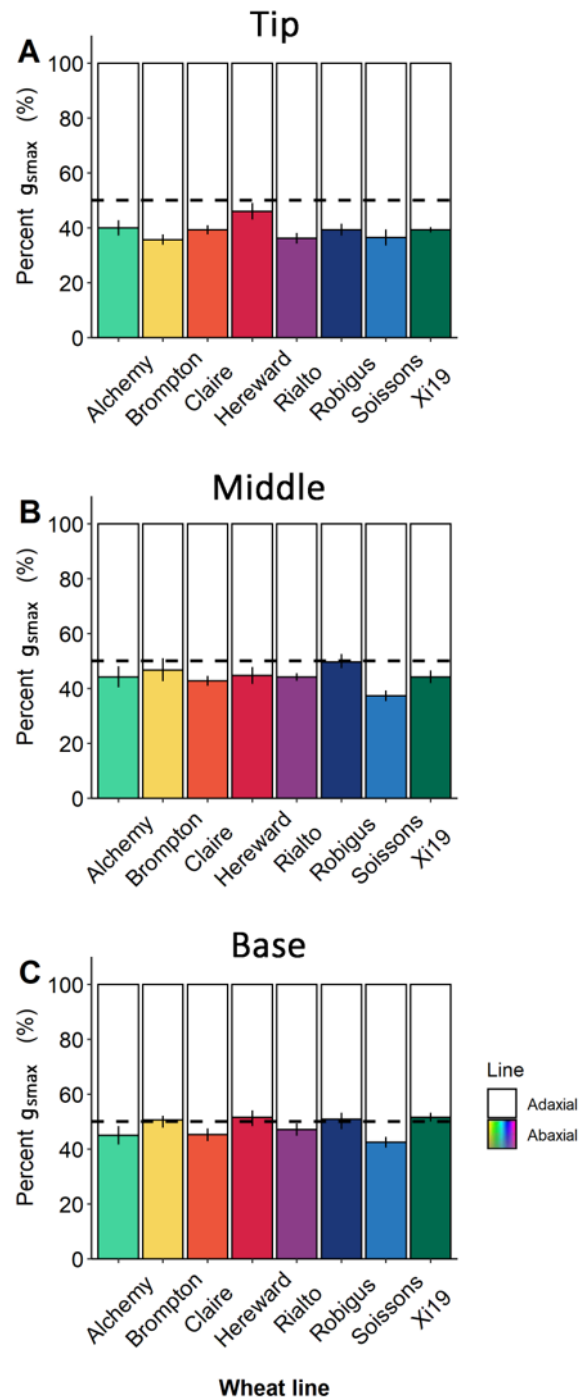


Figure 3.11. Flag leaf g_{smax} as percentage (%) for the abaxial (coloured bars) and adaxial (white bars) leaf surfaces, calculated from stomatal density and dimensions, for the tip (A), middle (B) and base (C) leaf locations for eight MAGIC wheat cultivars. Dark grey dashed line represents 50 % mark. Error bars represent mean \pm SE ($n = 6$).

Table 3.3: Tukey post-hoc test comparisons of group g_{smax} means between flag leaf opposing leaf surfaces (abaxial vs adaxial) for eight MAGIC wheat cultivars (Alchemy, Brompton, Claire, Hereward, Rialto, Robigus, Soissons and Xi19) at different leaf location, indicating p values, highlighting where significant differences have been observed. Significance codes: 0 '***' 0.001 '**' 0.01 '*' 0.05 '.'

Cultivar	Location	p adj	sig.
Alchemy	Base	9.99E-01	
Brompton	Base	1	
Claire	Base	1	
Hereward	Base	1	
Rialto	Base	1	
Robigus	Base	1	
Soissons	Base	6.87E-01	
Xi19	Base	1	
Alchemy	Middle	9.76E-01	
Brompton	Middle	1	
Claire	Middle	7.69E-01	
Hereward	Middle	9.97E-01	
Rialto	Middle	9.86E-01	
Robigus	Middle	1	
Soissons	Middle	1.11E-03	*
Xi19	Middle	9.85E-01	
Alchemy	Tip	6.74E-02	.
Brompton	Tip	4.53E-05	***
Claire	Tip	2.87E-02	.
Hereward	Tip	1	
Rialto	Tip	1.45E-04	***
Robigus	Tip	2.92E-02	.
Soissons	Tip	1.83E-04	***
Xi19	Tip	3.04E-02	.

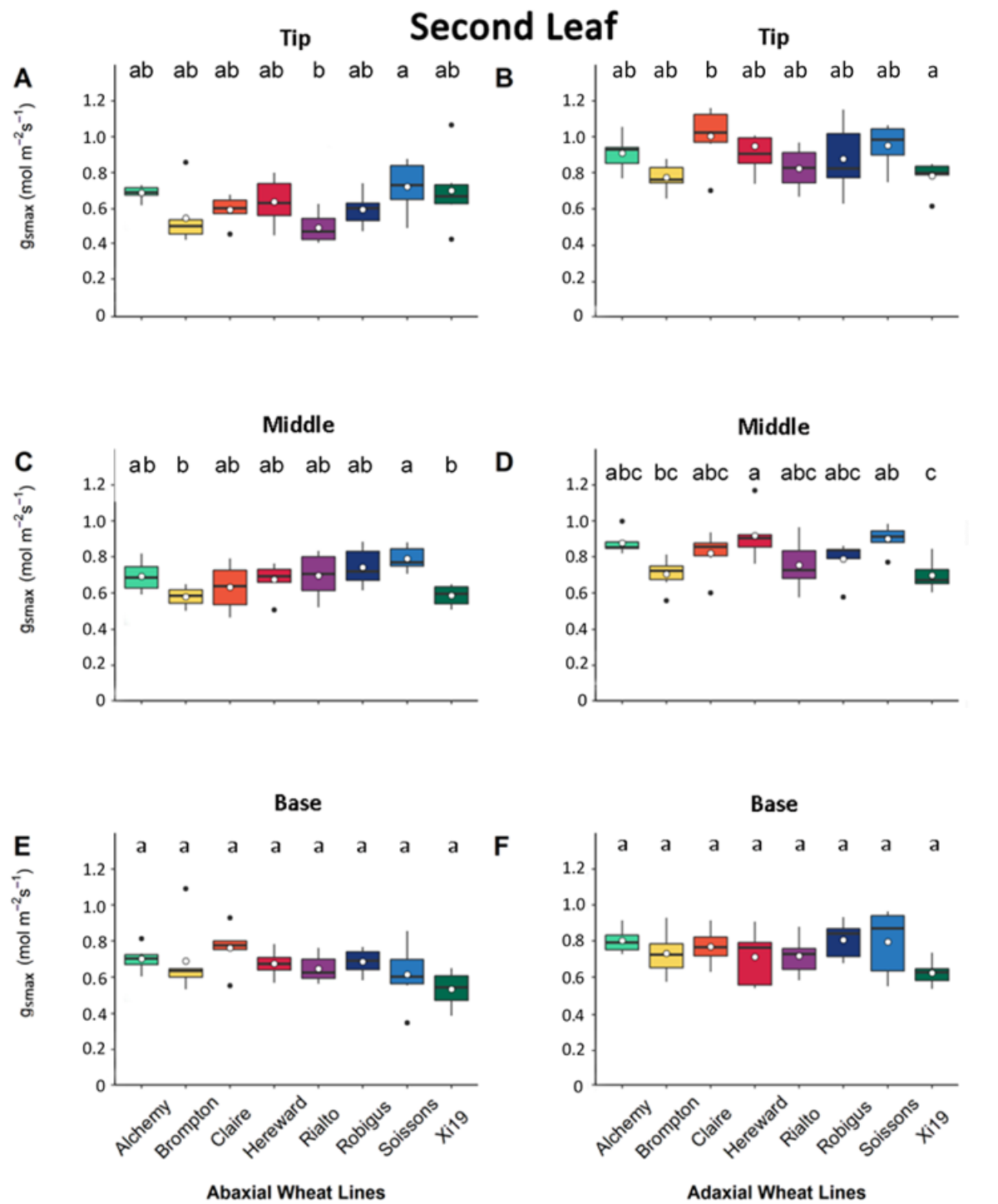


Figure 3.12. Variation (box and whisker plots displaying distribution of biological replicates) and mean (white dot) of second leaf g_{smax} (mol m⁻¹ s⁻¹), calculated from stomatal density and dimensions, for the abaxial (A, C, E) and adaxial (B, D, F) leaf surfaces at the tip (A, B), middle (C, D) and base (E, F) leaf locations for eight MAGIC wheat cultivars. Different letters represent statistically significant differences ($P < 0.05$) between means of different cultivars ($n = 6$).

3.3.2 Leaf gas exchange

3.3.2.1 Response of g_s and A to a step change in PPFD

To assess stomatal kinetics between cultivars, gas exchange measurements were performed on the flag leaf at the middle leaf location. The leaf surface response of g_s and A to a single step increase in light (100 to 1000 $\mu\text{mol m}^{-2} \text{s}^{-1}$ PPFD) are shown in Fig. 3.13. All cultivars exhibited the expected increase in g_s and A following a step increase in light intensity.

During the first 10-min of the protocol at 100 $\mu\text{mol m}^{-2} \text{s}^{-1}$ PPFD, and the final 10 min of the protocol at 1000 $\mu\text{mol m}^{-2} \text{s}^{-1}$ PPFD there was a considerable range in g_s , A and W_i mean values between cultivars. Most cultivars had not attained their maximum g_s values within the 70 min timeframe (Fig. 3.13). It is possible that the exposure time to low light of 20 minutes was insufficient for complete steady state g_s to be achieved under low light; however, this did not greatly impact the stomatal responses to the initial rapid opening response of the stomata. Steady state g_s at the initial PPFD of 100 $\mu\text{mol m}^{-2} \text{s}^{-1}$ varied among the cultivars (Fig. 3.13), with the lowest values observed for Alchemy and the highest for Xi19 with all values under 0.21 $\text{mol m}^{-2} \text{s}^{-1}$. Furthermore, steady state A at the initial PPFD of 100 $\mu\text{mol m}^{-2} \text{s}^{-1}$ also varied among the cultivars although more concisely with A values for all cultivars under 7 $\mu\text{mol m}^{-2} \text{s}^{-1}$ (except for a minimal amount of variations that were probably artefactual for technical reasons). An increase in PPFD to 1000 $\mu\text{mol m}^{-2} \text{s}^{-1}$ led to an immediate and rapid increase in A compared to g_s for all cultivars and after this initial period, the increase in A slowed to a magnitude similar to the increase in g_s , and A reached steady state while g_s continued to increase. The lack of synchrony between the responses of A and g_s to a step increase in PPFD had a consequential effect demonstrated by the temporal responses of W_i (Fig. 3.13; C). The lowest steady state W_i values were

observed in cultivar Xi19 and the highest in Alchemy. Following the step change in PPFD, A rapidly increased compared to g_s and therefore W_i reached a maximum value minutes after the increase on PPFD. Further increases in g_s over time drove a continuous decrease in W_i after A had reached a steady state until the end of the protocol.

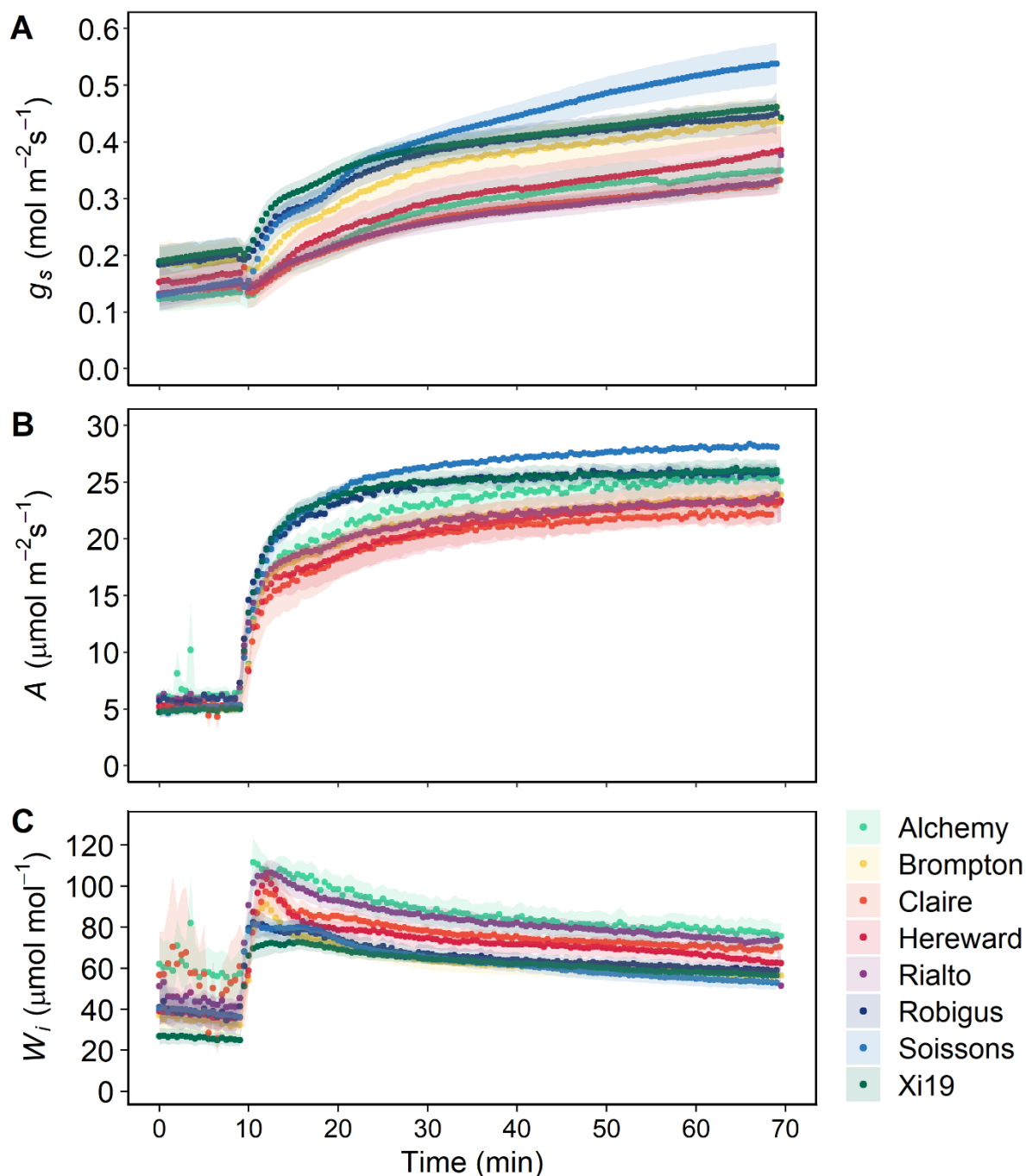


Figure 3.13. Temporal response of stomatal conductance (g_s ; A), net CO₂ assimilation (A ; B), and intrinsic water use efficiency (W_i ; C), to a step increase in light intensity (from $100 \mu\text{mol m}^{-2} \text{s}^{-1}$ for 20 minutes to $1000 \mu\text{mol m}^{-2} \text{s}^{-1}$ for 60 minutes) for eight MAGIC wheat cultivars (Alchemy, Brompton, Claire, Hereward, Rialto, Robigus, Soissons and Xi19). Gas exchange parameters (g_s and A) were recorded at 30s intervals, leaf temperature maintained at 22°C , and leaf VPD at $1 \pm 0.2 \text{ KPa}$. Error ribbons represent mean \pm SE. $n = 4-6$.

3.3.2.2. Speed of g_s response to a step change in light intensity

Stomatal responses to a step increase in light intensity (100 to 1000 $\mu\text{mol m}^{-2} \text{s}^{-1}$ PPFD) were used to determine natural variation in the speed of g_s and A response to light amongst eight MAGIC wheat cultivars. The time constants to reach 63 % of final value for g_s (τ_{g_s} ; Fig. 3.14, A) and for A (τ_A ; Fig. 3.14, B) final value of g_s (g_{sF} , Fig. 3.14, C) and A (A_F , Fig. 3.14, D) at 1000 $\mu\text{mol m}^{-2} \text{s}^{-1}$ and finally the magnitude of change in g_s (Δg_s , Fig. 3.14, E) and A (ΔA , Fig. 3.41, F) between 100 $\mu\text{mol m}^{-2} \text{s}^{-1}$ - 1000 $\mu\text{mol m}^{-2} \text{s}^{-1}$.

Time constants for the increases in g_s (τ_{g_s} ; Fig. 3.14, A) were significantly longer ($p < 0.05$) in wheat cultivars Rialto and Soissons despite Rialto having the lowest magnitude of change in g_s between steady state values between 100 $\mu\text{mol m}^{-2} \text{s}^{-1}$ - 1000 $\mu\text{mol m}^{-2} \text{s}^{-1}$ at 60 min (Δg_s , Fig. 3.14, E). In contrast, wheat cultivar Soissons, although having the one of the slowest ($p < 0.05$) responses for increasing g_s (τ_{g_s} ; Fig. 3.14, A), this cultivar had the highest ($p < 0.05$) magnitude of change in g_s (Δg_s , Fig. 3.14, E), and highest final g_s value (g_{sF} , Fig. 3.14, C). Significantly faster ($p < 0.05$) changes in g_s (τ_{g_s} ; Fig. 3.14, A) were observed in cultivar Brompton and Robigus, almost 10 min faster, than in Robigus which had the second highest magnitude of changes in g_s (Δg_s , Fig. 3.14, E), and one of the highest final g_s values (g_{sF} , Fig. 3.14, C).

A positive relationship was observed (Fig. 3.15) between the final values of g_s at 1000 $\mu\text{mol m}^{-2} \text{s}^{-1}$ and the time constant of change in g_s between the eight MAGIC wheat cultivars. In this case, as the time constant increased, the final values of g_s increased, indicating that the longer the g_s response to a step change in light intensity, the higher the final g_s value. The time constants for increasing A (τ_A ; Fig. 3.14, B) in response to a step increase in light intensity (100 - 1000 $\mu\text{mol m}^{-2} \text{s}^{-1}$) were longest

($P < 0.05$) in cultivars Claire, Rialto and Robigus and shortest in the cultivar Hereward. The cultivar Soissons had a significantly higher final A value (A_F , Fig. 3.14D), with no significant differences observed between the remaining seven cultivars. The magnitude of change in A (ΔA , Fig. 3.14, F) was higher ($P < 0.05$) in Soissons than any other cultivar and Rialto had a lower magnitude of change in A ($P < 0.05$) than all other cultivars except Hereward.

Flag Leaf

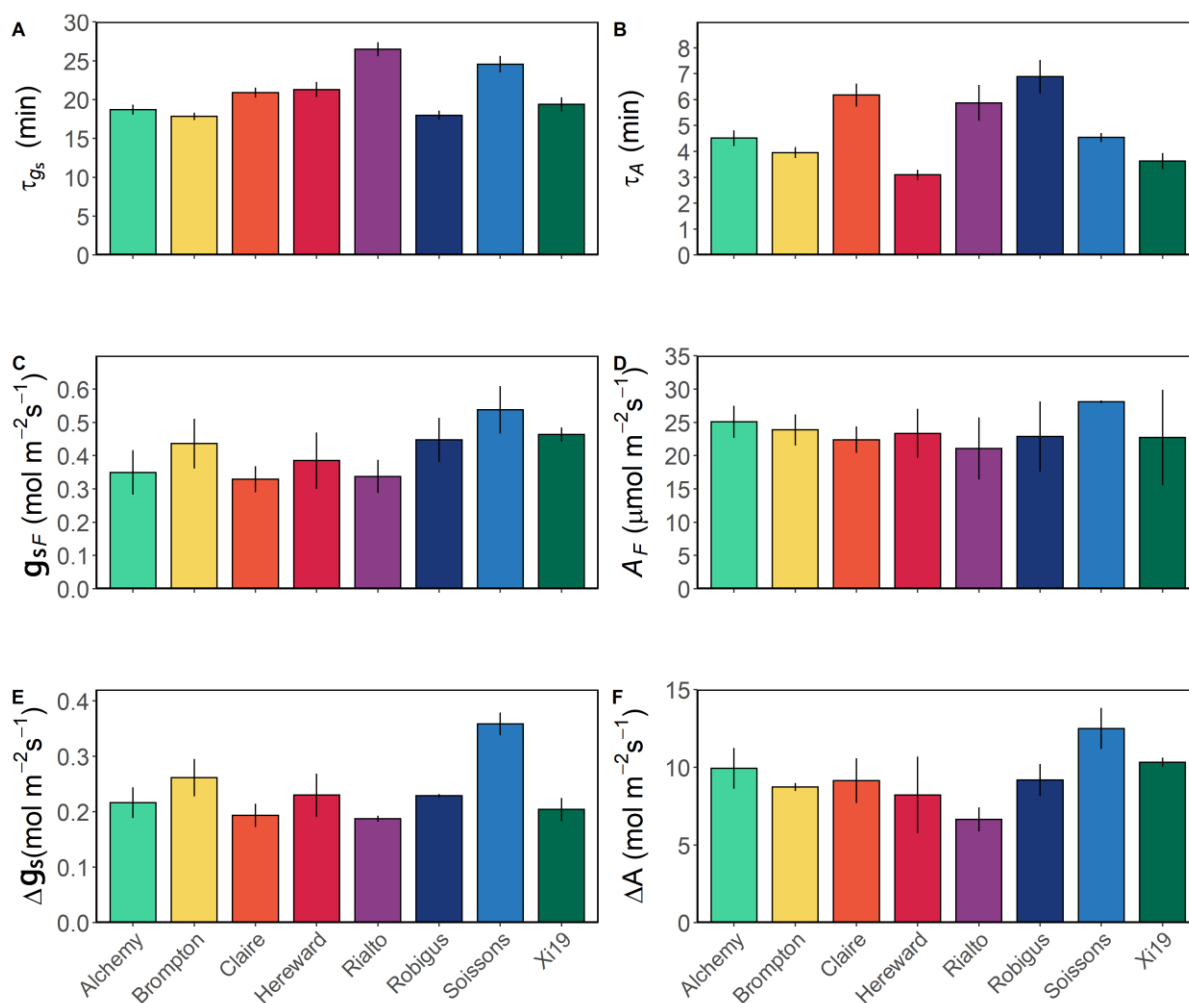


Figure 3.14. Time constant for stomatal opening (τ_{gs} , A) in minutes, final values of stomatal conductance ($1000 \mu\text{mol m}^{-2} \text{s}^{-1}$ PPFD) after an increased step change in light intensity (g_{sF} , C) and difference in g_s between 100 and $1000 \mu\text{mol m}^{-2} \text{s}^{-1}$ PPFD (Δg_s , E) following the step increase in light intensity. Time constant for light saturated carbon assimilation (τ_A , B) in minutes, final values light saturated carbon assimilation ($1000 \mu\text{mol m}^{-2} \text{s}^{-1}$ PPFD) after an increased step change in light intensity (A_F , D) and difference in A between 100 and $1000 \mu\text{mol m}^{-2} \text{s}^{-1}$ PPFD (ΔA , F) following the step increase in light intensity. All results for eight MAGIC wheat cultivars (Alchemy, Brompton, Claire, Hereward, Rialto, Robigus, Soissons and Xi19). Error bars represent 95% confidence intervals. $n=4-6$.

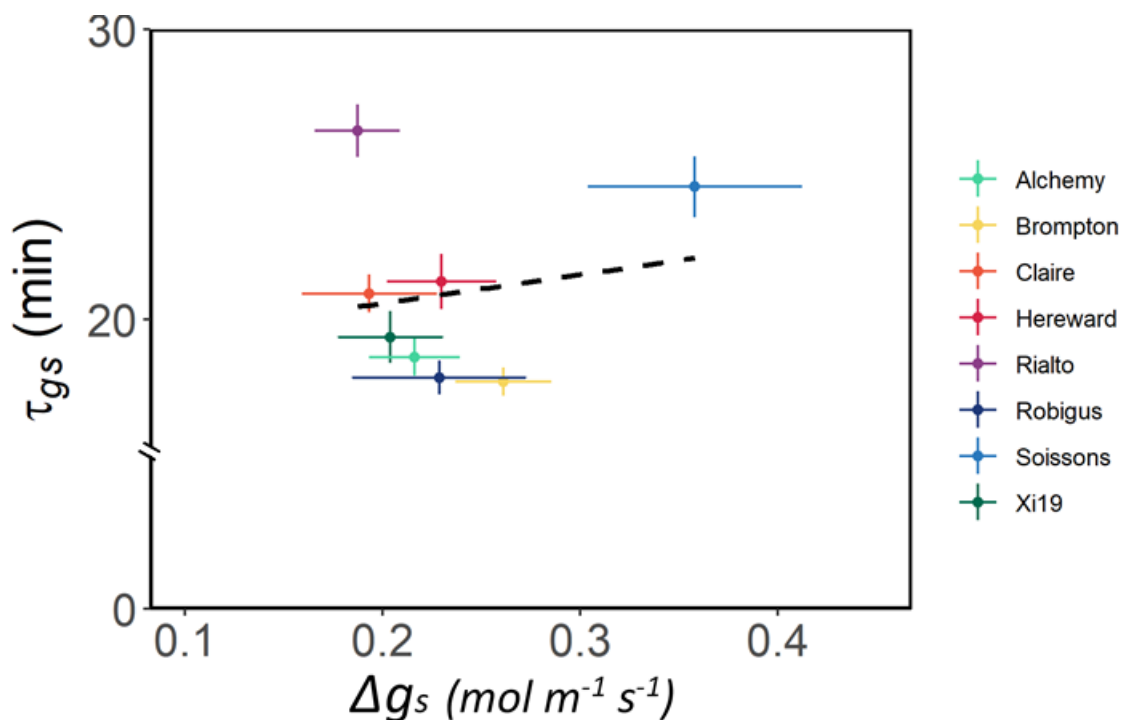


Figure 3.15. Correlations between time constant for stomatal opening (τ_{g_s}) in minutes and difference in g_s between 100 and 1000 $\mu\text{mol m}^{-2} \text{s}^{-1}$ (Δg_s) following the step increase in light intensity, for eight MAGIC wheat cultivars. Black dotted line represents the trend in the data for all individuals.

Differences ($P < 0.001$) between g_s mean values at 1000 $\mu\text{mol m}^{-2} \text{s}^{-1}$ PPFD (operational g_s) of the flag leaf at the middle leaf location and flag leaf $g_{s_{max}}$ (an average of abaxial and adaxial leaf surface $g_{s_{max}}$ values) were observed (Fig. 3.16). Measurements were either performed (operational g_s) or utilised ($g_{s_{max}}$ calculation) from the middle leaf location. Operational g_s values range between 0.3 and 0.55 $\text{mol m}^{-2} \text{s}^{-1}$ whereas the potential anatomical maximum g_s calculated from anatomical measurements range between 0.6 and 2.0 $\text{mol m}^{-2} \text{s}^{-1}$ suggesting an 85 % decrease from the highest potential anatomical g_s to lowest observed operational g_s values (Fig. 3.16).

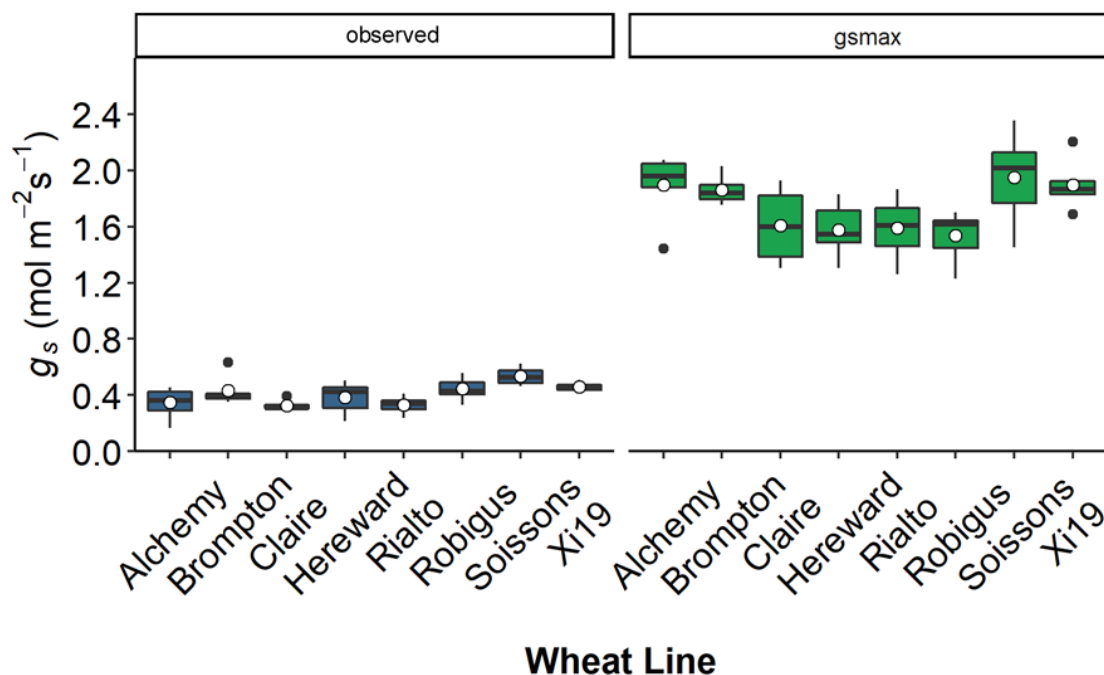


Figure 3.16. Variation (box and whisker plots displaying distribution of biological replicates) and mean (white dot) of g_s at $1000 \mu\text{mol m}^{-2} \text{s}^{-1}$ PPFD (observed g_s ; $\text{mol m}^{-1} \text{s}^{-1}$) and potential maximum anatomical stomatal conductance (g_{smax} ; $\text{mol m}^{-1} \text{s}^{-1}$) calculated from stomatal density and dimensions from the flag leaf at the middle leaf location for eight MAGIC wheat cultivars. ($n = 4-6$).

3.3.2.3. A/C_i response analysis

The response of CO_2 assimilation (A) as a function of internal $[\text{CO}_2]$ (C_i ; A/C_i – Figure 3.17) were performed on the flag leaf for all eight MAGIC wheat cultivars to determine any differences in photosynthetic capacity between the cultivars. All cultivars exhibited the expected increase in A with increased C_i up to a certain point before reaching a plateau. The maximum A (A_{max}) at CO_2 $1500 \mu\text{mol m}^{-2} \text{s}^{-1}$ and $1300 \mu\text{mol m}^{-2} \text{s}^{-1}$ PPFD (determined from a light response protocol), maximum rate of carboxylation (V_{cmax}) and maximum rate of electron transport (J_{max}) were determined (Fig. 3.18; A, B and C respectively). No significant differences were observed between the cultivars in A_{max} (Fig. 3.18; A), V_{cmax} (Fig. 3.18; B) or J_{max} (Fig. 3.18; C).

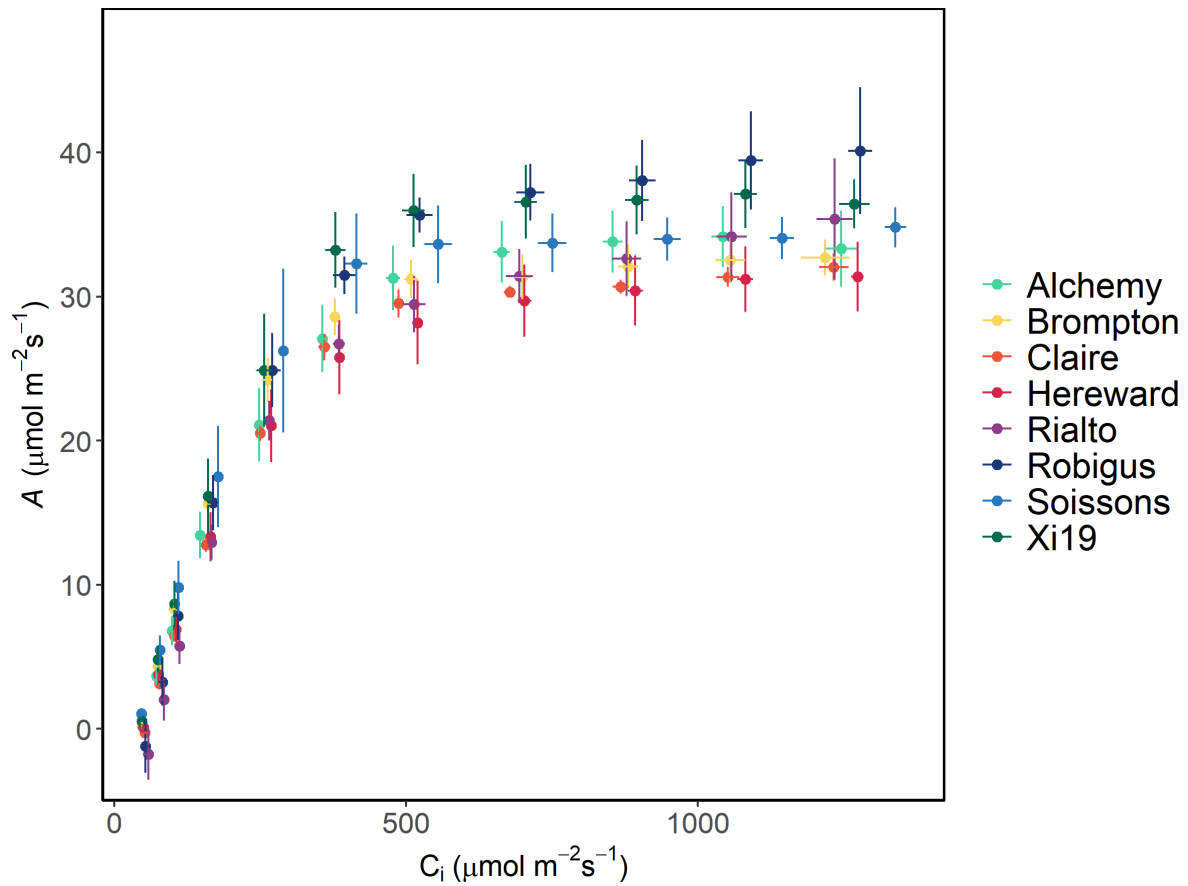


Figure 3.17. The response of CO₂ assimilation (*A*) to intercellular [CO₂] (*C_i*) between 50 and 1500 $\mu\text{mol m}^{-2}\text{s}^{-1}$, under saturating PPFD ($1300 \mu\text{mol m}^{-2}\text{s}^{-1}$), for eight MAGIC wheat cultivars. Error bars represent mean \pm SE. *n* = 4-6.

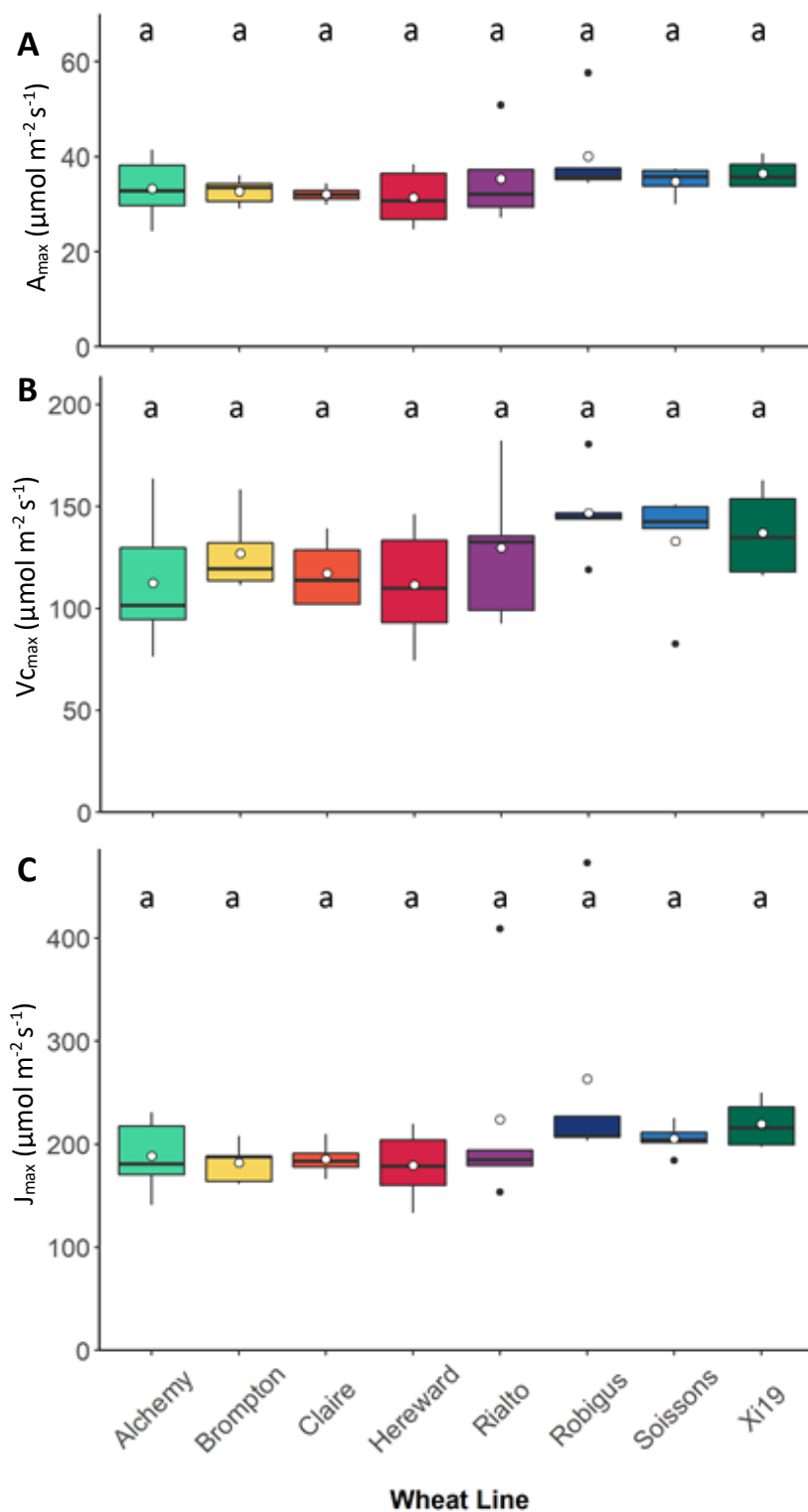


Figure 3.18. Variation (box and whisker plots displaying distribution of biological replicates) and mean (white dot) and the measured CO_2 -saturated ($1500 \mu\text{mol m}^{-2} \text{s}^{-1}$) rate of photosynthesis at light $1300 \mu\text{mol m}^{-2} \text{s}^{-1}$ (A; A_{max}), the maximum rate of carboxylation (B; $V_{c,max}$) and maximum rate of electron transport (C; J_{max}) from eight MAGIC wheat cultivars. Different letters represent statistically significant differences ($P < 0.05$) between means of different cultivars ($n = 4-6$).

3.4. Discussion

Many studies have reported that heterogeneity in stomatal characteristics can be found in stomatal size, density, patterning and distribution and observed both between and within cultivars, moreover heterogeneity is influenced by environmental growth conditions (Ticha, 1982; Poole *et al.*, 1996; Willmer & Fricker, 1996; Weyers & Lawson, 1997; Bettarini *et al.*, 1998; Lawson & Weyers, 1999; Royer, 2001; Franks & Farquhar, 2007). Furthermore, heterogeneity in anatomical features influences the maximal potential anatomical stomatal conductance (g_{smax} ; Dow *et al.*, 2014; Matthews *et al.*, 2017) and the realised or operational g_s , although ultimately infinite combinations of stomatal size, density, patterning and distribution can achieve the same g_{smax} . Stomatal conductance is regulated to optimize carbon uptake and reduce water loss (Cowan, 1977; Hetherington & Woodward, 2003) and in this way, regulating stomatal characteristics to a given environment which will put constraints on overall g_{smax} as well as operational g_s and has been linked to the evolution of stomatal anatomy and function (McElwain *et al.*, 2015) and therefore essential to optimal function in higher plants.

The investigations reported in this study were designed to determine and quantify variation in stomatal characteristics, specifically size and density, of the eight MAGIC wheat parental cultivars. Variation was assessed between leaves (flag leaf and second leaf), between leaf surfaces (abaxial and adaxial) and at different leaf locations (base, middle and tip). Heterogeneity in both stomatal density (Fig. 3.2, 3.3 and 3.4) and size (Fig. 3.6, 3.7 and 3.8) was observed between cultivars, flag and second leaves, leaf surfaces and leaf locations (see also tables 1 and 2). An overall observation was that the flag leaf of all MAGIC wheat parental cultivars had a higher density of smaller stomata than those of the second leaf, using GCL as a proxy for

stomatal size (Fig. 3.9) and as previously reported stomatal density and size are negatively correlated with each other (Hetherington & Woodward, 2003; Franks & Beerling, 2009). Such strong relationships have often been observed in species from the same families (Drake *et al.*, 2013) or over long periods of geological time (Franks & Beerling, 2009), whilst across vastly different species this relationships had not always held (McAusland *et al.*, 2016). De Boer *et al.* (2016) suggested that the evolution of stomatal traits involved an epidermis trade-off which sought to maximise gas exchange capacity and minimise the epidermis covered, and by reducing the size of stomata, not only could stomatal numbers be increased but gaseous diffusivity in and out of the leaf interior could be improved by reduction of the pore depth (decreased cross sectional area of guard cells), and without compromising the “one cell spacing” rule (Nadeau & Sack, 2002; Franks & Farquhar, 2007; Franks & Beerling, 2009; Doheny-Adams *et al.*, 2012; Lawson & Blatt, 2014). The “one cell spacing” rule states that for efficient functioning, stomata must be separated by at least intervening pavement cell in the leaf epidermis and cover a single substomatal cavity within the mesophyll layer to ensure optimal gaseous fluxes (Nadeau & Sack, 2002; Peterson *et al.*, 2010). Smaller stomata are also reported to have faster stomatal responses compared with larger stomata which results from an increased membrane surface area to guard cell volume ratio increasing the rate of ionic fluxes back and forth from subsidiary cells (Hetherington & Woodward, 2003; Franks & Beerling, 2009; Drake *et al.*, 2013; Lawson & Blatt, 2014). Therefore, together the size-speed association with the size-density relationship could represent different/alternative strategies for modifying overall g_{smax} as well as operational g_s (McElwain *et al.*, 2015) to maximize plant performance in a specific environment.

The flag leaf (the last leaf to develop before the ear emergence) is situated at the top of the canopy and therefore intercepts high levels of light throughout the hottest parts of the growing season than lower leaves, and is the most photosynthetically active during grain filling stages (Gooding *et al.*, 2000). The higher stomatal densities in the flag leaf compared with the second leaf and variation in these numbers in some cultivars could be an adaptation of the flag leaf emerging later in the growing season when typically, temperatures are higher and light intensity greater, increasing the need for higher transpiration and leaf cooling as well as an enhanced influx of CO₂ for A. As the flag leaf is in closer vascular proximity to the ear than other leaves, it is thought that the movement of photo-assimilates from the flag leaf to the ear is essential for an optimal grain filling stage with approximately 45 % transferred from the flag leaf, while only approximately 5 % comes from the second leaf, while 25 % comes from ear photosynthesis itself (Simkin *et al.*, 2020), and the remaining coming from other parts of the plant, although the proportion differs between species and the environmental conditions (Buttrose & May, 1959; Stoy, 1963; Lupton, 1972; Stamp & Herzog, 1976).

Higher stomatal densities were generally observed on the adaxial leaf surfaces of both the flag and second leaf (Table 1; Fig. 3.4 & 3.5). It should be noted that it is more common to view higher stomatal densities on the abaxial leaf surface of amphistomatous leaves as the adaxial leaf surface is typically exposed to higher light intensities which could drive severe water loss (Gooding *et al.*, 2000). Wheat abaxial/adaxial polarity, or amphistomaty is under genetic control and is established early on in leaf development. Wheat leaves have polarized growth from a collection of proliferative cells at the tiller growing from the leaf base, creating a leaf blade with the oldest cells at the tip of the leaf (Croxdale, 2000). Croxdale (2000) reported that monocots, such as wheat, consist of regular longitudinal files of cells in visibly ordered

arrays adjacent to cell files near the midrib. This suggests wheat species *could* have an advantageous relationship between its stomatal positioning (longitudinal files near the midrib) and having smaller, faster stomata to aid a quicker stomatal response to either increased water availability or water stress. Amphistomatous species, such as wheat, have also been suggested to have operational independence, whereby abaxial and adaxial leaf surfaces can respond separately to external stimuli such as differences in evaporative demand and sensitivity to light (Wong *et al.*, 1985; Lu *et al.*, 1993; Richardson *et al.*, 2017).

In general amphistomatous species tend to have higher gas exchange capacity compared with hypostomatous species (Mott & O'Leary, 1984; Beerling & Kelly, 1996), which could be due to shorter diffusion pathways, and differences in boundary layer, as well as having two potentially high functioning leaf surfaces (de Boer *et al.*, 2012; Drake *et al.*, 2019; Xiong & Flexas, 2020). Several studies have suggested that stomata on each surface responded to changes in evaporative demand (Mott & Parkhurst, 1991; Richardson *et al.*, 2017) and light and CO₂ (Mott & Peak, 2018) independently of each other in amphistomatous leaves. Differences in stomatal characters (SD and SS) and therefore operational differences could be advantageous in wheat during grain filling stages for achieving optimal *A* for yield, which outweighs desiccation, as the adaxial leaf surface of upper leaves (especially the flag leaves) occupy higher light environments of both intensity and wavelength (Muir, 2019). Although no significant differences were found between SS on flag leaf surfaces (table 1).

Spatial distribution of stomatal characters across the leaf lamina exists (Poole *et al.*, 1996; Weyers *et al.*, 1997; Lawson *et al.*, 1998; Lawson & Weyers, 1999; Fiorin *et al.*, 2016) non-uniformly (Weyers & Lawson, 1997) and occurs due to both cell

expansion and cell differentiation (Croxdale, 2000). For example, Smith *et al.*, (1989) showed spatial variation in stomatal aperture across the entire leaf lamina of *Commelina communis* illustrating the variation impacted on A (Weyers & Lawson, 1997; Weyers *et al.*, 1997). This non-uniform trend was found in the eight MAGIC wheat cultivars between the base, middle and tip leaf locations for SD and SS. In this study, the highest values of flag leaf SD means (Fig. 3.3) were found at the middle leaf location in all cultivars with predominantly the lowest values of SS means (Fig. 3.7), the highest values SS means were found at the tip leaf location. The second leaf followed in this trend with the highest values of SD means (Fig. 3.4) found predominantly at the middle leaf location and the highest values SS means (Fig. 3.8) were found at the tip leaf location. Crop canopies intercept solar radiation based on multiple factors including leaf area per unit soil surface area, or the leaf area index, and also on characteristics such as leaf angle and the spatial arrangement of leaves (Araus *et al.*, 1993). An observed characteristic of the eight magic wheat cultivars was that flag leaves, when fully expanded, are in a horizontal position and have a 'draped' leaf angle where the middle of the leaf is at a higher position than the leaf tip, which is angled downward, with the middle leaf location at the highest point of the canopy which intercept the highest light intensities. With this in mind, and the results of this study for the size and density of stomata distribution over the leaf lamina, it would be an advantage for higher densities of smaller stomata for a more rapid stomatal opening and closing (Drake *et al.*, 2013; Raven, 2014) to be situated in the middle leaf location and therefore benefit from a faster stomatal kinetics, higher rates of g_s for photosynthesis and leaf cooling.

The variation in stomatal characters (SD, SS, and stomatal distribution) led to significant differences ($p < 0.05$) in g_{smax} (Table1) in the flag leaf and between leaves,

surfaces and locations (Fig. 3.10) but not in the second leaf (Fig. 3.12). In the flag leaf, differences in g_{smax} between cultivars were a result of differences ($p < 0.05$) in SD without differences in SS, whereas in the second leaf, the higher SD were offset by SS which counteracted the differences in g_{smax} . Plants do not operate at their g_{smax} due to the inefficiency of the turgor pressures control in the guard cells, which drive pore aperture with modern crop species generally operating at approx. 20 % of their potential maximum capacity (Franks *et al.*, 2012a; Dow *et al.*, 2014b), and in this study (Fig. 3.16) plants were operating at approximately 25-30 % of their g_{smax} . This indicates that these eight-elite wheat operate at a capacity where guard cell turgor pressure can most efficiently control stomatal apertures for opening (Hetherington & Woodward, 2003; Elliott-Kingston *et al.*, 2016).

Although significant variation in anatomical features was observed between and within cultivars, resulting in variation to the g_{smax} , no differences were observed between the CO₂-saturated ($1500 \mu\text{mol m}^{-2} \text{s}^{-1}$) rate of photosynthesis at light $1300 \mu\text{mol m}^{-2} \text{s}^{-1}$ (A_{max} ; Fig. 3.18; A), the maximum velocity of Rubisco for carboxylation (V_{cmax} ; Fig. 3.18; B) or the potential rate of electron transport under saturating light (J_{max} ; Fig. 3.18; C). Elite wheat cultivars are bred for superior traits that lead to higher seed yield and it is not surprising that these eight elite wheat cultivars are all operating at a similar high functioning photosynthetic capacity. However, considerable differences in the rates of g_s , A , W_i and stomatal rapidity (Figs. 3.13 and 3.14) were found.

This study highlights that there is heterogeneity of SD and SS between the eight MAGIC cultivars, flag and second leaves, leaf surfaces, and leaf locations. There was also a negative relationship observed between stomatal density and size in which density appears to supersede size when determining g_{smax} . Moreover, because g_s , A

and therefore W_i is determined predominantly by both these anatomical factors, they are demonstrably a key target for either manipulation or detection of natural variants for the improvement of stomatal behaviour (Doheny-Adams *et al.*, 2012; Hepworth *et al.*, 2015; Caine *et al.*, 2018; Dunn *et al.*, 2019; Faralli & Lawson, 2020), focusing on the speed of stomatal response to dynamic environmental conditions (Matthews *et al.*, 2018).

CHAPTER 4

**The dark side of stomatal conductance:
does photosynthesis on the abaxial and
adaxial leaf surface contribute independently
to overall gas exchange in wheat?**

In preparation for journal article

Modelling completed by Silvere Vialet-Chabrand

4.1 Introduction

For plants to function efficiently, stomata open and close in response to various external and internal stimuli to carefully balance CO₂ uptake to maintain photosynthetic carbon assimilation (A) and water loss via transpiration. Stomatal conductance (g_s) is used to assess stomatal behaviour and functional responses to different environmental conditions. High g_s facilitates the CO₂ uptake and supply for A but is also associated with high water loss through transpiration, with implication for plant water status. However, transpirational water loss also facilitates nutrient uptake and is an essential for maintaining appropriate leaf temperature for optimal photosynthesis (particular under conditions of high light that drive high photosynthesis; Willmer & Fricker, 1996; Shimazaki *et al.*, 2007; Morison *et al.*, 2008; Lawson & Blatt, 2014).

Stomatal conductance is determined by both anatomical characteristics, including stomatal density (SD), size (SS) and patterning (SP) as well as functional responses that alter the pore aperture (Willmer & Fricker, 1996; Weyers & Lawson, 1997; Hetherington & Woodward, 2003; Casson & Hetherington, 2010; Lawson & Blatt, 2014). Anatomical characters are fixed early in leaf development and can be used to determine the potential anatomical maximum stomatal conductance (g_{smax}) (McElwain *et al.*, 2015) and therefore dynamic changes in g_s are driven completely by changes in function (aperture). Stomatal density is one of the main components in determining both g_s and g_{smax} and known to vary depending on species (Tichá, 1982) and environmental conditions (Woodward, 1987; Stevens *et al.*, 2020). Stomatal distribution can either be confined to one leaf surface, the abaxial surface (hypostomatous), or much less commonly, only on the adaxial surface (hyperstomatous), or they can be present on both leaf surfaces (amphistomatous;

Parkhurst, 1978; Morison & Lawson, 2007). Amphistomatous leaves can also differ in SD on each leaf surfaces (Willmer & Fricker, 1996; Taylor *et al.*, 2012), but typically SD in most species is often much greater on the abaxial surface compared with adaxial (Driscoll *et al.*, 2006). . Amphistomatous leaves can be further subdivided into dorsiventral or isobilateral species, where dorsoventrality presents palisade mesophyll cells, the tissue performing most of the CO₂ uptake, positioned nearest to the upper epidermis (for example, *Rhododendron catawbiense*) and the term Isobilateral describes species with palisade mesophyll cells at both the upper and lower epidermis (for example, *Triticum aestivum* L.; Rudall, 1980; Brodribb *et al.*, 2007; Drake *et al.*, 2019). Isobilateral amphistomatous species have been suggested to have operational independence, whereby abaxial and adaxial leaf surfaces can respond separately to external stimuli such as differences in evaporative demand and sensitivity to light (Wong *et al.*, 1985; Lu *et al.*, 1993; Richardson *et al.*, 2017). Characteristically, dorsiventral leaves are found in fast-growing dicotyledonous herbaceous crops whereas isobilateral leaves are typically adapted to arid conditions due to the high-water potential of the leaf morphology (Buckley *et al.*, 2015; Richardson *et al.*, 2020).

In general, amphistomatous species tend to have higher gas exchange capacity compared with hypostomatous species (Mott & O'Leary, 1984; Beerling & Kelly, 1996), which could be due to shorter diffusion pathways, and differences in boundary layer (de Boer *et al.*, 2012; Drake *et al.*, 2019; Xiong & Flexas, 2020). Several studies have suggested that stomata on each surface responded to changes in evaporative demand (Mott & Parkhurst, 1991; Richardson *et al.*, 2017) and light and [CO₂] (Mott & Peak, 2018) independently of each other. The higher functionality of amphistomatous species creates a higher risk of desiccation and therefore these plant must invest in higher vein density to increase hydraulic efficiency (Brodribb *et al.*, 2007; Buckley *et*

al., 2015). Richardson *et al.* (2020) observed a lack of asymmetry in vein position in *Helianthus annuus*, with minor veins closer to the abaxial compared with the adaxial leaf surface. The same authors also reported a decrease of coordination between stomata on the two leaf surfaces that were driven by leaf hydraulics, demonstrating the tight coupling between stomatal behaviour and leaf water supply. Amphistomaty has therefore adapted to experience greater irradiance, temperature and evaporative demand to avoid desiccation.

The extent to which wheat leaves intercept solar radiation depends on characteristics such as leaf angle and the spatial arrangement (Araus *et al.*, 1993). Wheat flag leaves are the last to appear before the ear and grow vertically until fully emerged, when they droop. Wheat leaves therefore occupy differing light environments in both intensity and wavelength, on the adaxial and abaxial leaf surfaces (Vergara-Díaz *et al.*, 2018). Wang *et al.* (2008) suggested that the different stomatal responses of the two surfaces of the same leaf is due to the differential light exposure, as the adaxial leaf surface is exposed to more direct radiation, whilst the abaxial leaf surface is shaded by itself, receiving light transmitted through the mesophyll and reflected from its surroundings. To evaluate the functional impact of different stomatal densities on the two surfaces on gas exchange and photosynthesis we developed a split chamber to separately determine A and g_s on both surface simultaneously in eight MAGIC wheat cultivars that represent 80% of the SNP variation in North–West European bread wheat (Faralli *et al.*, 2019a).

4.2 Materials and Methods

This section outlines methods specific to this chapter and modifications made to protocols outlined in Chapter 2 – “Materials and Methods”.

4.2.1 Plant material and growth conditions

Wheat cultivars Alchemy, Brompton, Claire, Hereward, Rialto, Robigus, Soissons and Xi19 were grown as outlined in Chapter 2 – “Materials and Methods” – 2.2.1.

4.2.2 Leaf and stomatal characteristics

4.2.2.1 Leaf epidermal impressions

Leaf epidermal impressions were generated following the method in section 2.2.1. All impressions were taken from fully expanded flag leaves of similar positions at the middle of the leaf avoiding major veins and leaf edges before anthesis (Zadok’s growth stage 49-59).

4.2.2.2 Stomatal anatomical measurements

Stomatal density, guard cell length and pore length were measured via light microscopy (Olympus BX60, Southend-on-Sea, Essex, UK) following the method in section 2.2.2 and 2.2.3 respectively. Guard cell length and pore length measurements were used to generate anatomical potential maximum stomatal conductance (g_{smax} mol m⁻² s⁻¹) following the calculation in method in section 2.2.4.

4.2.3 IRGA measurements using split leaf chamber

The design and construction of split leaf chamber for measuring each surface individually and simultaneously was conducted using methods in section 2.4.1. All gas exchange parameters were recorded using a Li-Cor 6400XT portable gas exchange system (Li-Cor, Lincoln, Nebraska, USA) following the method in section 2.4.2.

4.2.3.1 Single leaf surface response of g_s and A to a step change in PPFD

The response of net CO₂ assimilation rate (A) and stomatal conductance (g_s) on each leaf surface to a step change in PPFD was carried out as described in method in section 2.4.4.

4.2.3.2 Greased intracellular CO₂ (A/C_i) response curves

A/C_i response curves (net CO₂ assimilation rate (A) to intercellular CO₂ concentration (C_i)) were measured as described in method in section 2.4.3.

4.2.4 Modelling gas exchange parameters

4.2.4.1. Determining the rapidity of stomatal conductance response

The split chamber modelling of gas exchange parameters achieved using the method in section 2.7.

4.2.5 Statistical analysis

Statistics were conducted using R software (www.r-project.org; version 3.5.3). Stomatal density, size and g_{smax} was analysed using the methods in section 2.6.

4.3 Results

4.3.1 Stomatal anatomy

Total flag leaf stomatal density (SD) varied depending upon cultivar (Fig. 4.1), with Soissons and Brompton exhibiting significantly higher total SD compared with all other cultivars ($P < 0.001$). These differences were driven primarily by higher SD on the adaxial leaf surface (Fig. 4.2) with Soissons having significantly ($P < 0.05$) more stomata on this surface (adaxial) compared with all cultivars except Brompton. No significant differences in SD were observed on the abaxial surface. Overall SD was higher ($P < 0.001$) on the adaxial than the abaxial surface considering the interaction between surface and cultivar. Variation in stomatal size was also observed on each leaf surface, Xi19 had significantly larger ($P < 0.05$) stomata than Brompton, on the abaxial surface and on the adaxial surface Brompton, Rialto and Robigus was significantly smaller ($P < 0.05$) than Xi19 and no other differences were observed between cultivars. Together the anatomical features SD and SS were used to calculate the maximum anatomical g_{smax} assuming fully open stomata. Differences in total g_{smax} was observed (Fig. 4.1) between cultivars ($p < 0.001$), with Robigus significantly lower ($p < 0.05$) than Soissons. When g_{smax} was broken down into individual surface values (Fig. 4.2), no differences in g_{smax} on the abaxial surface were observed between cultivars, and on the adaxial leaf surface Robigus was significantly lower than Soissons and Xi19 and Soissons was also greater than Alchemy and Hereward (Fig. 4.2).

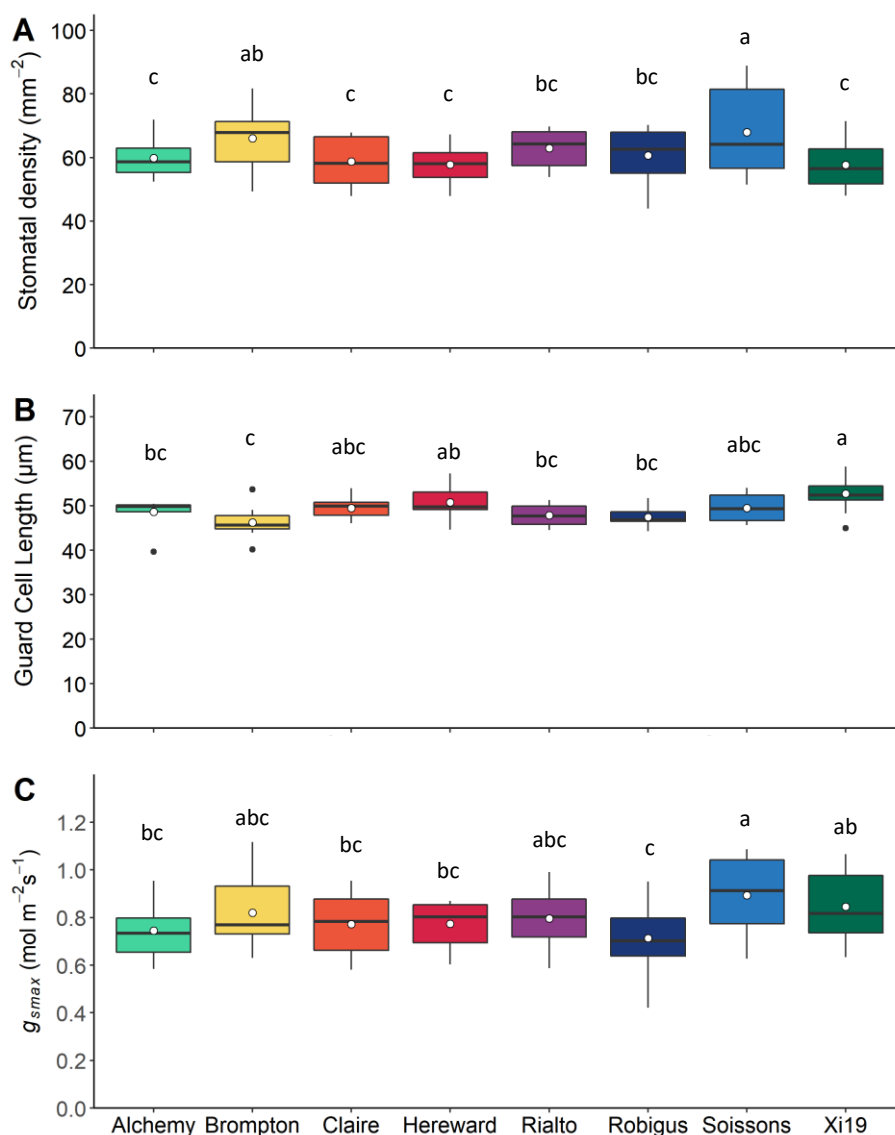


Figure 4.1: Variation (box and whisker plots displaying distribution of biological replicates) and mean (white dot) of total averaged abaxial and adaxial flag leaf stomatal density (A; mm^2), guard cell length representing stomatal size (B; μm) and potential maximum stomatal conductance (C; g_{smax} $\text{mol m}^{-1} \text{s}^{-1}$) calculated from stomatal density and dimensions, for eight MAGIC wheat cultivars (Alchemy, Brompton, Claire, Hereward, Rialto, Robigus, Soissons and Xi19; $n = 6$). Different letters represent statistically significant differences ($P < 0.05$) between means of different cultivars using the results of a Tukey post-hoc test following a one-way ANOVA.

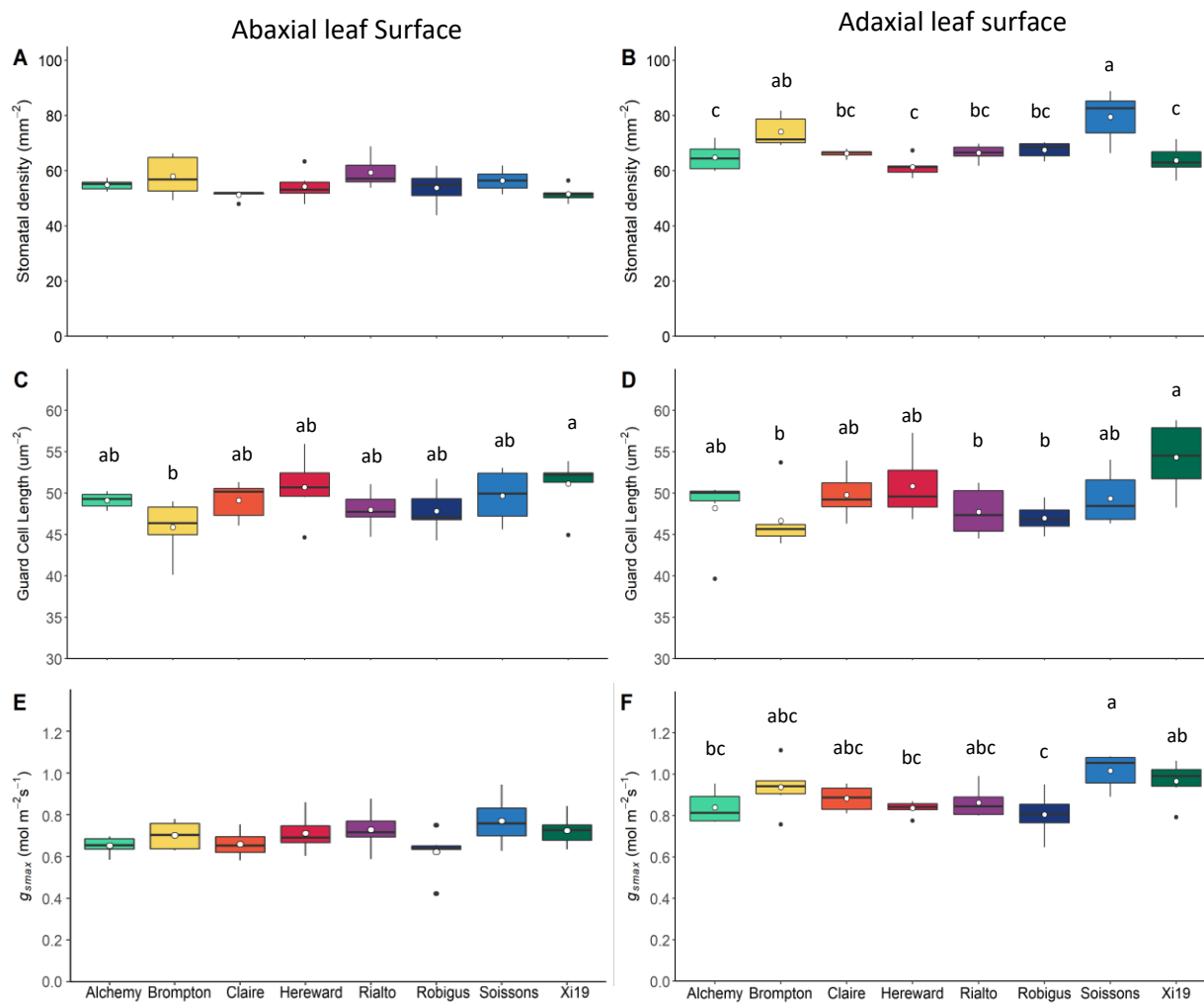


Figure 4.2: Variation (box and whisker plots displaying distribution of biological replicates) and mean (white dot) of flag leaf stomatal density (A and B; mm^2), guard cell length representing stomatal size (C and D; μm) and potential maximum stomatal conductance (E and F; g_{smax} $\text{mol m}^{-2} \text{s}^{-1}$) calculated from stomatal density and dimensions, for the abaxial (A, C and E) and adaxial (B, D and F) leaf surfaces of eight MAGIC wheat cultivars (Alchemy, Brompton, Claire, Hereward, Rialto, Robigus, Soissons and Xi19; $n = 6$). Different letters represent statistically significant differences ($P < 0.05$) between means of different cultivars using the results of a Tukey post-hoc test following a two-way ANOVA.

Further anatomical differences were observed between flag leaf area (LA), thickness (LT) and leaf absorbance (LAb) of the eight cultivars (Fig. 4.3). There were significant differences in flag LA ($p < 0.001$) between all cultivars, the smallest ($p < 0.05$) LA values was observed in cultivar Soissons and the highest ($p < 0.05$) LA values in the cultivar Hereward, a difference of ~ 60 % between the smallest and largest mean values for LA. Flag LT was also different ($P < 0.001$) between cultivars with the highest flag LT ($p < 0.05$) found in the cultivar Brompton and Hereward (Fig. 3; B), and the lowest mean values found in cultivar Soissons, a difference of ~ 35 % between the smallest and largest mean values for LA. Leaf absorption was also significantly different between (sig. $P < 0.001$) between cultivars (Fig. 3.3; C). Although there were differences between all cultivars, Soissons (87.5 %) was substantially lower than the highest cultivar, by 7 %, whereas the differences in range between all other cultivars was only 0.9%, with the lowest at 93.1 % for cultivar Robigus and highest 94.2 % for cultivar Hereward. Cultivar XI19 was significantly different from, the highest cultivar Soissons, and Robigus.

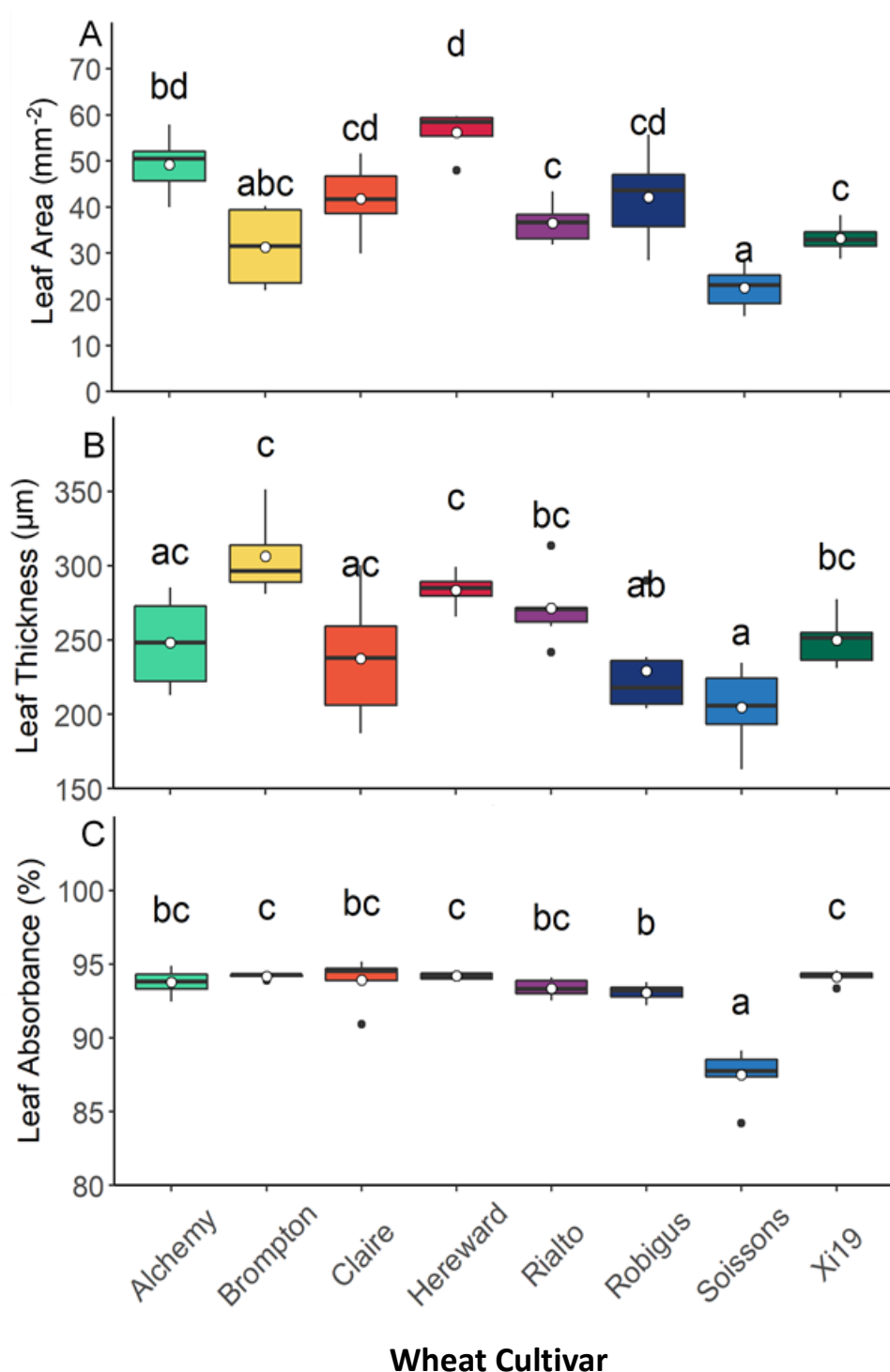


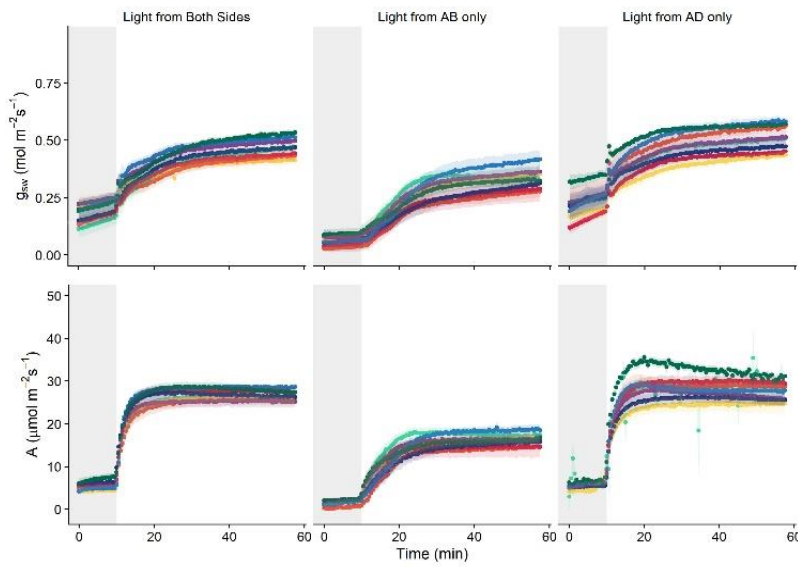
Figure 4.3: Variation (box and whisker plots displaying distribution of biological replicates) and mean (white dot) of flag leaf area (A; mm²), leaf thickness (B; μm) and leaf absorbance (C; %) of eight MAGIC wheat cultivars (Alchemy, Brompton, Claire, Hereward, Rialto, Robigus, Soissons and Xi19). (n = 6). Different letters represent statistically significant differences (P < 0.05) between means of different cultivars using the results of a Tukey post-hoc test following a one-way ANOVA.

4.3.2 Leaf gas exchange

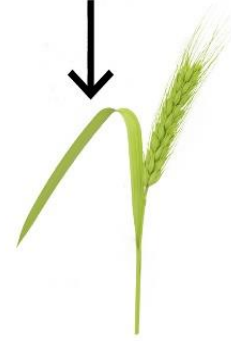
4.3.2.1 Response of g_s and A to a step change in PPFD

To assess the impact of these differences in anatomy on function, flag leaf A and g_s responses to a step a change in irradiance was evaluated. The individual and combined leaf surface response of g_s and A to a single step increase in PPFD (100 to 1000 $\mu\text{mol m}^{-2} \text{s}^{-1}$ PPFD) is shown in Fig. 4.4. There were no significant differences in A and g_s between the eight cultivars for either the adaxial, abaxial or combined leaf surface responses. All cultivars exhibited the expected increase in steady state g_s and A with increased PPFD (Fig. 4.4). There was however a range of steady state rates between the cultivars, for example, adaxial g_s and A were approximately 45 % higher in Xi19 than Brompton. In all cultivars, g_s and A were consistently higher in the adaxial leaf surface responses than the abaxial leaf surface responses, for example, Soissons abaxial A and g_s were typically half of that measured for the adaxial leaf surface A and g_s . The direction of illumination had no consistent effect on the magnitude of A or g_s ; the only exception was adaxial A and g_s , where rates were significantly lower when illuminated from the abaxial surface only, see Fig. 4.4.

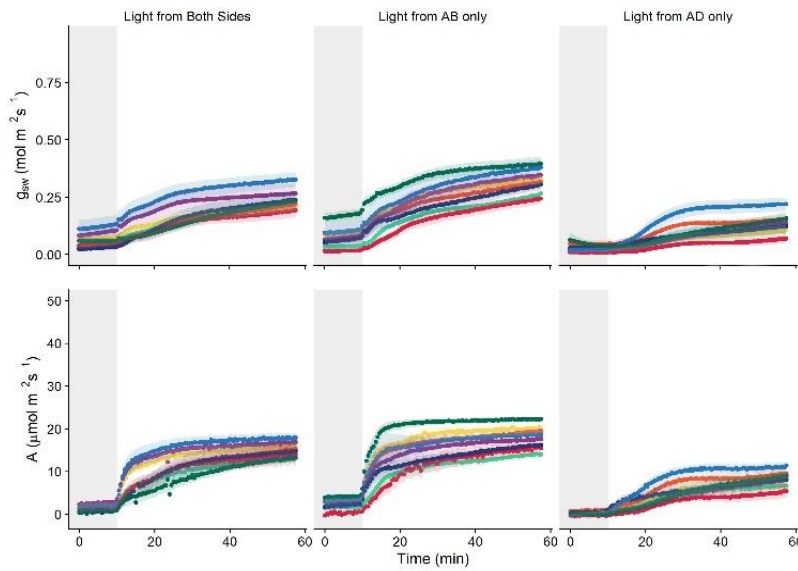
Adaxial leaf surface



Response



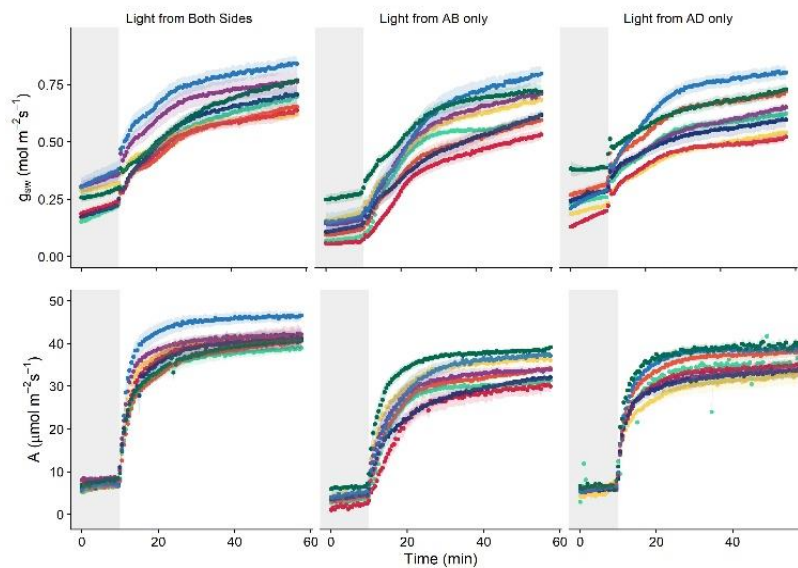
Abaxial leaf surface



Response



Both leaf surfaces



Response

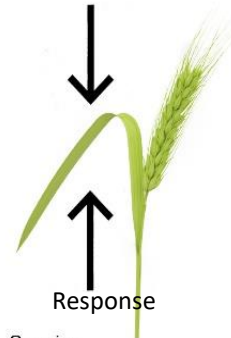


Figure 4.4: Temporal response of stomatal conductance (g_s) and net CO₂ assimilation (A) to a step increase in light intensity for eight MAGIC wheat cultivars (Alchemy, Brompton, Claire, Hereward, Rialto, Robigus, Soissons and Xi19). The headings “Adaxial leaf surface” and “Abaxial leaf surface” denotes data from the adaxial and abaxial leaf surface respectively and “Both leaf surfaces” denotes data from the adaxial and abaxial leaf surface combined. Headings “Light from AD only” and “Light from AB only” represents the lighting regime, where plants were lit from the adaxial and abaxial leaf surface respectively (100 – 1000 $\mu\text{mol m}^{-2} \text{s}^{-1}$ PPFD) and “Light from Both sides” represents plants lit from both sides (50 – 500 $\mu\text{mol m}^{-2} \text{s}^{-1}$ PPFD). Gas exchange parameters (A and g_s) were recorded at 30s intervals for 60 minutes, leaf temperature, CO₂ supply and leaf VPD were maintained at 22°C, 400 $\mu\text{mol mol}^{-1}$ and 1 ± 0.2 KPa respectively. Error ribbons represent mean \pm SE (n = 4-6).

4.3.2.2. Speed of g_s response to a step change in light intensity

As no cultivar specific functional differences were observed, the subsequent experimental results are presented for combined data from all cultivars, focussing on the differences between surface irrespective of cultivar. Figure 4.5 highlights the combined cultivars responses of A and g_s separated between the adaxial and abaxial surfaces for each light treatment. Stomatal conductance was significantly higher on the adaxial leaf surface (AD) and was doubled that observed on the abaxial leaf surface (AB) when the leaf was illuminated from both side (BS) or from the adaxial leaf surface (Fig. 4.5; A). Net CO_2 assimilation (A) followed a similar pattern with the adaxial leaf surface reaching values three times higher than the abaxial leaf surface when illuminated from the adaxial leaf surface (Fig. 4.5; B). In contrast, when the leaf was illuminated from the abaxial leaf surface, there was an equal contribution of A and g_s from each leaf surface. The temporal response of g_s was characterised by an increase in the initial delay (or lag time) before g_s started to rise on the abaxial leaf surface when the leaf was illuminated from the adaxial leaf surface compared to the other light treatments (Fig. 4.5; C). The increase in g_s following the delay was significantly faster on the adaxial leaf surface compared to the abaxial leaf surface under all light treatments, as shown by the difference in time constants (Fig. 4.5;D).

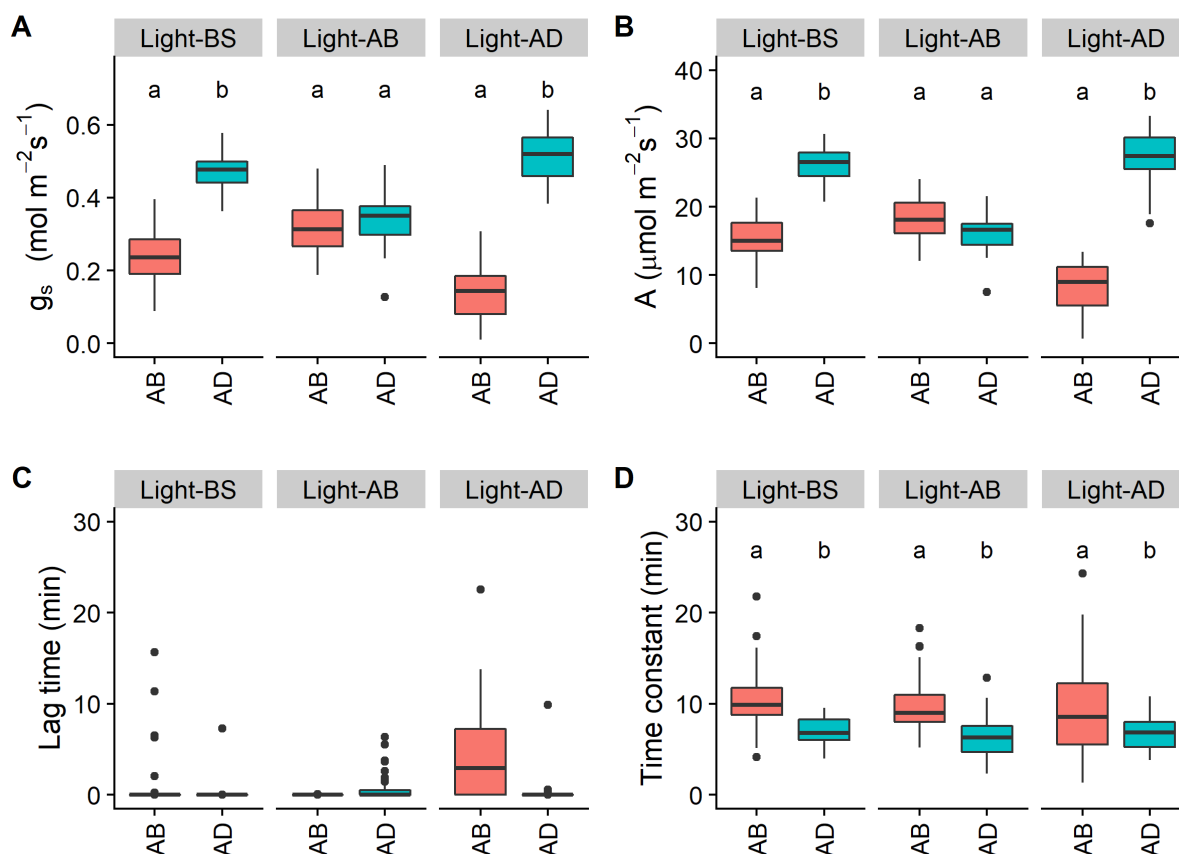


Figure 4.5: Variation (box and whisker plots displaying distribution of biological replicates) of Stomatal conductance (g_s : A), net CO₂ assimilation (A: B), Lag time in stomatal opening (C) in minutes and the time constant of 63% of projected full stomatal opening (D) in minutes for the abaxial (AB) and adaxial (AD) leaf surfaces of eight MAGIC wheat cultivars (Alchemy, Brompton, Claire, Hereward, Rialto, Robigus, Soissons and Xi19) to a single step change in PPFD. Headings “Light-AD” and “Light-AB” (grey banner) represents the lighting regime, where plants were lit from the adaxial and abaxial leaf surface respectively ($100 - 1000 \mu\text{mol m}^{-2} \text{s}^{-1}$ PPFD) and “Light-BS” (grey banner) represents plants lit from both sides ($50 - 500 \mu\text{mol m}^{-2} \text{s}^{-1}$ PPFD). Different letters represent statistically significant differences ($P < 0.05$) between means of different leaf surfaces ($n = 4-6$).

To further assess the contribution of the abaxial leaf surface stomata to g_s and A , and to determine if adaxial leaf surface stomatal behaviour could compensate for any changes in abaxial leaf surface g_s , we examined gas exchange responses following a step change in light intensity when vertical gaseous flux from the abaxial surface was prevented by blocking stomata with grease applied to the leaf surface (Fig. 4.6). Two cultivars were selected (Brompton and Xi19; Fig. 4.6) based on the fact that Brompton consistently showed different anatomical features and g_{smax} values compared with Soissons and Xi19, and Xi19 was chosen as it was the cultivars that was most different to Brompton in terms of anatomy and physiological responses and a cultivar without awns.

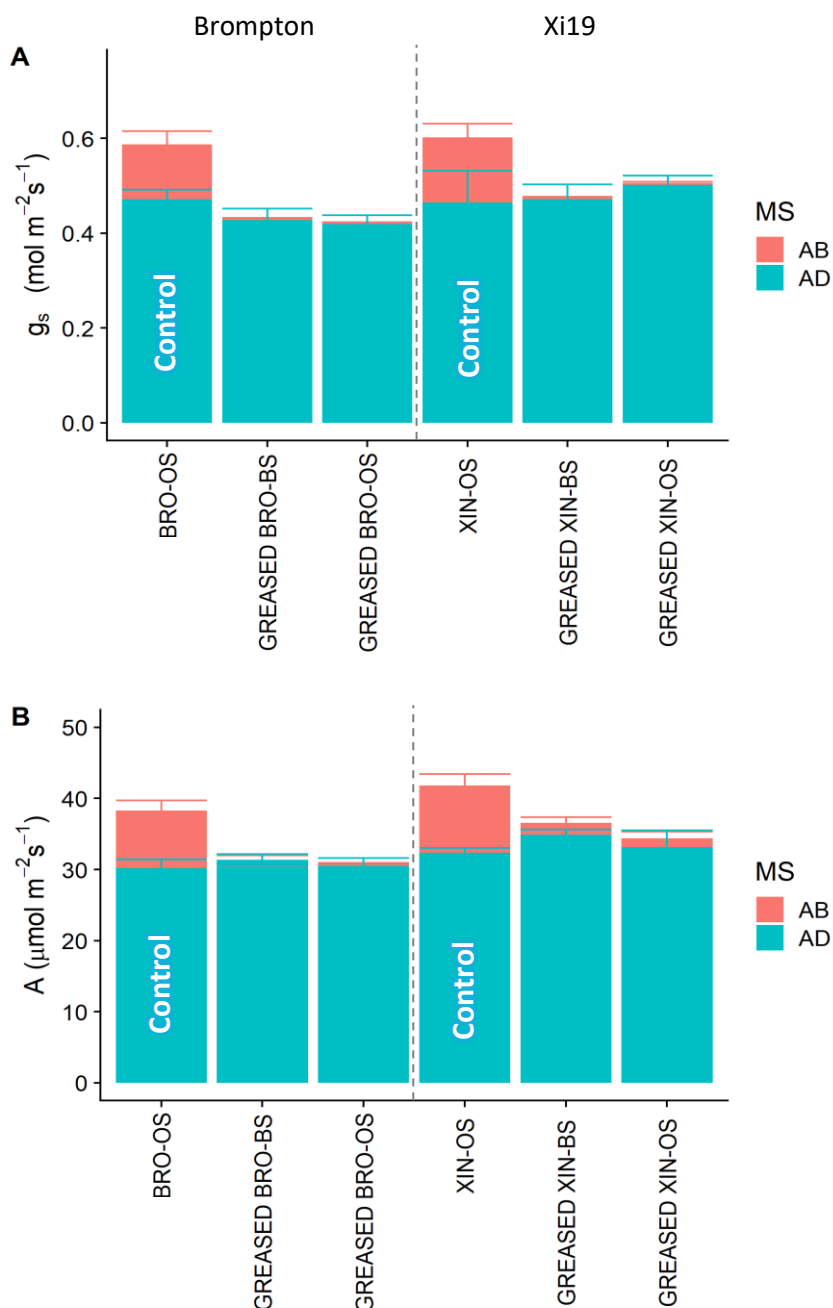


Figure 4.6: Stomatal conductance (g_s ; A) and net CO_2 assimilation (A ; B) for two selected MAGIC wheat cultivars; Brompton and XI19. Control OS bars represents the mean of the final 5 response points of A and g_s to a single step change in PPFD ($100 - 1000 \mu\text{mol m}^{-2} \text{s}^{-1}$ PPFD) for the adaxial leaf surface leaving the abaxial leaf surface with no direct light. Greased BS bars represents the mean of the final 5 response points of A and g_s to a single step change in PPFD ($50 - 500 \mu\text{mol m}^{-2} \text{s}^{-1}$ PPFD) on both leaf surfaces with the abaxial leaf surface covered with silicone grease to prevent gaseous flux from the abaxial surface by blocking stomata. Greased OS bars represents the mean of the final 5 response points of A and g_s to a single step change in PPFD ($100 - 1000 \mu\text{mol m}^{-2} \text{s}^{-1}$ PPFD) for the adaxial leaf surface with the abaxial leaf surface greased to prevent gaseous flux from the abaxial surface by blocking stomata. Error bars represent mean 95 % confidence intervals ($n = 4$).

4.3.2.4. intracellular CO₂ (A/C_i) response curves

The response of net CO₂ assimilation (A) as a function of internal [CO₂](C_i ; A/C_i – Fig. 4.7) was performed on the flag leaf for cultivar Brompton. All replicates exhibited the expected increase in A with increased C_i up to a certain point before reaching a plateau. The results in Fig. 4.7 displayed the ungreased replicates reached the highest A . When the adaxial leaf surface was covered with silicone grease to prevent gaseous flux from the adaxial surface by blocking stomata, the lowest A values were observed. When the abaxial leaf surface was greased the A values fell between the lower adaxial greased values and the higher ungreased values. Final values of A (at 1500 $\mu\text{mol mol}^{-1} C_i$ and 2000 $\mu\text{mol m}^{-2} \text{s}^{-1}$ PPF) reached $\sim 41 \mu\text{mol m}^{-2} \text{s}^{-1}$ for the ungreased replicates, $\sim 37 \mu\text{mol m}^{-2} \text{s}^{-1}$ for the abaxial greased replicates and $\sim 30 \mu\text{mol m}^{-2} \text{s}^{-1}$ for the adaxial replicates, a decrease of $\sim 27 \%$ from the ungreased to the adaxial greased A values.

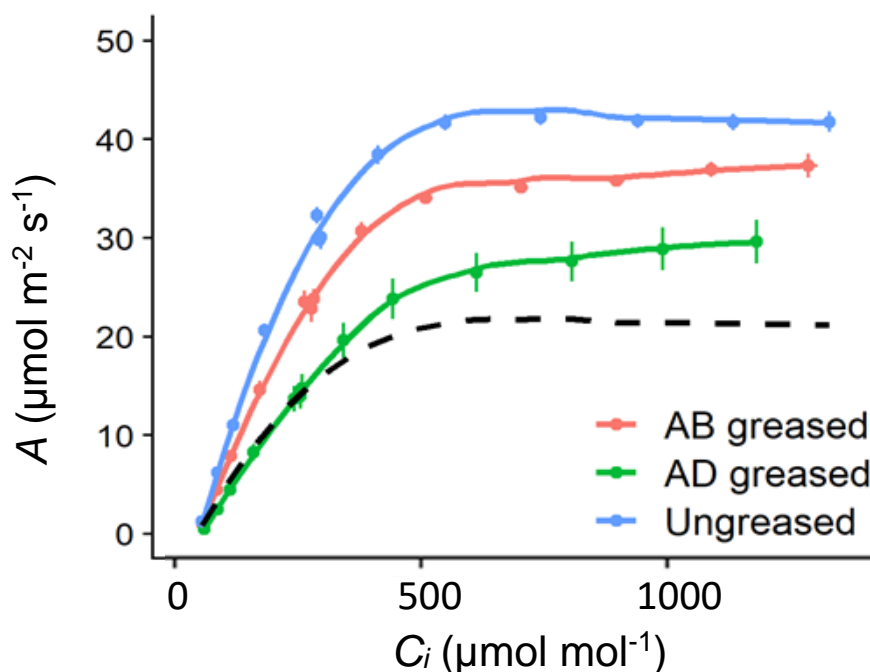


Figure 4.7: The response of net CO_2 assimilation (A) to intercellular $[\text{CO}_2]$ (C_i) between 50 and 1500 $\mu\text{mol m}^{-2} \text{s}^{-1}$ in 2000 $\mu\text{mol m}^{-2} \text{s}^{-1}$ PPFD for wheat cultivars Brompton. Blue points (and lines) indicate standard A/C_i curve (ungreased), with the black dotted lines indicating half the standard A/C_i curve (ungreased). The term 'greased' refers to the covering with silicone grease to prevent gaseous flux by blocking stomata. The pink points (and lines) represent the abaxial leaf surface being 'greased' showing gas exchange from the adaxial leaf surface only while the green points (and lines) represent the adaxial leaf surface being 'greased' showing the gas exchange from the abaxial leaf surface only. Error bars represent mean \pm SE ($n = 5-7$).

4.4 Discussion

Stomatal conductance (g_s) is determined by both anatomical features, including density and size, as well as functional responses to changing external and internal cues (Lawson *et al.*, 2010) and considerable variation in both is known to exist between and within species (Ticha, 1982; Pospíšilová & Šantrůček, 1994; Weyers & Lawson, 1997; Lawson & Blatt, 2014). It has been demonstrated that SD is influenced by light (Gay & Hurd, 1975), $[CO_2]$ (Woodward, 1987), water status (Xu & Zhou, 2008) and other environmental stimuli in most likely a hierarchical manner (Stevens *et al.*, 2020). Furthermore, large difference in the distribution of stomata between abaxial and adaxial leaf surfaces is well studied, although the functional differences in leaf surface is less well established. The functional advantages or disadvantage of such differences in distribution are further complicated by considerable heterogeneity across individual leaf surface in SD (Smith *et al.*, 1989a; Weyers & Lawson, 1997; Weyers *et al.*, 1997) and patterning (Lehmann & Or, 2015) that have consequences for functional responses (Lawson *et al.*, 1998a; Dow & Bergmann, 2014; de Boer *et al.*, 2016) and these patterns are not necessarily identical between surfaces of amphistomatous leaves. Amphistomaty has previously been reported to have greater capacity for gaseous diffusion by increased CO_2 supply to the mesophyll (Parkhurst, 1978; Beerling & Kelly, 1996; Richardson *et al.*, 2020) by the reduction in the pathway of CO_2 from atmosphere to site of photosynthesis (Parkhurst, 1978, 1994; Franks & Beerling, 2009) and increasing the amount of epidermis allocated to stomata (Muir, 2018). Amphistomaty has also previously been reported to have higher photosynthetic rates and high water use efficiency (Richardson *et al.*, 2017) associated with high g_s to CO_2 , an advantage to plants in high light and temperature environments (Muir, 2019).

Here we have shown that there is considerable variation in anatomical features specifically SS and SD on both leaf surfaces of the eight wheat cultivars that account for 80% of the United Kingdom single nucleotide polymorphism variability (Gardner *et al.*, 2016) represent the diversity of UK wheat germplasm. The anatomical differences did not translate into any differences in functional g_s responses between the cultivars (Fig. 4.4). When we examined g_s responses to a step increase in PPFD there were no significant differences between cultivars in the overall A and g_s values attained or the kinetics of these responses.

As no cultivar functional differences were observed, individual responses were combined to focus on the differences between the two leaf surfaces. What was immediately obvious was the significantly ($p < 0.05$) higher g_s and A achieved on the adaxial leaf surface compared with the abaxial leaf surface (when illuminated from either both sides or the adaxial surface only). This could be due to a higher photosynthetic capacity in the mesophyll cells associated with the adaxial leaf surface compared with those associated with the abaxial leaf surface, as has previously been shown for maize (Driscoll *et al.*, 2006). A higher photosynthetic capacity on the adaxial leaf surface would require a greater CO_2 flux into the leaf and would therefore require a higher g_s to facilitate this (Lawson & Blatt, 2014; Lawson & Matthews, 2020) as observed in Fig. 4.5. Furthermore, no differences in abaxial g_s or A were observed when illumination was received on both sides of the leaf surface ($500 \mu\text{mol m}^{-2} \text{s}^{-1}$ PPFD each surface), compared with illumination received on the adaxial leaf surface only ($1000 \mu\text{mol m}^{-2} \text{s}^{-1}$ PPFD), suggesting photosynthesis is light saturated at $500 \mu\text{mol m}^{-2} \text{s}^{-1}$ PPFD and/or diffusionally constrained at these g_s values. These findings also imply limited contribution from abaxial g_s in the supply of CO_2 for adaxial assimilation. Abaxial g_s and A rates (Fig. 4.5), when illuminated on both leaf surfaces,

were greater than when illumination was received on only the adaxial leaf surface, as though demonstrating that the abaxial leaf surface stomata and associated mesophyll cells were limited by light intensity (or spectral quality), due to self-shading and receiving transmitted light only on this surface (Wang *et al.*, 2008b). When illuminated from the abaxial leaf surface only (Fig. 4.5), A and g_s values were approaching equal values to the abaxial leaf surface observed when illumination was received on both sides. These findings further confirm a likely lower photosynthetic capacity in mesophyll cells associated with the abaxial leaf surface compared with the adaxial leaf surface. Whilst the lower A rates observed on the abaxial leaf surface when light was received on both leaf surfaces could be the result of the reduction in light (from 1000 to 500 $\mu\text{mol m}^{-2} \text{s}^{-1}$ PPFD) reaching the mesophyll cell associated with the abaxial leaf surface (Wang *et al.*, 2008b) and/or greater diffusion constraints due to the reduced g_s .

Previous studies have demonstrated different stomatal sensitivities to both incident and transmitted light on the different leaf surfaces (Turner & Singh, 1984; Wang *et al.*, 2008b) whilst other have suggested no such differences in sensitivity (Yera *et al.*, 1986). Several studies have also demonstrated a co-ordinated stomatal response between the upper and lower surfaces (Yera *et al.*, 1986) whilst other studies have demonstrated that stomata on the two surfaces behave independently (Mott *et al.*, 1993). Furthermore, several studies that have demonstrated co-ordinated responses between stomata on the adaxial and abaxial surface have suggested that stomata in these plants do not respond to light alone and that additional factors in the bulk tissue contribute to this co-ordinated stomatal opening responses to meet the photosynthetic requirements of the whole leaf for CO_2 (Yera *et al.*, 1986). The idea of a mesophyll driven metabolite or signal that acts as a messenger to signal to stomatal

opening was first proposed by Dittrich & Raschke (1977) and supported by Wong *et al.*, (1979). Since then several studies have attempted to elucidate the signal (e.g. Lee & Bowling, 1992) and various suggestions have been put forward including vapour ion signals, (Mott *et al.*, 2008; Sibbersen & Mott, 2010) sucrose (Outlaw & Tarczynski, 1984; Outlaw & De Vlieghere-He, 2001; Daloso *et al.*, 2016) along with many others (Fujita *et al.*, 2013; Lawson *et al.*, 2014; Kottapalli *et al.*, 2018).

Our findings do not support the suggestion of a co-ordinated stomatal responses between the two leaf surfaces as proposed by Yera *et al.* (1986) to meet the photosynthetic requirements of the whole leaf. To examine this idea cultivars Brompton and Xi19 were further examined using silicone grease to prevent vertical gaseous flux by blocking stomata on the abaxial leaf surface to examine the impact of a step change in irradiance on the g_s and A response (Fig. 4.6) when illuminated from both surfaces ($500 \mu\text{mol m}^{-2} \text{s}^{-1}$ PPFD) or the adaxial surface ($1000 \mu\text{mol m}^{-2} \text{s}^{-1}$ PPFD). No significant difference in adaxial g_s or A were observed between the greased protocols (Fig. 4.6) and the non-greased control protocol indicating that the abaxial gaseous fluxes contribute very little to the adaxial leaf surface A . From these findings it appears most likely that both surface act independently from each other and supports the earlier observations that adaxial A and g_s is substantially greater than abaxial, however both are essential in their contribute to the overall leaf A and g_s . This does not agree with the findings of Mott and Peak (2018) who demonstrated that stomata on the abaxial surface opened further when gas exchange on the adaxial surface was blocked. The fact that no differences in A were observed when illuminated with 500 or $1000 \mu\text{mol m}^{-2} \text{s}^{-1}$ PPFD further supports the idea that these are light saturated (or diffusional constrained at the observed g_s values). The high rate of A particularly on the upper surface would suggest that the vertical profile of $[\text{CO}_2]$ through

the leaf will be relative high due to high consumption rates in the upper palisade layer associated with the adaxial surface (Evans *et al.*, 2009). Studies by Lawson & Morison (2004) and Morison & Lawson (2007) examined lateral diffusion through the leaf and demonstrated that any flux was greatly constrained by the photosynthetic consumption of CO₂ along the path, and this was more important than any anatomical constraints such as vein spacing or extensions, cell size, spacing and airspace volume (Lawson & Morison, 2006), and that these fluxes were in the same order of magnitude as vertical conductance (Evans *et al.*, 2009). The relative high *A* rate observed in wheat (for both surfaces) would suggest that high CO₂ consumption rate through the vertical pathway would limit CO₂ supply from the adaxial surface to the abaxial surface and *vice versa*.

To evaluate potential vertical fluxes, we examine *A* as a function of internal CO₂ concentration in leaves a protocol was used with either the adaxial or abaxial surface greased to prevent gaseous flux by blocking stomata (Fig. 4.7) and compared with a non-greased control. As expected, *A* increased with increasing *C_i* up to a certain concentration, after which maximum *A* was reached. When either of the surface were greased to prevent vertical CO₂ fluxes through that surface, *A* was reduced, and this reduction was greater when the adaxial surface was greased due to the higher photosynthetic capacity. However, it was apparent that at 2000 μmol m⁻² s⁻¹ PPFD and 1500 μmol mol⁻¹ each surface was both light and CO₂ saturated with only a very small amount of CO₂, if any, able to be “pushed” from one surface and used by the other. This demonstrates that the higher *g_s* in the adaxial leaf surface is coupled with a higher adaxial photosynthetic capacity resulting in higher *A* and potentially higher leaf cooling.

Many studies have reported differences in anatomy, such as SD and SS between the two leaf surfaces of amphistomatous leaves (Royer, 2001; Taylor *et al.*, 2012; Vergara-Díaz *et al.*, 2018; Drake *et al.*, 2019) as well as function (Mott & O'Leary, 1984; Soares *et al.*, 2008; Wang *et al.*, 2008b; Tominaga & Kawamitsu, 2015; Richardson *et al.*, 2017, 2020; Mott & Peak, 2018; Tominaga *et al.*, 2018; Xiong & Flexas, 2020), and suggested the advantages of amphistomaty over hyper/hyper stomatous leaves in high light and temperature environments (Mott *et al.*, 1982; Muir, 2019). To our knowledge this is the first study that measures the simultaneous but separate gas exchange of two leaf surfaces in real time on wheat. Uncoordinated function of the two leaf surfaces have previously been attributed to adaptations to environments of high light and temperature, but they could also be an adaptation to leaf angle.

In the early stage of wheat flag leaf development, the leaf emerges vertically to the plant with both leaf surfaces exposed to direct sunlight and therefore it would be expected that both leaf surfaces contributed to overall leaf photosynthesis. However, later in development when the Inflorescence (ear) start to emerge (~ GS 50-55), the flag leaf drops to a horizontal position and therefore most irradiance will be intercepted by the adaxial leaf surface. This would support higher SD and g_s on the adaxial leaf surface, to not only support a higher A , as well facilitate a more effective transpiration for leaf cooling to ensure an optimal leaf temperature for photosynthesis. Wheat leaf angle could therefore have an effect on photosynthesis which is important for grain filling; it has been estimated that a large proportion, up to 45%, of the grain carbohydrate is derived from the flag leaves (Stoy, 1963; Lupton, 1972; Stamp & Herzog, 1976) while 25 % comes from ear photosynthesis itself (Simkin *et al.*, 2020). Additionally, the adaxial surface of the flag leaf would benefit further from higher rates

of g_s due to the fully expanded flag leaf being situated at the top of the canopy where it intercepts higher light intensities and differing qualities of spectral light to that of the lower leaves of the plant throughout the canopy, and that of the differing leaf surfaces of lower leaves (Gooding *et al.*, 2000).

The results from this chapter indicate that both abaxial and adaxial leaf surfaces are crucial to the overall flag leaf contribution of g_s and A , albeit unequal contributions, and if gas exchange from either surface is impeded the leaf will not be able to compensate for the loss. Future experiments include the study of wheat function on the separate leaf surfaces in response to differing CO_2 , light and temperature treatments, and to follow both the results of this study and those of future studies into quantitative trait loci analysis (Ishimaru *et al.*, 2001). The interest in understanding plant adaptations are to assist in targeting traits for enhanced water-use efficiency and, moreover, crop productivity on individual leaf surfaces which is hopefully a prerequisite for a suite of leaf traits aimed at improving overall productivity in wheat.

CHAPTER 5

Heterogeneity in anatomical features and functional traits in landraces and wheat wild relatives

5.1. Introduction

The FOA report (2015) predicted the global demand for food is to increase by 50% by the year 2030 and therefore greater priority is needed in agricultural research and development to achieve the yield and productivity gains needed with a changing climate (Wheeler & von Braun, 2013). Rice, wheat, and maize staple foods for 80 % of the world population (Maclean et al., 2013). Wheat, is one of the largest primary commodities and a major renewable resource for food, feed, and industrial raw materials (Charmet, 2011). Global production reaches seven hundred million tons annually and provides approximately 20% of the total global available calories (2009-2011) (FOA, 2014) .

In recent years, increases in global wheat yields have slowed, averaging between 0 and 1.1% annually, but an increase of 1.6 and 2.4% per annum over the next 50 y is needed to keep up with demand (Dixon *et al.*, 2009). If rates of crop yield improvement per hectare are only maintained rather than increased in the future, supply will not keep up with demand (Brisson *et al.*, 2010; Ray *et al.*, 2013; Long *et al.*, 2015). Not only do crop yields need to increase, they need to increase without encumbering land and water resources and without overloading the environment with an excess of fertilisers or nitrogen-rich manure (Janssen *et al.*, 2014; Nair, 2014).

In the past decades breeding efforts have increased yields by focusing on a combination of genetic improvement and selecting genotypes that partitioned more biomass into harvested product, resulting in high-yielding varieties, most notably the semi-dwarf wheat species and matched these with a better management of pest and diseases and higher applications of fertilisers (Semenov *et al.*, 2012; Long *et al.*, 2015). The traits that drove yield increases appear to have reached a genetic 'bottleneck' and have modest remaining potential for further increases. This reduction

in genetic diversity among the elite wheat (EW) species used for food, feed and industrial raw materials has been initiated by the domestication and intensive selection for agronomically important traits over the past 10000 y (Charmet, 2011; Faris, 2014; McAusland *et al.*, 2020). One future option for increasing wheat yield depends on understanding and exploiting the extensive natural variation in wild relatives of modern wheat. Wheat wild relatives (WWR) represent an underutilized source of genetic and phenotypic diversity that are of interest to breeders due to their wide adaptation to different environments (McAusland *et al.*, 2020).

The development of western agriculture originated in the 'Fertile Crescent' situated between south-eastern Turkey and northern Syria approximately 10,000 years ago, after the last ice age, lasting several centuries (Heun *et al.*, 1997; Lev-Yadun *et al.*, 2000; Salamini *et al.*, 2002; Riehl *et al.*, 2013; Faris, 2014). The understanding of the evolution and domestication of wheat has come from assembling evidence from botany, genetics, archaeology, and a knowledge of the present distribution of grass species. Modern wheat domestication occurred from polyploidization, referring to the multiplication of a complete chromosome set, resulting in multi-copy genes that exist as paralogs to each other to establishing useful agronomic traits (Hancock, 2005; Renny-Byfield & Wendel, 2014; Zhang *et al.*, 2019) see figure 5.1. The evolution of wheat from the primitive to the cultivated forms saw the acquisition of valuable agronomic traits such as non-brittle rachis, which limited the natural seed dispersal mechanisms, glume tenacity for free-threshing, spikelet articulation, awn development and an increase in grain size (see Figure 5.2), which allowed for mechanised cultivation on a large scale (Kerber & Rowland, 1974).

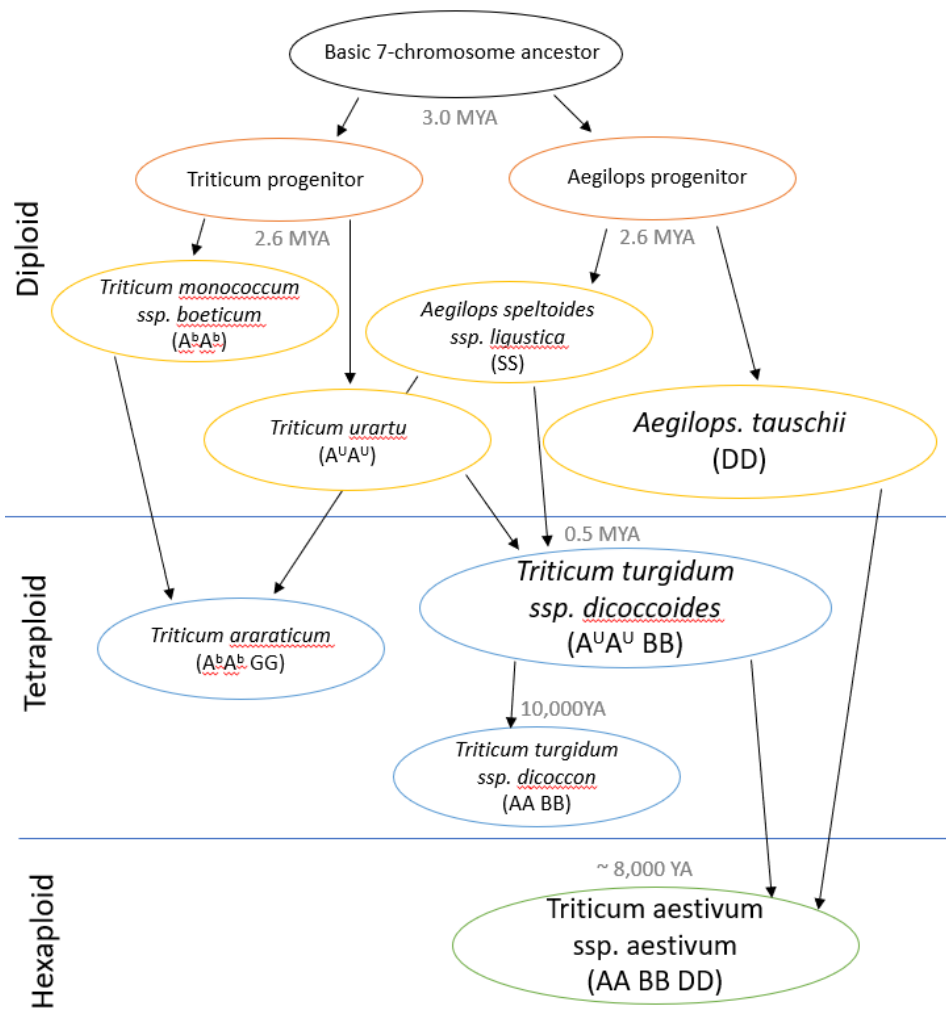


Figure 5.1. The evolutionary lineages involving Triticum wheat species with sub-genome lettering. Diploid, tetraploid, and hexaploid species are separated by blue lines. Grey wording indicates time passed since event YA = years ago, MYA = million years ago (reproduced from Faris, 2014)

Wheat is a ubiquitous crop with nearly 800,000 accessions (Crop Wild Relative Diversity, 2019) which have evolved, before the domestication events, in diverse habitats and climates acquiring traits depending on their environmental origin. These wild relatives of modern wheat may harbour traits that are unavailable in the existing EW germplasm. To improve future productivity and resilience in EW it may benefit from looking at wheat wild progenitors which grew and thrived in environment that modern day wheat find difficult, such as high temperatures, low water supply, high CO₂ and maybe have the ability to resist current diseases (Faris, 2014; McAusland et al., 2020) as an unexploited resources to explore wilds wheat traits for modern breeding programmes and relatives. This study assessed phenotypic variation in photosynthetic, stomatal behaviour, and morphological traits such as stomatal size and density and related this productivity and yield in wild wheat progenitors and relatives such as *Aegilops tauschii*, *Triticum turgidum* ssp. *Dicoccoides* and *Triticum turgidum* ssp. *Dicoccon*, and compared to an EW variety, *Triticum aestivum* ssp. *Xi19*.

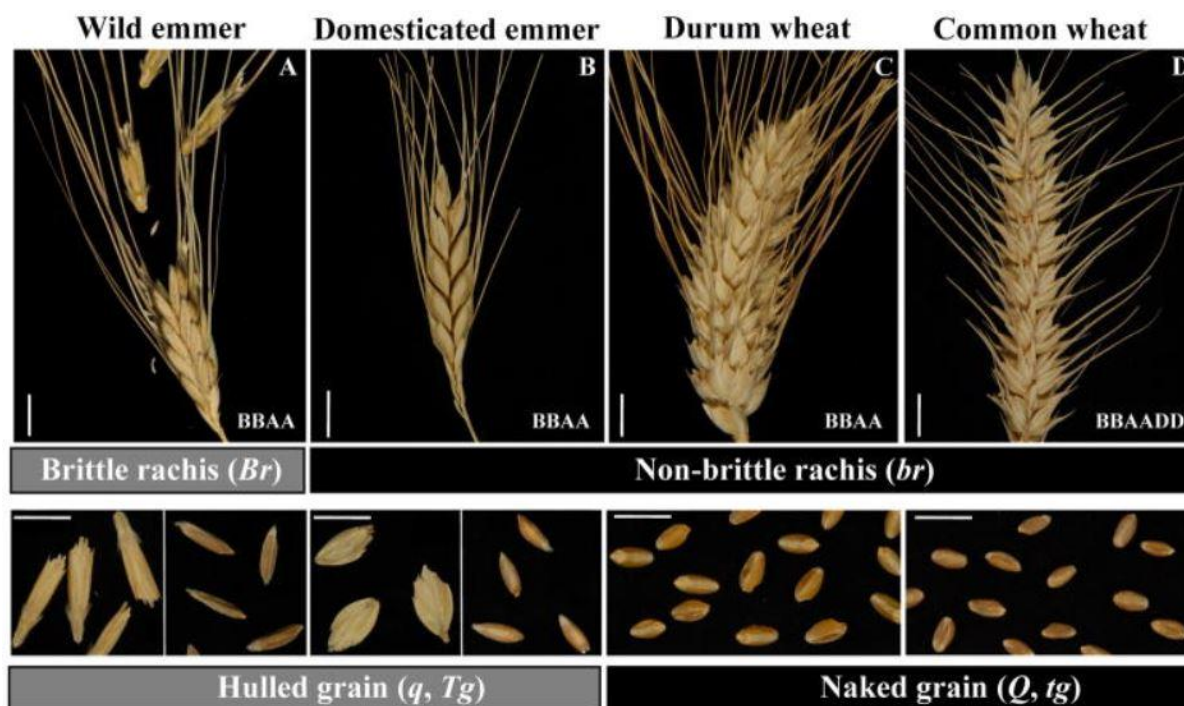


Figure 5.2. Wheat spikes showing a brittle rachis (A), non-brittle rachis (B to D), hulled grain (A and B), and naked grain (C and D). Wild emmer wheat (*T. dicoccoides*; A), domesticated emmer (*T. dicoccum*; B), durum (*T. durum*; C), and common wheat (*T. aestivum*; D). White scale bars represent 1 cm. Letters at the lower right corner indicate the genome formula of each type of wheat. Gene symbols: Br = brittle rachis, Tg = tenacious glumes, and Q = square head (Image from Dubcovsky & Dvorak, 2007)

The first aim of the work presented in this chapter was to assess the extent of phenotypic variation in morphological traits between the 16 wild wheat relatives (WWR) and 1 elite wheat (EW) species, see figure 5.1 and Table 5.1. Secondly, to ascertain whether there is variation in g_{smax} between the 16 wild wheat relatives (WWR) and 1 elite wheat (EW). Secondly, to evaluate the impact of any phenotypic variation on the rapidity of stomatal responses and its effect on CO₂ assimilation, and photosynthetic capacity. The hypothesis being that although the 17 species will be grown in an similar environment, there will be variation within the stomatal size and density between species, and this will influence g_{smax} and stomatal kinetics and photosynthetic capacity between the different species.

5.2 Materials and Methods

This section summarises methods specific to this chapter and modifications made to protocols outlined in Chapter 2 – “Materials and Methods”.

5.2.1 Plant material and growth conditions

Wheat species (Table 5.1) were grown in the BASF Crop solutions facilities in Ghent, Belgium, with slight adaptations to the method in section 2.1 (see below).

Table 5.1 Species selected for this chapter including ploidy and common name. Species abbreviation is how the species will be referred to in the text.

Species Abbreviation	Species	Common Name	Ploidy
Xi19	<i>Triticum aestivum</i>	Common or Bread Wheat	Hexaploid
AE 146	<i>Aegilops tauschii</i>	Goatgrass or rough-Spike Hard Grass	Diploid
AE 472/87	<i>Aegilops tauschii</i>	Goatgrass or rough-Spike Hard Grass	Diploid
IG 48509	<i>Aegilops tauschii</i>	Goatgrass or rough-Spike Hard Grass	Diploid
IG 48514	<i>Aegilops tauschii</i>	Goatgrass or rough-Spike Hard Grass	Diploid
IG 48556	<i>Aegilops tauschii</i>	Goatgrass or rough-Spike Hard Grass	Diploid
KU 2010	<i>Aegilops tauschii</i>	Goatgrass or rough-Spike Hard Grass	Diploid
KU 2018	<i>Aegilops tauschii</i>	Goatgrass or rough-Spike Hard Grass	Diploid
KU 2036	<i>Aegilops tauschii</i>	Goatgrass or rough-Spike Hard Grass	Diploid
KU 2043	<i>Aegilops tauschii</i>	Goatgrass or rough-Spike Hard Grass	Diploid
KU 2056	<i>Aegilops tauschii</i>	Goatgrass or rough-Spike Hard Grass	Diploid
KU 2636	<i>Aegilops tauschii</i>	Goatgrass or rough-Spike Hard Grass	Diploid
TRI 11502	<i>Triticum dicoccoides</i>	Wild Emmer	Tetraploid
TRI 17137	<i>Triticum urartu</i>	Red Wild Einkorn	Diploid
TRI 17162	<i>Triticum urartu</i>	Red Wild Einkorn	Diploid
TRI 18510	<i>Triticum araraticum</i>	Araratian or Armenian Wild Emmer	Tetraploid
TRI 3432	<i>Triticum dicoccon</i>	Emmer	Tetraploid

In the BASF Crop solutions facilities, the plants were germinated and vernalised in the same way using an in house made 60/40 peat-based sowing and cutting soil (including NPK Compound Fertilizer 12-14-24 (0.8 kg m⁻³)) and transferred into 4 l pots using a peat-based, boron free potting soil (including NPK Compound Fertilizer 12-14-24 (2 kg m⁻³)) and grown in glasshouse conditions between the months of September and

November 2018. Plants were well watered throughout the day using a drip irrigation system, watering to the roots of plants. In the glasshouse, supplementary high-pressure sodium vapor lighting was provided with (table level) $200 \mu\text{mol m}^{-2} \text{s}^{-1}$ PPFD (supplied by Master Greenpower CGT 400 W E40 bulbs) when external solar radiation fell below 8 K LUX (PPFD of $\sim 500 \mu\text{mol m}^{-2} \text{s}^{-1}$), over a 15-hour photoperiod, air temperature was maintained at $20 \text{ }^\circ\text{C} \pm 3^\circ\text{C}$ during the day and $17 \text{ }^\circ\text{C} \pm 3 \text{ }^\circ\text{C}$ at night.

5.2.2 Leaf and stomatal characteristics

5.2.2.1 Leaf epidermal impressions

Leaf epidermal impressions were generated following the method in section 2.2.1. All impressions were taken from fully expanded single leaves of similar positions at the middle of the flag leaf, on both the abaxial and adaxial leaf surfaces, avoiding major veins and leaf edges before anthesis (growth stage 49-59). Impressions were taken from the same lead tillers of six wheat plant replicates per species.

5.2.2.2 Stomatal anatomical measurements

Stomatal density, guard cell length and pore length were measured via light microscopy (Olympus BX60, Southend-on-Sea, Essex, UK) following the methods in sections 2.2.2 and 2.2.3 respectively. Guard cell length and pore length measurements were used to generate potential anatomical maximum stomatal conductance ($g_{\text{smax}} \text{ mol m}^{-2} \text{ s}^{-1}$) following the calculation in method 2.2.4.

5.2.3 Leaf gas exchange

All gas exchange parameters were recorded using a Li-Cor 6400XT portable gas exchange system (Li-Cor, Lincoln, Nebraska, USA) following the method 2.2

5.2.3.1 PPFD-step measurements

The response of net CO₂ assimilation rate (A) and stomatal conductance (g_s) to a step change in photosynthetic photon flux density ($PPFD$) was carried out as described in method 2.3.1.

5.2.3.2 Intracellular CO₂ response curves (A/C_i)

A/C_i response curves (net CO₂ assimilation rate (A) to intercellular CO₂ concentration (C_i)) were measured as described in method 2.3.2.

5.2.4 Modelling gas exchange parameters

5.2.4.1. Estimating photosynthetic capacities

The maximum rate of electron transport for RuBP regeneration (J_{max} ; $\mu\text{mol m}^{-2} \text{s}^{-1}$), the maximum velocity of Rubisco for carboxylation (V_{cmax} ; $\mu\text{mol m}^{-2} \text{s}^{-1}$) and the light and CO₂ saturated assimilation rate (A_{max} ; $\mu\text{mol mol}^{-1}$) at 1500 $\mu\text{mol mol}^{-1}$ CO₂ and 1500 $\mu\text{mol m}^{-2} \text{s}^{-1}$ PPFD were estimated from the A/C_i response curves using method 2.5.1.

5.2.4.2. Determining the rapidity of stomatal conductance response

The rapidity of the stomatal response following a step change in light intensity was assessed using method 2.5.3.

5.2.4.3. Determining the rapidity of net CO₂ assimilation response

The rapidity of the photosynthesis response following a step change in light intensity was assessed using method 2.5.4.

5.2.5 Statistical analysis

Statistics were conducted using R software (www.r-project.org; version 3.5.3) following the methods in section 2.6.

5.3. Results

5.3.1 Stomatal anatomy

Stomatal impressions were made from each of the 17 wheat species to measure stomatal density (SD; mm^{-2}), guard cell length (GCL; μm) as a proxy for stomatal size (SS), and pore length (PL; μm) and were subsequently used to calculate the maximum potential anatomical g_s ($g_{s\text{max}}$; $\text{mol m}^{-2} \text{s}^{-1}$). Densities (Figures 5.3 and 5.4), SS (Figures 5.5 and 5.6) and $g_{s\text{max}}$ (Figures 5.8 and 5.9) were compared between species and leaf surfaces and displayed in Table 5.2.

5.3.1.1 Stomatal Density

Significant differences ($P < 0.0001$) of SD were observed (Table 5.2) between species and leaf surface but no interaction between species and surface was found. Figure 5.3 presents the average of abaxial and adaxial SD counts, and shows that three species with significantly higher ($p < 0.05$) SD than the others, TRI 17137 had the highest mean SD ~ 100 per mm^2 , KU 2010 was about 20% lower with a mean SD of at ~ 78 per mm^2 and TRI 17162 at the third highest at ~ 72 per mm^2 . Two species exhibited significantly ($p < 0.05$) lower SD, Xi19 was the lowest at ~ 48 per mm^2 , 55 % less than the species with the highest SD, and AE 146 had only ~ 54 per mm^2 . The SD of the remaining species fell between 57 -74 per mm^2 .

Table 5.2: Two-way analysis of variance (ANOVA) results between flag leaf species and surfaces for stomatal density, guard cell length and $g_{s\text{max}}$ of 17 wheat species, indicating F values and P values, highlighting where significant differences have been observed. Sig. codes: 0 '***' 0.01 '**' 0.05 '.'

Flag Leaf	Stomatal Density			Guard Cell Length			$G_{s\text{max}}$		
	F value	Pr(>F)	Sig	F value	Pr(>F)	Sig	F value	Pr(>F)	Sig
Species	24.3	2.00E-16	***	9.702	2.00E-16	***	3.651	1.08E-05	***
Surface	16.5	7.49E-05	***	29.738	1.78E-07	***	46.903	1.43E-10	***
Line: Surface	1.291	2.08E-01		1.108	3.52E-01		1.094	0.364	

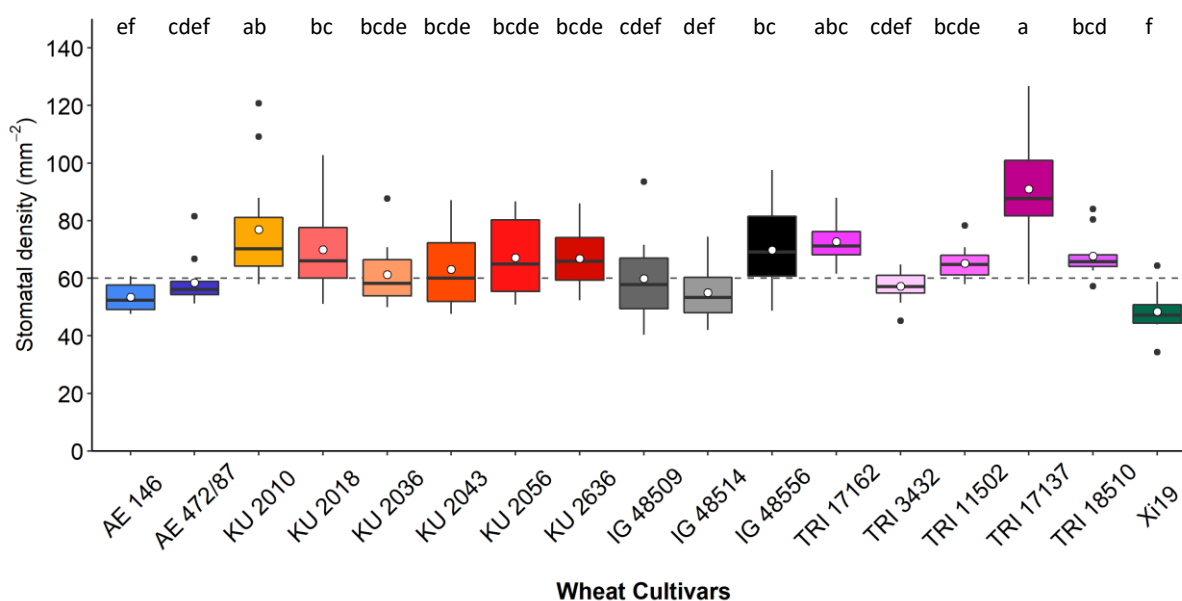


Figure 5.3. Variation (box and whisker plots displaying distribution of biological replicates) and mean (white dot) of flag leaf stomatal density (mm^2) from an average of the two leaf surfaces for 17 wheat species. Different letters represent statistically significant differences ($P < 0.05$) between means of different species, using the results of a Tukey test following a one-way ANOVA. Dotted line represents 60 mm^2 ($n = 12$).

Stomatal density was assessed on the abaxial and adaxial leaf surface as wheat is amphistomatous. When separating total SD between the abaxial and adaxial leaf surface (Figure 5.4) a similar trend was observed whereby higher ($p < 0.05$) SD values were found in species TRI 17137 and the lowest ($p < 0.05$) were found in species Xi19 on both the abaxial and adaxial surfaces. An overall significant difference ($p < 0.001$) between the leaf surfaces was observed (Figure 5.4) with higher SD values found on the adaxial leaf surface by ~ 5-10% excluding the species TRI 17162, TRI 3432, TRI 11502 and TRI 18510 which were approximately equal between the two leaf surfaces, although no differences of SD were found between leaf surfaces of the same species, for example, between Xi19 abaxial and Xi19 adaxial.

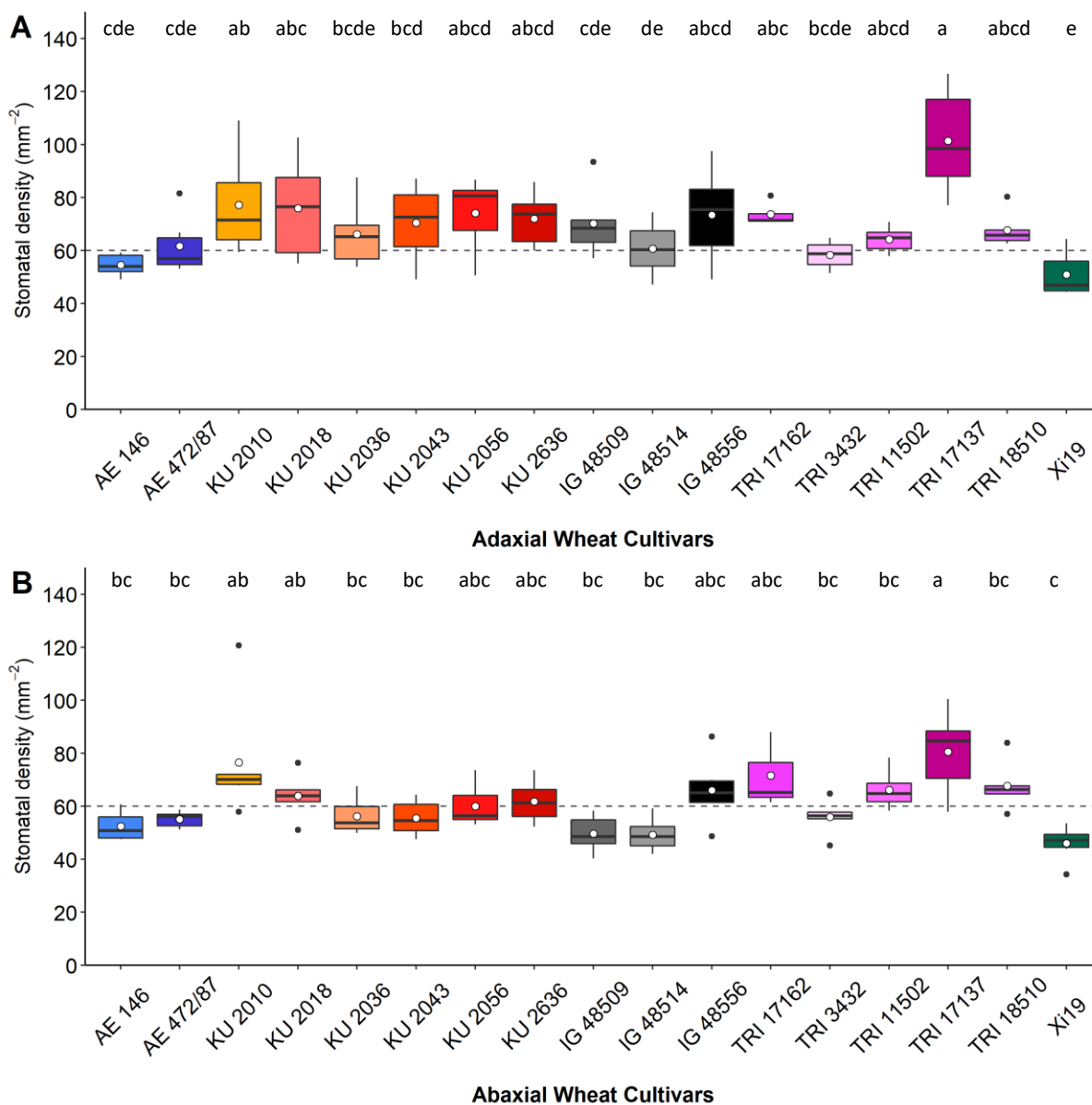


Figure 5.4. Variation (box and whisker plots displaying distribution of biological replicates) and mean (white dot) of flag leaf stomatal density (mm^{-2}), calculated for the adaxial (A) and abaxial (B) leaf surfaces for 17 wheat species. Different letters represent statistically significant differences ($P < 0.05$) between means of different species using the results of a Tukey test following a two-way ANOVA. Dotted line represents 60 mm^{-2} ($n = 6$).

5.3.1.2 Guard Cell Length

A significant difference ($P < 0.0001$) in stomatal size (SS; measured as guard cell length; μm) was observed (Table 5.2) between species and leaf surfaces. Figure 5.5 displays the average of abaxial and adaxial SS, with two species exhibiting larger ($p < 0.05$) SS, Xi19 was found to have the largest SS mean $\sim 52 \mu\text{m}$ and TRI 18510 had the second largest SS mean $\sim 50 \mu\text{m}$. Ten species displayed lower SS ($p < 0.05$) with TRI 17137 having the smallest SS mean $\sim 37 \mu\text{m}$, $\sim 29\%$ less than the largest SS mean (Fig. 5.6). The SS values of the remaining species fell between 38 and 46 μm .

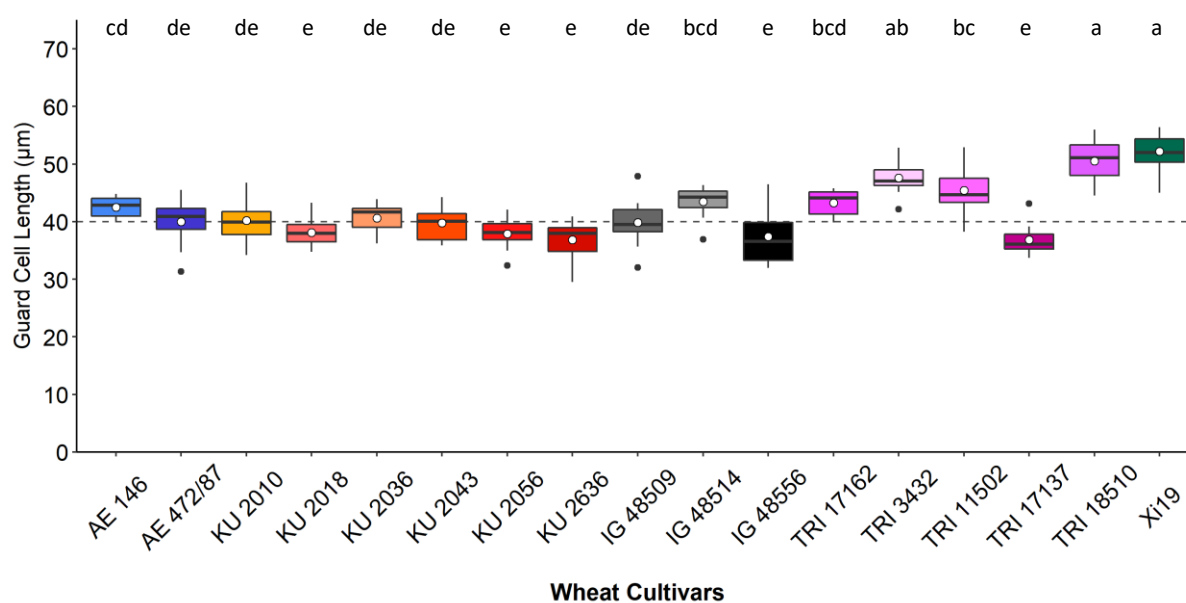


Figure 5.5. Variation (box and whisker plots displaying distribution of biological replicates) and mean (white dot) of flag leaf guard cell length (μm) from an average of the two leaf surfaces for 17 wheat species. Different letters represent statistically significant differences ($P < 0.05$) between means of different species using the results of a Tukey test following a one-way ANOVA. Dotted line represents $40 \mu\text{m}$ ($n = 12$).

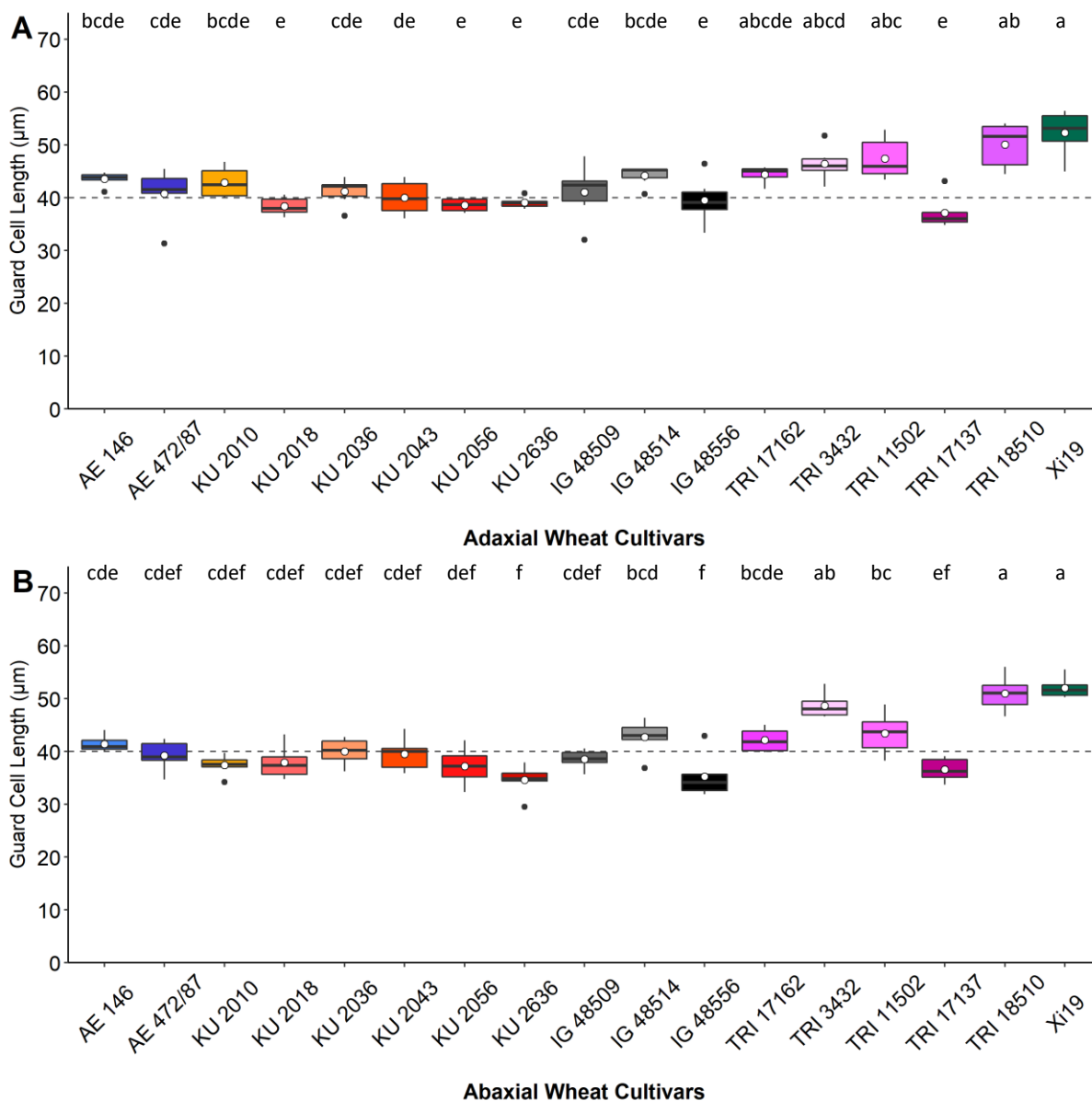


Figure 5.6. Variation (box and whisker plots displaying distribution of biological replicates) and mean (white dot) of flag leaf guard cell length (μm), calculated for the adaxial (A) and abaxial (B) leaf surfaces for 17 wheat species. Different letters represent statistically significant differences ($P < 0.05$) between means of different species using the results of a Tukey test following a two-way ANOVA. Dotted line represents $40 \mu\text{m}$ ($n = 6$).

When assessing SS between the abaxial and adaxial leaf surface (Figure 5.6) a significant difference ($p = 7.49e-05$) was found between surfaces of all species although no differences were found between leaf surfaces of the same species, for example of Xi19 abaxial and XI19 adaxial. The largest SS values (Figure 5.6) were found on Xi19 on both the adaxial and abaxial leaf surface $\sim 52 \mu\text{m}$ and $\sim 54 \mu\text{m}$ respectively. The smallest SS values were found on TRI 17137 with $\sim 37 \mu\text{m}$ on the adaxial leaf surface and IG 48556 and KU 2636 with both SS values at $\sim 35 \mu\text{m}$. The remaining SS (Figure 5.6) values fell between $\sim 38 \mu\text{m}$ and $\sim 50 \mu\text{m}$ on the adaxial leaf surface and similarly $\sim 36 \mu\text{m}$ and $\sim 53 \mu\text{m}$ on the abaxial leaf surface.

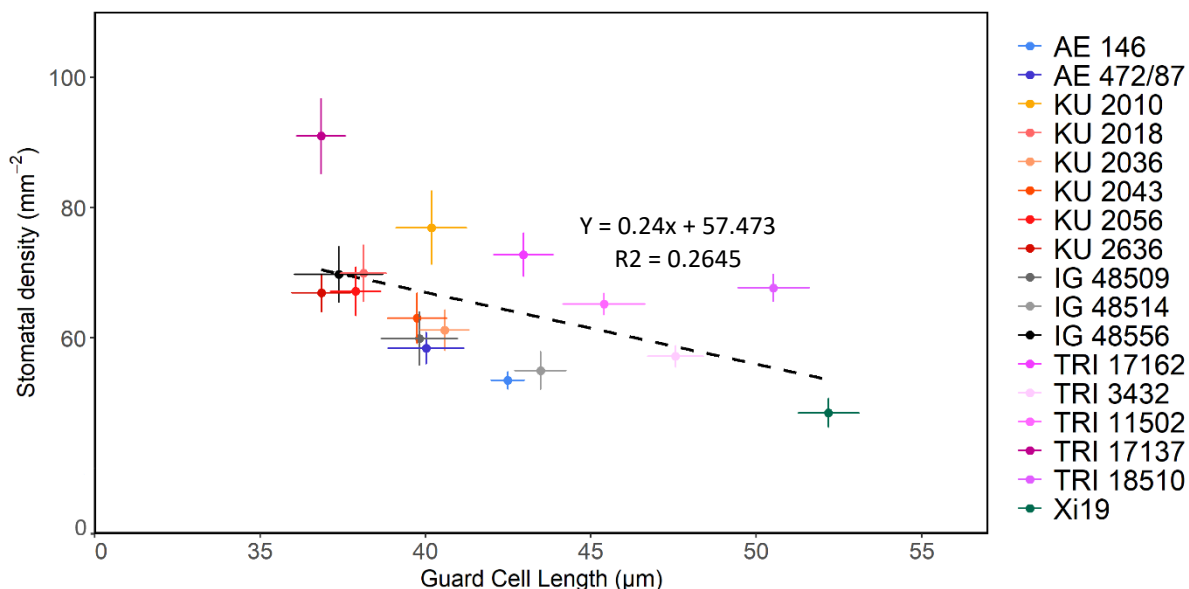


Figure 5.7. Correlation between total stomatal density (mm²) and total guard cell length (μm) for each species from an average of the two leaf surfaces for 17 wheat species. Black dotted line represents the trend in the data between the two variables ($p=0.035$) using the results of a Pearson's correlation test. Error bars represent standard error ($n = 12$).

A negative correlation ($p=0.035$) between SD and SS was observed (Figure 5.7), demonstrating that SS increases as SD decreases. The species with the highest SD mean, TRI 17137, had the smallest SS and the species with the lowest SD mean, Xi19, had the largest SS.

5.3.1.3 Maximum potential stomatal conductance (g_{smax})

A significant difference ($P < 0.0001$) in the anatomical maximum potential g_s (g_{smax} ; $\text{mol m}^{-2} \text{s}^{-1}$) was observed (Table 5.2) between species and leaf surfaces, highlighting variation in g_{smax} owing to differences in SD and SS. Total g_{smax} (an average of abaxial and adaxial measurements; Fig. 5.8) is higher ($p < 0.05$) in species TRI 18510, at $\sim 1.8 \text{ mol m}^{-2} \text{ s}^{-1}$. AE 146, AE 472/87 and Xi19 exhibit the lowest g_{smax} values at $\sim 1.15 \text{ mol m}^{-2} \text{ s}^{-1}$ and $\sim 1.16 \text{ mol m}^{-2} \text{ s}^{-1}$ respectively, with species AE 146 being $\sim 20\%$ lower than the species highest (TRI 18510). The g_{smax} values of the remaining species fell between 1.25 and $1.7 \text{ mol m}^{-2} \text{ s}^{-1}$.

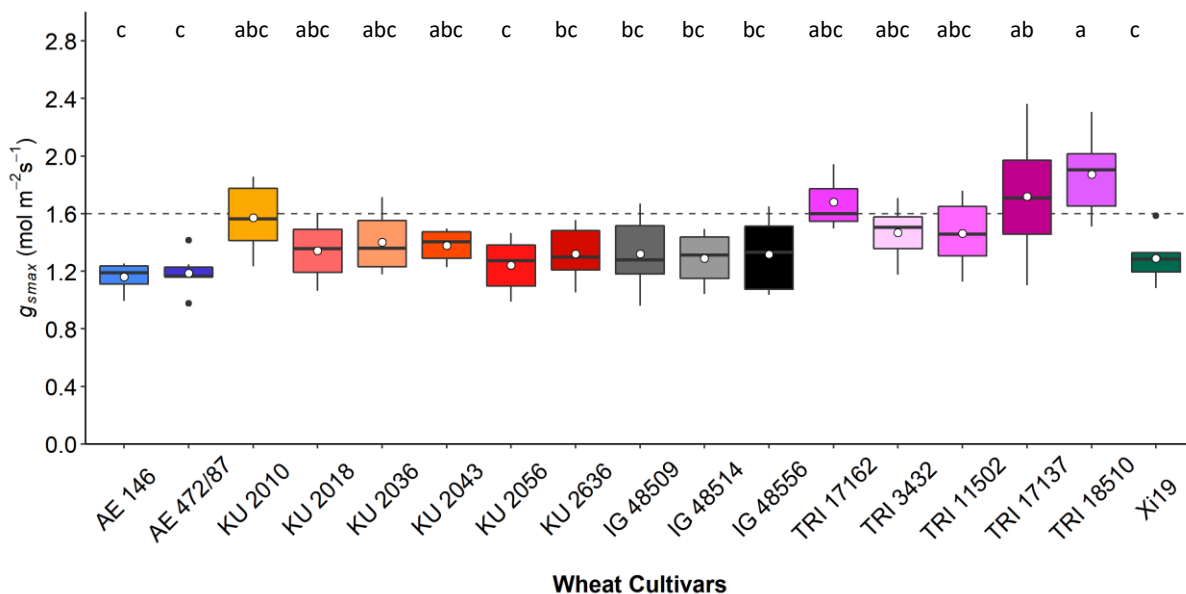


Figure 5.8. Variation (box and whisker plots displaying distribution of biological replicates) and mean (white dot) of flag leaf g_{smax} (mol m⁻² s⁻¹), calculated from an average of the two leaf surfaces stomatal density and guard cell length dimensions, for 17 wheat species. Different letters represent statistically significant differences ($P < 0.05$) between means of different species using the results of a Tukey test following a one-way ANOVA. Dotted line represents 1.6 mol m⁻² s⁻¹ ($n = 12$).

Both abaxial and adaxial leaf surface g_{smax} (Figure 5.9) was significant different ($p = 0.000152$) between species, although no differences were observed between surfaces of the same species (Table 5.3). No significant differences were observed between g_{smax} values of the adaxial leaf surface. On the abaxial leaf surface g_{smax} differences ($p < 0.05$) were found between TRI 18510 and eight other species (Figure 5.9), although differences were found between the remaining eight mid-range species which fell between ~ 0.5 mol m⁻² s⁻¹ and ~ 0.9 mol m⁻² s⁻¹.

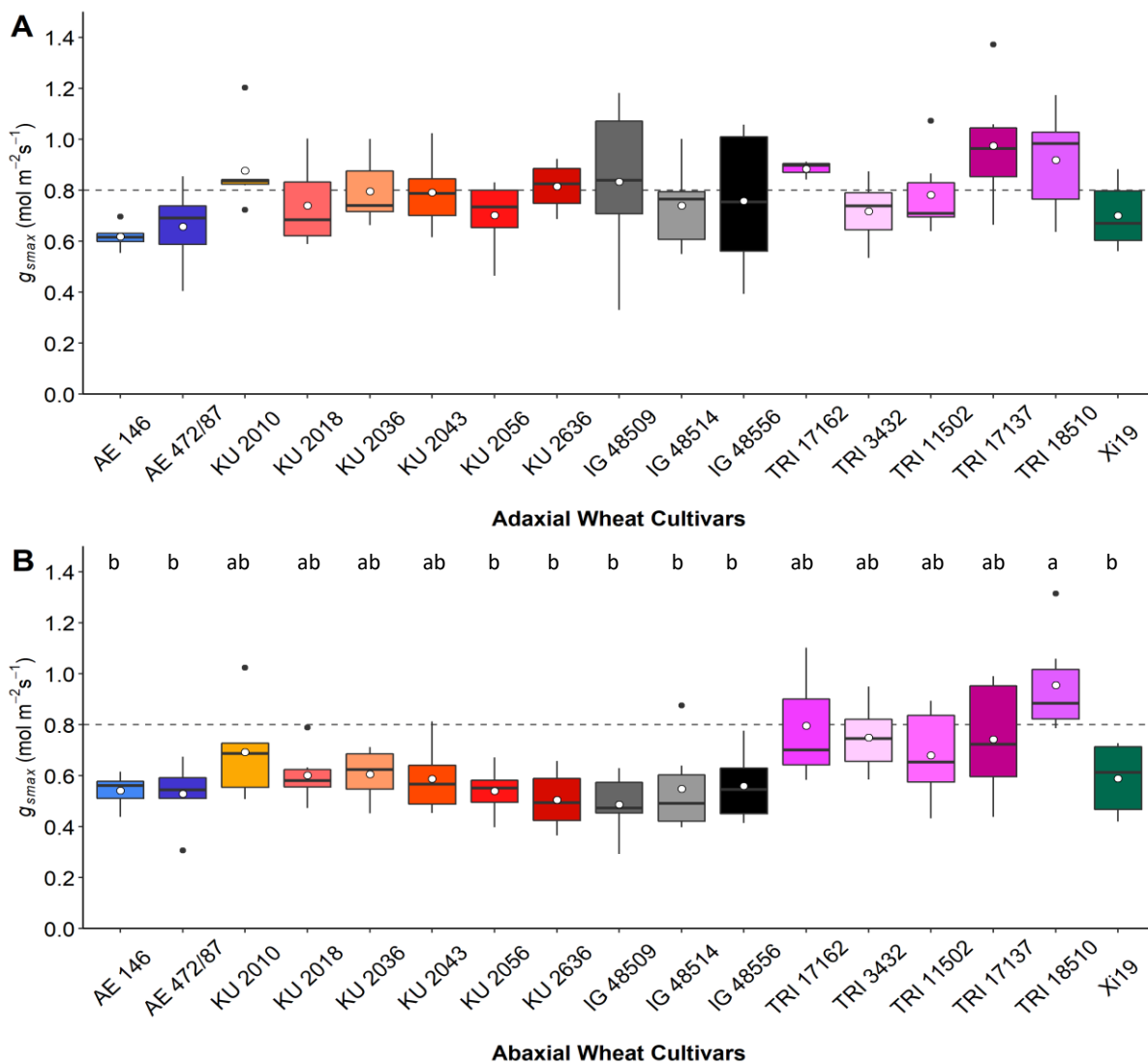


Figure 5.9. Variation (box and whisker plots displaying distribution of biological replicates) and mean (white dot) of flag leaf g_{smax} (mol m⁻² s⁻¹), calculated from stomatal density and guard cell length dimensions of the adaxial (A) and abaxial (B) leaf surfaces for 17 wheat species. Different letters represent statistically significant differences ($P < 0.05$) between means of different species using the results of a Tukey test following a two-way ANOVA. Dotted line represents 0.8 mol m⁻² s⁻¹ ($n = 6$).

5.3.2 Leaf gas exchange

5.3.2.1 Response of g_s and A to a step change in PPFD

To assess stomatal kinetics between species, gas exchange measurements were performed on the flag leaf at the middle leaf location. The leaf surface response of g_s and A to a single step increase in light (100 to 1000 $\mu\text{mol m}^{-2} \text{s}^{-1}$ PPFD) are shown in figure 5.10. To assist with visualizing the data, species were separated into groups (based on their first two identifying letters) and plotted along with the EW Xi19 for comparison. All species exhibited the expected increase in g_s and A to the increased light intensity. Some species had not attained their maximum g_s values within the 50 min timeframe (Fig. 5.10). Also, the exposure time to low light of 20 minutes might have been insufficient for complete low light steady state g_s ; however, this does not greatly impact the stomatal responses to the initial rapid opening response of the stomata. Steady state g_s at the initial PPFD of 100 $\mu\text{mol m}^{-2} \text{s}^{-1}$ varied among the species (Fig. 5.10; A-D), with a substantial range in values (approximately 0.2 $\text{mol m}^{-2} \text{s}^{-1}$). Although, a larger range in g_s values was found from the final measurements of the protocol (after 45 min at 1000 $\mu\text{mol m}^{-2} \text{s}^{-1}$ PPFD) with an approximate 0.5 $\text{mol m}^{-2} \text{s}^{-1}$ difference between the highest values, in two species (TRI 17137 and KU 2056), and the lowest (IG 48514).

Steady state A at the initial PPFD of 100 $\mu\text{mol m}^{-2} \text{s}^{-1}$ (Fig. 5.10 E-H) varied among species with values for all species under 12 $\mu\text{mol m}^{-2} \text{s}^{-1}$ (except for a minimal number of artifacts). A large range in mean A values was also found during the final measurements of the protocol (after 45 min at 1000 $\mu\text{mol m}^{-2} \text{s}^{-1}$ PPFD) with over 10 $\mu\text{mol m}^{-2} \text{s}^{-1}$ difference between the highest mean value in species TRI 3432, to the lowest mean value in species IG 48509 (Figure 5.10; E-H). This indicates that the

starting position of A does not necessarily reflect the final position of A values, furthermore, the magnitude of change in g_s is not related to magnitude of change in A .

An increase in PPFD to $1000 \mu\text{mol m}^{-2} \text{s}^{-1}$ led to an immediate and rapid increase in A compared to g_s for all species and after this initial period, the increase in A slowed to a magnitude similar to the increase in g_s , and A reached steady state while g_s continued to increase. The lack of synchrony between the responses of A and g_s to a step increase in PPFD had a consequential effect demonstrated by the temporal responses of W_i (A/g_s ; Figure 5.10; I-L). Following the step change in PPFD, A rapidly increased compared to g_s and therefore W_i reached a maximum value minutes after the increase on PPFD. Further increases in g_s over time drove a continuous decrease in W_i after A had reached a steady state until the end of the protocol. By the end of the protocol (at $1000 \mu\text{mol m}^{-2} \text{s}^{-1}$ PPFD) variation in mean W_i values (Figure 5.10; I-L) had returned to a range between species of $\sim 30 \mu\text{mol m}^{-2} \text{s}^{-1}$ between the highest (IG 48514) and the lowest values (KU 2056).

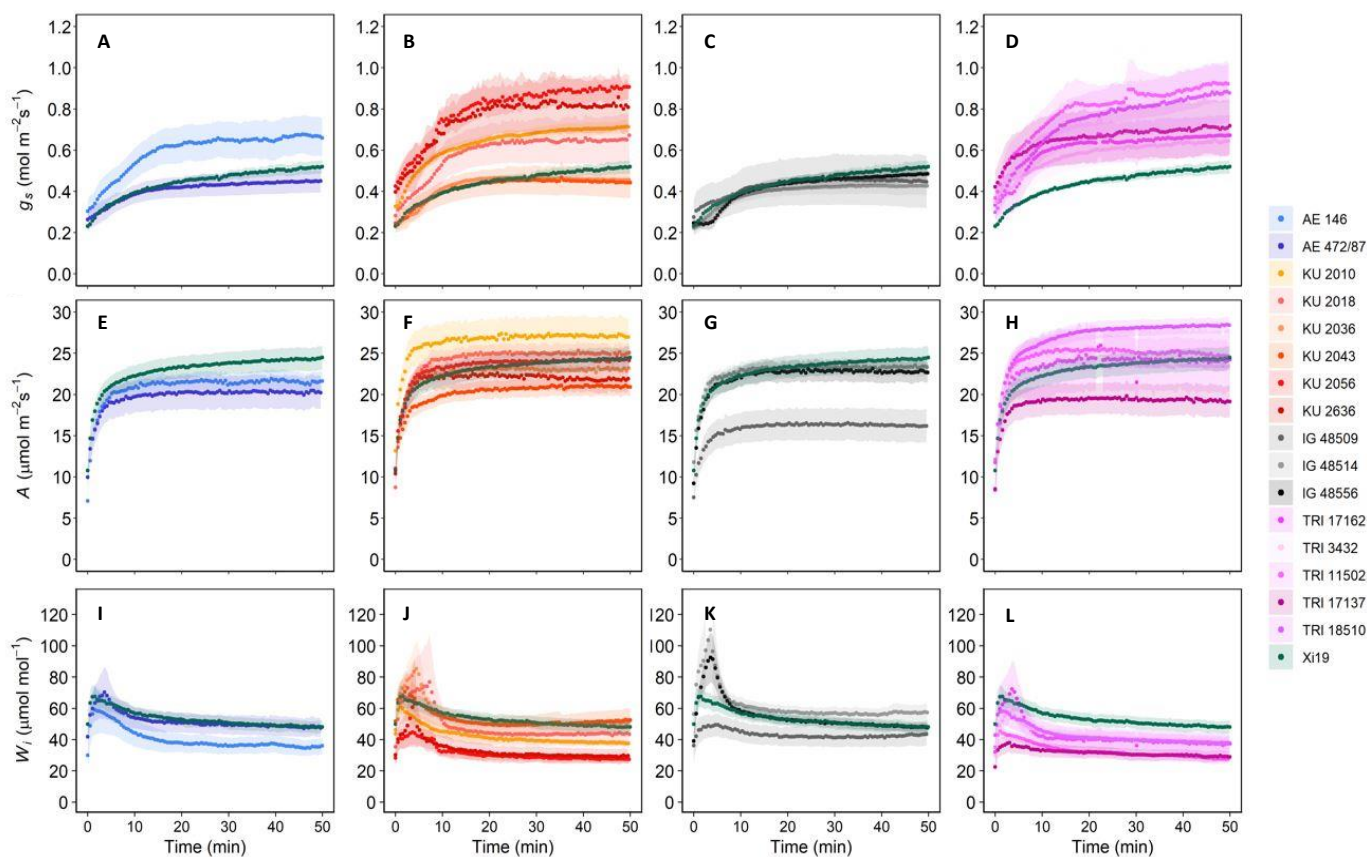


Figure 5.10. Temporal response of stomatal conductance (g_s ; A-D), net CO₂ assimilation (A ; E-H), and intrinsic water use efficiency (W_i ; I-L), to a step increase in light intensity (from $100 \mu\text{mol m}^{-2} \text{s}^{-1}$ for 20 minutes to $1000 \mu\text{mol m}^{-2} \text{s}^{-1}$ for 50 minutes) for 17 wheat species. Species were separated into groups by first two identifying letters with the elite wheat Xi19 in each group for comparison. Gas exchange parameters (g_s and A) were recorded at 30s intervals, leaf temperature maintained at 22°C , and leaf VPD at $1 \pm 0.2 \text{ kPa}$. Error ribbons represent mean \pm SE ($n = 5-7$).

5.3.2.2. Speed of g_s response to a step change in light intensity

Stomatal responses to a step increase in light intensity (100 to 1000 $\mu\text{mol m}^{-2} \text{s}^{-1}$ PPFD) were used to determine natural variation in the speed of g_s and A response to light amongst 17 wheat species. The time constants to reach 63 % of final value for g_s (τ_{g_s} ; Figure 5.11, A) and A (τ_A ; Figure 5.11, B) final value of g_s (g_{sF} , Figure 5.11, C) and A (A_F , Figure 5.11, D) at 1000 $\mu\text{mol m}^{-2} \text{s}^{-1}$ and finally the magnitude of change in g_s (Δg_s , Figure 5.11, E) and A (ΔA , Figure 5.11, F) between 100 $\mu\text{mol m}^{-2} \text{s}^{-1}$ - 1000 $\mu\text{mol m}^{-2} \text{s}^{-1}$.

Time constants for stomatal opening (τ_{g_s} ; Figure 5.11, A) revealed that Xi19, the only EW variety, was significantly ($p < 0.05$) longer than all other species by 5 minutes and the shortest ($p < 0.05$) species was KU 2036. Although, the time constants for A (τ_A ; Figure 5.11, B) indicate that both Xi19 and KU 2036 reached 63 % of A only 30 s apart, despite the time take for g_s to reach 63% took much longer to be reach. The slowest time constant for A was found in KU 2043, although again, this species also had one of the shortest time constants for stomatal opening at approx. 7 min. The time constants for stomatal opening (τ_{g_s} ; Figure 5.11, A) for the remaining species were all within 8 min of each other and the time constants for A (τ_A ; Figure 5.11, B) within 1 min of each other.

Final g_s values (g_{sF} , Figure 5.11, C), at 50 min, range from $\sim 0.42 \text{ mol m}^{-2} \text{s}^{-1}$ to $\sim 0.94 \text{ mol m}^{-2} \text{s}^{-1}$ with a group of 7 species (including the EW species Xi19) showing significantly lower ($p < 0.05$) values compared with the three species with the highest values. Final A values ranged from $\sim 15 \mu\text{mol m}^{-2} \text{s}^{-1}$ to $\sim 28 \mu\text{mol m}^{-2} \text{s}^{-1}$, in species IG 48509 and TRI 3432 respectively. The EW species Xi19 was 40% higher than IG 48509 at $\sim 25 \mu\text{mol m}^{-2} \text{s}^{-1}$.

The magnitude of change in g_s (Δg_s , Figure 5.11, E) and A (ΔA , Figure 5.11, F)

between $100 \mu\text{mol m}^{-2} \text{s}^{-1}$ - $1000 \mu\text{mol m}^{-2} \text{s}^{-1}$ followed the same pattern as the final g_s and A values where species that had low, mid-range or high final g_s and A values also had a corresponding low, mid-range or high magnitude of change in g_s and A . The smallest magnitude of change in g_s values (Δg_s , Figure 5.11, E) belong to species IG 48509 and the highest values were found in species TRI 3432 which with an approx. 35 % difference between the lowest and the highest. The greatest magnitude of change in A (Δg_s , Figure 5.11, F) was observed in species KU 2018 and the lowest was found in KU 2043 at $8 \mu\text{mol m}^{-2} \text{s}^{-1}$, almost 50 % lower magnitude of change in A than that of KU 2018.

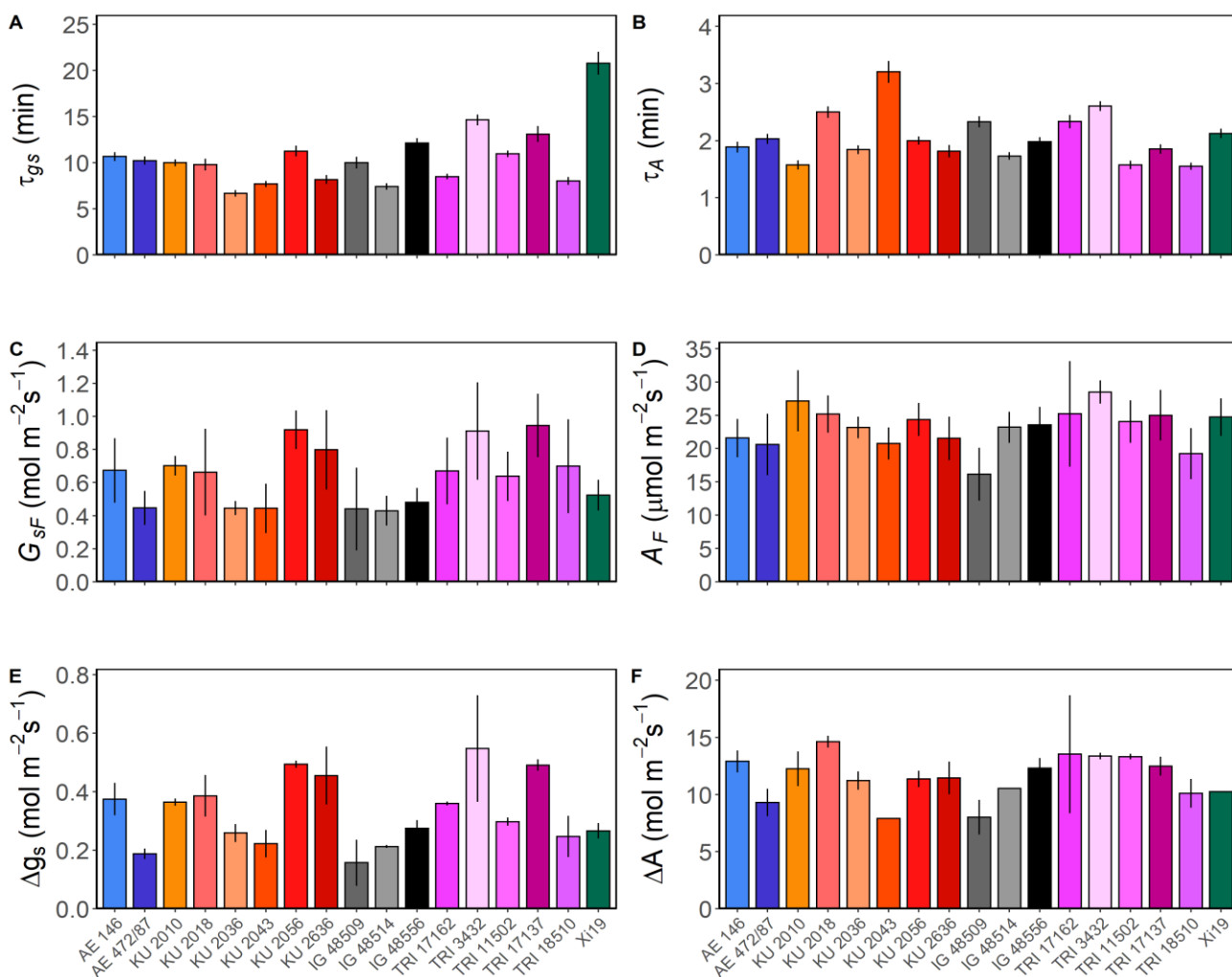


Figure 5.11. Time constant for stomatal opening (τ_{gs} , A) in minutes to reach 63% of final value, final values of stomatal conductance (1000 $\mu\text{mol m}^{-2} \text{s}^{-1}$ PPFD) after an increased step change in light intensity (g_{sF} , C) and difference in g_s between 100 and 1000 $\mu\text{mol m}^{-2} \text{s}^{-1}$ PPFD (Δg_s , E) following the step increase in light intensity. Time constant for light saturated carbon assimilation (τ_A , B) in minutes to reach 63% of final value, final values light saturated carbon assimilation (1000 $\mu\text{mol m}^{-2} \text{s}^{-1}$ PPFD) (A_F , D) and difference in A between 100 and 1000 $\mu\text{mol m}^{-2} \text{s}^{-1}$ PPFD (ΔA , F) following the step increase in light intensity. All results for 17 wheat species. Error bars represent 95% confidence intervals using the results of a Tukey test following a two-way ANOVA ($n = 5-7$).

The six parameters from figure 5.11 were correlated against each other (Figure 5.12) which reveal three significant positive correlations; the time constant for stomatal opening (τ_{gs} , A, B, C), final values of stomatal conductance ($1000 \mu\text{mol m}^{-2} \text{s}^{-1}\text{PPFD}$; g_{sF} , G, H, I), the difference in g_s between 100 and $1000 \mu\text{mol m}^{-2} \text{s}^{-1}\text{PPFD}$ (Δg_s , D, E, F) and time constant for light saturated carbon assimilation (τ_A , A, D, G), final values light saturated carbon assimilation ($1000 \mu\text{mol m}^{-2} \text{s}^{-1} \text{PPFD}$; A_F , C, F, I) and difference in A between 100 and $1000 \mu\text{mol m}^{-2} \text{s}^{-1}\text{PPFD}$ (ΔA , B, E, H). A positive correlation ($p = 0.001375$) between τ_{gs} and ΔA (Fig 5.12B) highlights that species with slow stomatal opening also have the greatest magnitude of change in A . Secondly, a positive correlation ($p = 0.003852$) was observed (Figure 5.12 F) between A_F and Δg_s , whereby, species with the higher change in g_s a higher final A values was also observed. A positive correlation ($p = 0.04226$) was also observed (Figure 5.12I I) between g_{sF} and A_F .

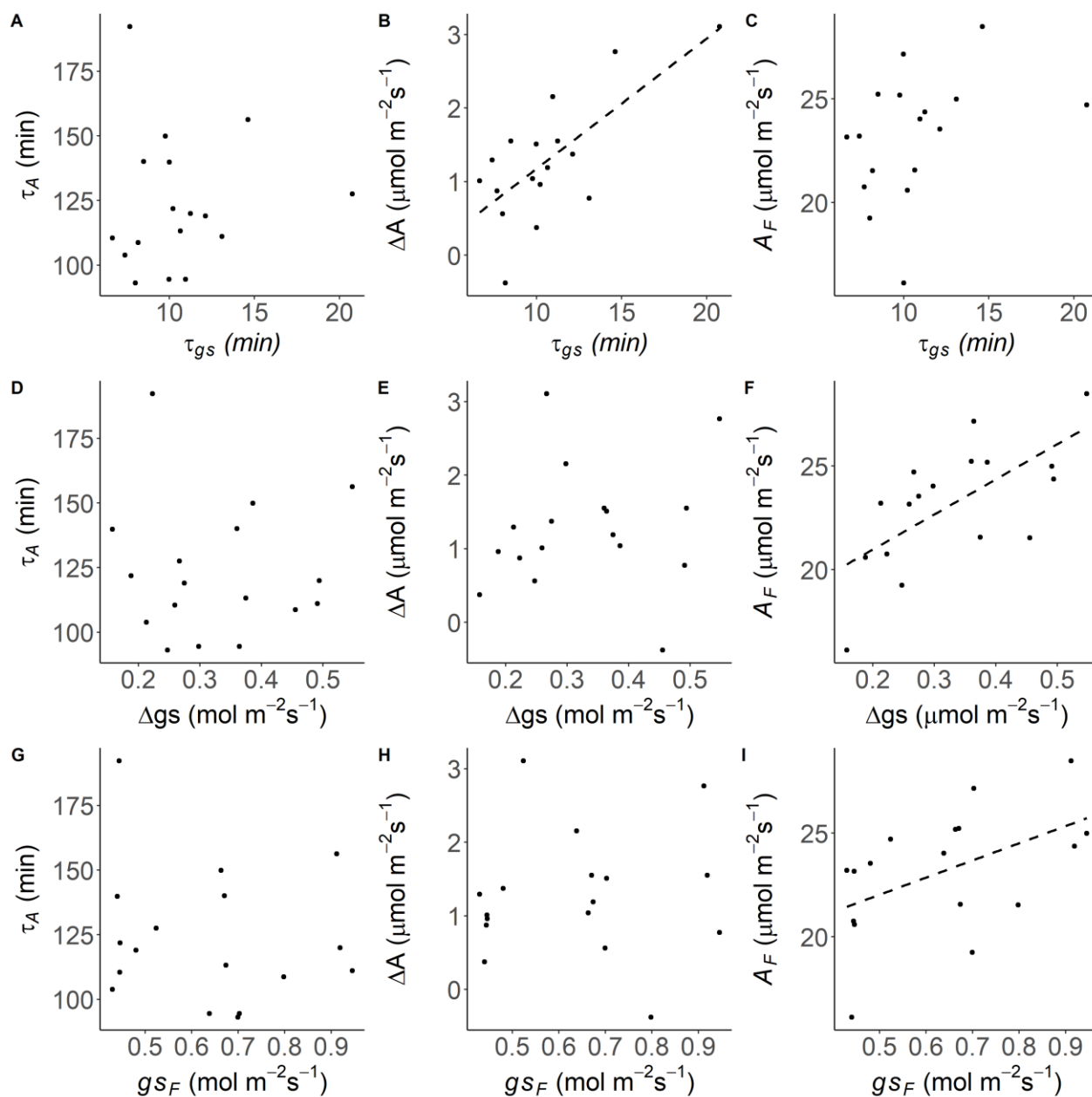


Figure 5.12. Correlations between time constant for stomatal opening (τ_{gs} ; A, B, C) in minutes, final values of stomatal conductance ($1000 \mu\text{mol m}^{-2} \text{s}^{-1}$ PPF) after an increased step change in light intensity (g_{sF} ; G, H, I) and difference in g_s between 100 and $1000 \mu\text{mol m}^{-2} \text{s}^{-1}$ PPF (Δg_s ; D, E, F) following the step increase in light intensity and time constant for light saturated carbon assimilation (τ_A ; A, D, G) in minutes, final values light saturated carbon assimilation ($1000 \mu\text{mol m}^{-2} \text{s}^{-1}$ PPF) after an increased step change in light intensity (A_F ; C, F, I) and difference in A between 100 and $1000 \mu\text{mol m}^{-2} \text{s}^{-1}$ PPF (ΔA ; B, E, H) following the step increase in light intensity for 17 wheat species. Black dotted line represents a significant ($p < 0.05$) trend in the data between the two variables ($n = 5-7$).

5.3.2.2. A/C_i response analysis

The response of CO_2 assimilation (A) as a function of internal $[\text{CO}_2]$ (C_i ; A/C_i – Figure 5.13) were performed on the flag leaf for 13 of the original 17 species of wheat (with KU 2010, KU 2056, TRI 17137 and TRI 18510 missing due to desiccation). All species exhibited the expected increase in A with increased C_i up to a certain point before reaching a plateau.

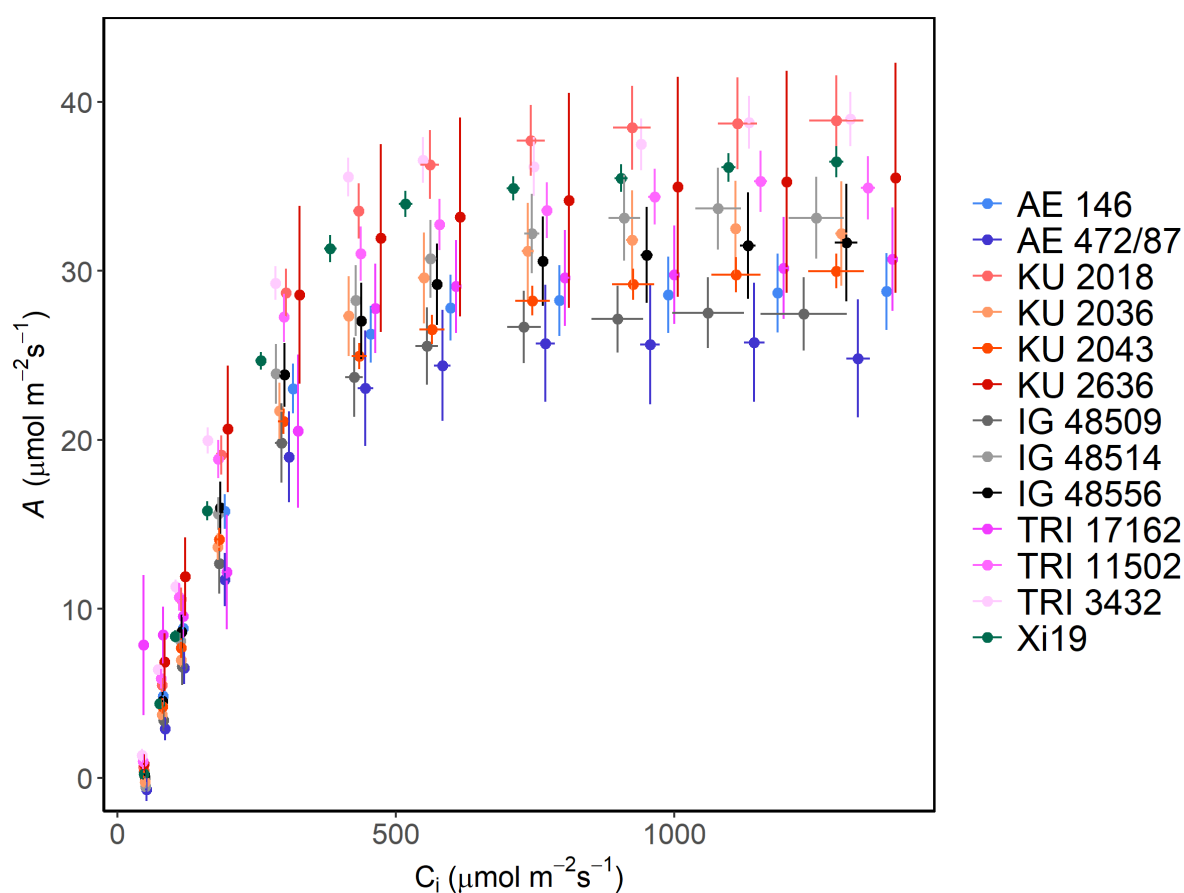


Figure 5.13. The response of CO_2 assimilation (A) to intercellular $[\text{CO}_2]$ (C_i) between 50 and 1500 $\mu\text{mol m}^{-2} \text{s}^{-1}$, under saturating PPFD ($1300 \mu\text{mol m}^{-2} \text{s}^{-1}$), for 17 wheat species. Error bars represent mean \pm SE ($n = 5-7$).

The maximum rate of carboxylation (V_{Cmax}), the maximum rate of electron transport (J_{max}) and the light and CO₂ saturated assimilation rate (A_{max}) at 1500 $\mu\text{mol mol}^{-1}$ CO₂ and 1500 $\mu\text{mol m}^{-2} \text{s}^{-1}$ PPFD were determined for all measurements (Figure 5.14; A, B and C respectively). Significant differences ($p = 4.86\text{e-}05$) in V_{Cmax} (Figure 5.14; A) were found between species, with the highest values in TRI 3432 and the lowest AE 472/87 with a lower V_{Cmax} by $\sim 40\%$ between the highest and lowest. The remaining species fell between $\sim 90 \mu\text{mol m}^{-2} \text{s}^{-1}$ and $\sim 130 \mu\text{mol m}^{-2} \text{s}^{-1}$. The species with the highest V_{Cmax} was significantly different to five other species (AE 472/87, IG 48509, KU 2036, KU 2043 and TRI 17162) but was not significantly different to the EW species Xi19. The maximum electron transport rate (J_{max} ; Figure 5.14; B) was different ($p = 0.0044$) between species, and a post-hoc Tukey test showed only a difference ($p < 0.05$) between the highest J_{max} rate found in species TRI 3432 and the two lowest rates in species AE 472/87 and TRI 17162, which differed by $100 \mu\text{mol m}^{-2} \text{s}^{-1}$. The light and CO₂ saturated assimilation rate (A_{max} ; at 1500 $\mu\text{mol mol}^{-1}$ CO₂ and 1500 $\mu\text{mol m}^{-2} \text{s}^{-1}$ PPFD; Figure 5.14; C) ranged from $\sim 25 \mu\text{mol m}^{-2} \text{s}^{-1}$ in species AE 472/87 to $\sim 38 \mu\text{mol m}^{-2} \text{s}^{-1}$ in TRI 3432, a difference of $\sim 34\%$ between the lowest and highest values.

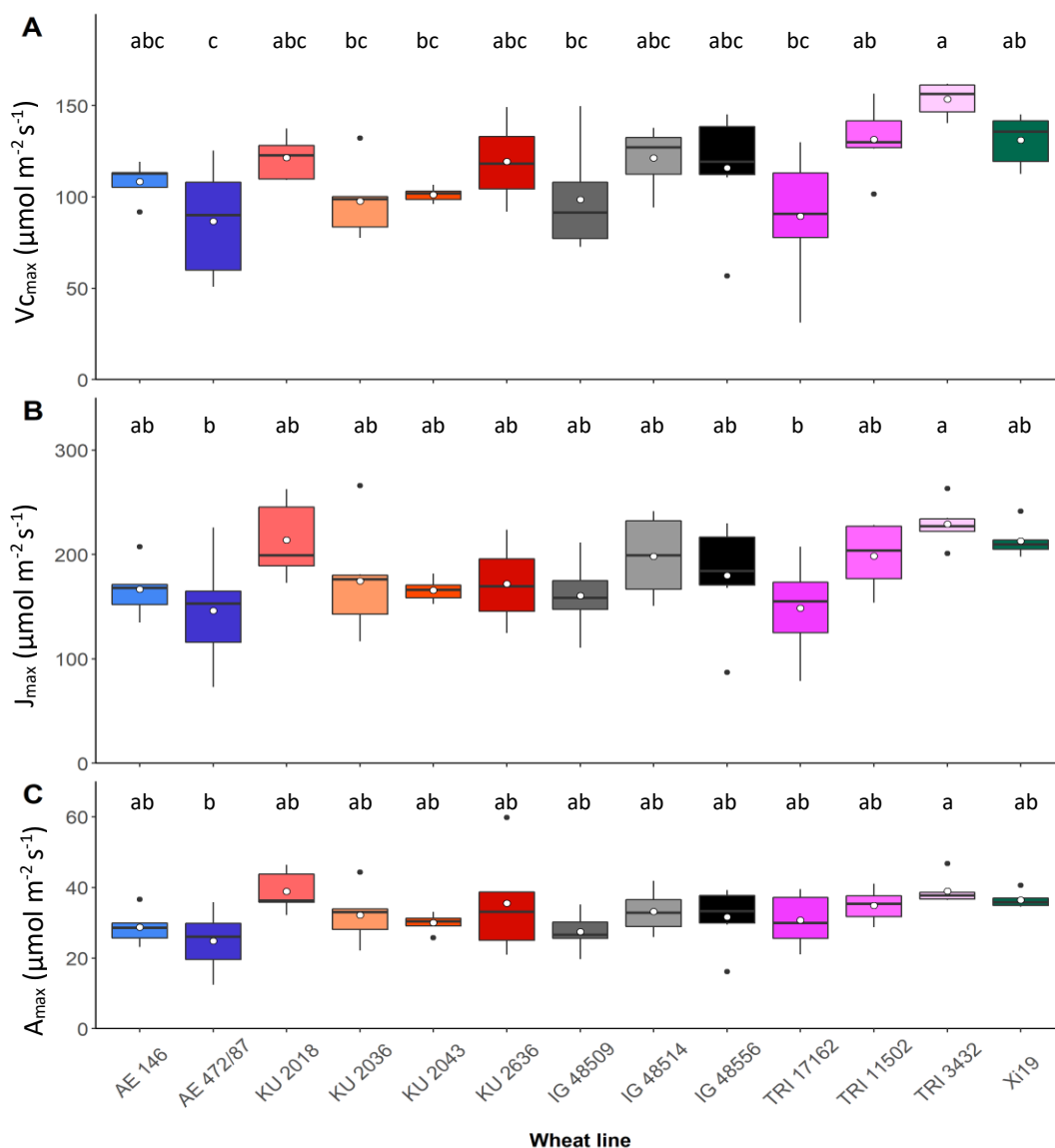


Figure 5.14. Variation (box and whisker plots displaying distribution of biological replicates) and mean (white dot) of the maximum rate of carboxylation (A; $V_{C_{max}}$), maximum rate of electron transport (B; J_{max}) and the measured CO_2 -saturated ($1500 \mu\text{mol m}^{-2} \text{s}^{-1}$) rate of photosynthesis, at light $1300 \mu\text{mol m}^{-2} \text{s}^{-1}$ (C; A_{max}) for 13 wheat species. Different letters represent statistically significant differences ($P < 0.05$) between species using the results of a Tukey test following a one-way ANOVA ($n = 5-7$).

5.4. Discussion

The introduction of genetically diverse traits from WWR into the EW species is becoming an increasing popular approach (King *et al.*, 2017; Prohens *et al.*, 2017) for increasing crop yield (McAusland *et al.*, 2020), although it requires a greater understanding of the depth in variety of traits accessible to breeding programmes, particularly those which encourage a more efficacious carbon acquisition (McAusland *et al.*, 2020). This study aimed to link g_s response to stomatal anatomy in WWR, specifically SS and SD, (Franks & Farquhar, 2007; Franks & Beerling, 2009; Drake *et al.*, 2013) which supports the identification and manipulation of stomatal anatomical characteristics to promote optimal stomatal responses, reducing limitations on CO₂ diffusion for photosynthesis and conserving water lost via transpiration to avoid desiccation (Cowan, 1977; Hetherington & Woodward, 2003; Ooba & Takahashi, 2003; Lawson *et al.*, 2010; Lawson & Blatt, 2014; Lawson & Violet-Chabrand, 2019). Large natural variation in stomatal characteristics were observed between the WWR and EW species, specifically in SD and SS. Anatomical maximum potential g_s (g_{smax}) was calculated to indicate the maximum potential g_s that could be achieved if pore aperture were at a maximum. A high g_{smax} value demonstrates a potential for a greater opening capacity to maximise CO₂ gain when water is not a limiting factor. No major differences in SS (measured as guard cell length) were observed between species, demonstrating that the differences in g_{smax} values observed was driven by SD (Dow *et al.*, 2014a) and not SS. Interestingly, the hexaploid EW species XI19 had the lowest SD coupled with the largest SS and the opposite was true of most diploid species, which displayed small SS and high SD. Moreover, the density to size trade-off, whereby decreasing stomatal size is offset by increasing density, reported in many EW species (Hetherington & Woodward, 2003; Franks & Beerling, 2009; Drake *et al.*,

2013; McElwain *et al.*, 2015; de Boer *et al.*, 2016; Henry *et al.*, 2019) is a trend that was conserved through diploid, tetraploid and hexaploid wheat species, shown in these results.

An evolutionary pressure on stomatal morphology is believed to be behind this trade-off in order to balance the benefits of increasing diffusional gas exchange with the cost associated with increasing the stomatal area to the leaf epidermal area (de Boer *et al.*, 2016). The SD/SS trade-off may have evolved due to SD variations being controlled by cell-to-cell signalling mechanisms that also regulate spacing between stomata (Lee *et al.*, 2015) and the phenotypic plasticity with environmental changes such as atmospheric CO₂ concentration (Ca) (Bergmann & Sack, 2007; Doheny-Adams *et al.*, 2012). Franks *et al.* (2012) suggests that fossil records imply that leaves have adapted to megacycles in Ca by adjusting leaf diffusivity to CO₂ which is achieved through adjusting the size and density of stomatal guard cells over the leaf surface, although SS is less plastic than SD (Zhang *et al.*, 2012) which may be attributed to changes in genome sizes. The study also suggests that smaller, more densely packed stomata are more effective in low Ca conditions, which may allow for faster dynamic responses in stomatal aperture and a shorter diffusional pathway (Drake *et al.*, 2013), benefits that may allow a more accurate control of stomata and confer a gas exchange advantage in lower CO₂ environments and in environments with higher temperatures, allowing the plants to cool using evapotranspiration but also avoid desiccation (Brodribb *et al.*, 2009; Mcadam & Brodribb, 2012, 2014).

The relationship of SD and SS on plant leaves, representing the proportion of leaf surface they occupy, signifies a critical investment in the functional economics of the plant, which in turn effects the g_{smax} , operational leaf gas exchange and plant productivity as a whole (McElwain *et al.*, 2015). The increase of g_{smax} , i.e. the increase

in SD and/or SS, is primarily constrained by leaf area that can be allocated to stomata, a spatial constraint to plant function, although this spatial constraint may not hinder amphistomatous species as much as hypostomatous species due to the doubling of available epidermal space (de Boer *et al.*, 2016). This is primarily due to the spacing of stomata to neighbouring subsidiary and/or guard cells, where clustered stomata can affect the mechanical advantage of having subsidiary cells by impeding the efficacy of guard cells opening and closing responses, and leads to increased interference/overlap between the diffusion shells (the semi-circular pattern of gaseous flux from the stomatal pore) of neighbouring stomata (Franks & Farquhar, 2007; Lehmann & Or, 2015; de Boer *et al.*, 2016; Lawson & Matthews, 2020). Furthermore, the energy cost for stomatal operation is high and therefore too many stomata may negatively affect the leaf carbon balance (Assmann & Zeiger, 1987).

The regulation of stomatal conductance is a mechanism utilised by plants to increase carbon gain and reduce water loss (Cowan, 1977; Cowan & Farquhar, 1977; Hetherington & Woodward, 2003). A significant limitation in this process, is the magnitude and speed of the g_s response to light, which can be affected by differences in stomatal anatomy and biochemistry (Hetherington & Woodward, 2003; Franks & Farquhar, 2007; McAusland *et al.*, 2016). A slow g_s response may impede carbon uptake for photosynthesis when a plant is in favourable light water and CO₂ conditions which can reduce the impact of water loss and maintains leaf turgor (Lawson & Morison, 2004; McAusland *et al.*, 2013, 2016) benefiting the plant, but if water is a limiting factor (Knapp *et al.*, 1993) and need to prioritise water conservation over carbon gain a slow g_s response can be beneficial (Lawson & Morison, 2004; Lawson *et al.*, 2010; Bertolino *et al.*, 2019).

As previously suggested, higher stomatal densities promote more rapid g_s

responses to changing light intensity (Franks & Farquhar, 2007; Franks & Beerling, 2009; Drake *et al.*, 2013; Lawson & Blatt, 2014). This is consistent with the results of this study, as the highest SD were observed in the WWR species TRI 17137 (diploid) with the smallest SS, which translated into one of the highest adaxial g_{smax} which displayed a fast speed of stomatal opening (to 63% of final the g_s values at $1000 \text{ m}^{-2} \text{ s}^{-1}$) and the highest final g_s values. Conversely, the EW Xi19 displayed the lowest SD and the largest SS translating into the lowest abaxial g_{smax} value and the second lowest total g_{smax} value (an average of both the abaxial and adaxial leaf surfaces). Xi19 had the slowest speed of stomatal opening (to 63% of final the g_s values at $1000 \text{ m}^{-2} \text{ s}^{-1}$) with a mid-range final g_s values, although the final A values were similar with only $1 \mu\text{mol m}^{-2} \text{ s}^{-1}$ difference between the two species. V_{cmax} and J_{max} data cannot be compared as TRI 17137 was among the group plants underwent heat stress and could not undergo further testing. Therefore, the EW species had lowest SD and the largest SS coupled with the slowest stomatal response and the WWR species had the highest SD and the fastest stomatal response. These results also confirmed that Xi19 had the second highest W_i (Figure 5.10: I-L) suggesting that diploid species exhibit a preference towards CO_2 uptake for photosynthesis over water conservation due to an increased g_s and lower W_i at high light intensities.

The results of this study revealed six WWR species (AE 472/87, KU 2036, KU 2043, IG 48509, IG 48554 and IG 48514) that had similar or lower g_s than Xi19 but also displayed similar or higher final A values, and a shorter τ_{gs} , therefore these species had increased carbon uptake for photosynthesis which has been correlated with increased grain yield (Fischer *et al.*, 1998; Carmo-Silva *et al.*, 2017). These WWR could be used for further testing to determine the optimal stomatal characteristics with the intent to exploit such targets for enhanced productivity. Although the EW species

has a much higher seed yield owing to the acquisition valuable agronomic traits such as non-brittle rachis, glume tenacity and a higher number of spikelets per spike (Wolde *et al.*, 2019). The lack of co-ordination between the g_s and A in crop species leads to decreases in W_i that could potentially have negative implications on yield. The improvements of W_i through manipulation of stomatal anatomy and responses has been widely studied (Doheny-Adams *et al.*, 2012; Franks *et al.*, 2015), with the aim of improving crop yields under water-limiting conditions (Lawson & Blatt, 2014; Raven, 2014). Furthermore, high g_s can be beneficial by providing leaf cooling through transpiration under high light conditions (Leakey *et al.*, 2003; Crawford *et al.*, 2012; Urban *et al.*, 2017a) and by allowing plants to utilise any increase in high light by the continual uptake of CO_2 with little or no stomatal limitation (Mooney *et al.*, 1983; Pearcy, 1990; Tinoco-Ojanguren & Pearcy, 1993; Yamori *et al.*, 2020) therefore increasing yield at high temperatures (Fischer *et al.*, 1998; Lu *et al.*, 1998). Increased SD and/or stomatal size requires further examination of the relationship between stomatal density and the mesophyll cell, and the surrounding air space required which would necessitate additional hydraulic supply at the expense of main photosynthesising cells (Lundgren *et al.*, 2019; Lawson & Matthews, 2020).

When measuring the photosynthetic capacities of the 13-wheat subset, by removing the stomatal limitation, there were no differences in J_{max} and A_{max} between all diploid and tetraploid species and the EW species. Although, one tetraploid species (TRI 3432) which had the highest A_{max} , V_{cmax} and J_{max} values suggested that this species might be better adapted to utilise both PPFD and CO_2 for photosynthesis. However, this species as it stands, with a high photosynthetic capacity possesses a low seed yield which are hulled, creating an even lower seed availability compared to EW varieties. Furthermore, there was no differences in photosynthetic capacity in the

A. tauschii (diploid) species, even though some species had higher W_i , demonstrating that stomatal anatomical characteristics are crucial in the futureproofing of crops to grow in the current changing climate, and this species is an example of a species to be further examined. However, these species are also known for having extremely small flag leaves, brittle rachis (which eases seed dispersal from the ear) and a low harvest index area (fraction of the biomass allocated to the grain; (Carmo-Silva *et al.*, 2017) which are not traits that are desirable in modern bread wheat.

Existing genotypic variation in photosynthetic efficiency can be exploited by identifying promising species and traits for subsequent integration into breeding programmes aimed at improving crop performance (Lawson *et al.*, 2012). WWR represent an unexploited target for the introduction of beneficial traits, specifically SD, SS and photosynthetic efficiency to improve yield (Muir *et al.*, 2014; Monda *et al.*, 2016; Faralli & Lawson, 2020; McAusland *et al.*, 2020; Yamori *et al.*, 2020). Moreover, the identification of WWR with potential for improving wheat productivity are a first step to inform follow-on gene discovery and pre-breeding programmes, specifically cultivar TRI 3432 (with a higher photosynthetic capacity than EW), TRI 18510 (higher g_{max} than EW), KU 2036 (shortest τ_{gs} than EW) and AE 472/87, KU 2043, IG 48514 and IG 48556 (higher W_i than EW) would be a good place to start.

CHAPTER 6

Effect of CO₂ concentration on anatomy and physiology of landraces and wheat wild relatives

6.1. Introduction

In the past, the atmospheric CO₂ concentration ([CO₂]) was maintained at figures close to 280 ppm for approximately 1000 years prior to the industrial revolution, since then anthropogenic CO₂ emissions, most notably the burning of fossil fuels, has facilitated the increase of [CO₂] to 409.8 ± 0.1 ppm in 2019 (NOAA, 2020), almost 40 % higher than at any time in the last 20 million years (Pagani *et al.*, 1999; Pearson & Palmer, 2000). With the current increases in CO₂ emissions associated with modern day demands, [CO₂] is projected to surpass 700 ppm by the end of the century (Prentice *et al.*, 2001). In this chapter, plants were grown at an elevated [CO₂](e[CO₂]) of 800 ppm, approximately double that of the current [CO₂]. Many studies have already emphasised the positive effect of e[CO₂] on C₃ crop yields, mainly driven by the enhancement of photosynthesis (Leahey *et al.*, 2009; Gray *et al.*, 2016; Xu *et al.*, 2016). Elevated [CO₂] increases C_i and in C₃ plants it can enhance CO₂ fixation by inhibiting the competing oxygenation reaction by ribulose-1,5-bisphosphate carboxylase-oxygenases (RuBisCO) known as photorespiration and consequently increasing plant growth and production (Long *et al.*, 2006; Ainsworth & Rogers, 2007; Xu *et al.*, 2016). This could lead to increases in biomass or yield of up to 30 % depending on species, environmental conditions and experimental [CO₂] (Leahey *et al.*, 2009). Furthermore, several lines of experimental evidence have demonstrated a mean reduction of g_s under e[CO₂] (for example, Ainsworth & Rogers, 2007) depending on species and photosynthetic pathway, which could limit the CO₂ fixation rate but in turn increase water use efficiency (W_i) benefiting plant growth (Leahey *et al.*, 2009; Sreeharsha *et al.*, 2015). The reduction in g_s and increased W_i , will lead to lower transpiration rates and therefore higher temperatures which could, in turn, have

deleterious effects on plant growth, especially if current global atmospheric temperatures continue to increase (Stevens *et al.*, 2020).

The reduction in g_s is facilitated by a multitude of factors, including a decrease in the numbers of stomata over the leaf lamina, which has been reported for a wide range of species grown under elevated $[\text{CO}_2]$ (Woodward & Kelly, 1995; Woodward *et al.*, 2002; Casson & Gray, 2008; Casson & Hetherington, 2010; Soh *et al.*, 2019). Although, wood species typically demonstrate little change in stomatal density with $e[\text{CO}_2]$ (Ainsworth & Rogers, 2007; Xu *et al.*, 2016) suggesting the mechanisms of $e[\text{CO}_2]$ on stomatal density are species-specific and genotype-dependent. Gray *et al.* (2000) explored the genetic mechanism of stomatal density reduction in arabidopsis at $e\text{CO}_2$ and demonstrated that the HIC (High Carbon dioxide) gene in arabidopsis disrupts the signal transduction pathway responsible for the control of stomatal patterning in response to $e\text{CO}_2$. Therefore, identifying a negative regulator of guard cell development which downregulates stomatal development in $e\text{CO}_2$.

This study assessed phenotypic variation in morphological traits such as stomatal size and density and compared six wheat wild relative (WWR) species including *Aegilops tauschii*, *Triticum turgidum ssp. Dicocoides* and *Triticum turgidum ssp. Dicoccon* to 5 elite *Triticum aestivum* (EW) cultivars, Claire, Rialto, Robigus, Soissons and Xi19. These wheat species were grown at two differing CO_2 concentrations (atmospheric at 408 ppm ($[\text{CO}_2]$) and elevated at 800 ($e[\text{CO}_2]$)). Wild relatives of modern wheat may harbour traits that are unavailable in the existing EW germplasm that could be useful for incorporation in modern breeding programmes. Similarly, the understanding of morphological and physiological differences in wheat to environmental conditions, such as $e[\text{CO}_2]$ is important for understanding the underlying mechanism for key biological processes.

To improve future productivity and resilience in EW in differing environments, it may benefit from looking at wheat wild progenitors which grew and thrived in environment that modern day wheat find difficult, such as high temperatures, low water supply, high CO₂ and possibly have the ability to resist current diseases (Faris, 2014; McAusland et al., 2020) which could be identified as an unexploited resources to explore wild wheat traits for modern breeding programmes and relatives, as described in the previous chapter (section 5.1). Furthermore, investigation into manipulating guard cell performance and or stomatal density may produce a more successful balance between CO₂ uptake and water loss through transpiration to enhance photosynthetic capacity with high W_i .

The first aim of the work presented in this chapter was to assess the extent of phenotypic variation in morphological traits between the 6 wild wheat relatives (WWR) and 5 elite wheat (EW) cultivars in two sets of wheat grown at two differing CO₂ concentrations (atmospheric at 408 ppm ([CO₂]) and elevated at 800 ppm (e[CO₂])) and to ascertain any variation in g_{smax} between the wheat species. Secondly to evaluate the impact of any physiological variation on the rapidity of stomatal responses and its effect on CO₂ assimilation, and photosynthetic capacity. The hypothesis being that those grown in elevated CO₂ conditions will present morphological differences such as lower stomatal densities, larger stomatal sizes which will influence g_{smax} , stomatal kinetics and photosynthetic capacity between the species, and moreover between the CO₂ concentrations.

6.2 Materials and Methods

This section outlines methods specific to this chapter and modifications made to protocols outlined in Chapter 2 – “Materials and Methods”.

6.2.1 Plant material and growth conditions

Wheat species (Table 6.1) were grown in the BASF Crop solutions facilities in Ghent, Belgium, with slight adaptations to the method 2.1.

Table 6.1 Species selected for this chapter including ploidy and common name. Species abbreviation is how the species will be referred to in the text.

Species Abbreviation	Species	Common Name	Ploidy
Claire-4	<i>Triticum aestivum</i>	Common or Bread Wheat	Hexiploid
RIALTO	<i>Triticum aestivum</i>	Common or Bread Wheat	Hexiploid
Robigus	<i>Triticum aestivum</i>	Common or Bread Wheat	Hexiploid
SOISSONS	<i>Triticum aestivum</i>	Common or Bread Wheat	Hexiploid
Xi19	<i>Triticum aestivum</i>	Common or Bread Wheat	Hexiploid
IG 48509	<i>Aegilops tauschii</i>	Goatgrass or rough-Spike Hard Grass	Diploid
IG 48514	<i>Aegilops tauschii</i>	Goatgrass or rough-Spike Hard Grass	Diploid
KU 2018	<i>Aegilops tauschii</i>	Goatgrass or rough-Spike Hard Grass	Diploid
KU 2036	<i>Aegilops tauschii</i>	Goatgrass or rough-Spike Hard Grass	Diploid
TRI 11502	<i>Triticum dicoccoides</i>	Wild Emmer	Tetraploid
TRI 3432	<i>Triticum dicoccon</i>	Emmer	Tetraploid

In the BASF Crop solutions facilities plants were germinated and vernalised in the same way using an in-house produced 60/40 peat-based sowing and cutting soil (including NPK Compound Fertilizer 12-14-24 (0.8 kg m⁻³)) and when finished vernalisation were transferred into 4 l pots using a peat-based, boron free potting soil (including NPK Compound Fertilizer 12-14-24 (2 kg m⁻³)). Plants were well watered throughout the day using a drip irrigation system, watering to the roots of plants. Plants were grown in two separate growth chambers of differing CO₂ concentrations

(atmospheric at 408 ppm CO₂ and elevated at 800 ppm CO₂) between the months of September and November 2019. Both growth chambers had a light intensity (table level) of +/- 200 $\mu\text{mol m}^{-2} \text{s}^{-1}$ with a 2 HPS/1MH lighting mix (Master Greenpower CGT 400 W E40 and Powerstar HQI-BT 400 W/D PRO 400 W Daylight E40 respectively) for a 15 hour day length. Both chambers air temperature was maintained at 20 °C \pm 1 °C during the day and 18 °C \pm 1 °C at night with relative humidity maintained at +/- 65%.

6.2.2 Leaf and stomatal characteristics

6.2.2.1 Leaf epidermal impressions

Leaf epidermal impressions were generated following the method 2.2.1. All impressions were taken from fully expanded single leaves of similar positions at the middle of the flag leaf, on both the abaxial and adaxial leaf surfaces, avoiding major veins and leaf edges before anthesis (Zadocks growth stage 49-59). Impressions were taken from the same lead tillers of six wheat plant replicates per cultivar.

6.2.2.2 Stomatal anatomical measurements

Stomatal density, guard cell length and pore length were measured via light microscopy (Olympus BX60, Southend-on-Sea, Essex, UK) following the method 2.2.2 and 2.2.3 respectively. Guard cell length and pore length measurements were used to generate potential anatomical maximum stomatal conductance (g_{smax} mol m⁻² s⁻¹) following the calculation in method in section 2.2.4.

6.2.2.2 Leaf thickness

Leaf thickness was calculated for 6 biological replicates of each cultivar using method in section 2.2.6.

6.2.2.3 Leaf anatomical measurements

Dry weight and leaf area were calculated for 6 biological replicates of each cultivars using methods in section 2.2.7.

6.2.3 Leaf gas exchange

All gas exchange parameters were recorded using a Li-Cor 6400XT portable gas exchange system (Li-Cor, Lincoln, Nebraska, USA) following the method in section 2.2. Both atmospheric CO₂ grown species (~ 408 ppm CO₂) and elevated CO₂ grown species (~ 800 ppm) had gas exchange measurements completed in atmospheric CO₂ conditions of ~ 408 ppm CO₂.

6.2.3.1 PPFD-step measurements

The response of net CO₂ assimilation rate (A) and stomatal conductance (g_s) to a step change in photosynthetic photon flux density ($PPFD$) was carried out as described in method in section 2.3.1.

6.2.3.2 Intracellular CO₂ response curves (A/C_i)

A/C_i response curves (net CO₂ assimilation rate (A) to intercellular CO₂ concentration (C_i)) were measured as described in method in section 2.3.2.

6.2.4 Modelling gas exchange parameters

6.2.4.1. Estimating photosynthetic capacities

Photosynthetic capacities ($V_{C_{max}}$ and J_{max}) were estimated from the A/C_i response curves using method in section 2.5.1.

6.2.4.1 Determining the rapidity of A and g_s response

The rapidity of the photosynthetic response following a step change in light intensity was assessed using method 2.5.3, whilst method 2.5.2 was used to determine the rapidity of the stomatal response following a step change in light intensity.

6.2.5 Statistical analysis

Statistics were conducted using R software (www.r-project.org; version 3.5.3) following the methods in section 2.6.

6.3. Results

6.3.1 Leaf and stomatal anatomy

Stomatal impressions were made for each of the wheat species, 5 elite *Triticum aestivum* cultivars, Claire, Rialto, Robigus, Soissons and Xi19 (EW, all hexaploid) and 6 wild wheat relative (WWR) species, IG 48509, IG 48514, KU 2018, KU 2036 (all 4 diploid), TRI 3432 and TRI 11502 (both tetraploid, grown in differing CO₂ concentrations (atmospheric (Ca) at ~ 408 ppm and elevated (e[CO₂]) ~ 800 ppm) to measure stomatal density (SD; mm⁻²), guard cell length (GCL; μm) as a proxy for stomatal size (SS), and pore length (PL; μm) which were used to calculate the anatomical maximum potential g_s (g_{smax} ; mol m⁻² s⁻¹). Densities (Fig. 6.1 and 6.2), SS (Fig. 6.3 and 6.4) and g_{smax} (Fig. 6.6 and 6.7) were compared between species, leaf surfaces and CO₂ growth concentrations using a two-way ANOVA (Table 6.2). A Tukey post-hoc test followed (Table 6.3) to show individual differences between opposing leaf surfaces of the same species, and CO₂ growth concentrations between the same species.

Table 6.2: Two-way analysis of variance (ANOVA) results between species, leaf surfaces (abaxial and adaxial) and CO₂ growth concentrations (atmospheric at ~ 408 ppm and elevated ~ 800 ppm) for stomatal density, guard cell length and g_{smax} of 11 wheat species, indicating F values and p values, highlighting where significant differences have been observed. Sig. codes: 0 '***' 0.001 '**' 0.01 '*' 0.05 '.' (n = 6)

Flag Leaf	Stomatal Density			Guard Cell Length			G_{smax}		
	F value	Pr(>F)	Sig	F value	Pr(>F)	Sig	F value	Pr(>F)	Sig
Species	81.564	2.00E-16	***	36.077	2.00E-16	***	25.019	2.00E-16	***
Surface	231.452	2.00E-16	***	35.735	9.24E-09	***	265.65	2.00E-16	***
CO ₂	78.616	2.93E-16	***	0.319	5.73E-01		16.832	5.79E-05	***
Species: Surface	10.249	4.53E-14	***	2.455	8.51E-03	**	7.413	4.28E-10	***
Species: CO ₂	50.619	2.00E-16	***	8.119	4.13E-11	***	13.739	2.00E-16	***
Surface: CO ₂	0.086	7.70E-01		0.413	5.21E-01		0.081	7.76E-01	
Species: Surface: CO ₂	2.549	6.31E-03	**	0.921	5.15E-01		2.228	0.0173	*

Table 6.3. Tukey results following a two-way ANOVA between CO₂ growth concentrations (atmospheric at ~ 408 ppm and elevated ~ 800 ppm) of the same species for stomatal density, guard cell length and g_{smax} of wheat species, indicating p-values, highlighting where significant differences have been observed. Sig. codes: 0 '***' 0.001 '**' 0.01 '*' 0.05 '.' (n = 6)

Flag Leaf CO ₂ Treatments	Stomatal Density		Guard Cell Length		G_{smax}	
	p adj	Sig	p adj	Sig	p adj	Sig
Atmospheric vs Elevated	0	***	5.73E-01		5.93E-05	***
Claire Atmospheric vs Claire Elevated	0	***	4.16E-04	***	1.00E-06	***
Rialto Abaxial vs Rialto Adaxial	3.81E-05	***	9.93E-01		5.18E-01	
Robigus Abaxial vs Robigus Adaxial	1		1		1	
Soissons Abaxial vs Soissons Adaxial	1		1		9.78E-01	
Xi19 Abaxial vs Xi19 Adaxial	9.99E-01		5.22E-01		1	
IG 48509 Abaxial vs IG 48509 Adaxial	2.67E-01		8.22E-01		3.60E-06	***
IG 48514 Abaxial vs IG 48514 Adaxial	0	***	1.16E-04	***	1.54E-04	***
KU 2018 Abaxial vs KU 2018 Adaxial	0	***	1		9.98E-01	
KU 2036 Abaxial vs KU 2036 Adaxial	0	***	1		9.90E-06	***
TRI 3432 Abaxial vs TRI 3432 Adaxial	9.96E-01		4.17E-02	.	2.43E-01	
TRI 11502 Abaxial vs TRI 11502 Adaxial	5.03E-05	***	1		1	

6.3.1.1 Stomatal Density

In this study, a difference ($p < 0.05$) in SD was found between species, leaf surfaces and CO₂ growth concentrations. Interactions were observed (Table 6.2) of SD between species and surfaces, species and CO₂ growth concentrations, and species, surfaces and CO₂ growth concentrations combined, although no further tests were performed to explain these interactions. Significant ($p < 0.05$) variation in total SD frequency was found between species grown at atmospheric CO₂ (Fig. 6.1 A) with the hexaploid EW cultivars ranging from ~ 60 mm² to ~100 mm². Between the WWR species there was an even larger SD range of ~ 60 mm² to ~150 mm², showing a 60 % difference between the lowest and the highest SD means. Species grown at elevated CO₂ (Fig. 6.1 B and Table 6.3) had less of a range in SD frequencies, especially between the WWR species. Five species of differing ploidies had a significant ($p < 0.05$) reduction in SD frequencies at e[CO₂] (Rialto, IG 48514, KU 2036, KU2018 and TRI 3432), five species of differing ploidies had no differences and (Robigus, XI19, Soissons, IG 48509 and TRI 3432), although two species, a tetraploid and a hexaploid, showed a significant ($p < 0.05$) increase in SD at e[CO₂] (Claire and TRI 11502).

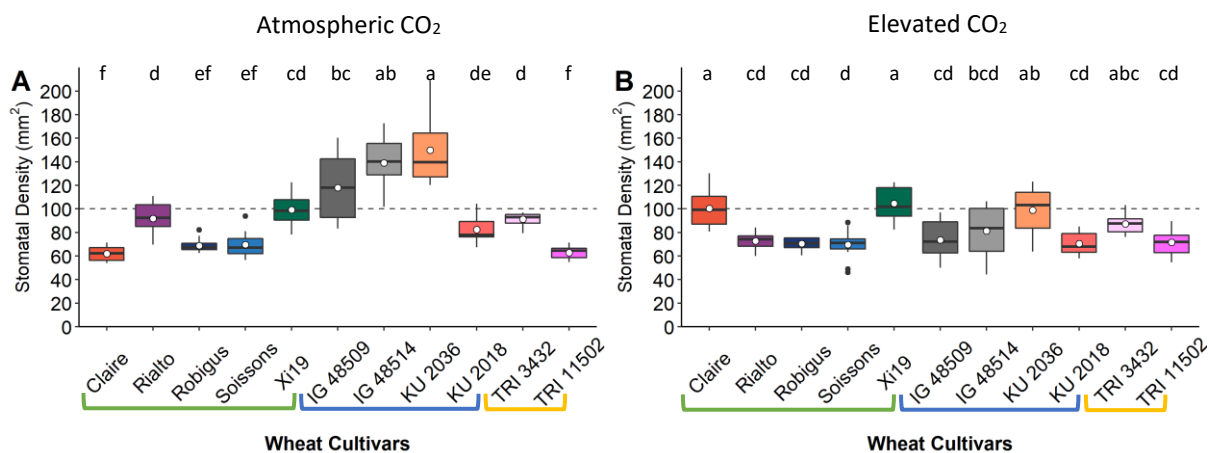


Figure 6.1 Variation (box and whisker plots displaying distribution of biological replicates) and mean (white dot) of flag leaf stomatal density (mm²) from an average of the two leaf surfaces of wheat species at both atmospheric CO₂ (~ 408 ppm; A) and elevated CO₂ (~ 800 ppm; B). Different letters represent statistically significant differences ($P < 0.05$) between means of different species using the results of a Tukey test following a two-way ANOVA. Dotted line represents 100 mm² ($n = 12$). Green bracket represents hexaploid species, blue bracket represents diploid species and yellow bracket represents tetraploid species.

When SD was separated by leaf surface a significant difference was found after a two-way ANOVA ($p < 0.0001$), a similar trend followed between the atmospheric CO₂ and elevated CO₂, with the adaxial leaf surface SD showing a larger range, driving the large range in total SD differences. A larger SD range of means were found on the adaxial leaf surface, predominantly on species grown at atmospheric CO₂. The adaxial leaf surface is most responsive to CO₂ induced reductions in SD. When species are separated by ploidy it was observed that all diploid species had a reduced SD at e[CO₂] from Ca, tetraploid species increased in density at e[CO₂] but no specific trends were observed for hexaploid cultivars.

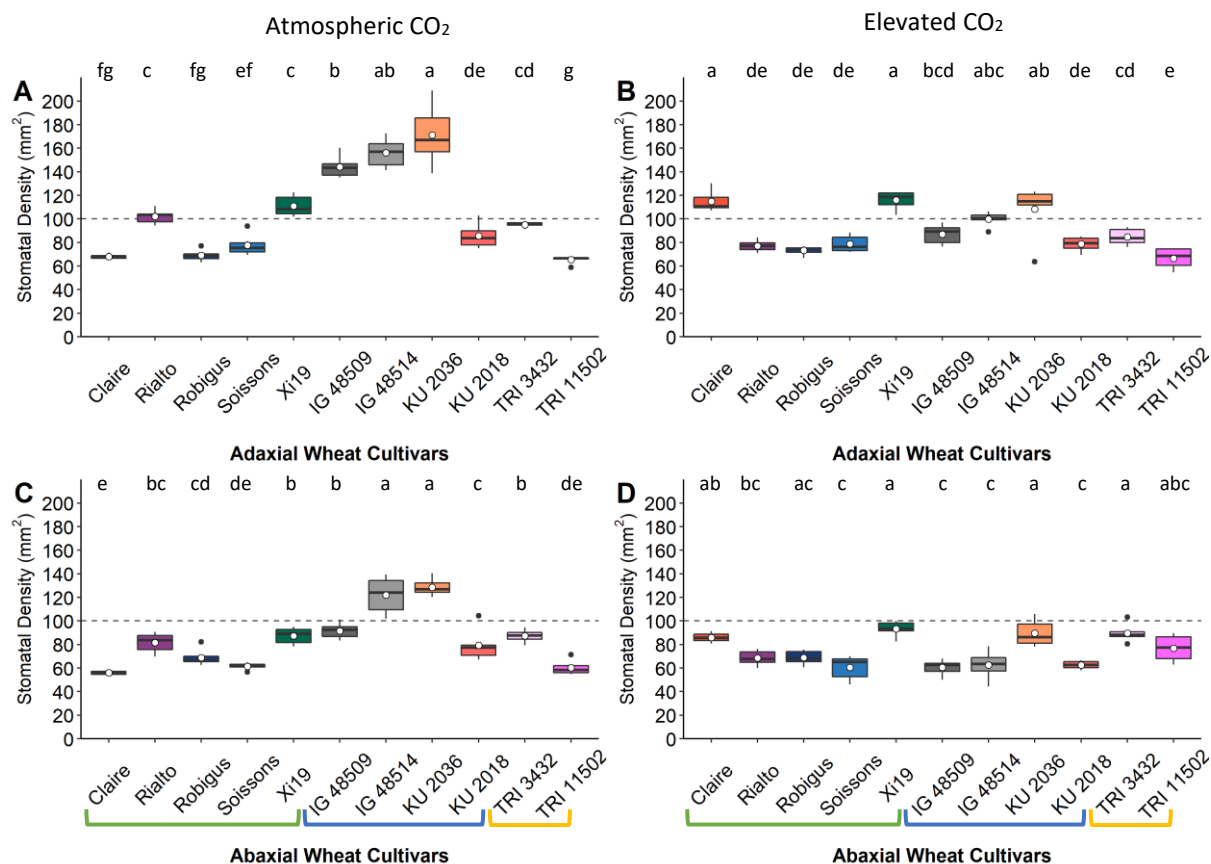


Figure 6.2 Variation (box and whisker plots displaying distribution of biological replicates) and mean (white dot) of flag leaf stomatal density (mm²), calculated for the adaxial (A and B) and abaxial (C and D) leaf surfaces for wheat species at both atmospheric CO₂ (~ 408 ppm; A and C) and elevated CO₂ (~ 800 ppm; B and D). Different letters represent statistically significant differences ($P < 0.05$) between means of different species using the results of a Tukey test following a two-way ANOVA. Green bracket represents hexaploid species, blue bracket represents diploid species and yellow bracket represents tetraploid species. Dotted line represents 100 mm² ($n = 6$).

6.3.1.2 Guard Cell Length

A difference ($p < 0.05$) in SS between species and leaf surfaces was found in these results (Table 6.2). A Tukey post-hoc test revealed significant differences ($p < 0.05$) between species grown at Ca, and species grown at e[CO₂]. Differences in GCLs from the same species between growth CO₂ concentrations were found on Claire, IG

48514 and TRI 3432. At Ca, a group of three species displaying the highest SD (IG 48514, KU 2036, KU2018; Fig. 6.3 A) also displayed the smallest SS (Fig. 6.3 A). A concise range of SS was observed between both CO₂ growth concentrations at approx. 40 µm. The smallest SS was found on KU 2036 at ~ 33 µm at Ca and ~ 35 µm at e[CO₂], while the largest SS was found on species XI19 at ~ 47 µm at Ca and species Robigus at ~ 45 µm at e[CO₂].

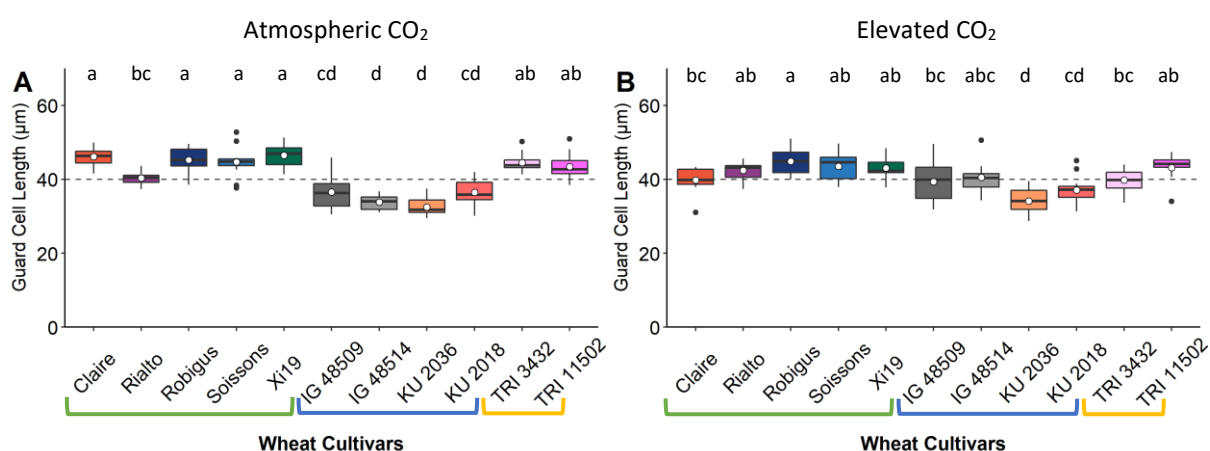


Figure 6.3 Variation (box and whisker plots displaying distribution of biological replicates) and mean (white dot) of flag leaf guard cell length (µm) from an average of the two leaf surfaces for 11 wheat species at both atmospheric CO₂ (~ 408 ppm; A) and elevated CO₂ (~ 800 ppm; B). Different letters represent statistically significant differences ($P < 0.05$) between means of different species using the results of a Tukey test following a two-way ANOVA. Green bracket represents hexaploid species, blue bracket represents diploid species and yellow bracket represents tetraploid species. Dotted line represents 40 µm ($n = 12$).

SS follows the same trend as total SS when separated between the adaxial and abaxial leaf surface (Fig. 6.4) whereby, larger SS were observed in the EW and as a trend the WWR had the smaller SS (except TRI 3432 and TRI 11502). All species have SS at approx. 40 µm with the largest adaxial SS observed in species XI19 for both CO₂ growth concentrations and the smallest SS was observed in species KU

2036 for both CO₂ growth concentrations. The largest abaxial SS observed (Fig. 6.4) in species XI19 and Robigus Ca and e[CO₂] respectively and the smallest SS was again observed in species KU 2036 for both CO₂ growth concentrations. When species are separated by ploidy it was observed that all diploid species had an increase of SS at e[CO₂] from Ca, tetraploid species showed a reduction of SS at e[CO₂] but no specific trends were observed for hexaploid cultivars.

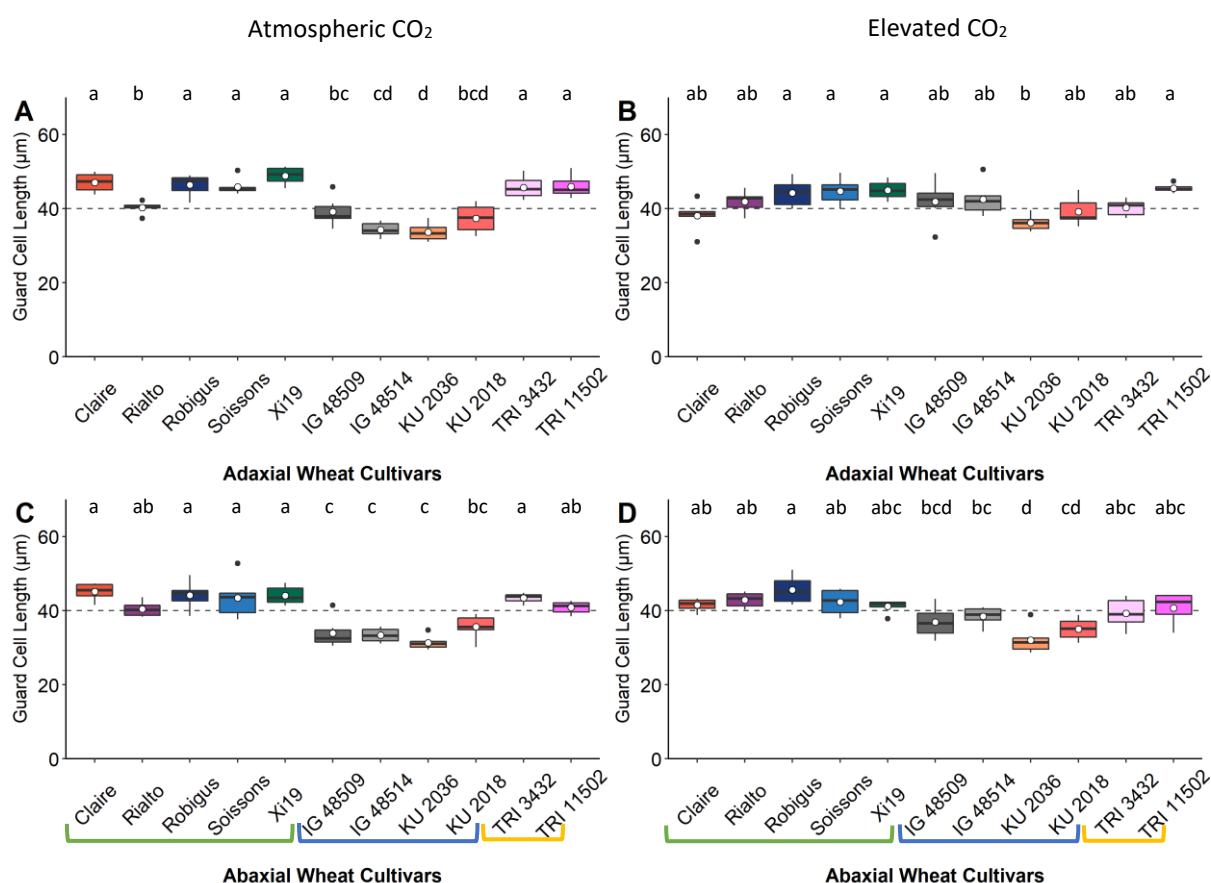


Figure 6.4 Variation (box and whisker plots displaying distribution of biological replicates) and mean (white dot) of flag leaf guard cell length (µm), calculated for the adaxial (A and B) and abaxial (C and D) leaf surfaces for 11 wheat species at both atmospheric CO₂ (~ 408 ppm; A and C) and elevated CO₂ (~ 800 ppm; B and D). Different letters represent statistically significant differences (P < 0.05) between means of different species using the results of a Tukey test following a two-way ANOVA. Green bracket represents hexaploid species, blue bracket represents diploid species and yellow bracket represents tetraploid species. Dotted line represents 40 µm (n = 6).

A significant ($p= 6.798e-12$) negative correlation was observed in Ca grown species between SD and SS (Fig. 6.5) and a negative correlation was found in e[CO₂] grown species, although not significant, demonstrating that SS increases as SD decreases although this is not as prevalent in a species grown at e[CO₂]. The Ca grown species (Fig. 6.5 A) with the highest SD mean (KU 2036) had the smallest SS, and the Ca grown species with the lowest SD mean (Claire) had one of the largest SS.

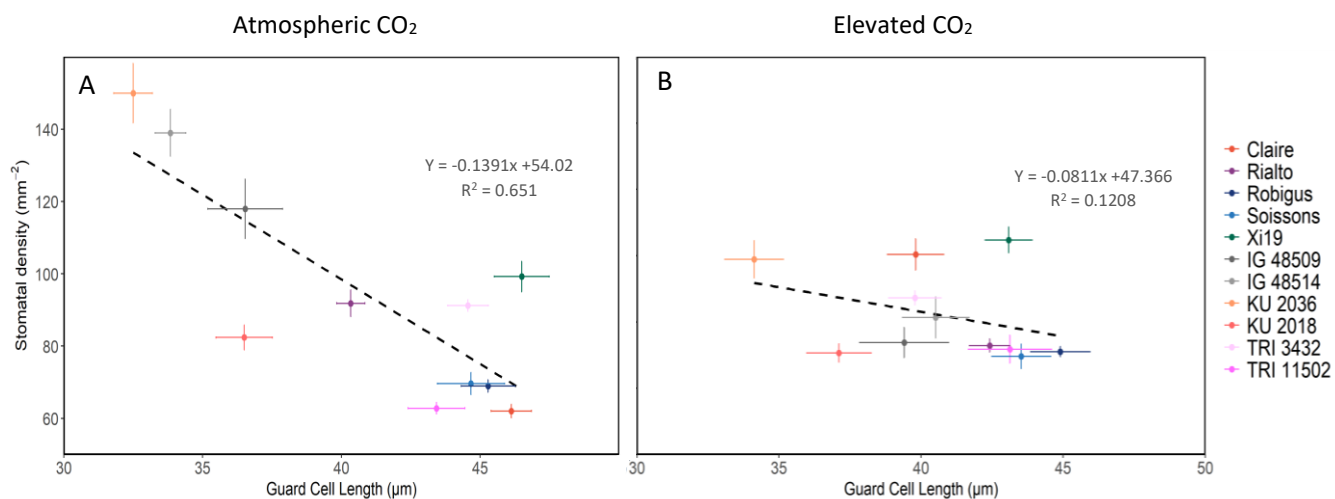


Figure 6.5 Correlation between total stomatal density (mm²) and total guard cell length (μm) for each species from two leaf surfaces for 11 wheat species at atmospheric CO₂ (~ 408 ppm; A) elevated CO₂ (~ 800 ppm; B). Black dotted line represents the trend in the data between the two variables. Atmospheric CO₂ correlation = -0.5520802 ($p= 6.798e-12$) and elevated CO₂ correlation = 0.06259211 ($p=0.4827$) using a Pearson's correlation test. Error bars represent standard error (n = 12)

3.3.1.3 Anatomical potential maximum rate of g_s

The results of a two-way ANOVA (Table 6.2) exhibited significant differences ($p < 0.05$) in anatomical potential maximum rate of g_s (g_{smax}) between species, leaf surfaces and CO_2 growth concentrations. Interactions were observed for g_{smax} between species and surfaces, species and CO_2 growth concentrations and species, surfaces and CO_2 growth concentrations combined although no further tests were performed to explain these interactions. At atmospheric CO_2 (Fig. 6.6 A) a considerable range of g_{smax} values was observed between species, with Soissons displaying the lowest values at $\sim 1.4 \text{ mol m}^{-2} \text{ s}^{-2}$ and the highest displayed in species KU 2036 at $\sim 2.4 \text{ m}^{-2} \text{ s}^{-2}$, an increase of $\sim 41\%$ between the lowest and the highest g_{smax} means. This considerable range in g_{smax} is driven predominantly by the differences in SD. The range in $e[CO_2]$ g_{smax} means (Fig. 6.6 A) from IG 48509 at $\sim 1.5 \text{ m}^{-2} \text{ s}^{-2}$ and Xi19 at $\sim 2.6 \text{ m}^{-2} \text{ s}^{-2}$ is also sizable, with an increase of 42 % between the lowest and the highest g_{smax} means, although eight species g_{smax} values fell between $1.55 \text{ m}^{-2} \text{ s}^{-2}$ and $1.75 \text{ m}^{-2} \text{ s}^{-2}$, a difference of less than 12 %. A significant difference ($p < 0.05$) of g_{smax} mean values were observed (Fig. 6.6 and Table 6.3) between Ca and $e[CO_2]$ growth concentrations of the same species (Claire, IG 48509, IG 48514 ad KU 2036).

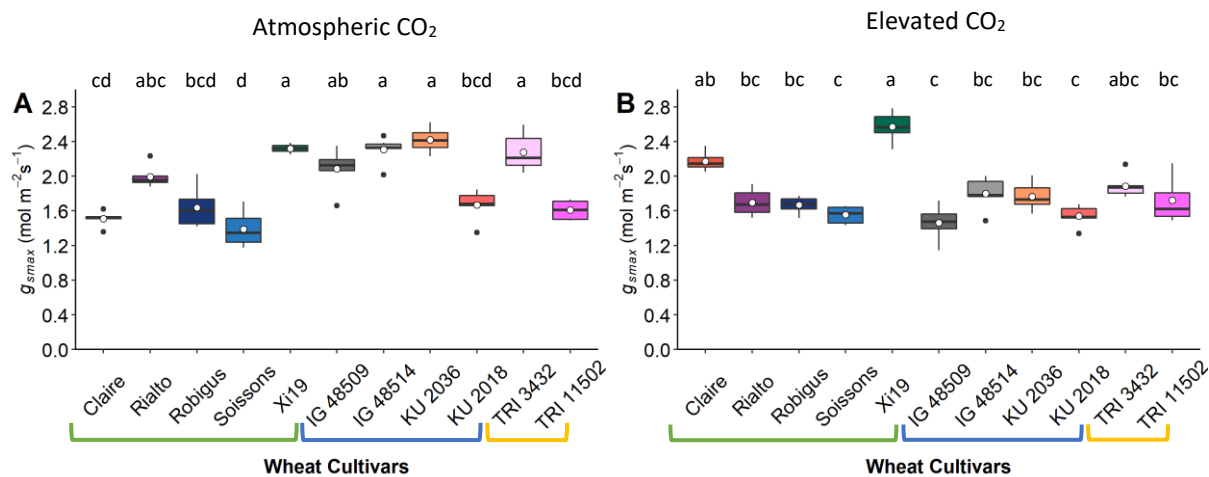


Figure 6.6 Variation (box and whisker plots displaying distribution of biological replicates) and mean (white dot) of flag leaf g_{smax} (mol m⁻¹ s⁻¹), calculated from an average of the two leaf surfaces stomatal density and guard cell length dimensions, for 11 wheat species at both atmospheric CO₂ (~ 408 ppm; A) and elevated CO₂ (~ 800 ppm; B). Different letters represent statistically significant differences ($P < 0.05$) between means of different species using the results of a Tukey test following a two-way ANOVA ($n = 12$). Green bracket represents hexaploid species, blue bracket represents diploid species and yellow bracket represents tetraploid species.

Leaf surface and CO₂ treatment g_{smax} (Fig. 6.7) was significant different ($p < 0.0001$) between species, with higher g_{smax} values observed on the adaxial leaf surface of both CO₂ growth concentrations. all abaxial species (except e[CO₂] species Xi19) fell under g_{smax} 1.0 mol m⁻² s⁻¹, whereas many adaxial species were observed above g_{smax} 1.0 mol m⁻² s⁻¹.

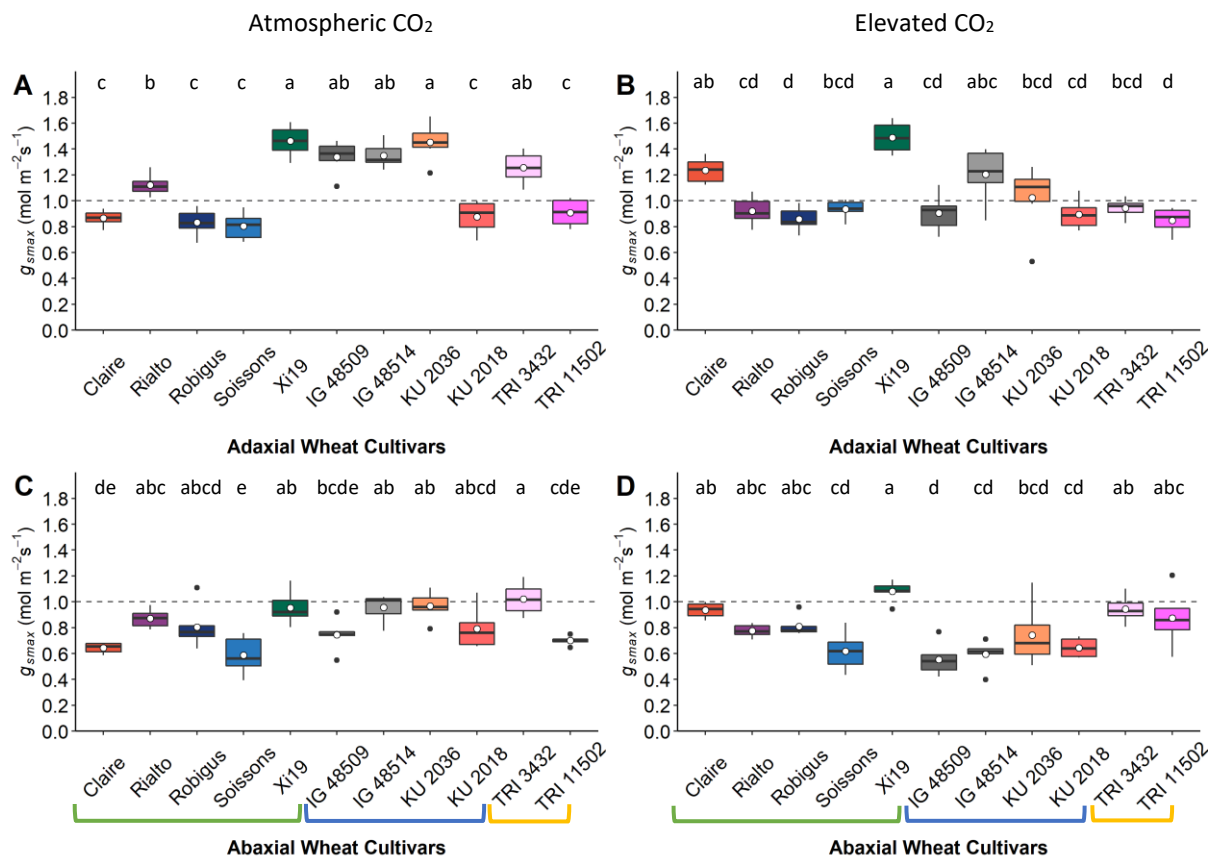


Figure 6.7 Variation (box and whisker plots displaying distribution of biological replicates) and mean (white dot) of flag leaf g_{smax} (mol m⁻¹ s⁻¹), calculated from stomatal density and guard cell length dimensions of the adaxial (A and B) and abaxial (C and D) leaf surfaces for 11 wheat species at both atmospheric CO₂ (~ 408 ppm; A and C) and elevated CO₂ (~ 800 ppm; B and D). Different letters represent statistically significant differences ($P < 0.05$) between means of different species using the results of a Tukey test following a two-way ANOVA. Green bracket represents hexaploid species, blue bracket represents diploid species and yellow bracket represents tetraploid species. Dotted line represents 1.0 mol m⁻¹ s⁻¹ ($n = 6$).

6.3.1.4 Leaf area, leaf dry weight, and leaf thickness

The EW and WWR wheat species grown in differing CO₂ growth concentrations were measured for leaf area (LA; cm²), dry weight (DW; g) and leaf thickness (LT; μm). LA (Fig. 6.8), DW (Fig. 6.9) and LT (Fig. 6.10) and were compared between species and CO₂ growth concentrations (Table 6.4). A Tukey post-hoc test showed individual differences between species (indicated on graphs) and between CO₂ growth concentrations of the same species (Table 6.5).

Table 6.4: Two-way analysis of variance (ANOVA) results between flag leaf species and CO₂ growth concentrations (atmospheric at ~ 408 ppm and elevated ~ 800 ppm) for Leaf dry weight, leaf area and leaf thickness of 11 wheat species, indicating F values and p values, highlighting where significant differences have been observed. Sig. codes: 0 '***' 0.001 '**' 0.01 '*' 0.05 '.' (n = 6)

Flag Leaf	Dry Weight			Leaf Area			Leaf Thickness		
	F value	Pr(>F)	Sig	F value	Pr(>F)	Sig	F value	Pr(>F)	Sig
Species	57.413	< 2e-16	***	5.381	1.94E-06	***	19.369	<2e-16	***
CO ₂	8.253	4.89E-03	**	2.975	8.74E-02	.	0.918	3.40E-01	
Species: CO ₂	3.848	1.76E-04	***	1.404	1.88E-01		2.243	2.02E-02	*

Table 6.5. Tukey results following a two-way ANOVA between CO₂ growth concentrations (atmospheric at ~ 408 ppm and elevated ~ 800 ppm) of the same species for Leaf dry weight, leaf area and leaf thickness of 11 wheat species, indicating p-values, highlighting where significant differences have been observed. Sig. codes: 0 '****' 0.001 '**' 0.01 '*' 0.05 '.' (n = 6)

Flag Leaf CO2 Treatments	Dry Weight		Leaf Area		Leaf Thickness	
	p adj	sig.	p adj	sig.	p adj	sig.
Atmospheric vs Elevated	4.91E-03	**	8.75E-02	.	3.40E-01	
Claire Atmospheric vs Claire Elevated	1		1		1	
Rialto Abaxial vs Rialto Adaxial	1		1.24E-01		9.99E-01	
Robigus Abaxial vs Robigus Adaxial	9.99E-01		1		1	
Soissons Abaxial vs Soissons Adaxial	5.18E-01		1		9.20E-01	
Xi19 Abaxial vs Xi19 Adaxial	1.48E-01		1		9.29E-01	
IG 48509 Abaxial vs IG 48509 Adaxial	5.37E-02	.	9.99E-01		1	
IG 48514 Abaxial vs IG 48514 Adaxial	1		1		1	
KU 2018 Abaxial vs KU 2018 Adaxial	1		1		1	
KU 2036 Abaxial vs KU 2036 Adaxial	4.66E-01		1		8.18E-01	
TRI 3432 Abaxial vs TRI 3432 Adaxial	9.88E-01		1		9.99E-01	
TRI 11502 Abaxial vs TRI 11502 Adaxial	1		1		8.00E-01	

Significant differences ($p < 0.001$) in LAs were observed (Table 6.4) between species. A post-hoc test revealed differences ($p < 0.05$) between species grown at Ca, and differences in species grown at e[CO₂], but no difference (Table 6.5) between CO₂ growth concentrations of the same species, for example, no difference were found in LAs between Claire grown at Ca and Claire grown at e[CO₂]. All EW species (Fig. 6.8) had larger LA than WWR, except for the species TRI 3432 for Ca. A similar trend followed for e[CO₂] species although less of a range was found between species. Species TRI 3432 (Fig. 6.8) had the largest ($p < 0.05$) LA in both CO₂ growth concentrations with IG 48509 having the smallest LA at Ca, a ~ 70 % reduction from the largest, and species KU 2036 had the smallest LA at e[CO₂], a ~ 75 % reduction from the largest e[CO₂] LA. At Ca there is a negative correlation between LA and SD, but not at e[CO₂], although both are not significant results. In hexaploid wheat flag LA is reduced when grown at e[CO₂], there was no similar trend in diploid or tetraploid species.

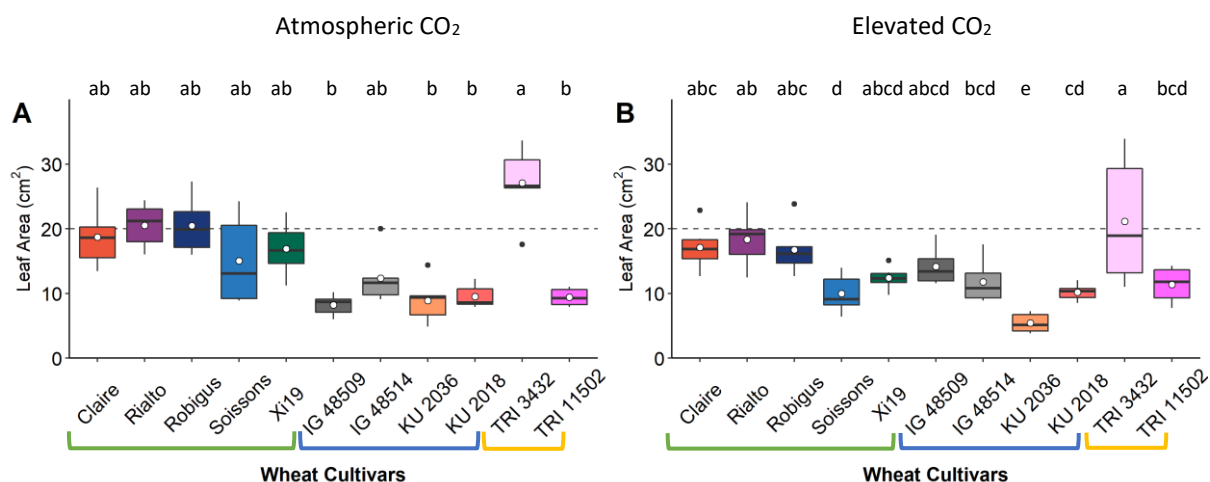


Figure 6.8 Variation (box and whisker plots displaying distribution of biological replicates) and mean (white dot) of flag leaf area (cm²) for 11 wheat species at both atmospheric CO₂ (~ 408 ppm; A) and elevated CO₂ (~ 800 ppm; B). Different letters represent statistically significant differences ($P < 0.05$) between means of different species. Green bracket represents hexaploid species, blue bracket represents diploid species and yellow bracket represents tetraploid species. Dotted line represents 20 cm² ($n = 12$).

Significant differences ($p < 0.001$) in DW were observed (Table 6.4) between species and CO₂ growth concentrations. A Tukey post-hoc test revealed significant differences ($p < 0.05$) between species grown at Ca, and species grown at e[CO₂], with no difference (Table 6.5) between CO₂ growth concentrations of the same species, also an interaction was observed between species and CO₂ growth concentrations although no further tests were performed to explain these interactions. As with the trend in LA, all EW species had higher DW (Fig. 6.9) than WWR, except for TRI 3432 for Ca grown species and for TRI 3432 and TRI 11502 for e[CO₂] grown species. EW species Rialto (Fig. 6.9) had the highest ($p < 0.05$) DW in both CO₂ growth concentrations with IG 48509 having the lowest DW at Ca, a ~ 84 % reduction from the largest, and species KU 2036 had the smallest LA at e[CO₂], an 80 % reduction from the largest LA. As with leaf area, all hexaploid DWs were reduced at e[CO₂] and no trends were observed for diploid and tetraploid species.

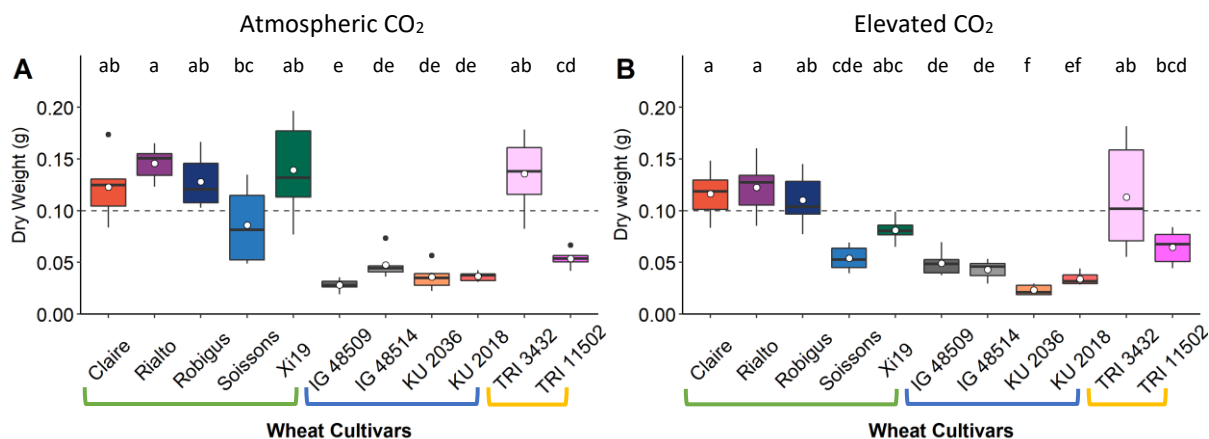


Figure 6.9 Variation (box and whisker plots displaying distribution of biological replicates) and mean (white dot) of flag leaf dry weight (g) for 11 wheat species at both atmospheric CO₂ (~ 408 ppm; A) and elevated CO₂ (~ 800 ppm; B). Different letters represent statistically significant differences ($P < 0.05$) between means of different species. Green bracket represents hexaploid species, blue bracket represents diploid species and yellow bracket represents tetraploid species. Dotted line represents 0.10 g ($n = 12$).

Significant differences ($p < 0.001$) in LT were observed (Table 6.4) between species. A Tukey post-hoc test revealed significant differences ($p < 0.05$) between species grown at Ca, and species grown at e[CO₂], with no difference (Table 6.5) between CO₂ growth concentrations of the same species. Both CO₂ growth concentrations had a large range of LT values that does not resemble the trends of LA and DW, indicating that LA drives DW rather than LT. The thickest and thinnest ($p < 0.05$) leaves in Ca grown species (Fig. 6.10) were Rialto and KU 2018 respectively with a ~ 45 % reduction from the largest, whereas the e[CO₂] grown species were thickest in Xi19 and thinnest in species Soissons, a ~ 40 % reduction from the largest. There were no LT trends for species with different ploidy.

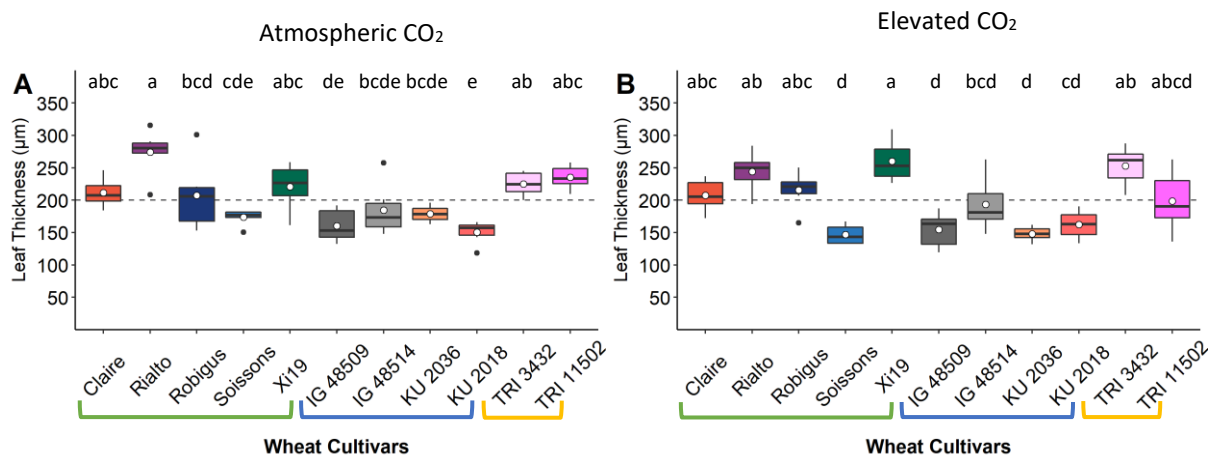


Figure 6.10 Variation (box and whisker plots displaying distribution of biological replicates) and mean (white dot) of flag leaf thickness (μm) for 11 wheat species at both atmospheric CO₂ (~ 408 ppm; A) and elevated CO₂ (~ 800 ppm; B). Different letters represent statistically significant differences ($P < 0.05$) between means of different species. Green bracket represents hexaploid species, blue bracket represents diploid species and yellow bracket represents tetraploid species. Dotted line represents $200 \mu\text{m}$ ($n = 12$).

6.3.2 Leaf gas exchange

6.3.2.1 Response of g_s and A to a step change in PPFD

To assess stomatal kinetics between wheat species grown in differing CO_2 growth concentrations, gas exchange measurements were completed in controlled CO_2 conditions of 400 ppm CO_2 . The response of g_s and A to a single step increase in light (100 to 1000 $\mu\text{mol m}^{-2} \text{s}^{-1}$ PPFD) was shown in figure 6.11 where all species exhibited the expected increase in g_s and A to the increased light intensity. Some species had not attained their maximum g_s values within the 50 min timeframe. Also, the exposure time to low light of 20 minutes might have been insufficient for complete low light steady state g_s ; however, this does not greatly impact the stomatal responses to the initial rapid opening response of the stomata. Considerable variation was observed in the A , g_s and W_i responses to step-changes in PPFD for both CO_2 growth concentrations although a higher range of variation was apparent in species grown in $e[\text{CO}_2]$. The increase in PPFD to 1000 $\mu\text{mol m}^{-2} \text{s}^{-1}$ led to an immediate and rapid increase in A compared to g_s for all species and after this initial period, the increase in A slowed to a magnitude similar to the increase in g_s , and A reached steady state while g_s continued to increase. The lack of synchrony between the responses of A and g_s to a step increase in PPFD had a consequential effect demonstrated by the temporal responses of W_i (A/g_s ; Fig. 6.11). Following the step change in PPFD, A rapidly increased compared to g_s and therefore W_i reached a maximum value minutes after the increase on PPFD. Further increases in g_s over time drove a continuous decrease in W_i after A had reached a steady state until the end of the protocol.

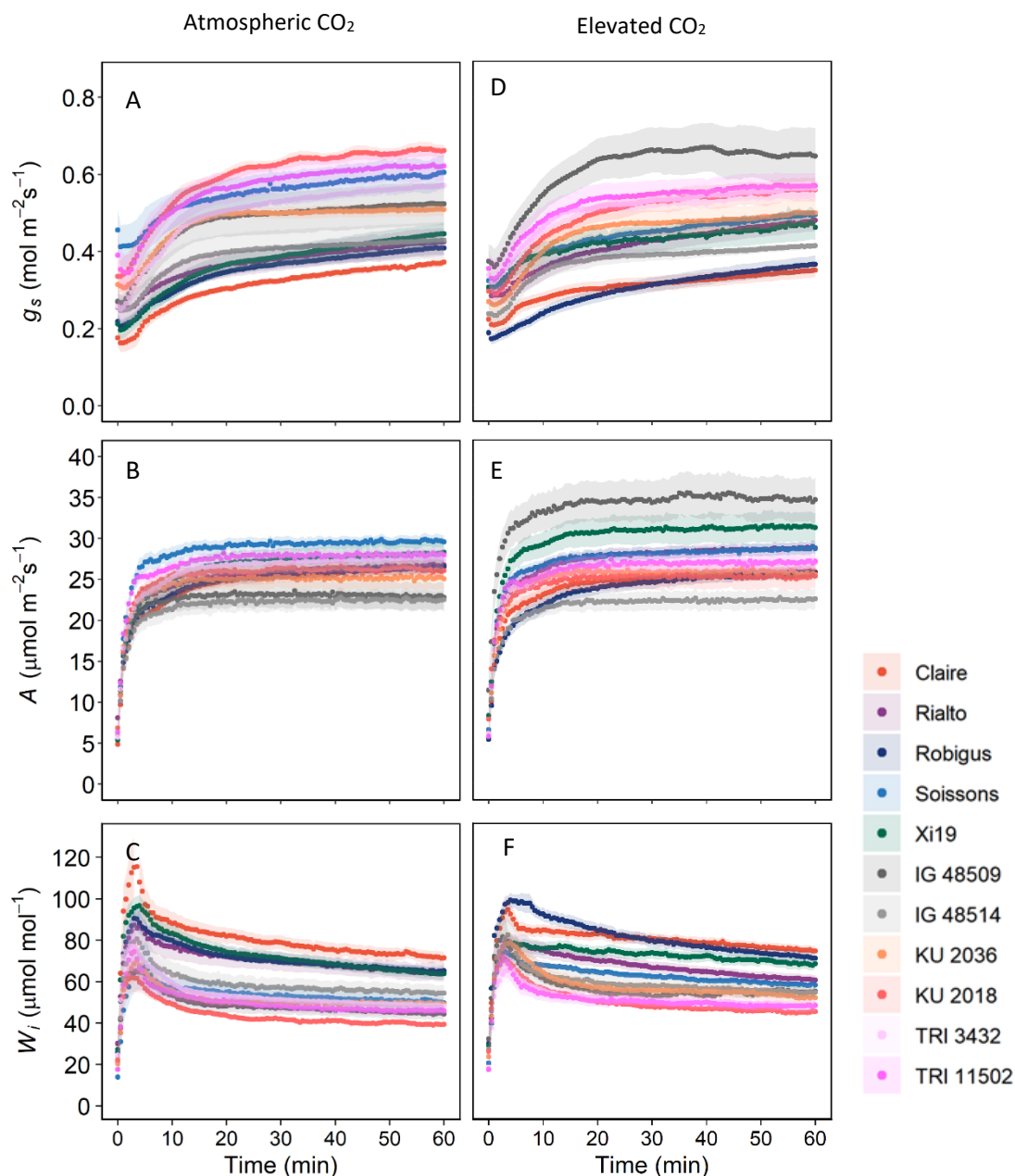


Figure 6.11 Temporal response of stomatal conductance (g_s ; A and D), net CO₂ assimilation (A ; B and E), and intrinsic water use efficiency (W_i ; C and F), to a step increase in light intensity (from $100 \mu\text{mol m}^{-2} \text{s}^{-1}$ for 20 minutes to $1000 \mu\text{mol m}^{-2} \text{s}^{-1}$ for 60 minutes) for wheat species at atmospheric CO₂ (~ 408 ppm) and elevated CO₂ (~ 800 ppm). Gas exchange parameters (g_s and A) were recorded at 30s intervals, leaf temperature maintained at 22°C , and leaf VPD at 1 ± 0.2 KPa. Error ribbons represent mean \pm SE (n = 5-7).

6.3.2.2. Speed of g_s response to a step change in light intensity

Stomatal responses to a step increase in light intensity (100 to 1000 $\mu\text{mol m}^{-2} \text{s}^{-1}$ PPFD) were used to determine natural variation in the speed of g_s and A response to light amongst the wheat species grown at differing CO_2 concentrations. Figure 6.12 displays the time constants to reach 63 % of final value for g_s (τ_{g_s} ; Fig. 6.12 A Ca and D $e[\text{CO}_2]$), final value of g_s (g_{sF} , Fig. 6.12 B Ca and E $e[\text{CO}_2]$) at 1000 $\mu\text{mol m}^{-2} \text{s}^{-1}$ PPFD and the magnitude of change in g_s (Δg_s , Fig. 6.12 C Ca and F $e[\text{CO}_2]$) between 100 - 1000 $\mu\text{mol m}^{-2} \text{s}^{-1}$ PPFD. Figure 6.13 displays the time constants to reach 63 % of final value for A (τ_A ; Fig. 6.13 A Ca and D $e[\text{CO}_2]$) final value of A (A_F , Fig. 6.13 B Ca and E $e[\text{CO}_2]$) at 1000 $\mu\text{mol m}^{-2} \text{s}^{-1}$ PPFD and finally the magnitude of change in A (ΔA , Fig. 6.13 C Ca and F $e[\text{CO}_2]$) between 100 - 1000 $\mu\text{mol m}^{-2} \text{s}^{-1}$ PPFD.

Time constants for the increases in g_s (τ_{g_s} ; Fig. 6.12 A Ca and D $e[\text{CO}_2]$) were significantly longer ($P < 0.05$) in the EW compared with the WWR for both CO_2 growth concentrations with the EW averaging 20 min and the WWR averaging 10 mins, a 50% reduction in time taken. The highest Ca and $e[\text{CO}_2]$ τ_{g_s} values observed were species Rialto and Robigus whereas the lowest τ_{g_s} values were species KU 2036 in Ca and TRI 11502 at $e[\text{CO}_2]$. The final value of g_s (g_{sF} , Fig. 6.12 B Ca and E $e[\text{CO}_2]$) were lower in the EW than the WWR species in both CO_2 growth concentrations (except Soissons at Ca) meaning higher g_{sF} was observed predominantly in WWR. The highest Ca g_{sF} observed was species KU 2018 with Soissons and TRI 11502 close behind with the highest $e[\text{CO}_2]$ g_{sF} observed was species IG 48509. The lowest g_{sF} observed in both CO_2 growth concentrations was species Claire. The magnitude of change in g_s (Δg_s , Fig. 6.12 C Ca and F $e[\text{CO}_2]$) between 100 $\mu\text{mol m}^{-2} \text{s}^{-1}$ - 1000 $\mu\text{mol m}^{-2} \text{s}^{-1}$ PPFD displayed lower values in the EW for both CO_2 growth concentrations (except species IG 48514), the highest being species KU 2018 at Ca and IG 48509 at

$e[\text{CO}_2]$. There was a ~ 43 % difference between the highest and lowest Δg_s at Ca and a ~ 55 % difference between the highest and lowest at $e[\text{CO}_2]$.

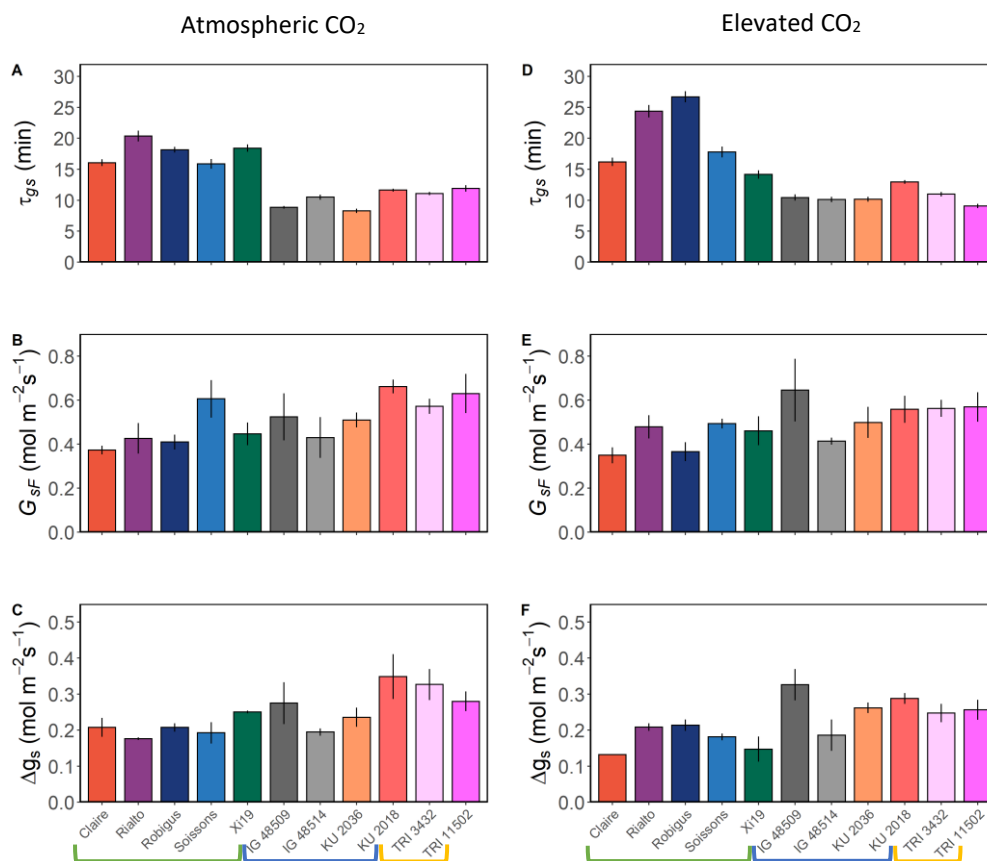


Figure 6.12 Time constant for stomatal opening (τ_{gs} ; A and D) in minutes, final values of stomatal conductance ($1000 \mu\text{mol m}^{-2} \text{s}^{-1}$ PPFD) after an increased step change in light intensity (G_{sF} ; B and E) and difference in g_s between $100 \mu\text{mol m}^{-2} \text{s}^{-1}$ PPFD (Δg_s ; C and E) following the step increase in light intensity. All results for 11 wheat species at atmospheric CO₂ (~408 ppm; A, B and C) elevated CO₂ (~800 ppm; D, E and F). Error bars represent 95% confidence intervals using the results of a Tukey test following a two-way ANOVA ($n = 5-7$). Green bracket represents hexaploid species, blue bracket represents diploid species and yellow bracket represents tetraploid species.

Time constants to reach 63 % of final value for A (τ_A ; Fig. 6.13 A Ca and D $e[\text{CO}_2]$) did not follow the same trend as τ_{gs} , all species over both CO_2 growth concentrations took approx. 2 mins, except 3 EW species at Ca (Claire, Robigus and XI19) and 1 EW species $e[\text{CO}_2]$ (Robigus) which all took approx. 30 sec to 1 min longer, although as A reaches 63 % of final value relatively quickly, the difference between the fastest and the slowest response was 46 % for Ca and 50 % $e[\text{CO}_2]$. The final value of A (A_F , Fig. 6.13 B Ca and E $e[\text{CO}_2]$) at $1000 \mu\text{mol m}^{-2} \text{s}^{-1}$ PPFD were similar in ranges at $\sim 25 \mu\text{mol m}^{-2} \text{s}^{-1}$ for both CO_2 growth concentrations although two significantly ($p < 0.05$) higher species were observed at $e[\text{CO}_2]$, 1 EW (Xi19, $\sim 32 \mu\text{mol m}^{-2} \text{s}^{-1}$) and 1 WWR (IG 48509, $\sim 35 \mu\text{mol m}^{-2} \text{s}^{-1}$), with the lowest in WWR species IG 48514 at $\sim 23 \mu\text{mol m}^{-2} \text{s}^{-1}$. The highest A_F on Ca grown species was observed in EW species Soissons at $\sim 29 \mu\text{mol m}^{-2} \text{s}^{-1}$, whereas the lowest significant ($p < 0.05$) difference was in the WWR species IG 48514 at $\sim 23 \mu\text{mol m}^{-2} \text{s}^{-1}$. The magnitude of change in A (ΔA , Fig. 6.13 C Ca and F $e[\text{CO}_2]$) between $100 \mu\text{mol m}^{-2} \text{s}^{-1}$ - $1000 \mu\text{mol m}^{-2} \text{s}^{-1}$ PPFD displayed a conserved variation in Ca grown species between approx. 15 and $17 \mu\text{mol m}^{-2} \text{s}^{-1}$, except 1 EW species (Soissons) and 1 WWR species (TRI 11502) which had significantly larger ΔA by 20 % and 30 % respectively. The $e[\text{CO}_2]$ ΔA presented a larger variation between both EW and WWR species with the highest being XI19 at $\sim 22 \mu\text{mol m}^{-2} \text{s}^{-1}$ and the lowest being IG 48514 at $\sim 14 \mu\text{mol m}^{-2} \text{s}^{-1}$.

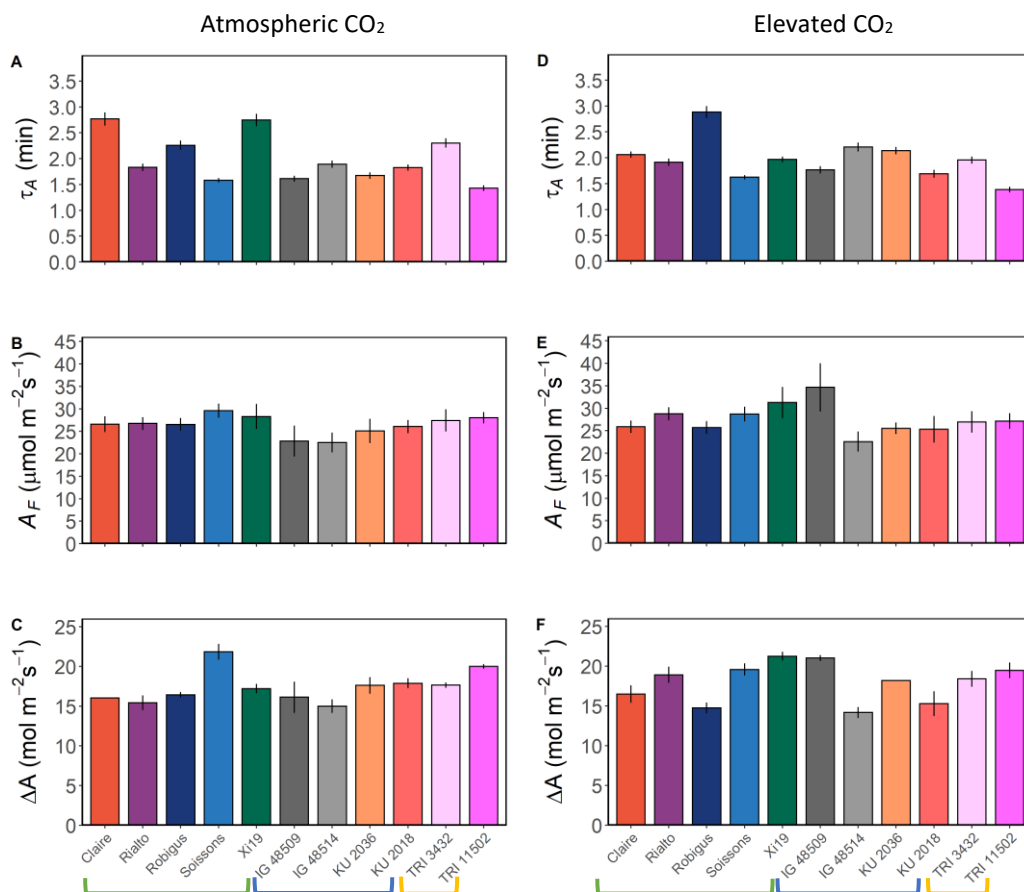


Figure 6.13 Time constant for light saturated carbon assimilation (τ_A ; A and D) in minutes, final values light saturated carbon assimilation ($1000 \mu\text{mol m}^{-2} \text{s}^{-1}$ PPFD) after an increased step change in light intensity (A_F ; B and E) and difference in A between 100 and $1000 \mu\text{mol m}^{-2} \text{s}^{-1}$ PPFD (ΔA ; C and F) following the step increase in light intensity. All results for 11 wheat species at atmospheric CO₂ (~ 408 ppm; A, B and C) elevated CO₂ (~ 800 ppm; D, E and F). Error bars represent 95% confidence intervals using the results of a Tukey test following a two-way ANOVA ($n = 5-7$). Green bracket represents hexaploid species, blue bracket represents diploid species and yellow bracket represents tetraploid species.

Although figure 6.12 (A Ca and D e[CO₂]) displays a distinct trend with longer ($P < 0.05$) τ_{gs} in the EW compared with the WWR for both CO₂ growth concentrations, there is no similar trend in τ_A (Fig. 6.13; A Ca and D e[CO₂]). Lower final values of g_s (Fig 6.12) were found predominantly in EW, which also showed slightly higher values for A_F (Fig 6.13). Species grown at e[CO₂] showed Robigus with the highest τ_{gs} and τ_A , and TRI 11502 had both the lowest τ_{gs} and τ_A , indicating that the time to reach the final g_s values was reflected in the time to reach final A value in these species. WWR species IG 48509 displayed the highest g_{sF} and A_F , and highest Δg_s . Species Claire had the lowest g_{sF} in both Ca and e[CO₂], whilst IG 48514 had the lowest A_F in both Ca and e[CO₂].

The six parameters from figure 6.13 were correlated against each other (Fig. 6.14 and 6.15) which reveal two significant positive correlations. Parameters include the time constant for stomatal opening (τ_{gs} ; A, B, C), final values of stomatal conductance (1000 $\mu\text{mol m}^{-2} \text{s}^{-1}$ PPFD; g_{sF} ; G, H, I), the difference in g_s between 100 and 1000 $\mu\text{mol m}^{-2} \text{s}^{-1}$ PPFD (Δg_s ; D, E, F) and time constant for light saturated carbon assimilation (τ_A ; A, D, G), final values light saturated carbon assimilation (1000 $\mu\text{mol m}^{-2} \text{s}^{-1}$ PPFD; A_F ; C, F, I) and difference in A between 100 and 1000 $\mu\text{mol m}^{-2} \text{s}^{-1}$ PPFD (ΔA ; B, E, H) for atmospheric CO₂ (~408 ppm, Fig. 6.14) and elevated CO₂ (~800 ppm, Fig. 6.15). Figures 6.14; B and 6.15; B found positive correlations ($p < 0.001$) for Ca and e[CO₂] between τ_{gs} and ΔA highlighting that in species with slow increases in g_s , the change in A is greater. Secondly, negative correlations ($p < 0.05$) for Ca and e[CO₂] (Fig. 6.14; G and 6.15; G) were observed between τ_A and g_{sF} , indicating that when the time taken for A to reach 63 % of its final value was higher, final values of g_s were higher.

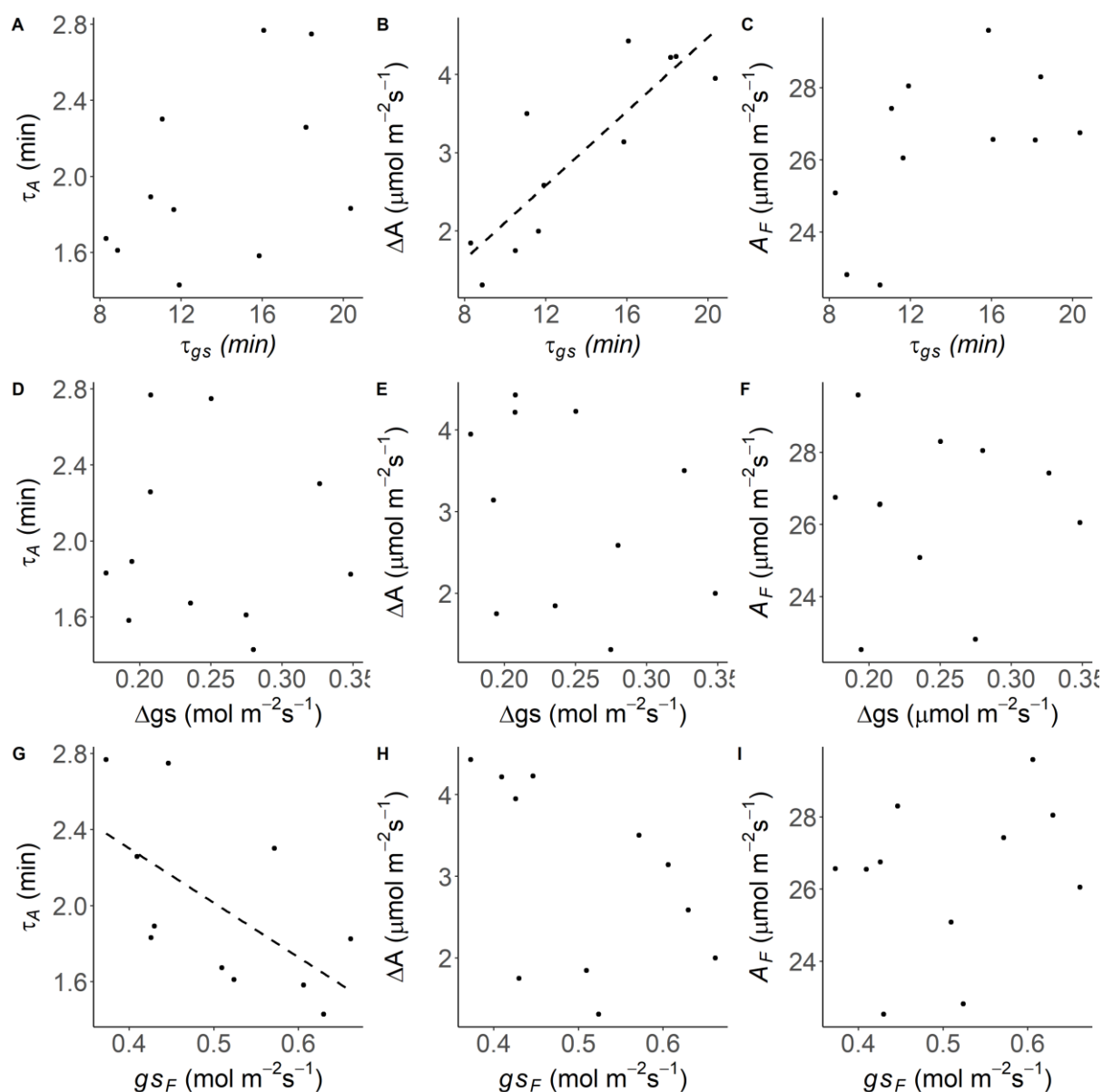
Atmospheric CO₂

Figure 6.14 Correlations between time constant for stomatal opening (τ_{gs} ; A, B, C) in minutes, final values of stomatal conductance ($1000 \mu\text{mol m}^{-2} \text{s}^{-1}$ PPFD) after an increased step change in light intensity (g_{sF} ; G, H, I) and difference in g_s between 100 and $1000 \mu\text{mol m}^{-2} \text{s}^{-1}$ PPFD (Δg_s ; D, E, F) following the step increase in light intensity and time constant for light saturated carbon assimilation (τ_A ; A, D, G) in minutes, final values light saturated carbon assimilation ($1000 \mu\text{mol m}^{-2} \text{s}^{-1}$ PPFD) after an increased step change in light intensity (A_F ; C, F, I) and difference in A between 100 and $1000 \mu\text{mol m}^{-2} \text{s}^{-1}$ PPFD (ΔA ; B, E, H) following the step increase in light intensity for 11 wheat species at atmospheric CO₂ (~408 ppm). Black dotted line represents a significant ($p < 0.05$) trend in the data between the two variables. Correlation found in graph B, between τ_{gs} and ΔA - correlation = 0.8608366 ($p=0.0006674$) and graph G, between τ_A and g_{sF} - correlation = -0.610793 ($p=0.04592$) using the results of a Pearson's correlation test. ($n = 5-7$).

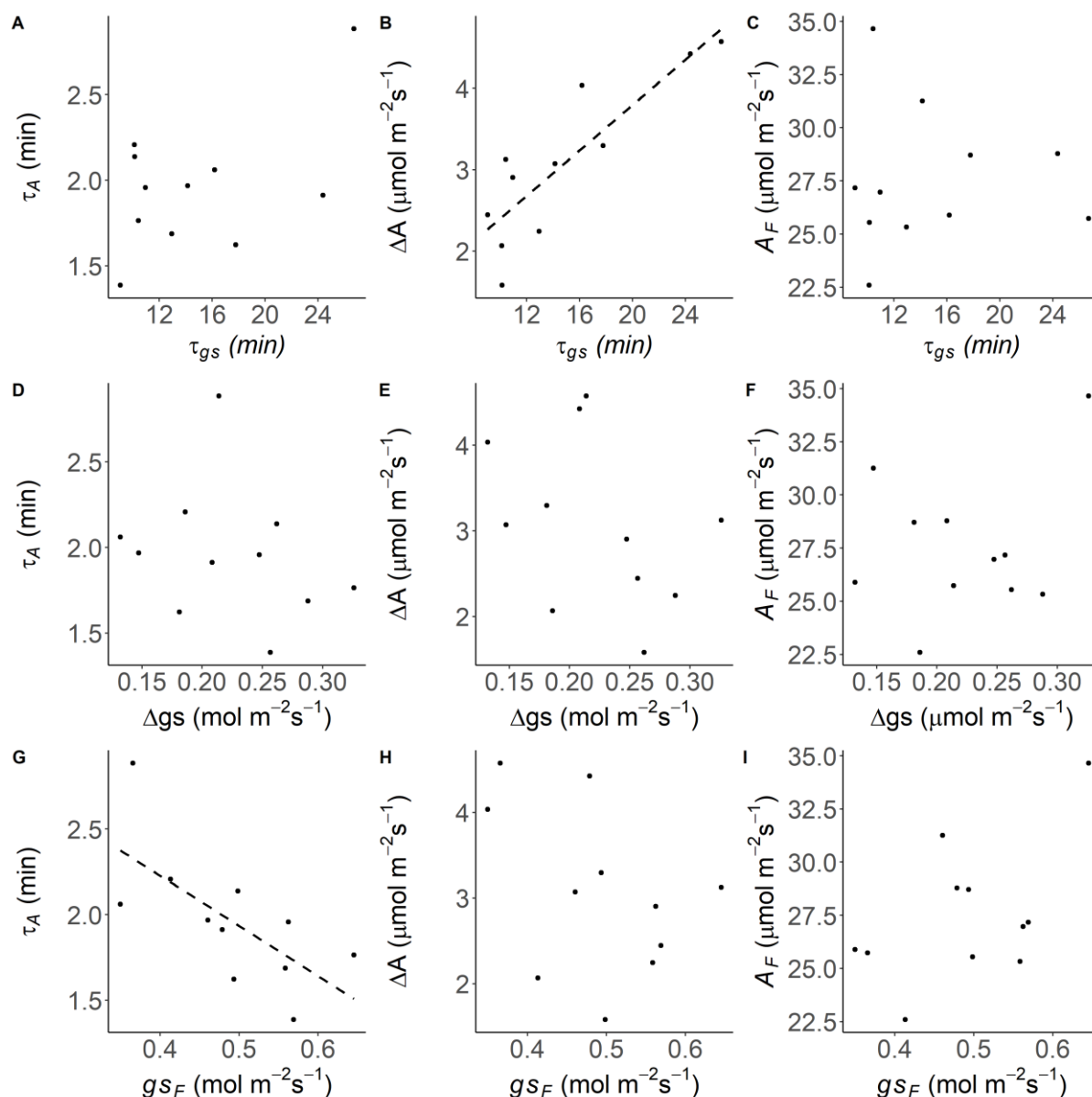
Elevated CO₂

Figure 6.15 Correlations between time constant for stomatal opening (τ_{gs} ; A, B, C) in minutes, final values of stomatal conductance ($1000 \mu\text{mol m}^{-2} \text{s}^{-1}$ PPFD) after an increased step change in light intensity (g_{sF} ; G, H, I) and difference in g_s between 100 and $1000 \mu\text{mol m}^{-2} \text{s}^{-1}$ PPFD (Δg_s ; D, E, F) following the step increase in light intensity and time constant for light saturated carbon assimilation (τ_A ; A, D, G) in minutes, final values light saturated carbon assimilation ($1000 \mu\text{mol m}^{-2} \text{s}^{-1}$ PPFD) after an increased step change in light intensity (A_F ; C, F, I) and difference in A between 100 and $1000 \mu\text{mol m}^{-2} \text{s}^{-1}$ PPFD (ΔA ; B, E, H) following the step increase in light intensity for 11 wheat species at elevated CO₂ (~800 ppm). Black dotted line represents a significant ($p < 0.05$) trend in the data between the two variables. Correlation found in graph B, between τ_{gs} and ΔA - correlation = 0.8611632 ($p=0.0006608$) and graph G, between τ_A and g_{sF} - correlation = 0.6843374 ($p=0.02019$) using the results of a Pearson's correlation test. ($n = 5-7$).

6.3.2.3. A/C_i response analysis

The response of CO_2 assimilation (A) as a function of internal $[\text{CO}_2]$ (C_i ; A/C_i – Fig. 6.16) were performed on the flag leaf on plants grown in differing CO_2 concentrations. All species exhibited the expected increase in A with increased C_i up to a certain point before reaching a plateau. Species grown at atmospheric CO_2 displayed a greater range in A at differing C_i values.

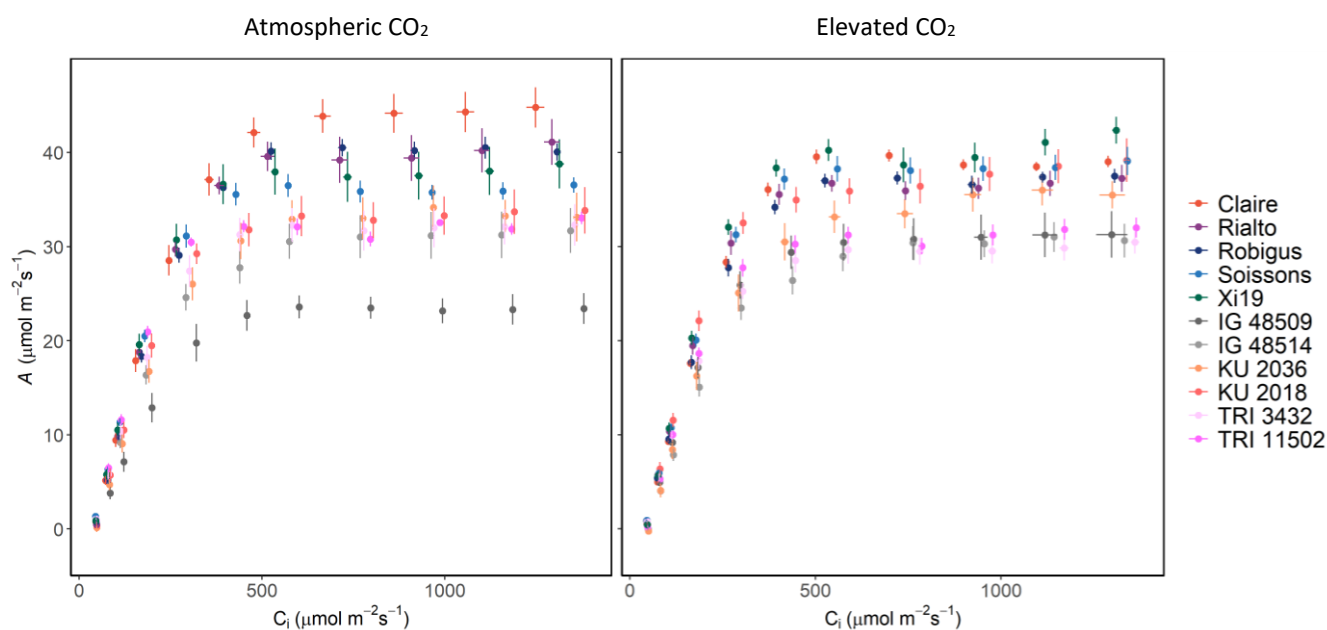


Figure 6.16 The response of CO_2 assimilation (A) to intercellular $[\text{CO}_2]$ (C_i) between 50 and 1500 $\mu\text{mol m}^{-2} \text{s}^{-1}$, under saturating PPFD (1500 $\mu\text{mol m}^{-2} \text{s}^{-1}$), for 11 wheat species at atmospheric CO_2 (~ 408 ppm; A) and elevated CO_2 (~ 800 ppm; B). Error bars represent mean \pm SE ($n = 5-7$).

Figure 6.16 displayed the maximum rate of carboxylation ($V_{C_{max}}$; A and B), the maximum rate of electron transport (J_{max} ; C and D) and the light and CO_2 saturated assimilation rate (A_{max} ; E and F) at 1500 $\mu\text{mol mol}^{-1} \text{CO}_2$ and 1500 $\mu\text{mol m}^{-2} \text{s}^{-1}$ PPFD were determined for all measurements from A/C_i measurement data. Significant

differences ($p < 0.001$) were found between all species for V_{Cmax} , J_{max} and A_{max} for both atmospheric and elevated CO_2 .

When observing figure 6.17, V_{Cmax} , J_{max} and A_{max} for both Ca and $e[CO_2]$ displayed a trend of higher rates in EW and lower rates in WWR except for the $e[CO_2]$ grown WWR species KU 2018 which saw higher rates in all parameters than other $e[CO_2]$ grown WWR. The highest $e[CO_2]$ grown species (Fig. 6.17; A, B, C, and E) was observed in EW species Xi19 in all parameters, which also exhibited the highest rates of V_{Cmax} for Ca grown species. The Ca grown species Claire displayed the highest rates of J_{max} and A_{max} . No one $e[CO_2]$ species displayed values for the lowest V_{Cmax} , J_{max} and A_{max} rates (Fig. 6.17; A, D, and F) although all were WWR, with species IG 48514, TRI 3432 and IG 48509 having the lowest rates for V_{Cmax} , J_{max} and A_{max} respectively. The lowest V_{Cmax} , J_{max} and A_{max} rates for plants grown at Ca (Fig. 6.17; B, D, and F) were all observed in WWR species IG 48509. Between the Ca grown species highest and lowest rates, there was a decrease of 30 % in V_{Cmax} , 36 % in J_{max} and 29 % in A_{max} , additionally, between the $e[CO_2]$ grown species highest and lowest rates, there was a decrease of 22 % in V_{Cmax} , 50 % in J_{max} and 45 % in A_{max} . Therefore, the EW species show a higher photosynthetic capacity than the WWR at both Ca and $e[CO_2]$.

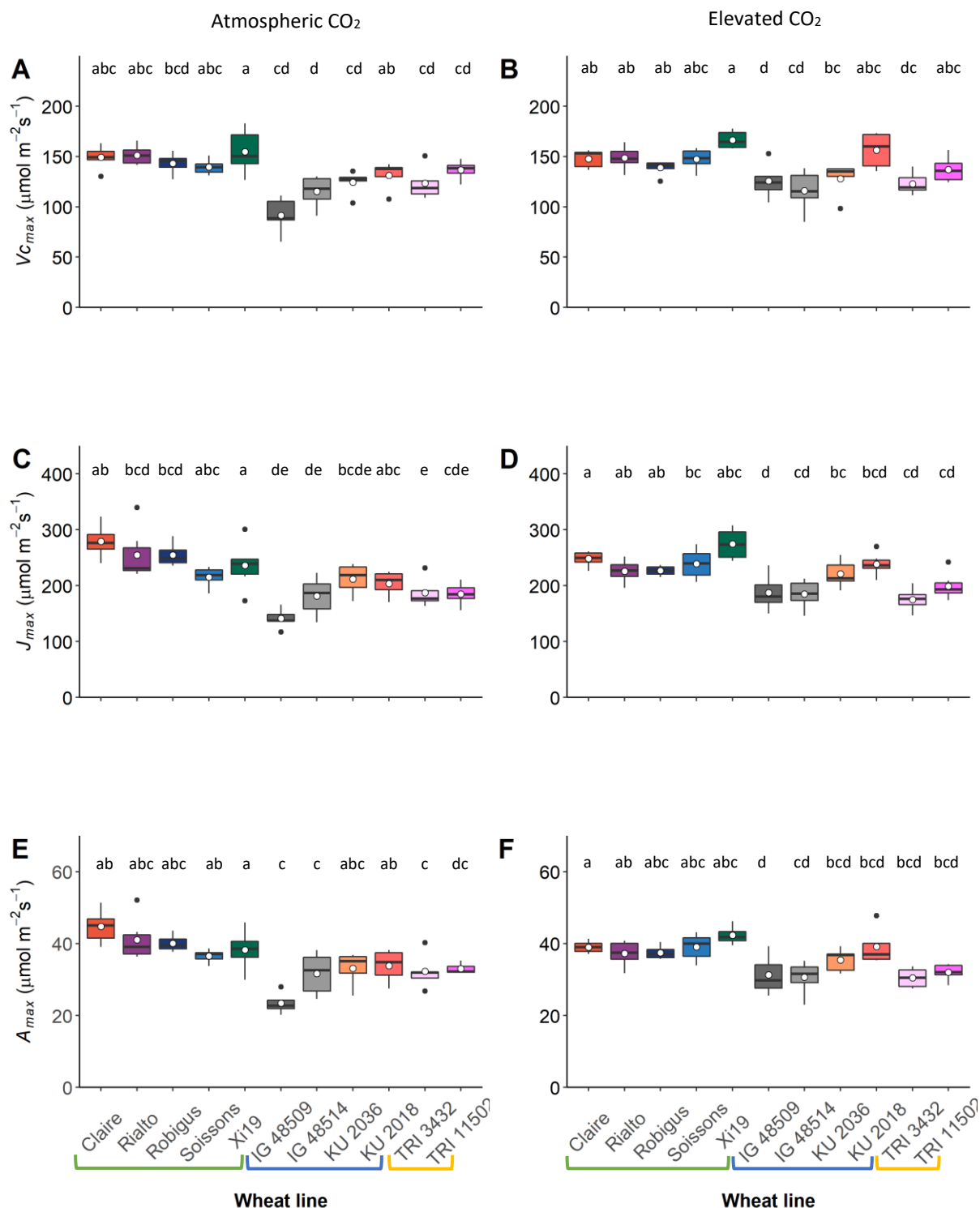


Figure 6.17 Variation (box and whisker) and mean (white dot) of light ($1500 \mu\text{mol m}^{-2} \text{s}^{-1}$) and CO_2 ($1500 \mu\text{mol m}^{-2} \text{s}^{-1}$) saturated photosynthesis (A_{max} ; E and F), the maximum rate of carboxylation (V_{cmax} ; A and B) and maximum rate of electron transport (J_{max} ; C and D) for 11 wheat species at atmospheric CO_2 ($\sim 408 \text{ ppm}$; A, C and E) and elevated CO_2 ($\sim 800 \text{ ppm}$; B, D and F). Different letters represent statistically significant differences ($P < 0.05$) between species using the results of a Tukey test following a two-way ANOVA ($n = 5-7$). Green bracket represents hexaploid species, blue bracket represents diploid species and yellow bracket represents tetraploid species.

6.4. Discussion

As stomata are the gatekeepers for major gaseous exchange between the atmosphere and the plant, studies which illustrate the impact of environmental change on the morphological and physiological response of stomata are essential for the prediction of climate change effects. Therefore, interpreting both anatomical and functional response to changes in environmental conditions will aid the identification of crop and ecosystem responses, and moreover potential feedback mechanisms associated with future climate change (Hetherington & Woodward, 2003; Buckley, 2005, 2017; Franks & Beerling, 2009). Environmental variables including C_a , air temperature and water availability are shifting in the face of climate change, influencing leaf and plant morphology and in turn impacting physiology of the plant (Hill *et al.*, 2014; Matthews & Lawson, 2019).

This study aimed to link changes in stomatal anatomy, specifically SS and SD, in a set of elite wheat (EW) and wheat wild relatives (WWR) grown at two differing CO_2 growth concentrations (atmospheric at 408 ppm (C_a), and elevated at 800 ppm ($e[CO_2]$)) with g_s responses and the impact on A (Franks & Farquhar, 2007; Franks & Beerling, 2009; Drake *et al.*, 2013). Future productivity could be improved using WWR through the identification of desirable traits in wild wheat germplasm currently eroded in elite wheat varieties by the domestication of wheat species. These WWR grew and thrived in environment that modern day wheat find difficult, such as high temperatures and the identification of their source traits could benefit EW in future breeding programmes (Faris, 2014; McAusland *et al.*, 2020). Furthermore, growing this set of wheat, which include diploid, tetraploid and hexaploid species, at two differing CO_2 concentrations produces information which is crucial for understanding

the potential impact of changing climate on crop fitness in the future (Matthews & Lawson, 2019).

As with previous chapters, a large natural variation in morphology was observed between the WWR and EW species at both CO₂ growth concentrations, specifically in SD. The anatomical maximum potential g_s (g_{smax}) was calculated from the SD and SS measurements to determine the maximum potential g_s that could be achieved if pore aperture were at a maximum. High g_{smax} demonstrates a potential for a greater opening capacity to maximise CO₂ gain when water is not a limiting factor. Although SS (guard cell length) was significantly different between species they were fairly conserved in range, with the four diploid species having the smallest SS. These results demonstrated that the lower g_{smax} values observed were driven by SD (Dow *et al.*, 2014a), specifically the adaxial SD, and not size differences irrespective of CO₂ concentration.

As in previous chapters, the hexaploid EW species had the lowest SD coupled with the largest SS with the opposite being true of two diploid species, which had the smallest SS and highest SD. Moreover, the density to size trade-off, whereby decreasing the stomatal size is offset by increasing density, reported in many EW species in past studies (Hetherington & Woodward, 2003; Franks & Beerling, 2009; Drake *et al.*, 2013; McElwain *et al.*, 2015; de Boer *et al.*, 2016; Henry *et al.*, 2019) is a trend that this study has shown to be conserved through diploid, tetraploid and hexaploid wheat species. Although interestingly the range of SD across the Ca grown wheat had a larger range than the e[CO₂] grown wheat, driven mainly by the high densities of the diploid species found in Ca grown species and the little change in SS between CO₂ growth concentrations, resulting in the Ca grown wheat displaying a greater correlation between SD and SS than in the e[CO₂] grown wheat. The extent to

which SD alter in response to $e[\text{CO}_2]$ can vary depending on the experimental set up, treatment duration, and other environmental factors experienced during growth (Lodge *et al.*, 2001; Ainsworth & Rogers, 2007; Haworth *et al.*, 2011; Xu *et al.*, 2016), with several studies reporting that the stomatal developmental response to $e[\text{CO}_2]$ differs greatly between and within species (Field *et al.*, 2015; Matthews & Lawson, 2019).

The four diploid species and one tetraploid species in this study had a higher anatomical g_{smax} in the Ca treatment which was reduced in the $e[\text{CO}_2]$, no other g_{smax} differences were found between CO_2 growth concentrations, except interestingly the EW species Claire had a significantly higher g_{smax} in the $e[\text{CO}_2]$ wheat, driven by the significant increase in SD from Ca to $e[\text{CO}_2]$. Again, in this study the evolutionary pressure on stomatal morphology is suggested to be behind the SD/SS trade-off, which strives to balance the benefits of increasing leaf diffusional gas exchange with the cost associated with increasing stomatal area to the leaf epidermal area and attempting to increase functionality (de Boer *et al.*, 2016). The trade-off between SD and SS may be regulated by the relationship between SS and genome size (Lomax *et al.*, 2008). Guard cells are amongst the smallest cells in the plant which restricts guard cell genome sizes due to the low plasticity of the genome sizes at low CO_2 , where smaller and perhaps more efficient (diffusionally and responsively (Drake *et al.*, 2013)) stomata are required (Lomax *et al.*, 2008). At higher concentrations of CO_2 , larger and arguably less efficient stomata are permitted larger genomes (Beaulieu *et al.*, 2008) owing to the larger guard cell nucleus size (Franks *et al.*, 2012). For example, during a period of falling Ca in the Palaeozoic era, greater numbers of smaller stomata were observed in plants, likely caused by the selection pressure to increase g_{smax} and maintain A under lower CO_2 (Crowley & Berner, 2001; Harrison *et al.*, 2020). The results in this study support cell size correlations with genome size (or ploidy level). In

diploid species, which have been shown to be SD-CO₂ responsive, SD can be reduced, and guard cell lengths (SS) can increase due to the diffusion path no longer being as important in plants grown at high CO₂, but EW (all hexaploid) have lost the ability to respond.

The findings of this study show that, in general, the EW species had a lower final value of g_s , the stomata took longer to reach 63% of the final g_s values and showed a smaller magnitude of change in g_s values from 100 to 1000 PPFD compared to the WWR over both CO₂ treatments. Furthermore, the effect of g_s on A showed differences between the EW and WWR final values of A , the stomata took longer to reach 63% of the final A and magnitude of change in A values from 100 to 1000 PPFD, they were minimal between CO₂ growth concentrations. There were no significant trends between species of different ploidy for A . This is interesting because the faster stomatal responses and higher g_s found in the WWR do not correspond into a higher A . The A in the WWR is either equal to, or in some diploid species lower than the EW. This suggests that the WWR, particularly the diploid species, prioritise photosynthesis over water conservation, which is backed up by the results of W_i shown in Figure 6.11, displaying all WWR had a lower W_i than EW in both CO₂ growth concentrations. Furthermore, this suggests that the WWR may be better able to deal with elevated temperatures as these plants have a faster stomatal speed of stomatal opening and a higher stomatal conductance and therefore greater evaporative cooling, however this would only hold true in situations where water was freely available, see Urban *et al.*, (2017a). In a situation where water is less available, the higher g_s would have deleterious effects on plants and the EW with its 'slow and steady' approach would most likely be beneficial. Urban *et al.*, (2017a) provided evidence that a direct stomatal response to temperature allows plants to benefit from increased evaporative leaf

cooling heat waves. They showed stomatal conductance increased by ~40% in a broadleaf and a coniferous species when temperature was increased by 10 °C, from 30 °C to 40 °C at a constant vapor pressure deficit of 1 kPa (Urban *et al.*, 2017a)

It has been forecast that under all carbon emissions scenarios climate change will lead to higher global temperatures with predictions up to 1.5°C, or more, by the end of this century (IPCC, 2014) furthermore, the frequency of extreme temperatures cycles including heat waves is predicted to increase in the near future (Perkins *et al.*, 2012). The impact of increasing temperature on photosynthesis has been well documented in a number of different species as either a sole variable (for example, Berry & Bjorkman, 1980; Bernacchi *et al.*, 2002), or in combination with other factors such as elevated [CO₂] (for example, Long, 1991; Reddy *et al.*, 2010; Bishop *et al.*, 2014). It has been suggested that for every 1°C increase in global temperature, yields of wheat could, on average, decline by up to 6% (Zhao *et al.*, 2017). The damaging effect of high temperatures are predicted to have general negative effect on plant growth and development which poses significant risks to global food security.

Urban *et al.* (2017) reported that temperature, either high or low, influences assimilation rate, transpiration, vapour pressure deficit (VPD) and plant water status which all indirectly impact stomatal behaviour (Lawson & Blatt, 2014). For example, stomatal responses to VPD are generally well characterised, with increases in VPD stimulating stomatal closure to conserve water, by means of reduction of leaf turgor and guard cell turgor (Mott & Peak, 2013) while decreases in VPD lead to stomata re-opening (Merilo *et al.*, 2018). Stomatal opening to increasing temperature could be due to changes in hydraulic conductance driven decreases in water viscosity (Urban *et al.*, 2017b). The influence of temperature on assimilation rate and transpiration in species at e[CO₂] is governed by the changes in the g_s which as previously mentioned

is facilitated by a multitude of factors, including a decrease in the numbers of stomata over the leaf lamina, reported for a wide range of species (Woodward & Kelly, 1995; Woodward *et al.*, 2002; Casson & Gray, 2008; Casson & Hetherington, 2010; Soh *et al.*, 2019). Although, wood species typically demonstrate little change in stomatal density with $e[\text{CO}_2]$, which was also seen in some species in this study (Ainsworth & Rogers, 2007; Xu *et al.*, 2016) suggesting the mechanisms of $e[\text{CO}_2]$ on stomatal density are species-specific and genotype-dependent. The results of this study, specifically the offset of SD with SS combination in the two differing CO_2 growth concentrations resulted in similar g_{smax} , which is expected due to, in principle, infinite combinations of either of the two parameters being able to achieve identical g_{smax} (Franks *et al.*, 2015). The results confirm that as well as temporal and spatial g_s responses, the anatomical stomatal traits for dealing with elevated temperature would be optimised in environments of $e[\text{CO}_2]$ which is of crucial importance for plant W_i (Lawson & Morison, 2004).

In this study, as a trend, the photosynthetic capacity is higher in the EW (hexaploid) for the Ca and $e[\text{CO}_2]$ grown wheat with two main species standing out as differing between the two CO_2 growth concentrations. The EW species Claire had a reduced V_{Cmax} and J_{max} and the WWR species IG 48509 had an increase in V_{Cmax} and J_{max} from the Ca grown wheat to the $e[\text{CO}_2]$ grown wheat. As previously mentioned, $e[\text{CO}_2]$ increases C_i and in C3 plants it can enhance CO_2 fixation by inhibiting photorespiration and consequently increasing plant growth and production (Long *et al.*, 2006; Ainsworth & Rogers, 2007; Xu *et al.*, 2016). Although with the change in stomatal anatomical features which can reduce transpiration and increase leaf temperature some C3 plants encountered an increase in photorespiration due to a reduction in Rubisco specificity for CO_2 (Peterhansel *et al.*, 2010), an increased affinity

for O₂, and stomatal closure (Mott, 1988). Also, enzymes of the Calvin–Benson cycle, Rubisco and Rubisco activase are very sensitive to increased temperature and can therefore be severely inhibited even at low levels temperature (Maestri *et al.*, 2002; Morales *et al.*, 2003).

In summary, the diploid WWR species have a faster g_s at both Ca and e[CO₂] meaning they could be better equipped to cope in higher temperatures as minimal difference in the speed of response for A between CO₂ growth concentrations were found in this study. The ability of plants to sense and respond to changes in the environment is crucial to their survival and reproductive success, and the impact of increased temperature and atmospheric CO₂ concentrations mediated by behavioural and developmental responses of stomata on crop performance remains a concern under all climate change scenarios, with wheat and maize already showing yield losses (IPCC, 2014; Zhao *et al.*, 2017). The diploid species therefore hold traits desirable for increased [CO₂] and temperatures predicted in future global climate change scenarios. Interestingly, identifying the effect that the higher densities of smaller faster stomata had g_s and its potential effect on transpiration for evaporative leaf cooling has the potential for improving wheat productivity in the future and their identification in WWR a first step to inform follow-on gene discovery for potential use in pre-breeding programmes.

CHAPTER 7

General Discussion

7.1 Main Discussion

7.1.1 Spatial heterogeneity of stomata

Stomatal anatomical characteristics including stomatal density (SD), stomatal size (SS) and pore aperture together determine stomatal conductance (g_s) (Lawson & Blatt, 2014). Heterogeneity in stomatal morphology is commonplace and found at many levels, including size and density which therefore has a direct influence on g_s , the stomatal kinetics, A and moreover the final whole plant biomass and yields (Ticha, 1982; Smith *et al.*, 1989a; Willmer & Fricker, 1996; Weyers & Lawson, 1997; Lawson & Vialet-Chabrand, 2019). Adding to this complexity, variability is found in both spatial and temporal senses at all these scales (Pospíšilová & Šantrůček, 1994; Weyers & Lawson, 1997; Weyers *et al.*, 1997).

Stomatal patterning in the grasses occur in parallel rows within predefined epidermal cell files which follows the 'one cell spacing rule' to avoid stomatal clustering which aims to provides optimal stomatal placement with intercellular airspaces and underlying photosynthetic tissue (Croxdale, 2000; Franks & Beerling, 2009; Doheny-Adams *et al.*, 2012). The patterning attempts to promote the best possible stomatal function by optimising ionic exchange with neighbouring cells in order to alter stomatal aperture (Outlaw, 1983; Kim *et al.*, 2010; Dow & Bergmann, 2014; Raissig *et al.*, 2016) whilst not bearing more stomata than the can supply of water can support, i.e. not crossing a vein density threshold (Drake *et al.*, 2019). Patterning in the MAGIC wheat parental species followed this patterning (mentioned above) over both the flag and the second leaves from base to tip. In chapter 3, stomata were found to be most dense and smaller in the middle of the leaf lamina, and larger and less dense at the base and tip of the leaf. Due to the convex leaf angle, the leaf boundary layer is thickest at the

centre of the lamina and thinner towards the base and tip of the leaf, meaning there will be less resistance to water loss (and enhanced leaf cooling) at these margins (Smith *et al.*, 1989a; Willmer & Fricker, 1996; Weyers & Lawson, 1997).

The results presented in Chapter 3 showed that flag leaves have higher density of smaller stomata than those of the second leaf. This could be due to, in part, to two factors, the first being the extent to which leaves higher in the canopy intercept more solar radiation (Araus *et al.*, 1993). Wheat flag leaves occupy a higher position on the leaf and therefore intercept differing light environments in both intensity and wavelength (Vergara-Díaz *et al.*, 2018) and therefore may require faster responding stomata facilitate evaporative leaf cooling to compensate for the higher temperatures. Secondly, the flag leaf shuttles assimilates to the ear for grain filling, with modelling approaches estimating that approximately 45% of the grain carbohydrate is derived from the flag leaves (Lupton, 1972), which would therefore require higher rates of A and a faster g_s to respond to a dynamic environmental.

Stomatal density and size were negatively correlated with each other in all chapters. . This density to size trade-off, whereby decreasing the SS is offset by increasing SD, reported in many species from past studies (Hetherington & Woodward, 2003; Franks & Beerling, 2009; Drake *et al.*, 2013; McElwain *et al.*, 2015; de Boer *et al.*, 2016; Henry *et al.*, 2019) is a trend that this study has shown to be conserved through diploid, tetraploid and hexaploid wheat species, on all differing leaves, at all leaf locations. The tetraploid and hexaploid species in all chapters had the lowest SD coupled with the largest SS and the opposite was true of diploid species which had the smallest SS and highest SD. The results in this study support cell size correlations with genome size (or ploidy level). In diploid species, which have been shown to be SD-CO₂ responsive, SD can be reduced, and guard cell lengths (SS) can

increase due to the diffusion path no longer being as important in plants grown at high CO₂, but EW (all hexaploid) have lost the ability to respond. Hetherington & Woodward (2003) suggested that smaller stomata have a more-rapid opening and closing speed of response partly due to less water and solute movement between guard cells and subsidiary cells (Franks & Farquhar, 2007), shorter diffusional pathways (Franks & Beerling, 2009) and a higher rate of movement due to a larger surface area to volume ratio of smaller guard cells. Photosynthesis accounts for the largest flux of CO₂ from the atmosphere into ecosystems and is the driving process for terrestrial ecosystem function and therefore it is crucial to understand the processes that determine rates of leaf-level A and g_s , which is determined in part by physiological traits such as stomatal anatomy and behaviour (Farquhar *et al.*, 1980; Bernacchi *et al.*, 2013).

7.1.2 Intra specific variation of anatomical traits leading to functional differences

Variation in SD and SS was observed between species in the finding presented in all chapters and between EW and WWR. The maximum potential anatomical stomatal conductance (g_{smax}), assuming all stomata are fully open, is calculated using empirical measurements of SD and SS, specifically pore area and pore depth, which can consequently dictate the theoretical capacity for gas exchange with infinite combinations of either of the two parameters achieving the same g_{smax} (Franks & Farquhar, 2001; Dow *et al.*, 2014a); Matthews *et al.*, 2017). Stomatal density were found to be the main drivers of changes in g_{smax} , as although SS were significantly different between species and wheat with differing ploidy, they were less plastic than SD (Zhang *et al.*, 2012). In this study, in general plants were operating at approximately 25-30 % of their g_{smax} , which is typical, as plants do not operate at their

g_{smax} due to the inefficiency of the turgor pressures control in the guard cells, which drive pore aperture with modern crop species generally operating at approx. 20 % of their potential maximum capacity (Franks *et al.*, 2012a; Dow *et al.*, 2014b) in modern plants. Furthermore, if plants operated near their g_{smax} in either fluctuating conditions or in a non-optimal environment, for example heat or water stress, there would be a higher prevalence of desiccation and/or an increase in photorespiration due to a reduction in Rubisco specificity for CO₂ (Peterhansel *et al.*, 2010), although earlier diverging lineages of plants do function much closer to their g_{smax} values (McElwain *et al.*, 2015). Also, enzymes of the Calvin–Benson cycle, specifically Rubisco and Rubisco activase, are very sensitive to increased temperature, especially in wheat species, and can therefore be severely inhibited even at low levels temperature (Maestri *et al.*, 2002; Morales *et al.*, 2003).

Whilst anatomical characters determine the g_{smax} (McElwain *et al.*, 2016), dynamic changes in g_s are driven completely by changes in function (aperture). This study found differences in g_s , A and therefore W_i and differences in stomatal kinetics such as speed of responses to a change in light between EW species and between EW and WWR. In general, between EW species, those with the more extreme combinations of SD and SS, either higher densities of smaller stomata or lower densities of larger stomata showed higher rates of g_s faster g_s kinetics which did not always translate into higher A and therefore lower W_i (for example in species Brompton and Soissons). However, if a mid-range combination of SD and SS was observed, then in general, those species would present lower rates of g_s with slightly slower kinetics (than the higher values found in species of this study) without excessive reductions in A but have an increased W_i . This trend is also seen in the differences between the EW and WWR, whereby higher g_{smax} values, driven by higher SD, were

found in WWR species which displayed higher rates of g_s and faster g_s kinetics which did not always translate into higher A and therefore had a lower W_i . These findings suggest that in fluctuating conditions and/or stressful environmental conditions smaller stomata are better equipped to deal with rapid fluctuating conditions (Violet-Chabrand *et al.*, 2017a; Matthews *et al.*, 2018) but in steady state conditions perhaps reduced stomatal densities may be beneficial. Future work could concentrate on adding to current studies using the natural variation of anatomical and physiological traits (Faralli *et al.*, 2019b; Faralli & Lawson, 2020) using the MAGIC wheat progeny to look at extreme SD and SS combinations in environments which are closer to those predicted in the future, such as higher temperatures, higher CO₂ concentration and with situations of high water stress (Bernacchi *et al.*, 2002; Hill *et al.*, 2014; Bellasio *et al.*, 2018; Caine *et al.*, 2018; Faralli *et al.*, 2019a).

Although significant variation in anatomical features was observed between and within species, resulting in variation to the g_{smax} , no differences were observed between the CO₂-saturated rate of photosynthesis at high light (A_{max}), the maximum velocity of Rubisco for carboxylation (V_{cmax}) or the potential rate of electron transport under saturating light (J_{max}). Although differences photosynthetic capacities were found between the EW and WWR species with higher capacities found in the EW species. Elite wheat species have been bred for superior traits that lead to higher seed yield and it is not surprising that these eight elite wheat species are all operating at a similar high functioning photosynthetic capacity which have been inadvertently selected for higher photosynthesis.

7.1.3 Amphistomaty in leaves and its effect on function

Higher stomatal densities were generally observed on the adaxial leaf surfaces of all species. Wheat abaxial/adaxial polarity, or amphistomaty is under genetic control and established early on in leaf development to ensure their correct formation and distribution of stomata is maintained throughout the leaf (Croxdale, 2000). To examine this disproportionate ratio of SD between the two leaf surfaces, a new leaf gas exchange chamber was constructed to measure the separate but simultaneous leaf gas exchange on each leaf surface in real time. In chapter 4 higher g_s and A was achieved on the adaxial leaf surface compared with the abaxial leaf surface (when illuminated from either both sides or the adaxial surface only).

These findings imply limited contribution from abaxial g_s in the supply of CO_2 for adaxial assimilation. Furthermore, abaxial g_s and A rates, when illuminated on both leaf surfaces, was greater than when illumination was received on only the adaxial leaf surface, as though demonstrating that the abaxial leaf surface stomata and associated mesophyll cells were limited by light intensity (or spectral quality), due to self-shading and receiving transmitted light only on this surface (Wang *et al.*, 2008b) and that abaxial gaseous fluxes contribute very little to the adaxial leaf surface A . We found an uncoordinated stomatal response between the two leaf surfaces to meet the photosynthetic requirements of the whole leaf, the opposite what has been proposed in previous studies by Yera *et al.* (1986). The finding from this study suggests that both surface act independently from each other which is supported by the earlier observations that adaxial A and g_s is substantially greater than abaxial, however both are essential in their contribute to the overall leaf A and g_s . The high rate of A found in these results, particularly on the upper surface, would suggest that the vertical profile

of $[CO_2]$ through the leaf will be relatively high due to high consumption rates in the upper palisade layer associated with the adaxial surface (Evans *et al.*, 2009).

This novel technique has a multitude of applications for further study in wheat species and in other crops species. Initially, further work should be completed on investigating the internal structure of wheat leaves with leaf cross-sections. Although it is already described that wheat are isobilateral amphistomatous species, indicating that the position of the tissue performing most of the CO_2 uptake (typically palisade mesophyll) is located near the upper and lower epidermis (Drake *et al.*, 2019), little is known on the size and distribution of the air spaces between the upper and the lower sections of the leaf and the impact this could have on leaf mechanisms such as mesophyll conductance. Furthermore, if high $[CO_2]$ were utilised on one leaf surface would the CO_2 'push' through and increase the other leaf surfaces photosynthesis? Additional following experiments could include using the split chamber to complete experiments on each leaf surface that included, but not limited to, responses to differing fluctuating light regimes on the two surfaces (following the work of Vialet-Chabrand *et al.*, 2017; Matthews *et al.*, 2018) and responses to red and blue light on the two surfaces (following the work of Hiyama *et al.*, 2017; Inoue & Kinoshita, 2017; Matthews *et al.*, 2020). This study highlighted that A and g_s were almost double on the adaxial leaf surface when illuminated on both leaf surfaces and up to three times higher when illuminated on the adaxial leaf surface only. When lit from the abaxial leaf surface only there was an almost equal contribution for A and g_s for each side of the leaf. The rationale for these results include a higher photosynthetic capacity on the adaxial leaf surface which therefore profits from a higher consumption of CO_2 , relinquishing less C_i for the abaxial leaf surface.

As mentioned in chapter 4, owing to the extent to which wheat leaves intercept solar radiation depends on characteristics such as leaf angle and the spatial arrangement (Araus *et al.*, 1993). Wheat leaves are the last leaf to appear before the ear and grow vertically until fully emerged, then, when the ear emerges the flag leaf falls into a horizontal position where it remains until senescence. It would be interesting to follow the leaf angle from emergence in the vertical position to pre-anthesis when the leaf is in a horizontal position with gas exchange measurements to 'map' gaseous exchange over the leaf and reveal how the difference in leaf angle alter the impact of this at the whole plant level.

7.1.4 The effect of high CO₂ on wheat species

Increases in the demand for our primary foodstuffs is already surpassing increases in yields and if rates of crop yield improvement per hectare are only maintained rather than increased in the future, supply will not keep up with demand by 2050 (Ray *et al.*, 2013; Long *et al.*, 2015). Factors affecting food shortages include the effects of a changing climate, losses of agricultural land to urbanization and increasing competition for non-food uses of crops for example biofuels and increased meat consumption (Zhu *et al.*, 2010; Ray *et al.*, 2013; Long *et al.*, 2015). As stomata are the gatekeepers for major gaseous exchange between the atmosphere and the plant, studies which illustrate the impact of environmental change on the morphological and physiological response of stomata are essential for the prediction of climate change effects. Environmental variables including Ca, air temperature and water availability are shifting in the face of climate change, influencing leaf and plant morphology and in turn impacting physiology of the plant (Hill *et al.*, 2014; Matthews & Lawson, 2019).

The impact of increasing temperature on photosynthesis has been well documented in a number of different species as either a sole variable (for example, Berry & Bjorkman, 1980; Bernacchi *et al.*, 2002), or in combination with other factors such as elevated [CO₂] (for example, Long, 1991; Reddy *et al.*, 2010; Bishop *et al.*, 2014). The damaging effect of high temperatures are predicted to have general negative effect on plant growth and development which poses significant risks to global food security with predictions of every 1°C increase in global temperature, yields of wheat could, on average, decline by up to 6% (Zhao *et al.*, 2017).

Chapter 6 explored 11 key EW and WWR species from previous chapters at differing CO₂ growth condition with an aim of examining anatomical variation and the

impact this may have on functionality with implications for A and g_s (and through both diffusional constraints and evaporative leaf cooling). Chapter 6 confirmed heterogeneity between leaf surfaces, species and between CO_2 growth conditions and these differences impacted functionality with a difference between g_s where EW has a slower g_s than the WWR species which did not always translate into a higher A . The diploid WWR species showed a faster g_s at both C_a and $e[\text{CO}_2]$ and higher g_s values, meaning they could be better equipped to cope in higher temperatures as minimal difference in the speed of response for A between CO_2 growth conditions were found in this study. These results propose that the WWR may be better able to deal with elevated temperatures as these plants have a faster stomatal speed of response to light and a higher stomatal conductance and therefore greater evaporative cooling (Leahey *et al.*, 2003; Crawford *et al.*, 2012; Urban *et al.*, 2017a) which is essential for a dynamic light environment. However, this would only hold true in situations where water was freely available. In a situation where water is less available, the higher g_s would have deleterious effects on plants and the EW with its 'slow and steady' approach would most likely be beneficial.

The ability of plants to sense and respond to changes in the environment is crucial to their survival and reproductive success, and the impact of increased temperature, mediated by behavioural and developmental responses of stomata on crop performance remains a concern under all climate change scenarios, with wheat and maize already showing yield losses (IPCC, 2014; Zhao *et al.*, 2017). The diploid species therefore hold traits desirable for increased $[\text{CO}_2]$ and temperatures predicted in future global climate change scenarios. This study clearly found heterogeneity between anatomical features which effect the variation shown in g_s and stomatal kinetics which has implication for evaporative leaf cooling. Interestingly responses

were found in this study to be different between the two leaf surfaces. This is an exciting find as it is a novel target to explore and potentially manipulate anatomical stomatal traits on the differing leaf surfaces.

CHAPTER 8

Reference List

8.1 References

- Aasamaa K, Söber A, Rahi M (2001) Leaf anatomical characteristics associated with shoot hydraulic conductance, stomatal conductance and stomatal sensitivity to changes of leaf water status in temperate deciduous trees. *Australian Journal of Plant Physiology*, **28**, 765–774.
- Abrash EB, Davies KA, Bergmann DC (2011) Generation of signaling specificity in Arabidopsis by spatially restricted buffering of ligand-receptor interactions. *The Plant cell*, **23**, 2864–79.
- Ainsworth EA, Rogers A (2007) The response of photosynthesis and stomatal conductance to rising [CO₂]: mechanisms and environmental interactions. *Plant, Cell & Environment*, **30**, 258–270.
- Amodeo G, Talbott LD, Zeiger E (1996) Use of Potassium and Sucrose by Onion Guard Cells during a Daily Cycle of Osmoregulation. *Plant and Cell Physiology*, **37**, 575–579.
- Araus JL, Reynolds MP, Acevedo E (1993) Leaf posture, grain yield, growth, leaf structure, and carbon isotope discrimination in wheat. *Crop Science*, **33**, 1273–1279.
- Assmann SM, Shimazaki KI (1999) The multisensory guard cell. Stomatal responses to blue light and abscisic acid. *Plant Physiology*, **119**, 809–815.
- Assmann SM, Zeiger E (1987) Guard cell bioenergetics. In: *Stomatal function* (eds Zeiger E, Farquhar GD, Cowan IR), pp. 163–193. Stanford University Press, Palo Alto, CA, USA.
- Beaulieu JM, Leitch IJ, Patel S, Pendharkar A, Knight CA (2008) Genome size is a strong predictor of cell size and stomatal density in angiosperms. *New Phytologist*, **179**, 975–986.
- Beerling DJ, Kelly CK (1996) Evolutionary comparative analyses of the relationship between leaf structure and function. *New Phytologist*, **134**, 35–51.
- Bellasio C, Quirk J, Beerling DJ (2018) Stomatal and non-stomatal limitations in savanna trees and C₄ grasses grown at low, ambient and high atmospheric CO₂. *Plant Science*, **274**, 181–192.
- Bergmann DC, Sack FD (2007) Stomatal development. *Annual review of plant biology*, **58**, 163–81.
- Bernacchi CJ, Portis AR, Nakano H, Von Caemmerer S, Long SP (2002) Temperature response of mesophyll conductance. Implications for the determination of Rubisco enzyme kinetics and for limitations to photosynthesis in vivo. *Plant Physiology*, **130**, 1992–1998.
- Bernacchi CJ, Bagley JE, Serbin SP, Ruiz-Vera UM, Rosenthal DM, Vanloocke A (2013) Modelling C₃ photosynthesis from the chloroplast to the ecosystem. *Plant, Cell and Environment*, **36**, 1641–1657.
- Berry J, Bjorkman O (1980) Photosynthetic Response and Adaptation to Temperature in Higher Plants. *Annual Review of Plant Physiology*, **31**, 491–543.

- Berry JA, Beerling DJ, Franks PJ (2010) Stomata: key players in the earth system, past and present. *Current Opinion in Plant Biology*, **13**, 232–239.
- Bertolino LT, Caine RS, Gray JE (2019) Impact of stomatal density and morphology on water-use efficiency in a changing world. *Frontiers in Plant Science*, **10**, 6.
- Bettarini I, Vaccari FP, Miglietta F (1998) Elevated CO₂ concentrations and stomatal density: observations from 17 plant species growing in a CO₂ spring in central Italy. *Global Change Biology*, **4**, 17–22.
- Bishop KA, Leakey ADB, Ainsworth EA (2014) How seasonal temperature or water inputs affect the relative response of C₃ crops to elevated [CO₂]: a global analysis of open top chamber and free air CO₂ enrichment studies. *Food and Energy Security*, **3**, 33–45.
- Blatt MR (2000) Cellular Signaling and Volume Control in Stomatal Movements in Plants. *Annual Review of Cell and Developmental Biology*, **16**, 221–241.
- de Boer HJ, Eppinga MB, Wassen MJ et al. (2012) A critical transition in leaf evolution facilitated the Cretaceous angiosperm revolution. *Nature Communications*, **3**, 1221.
- de Boer HJ, Price CA, Wagner-Cremer F, Dekker SC, Franks PJ, Veneklaas EJ (2016) Optimal allocation of leaf epidermal area for gas exchange. *New Phytologist*, **210**, 1219–1228.
- Braun HJ, Atlin G PT (2010) *Multi-location testing as a tool to identify plant response to global climate change*. In Reynolds MP, ed. *Climate change and crop production*. CABI, Climate Change Series, Surrey, UK, 115–138 pp.
- Brearley J, Venis MA, Blatt MR (1997) The effect of elevated CO₂ concentrations on K⁺ and anion channels of *Vicia faba* L. guard cells. **44**, 145–154.
- Brisson N, Gate P, Gouache D, Charmet G, Oury F-X, Huard F (2010) Why are wheat yields stagnating in Europe? A comprehensive data analysis for France 2000–2009. *Field Crops Research*, **119**, 201–212.
- Brodribb TJ, Feild TS (2010) Leaf hydraulic evolution led a surge in leaf photosynthetic capacity during early angiosperm diversification. *Ecology Letters*, **13**, 175–183.
- Brodribb TJ, Feild TS, Jordan GJ (2007) Leaf maximum photosynthetic rate and venation are linked by hydraulics. *Plant physiology*, **144**, 1890–8.
- Brodribb TJ, McAdam SAM, Jordan GJ, Feild TS (2009) Evolution of stomatal responsiveness to CO₂ and optimization of water-use efficiency among land plants. *New Phytologist*, **183**, 839–847.
- Buckley TN (2005) The control of stomata by water balance. *New Phytologist*, **168**, 275–292.
- Buckley TN (2017) Modeling stomatal conductance. *Plant Physiology*.
- Buckley TN, Mott KA (2013) Modelling stomatal conductance in response to environmental factors. *Plant, Cell & Environment*, **36**, 1691–1699.

- Buckley TN, John GP, Scoffoni C, Sack L (2015) How does leaf anatomy influence water transport outside the xylem? *Plant Physiology*, **168**, 1616–1635.
- Buttrose MS, May LH (1959) PHYSIOLOGY OF CEREAL GRAIN. 1. THE SOURCE OF CARBON FOR THE DEVELOPING BARLEY KERNEL. *Aust. J. biol. Sci.*, **12**, 40-52.
- von Caemmerer S, Farquhar GD (1981) Some relationships between the biochemistry of photosynthesis and the gas exchange of leaves. *Planta*, **153**, 376–387.
- Caine RS, Yin X, Sloan J et al. (2018) Rice with reduced stomatal density conserves water and has improved drought tolerance under future climate conditions.
- Cardon ZG, Mott KA, Berry JA (1994) Dynamics of patchy stomatal movements, and their contribution to steady-state and oscillating stomatal conductance calculated using gas-exchange techniques. *Plant, Cell and Environment*, **17**, 995–1007.
- Carmo-Silva E, Andralojc PJ, Scales JC et al. (2017) Phenotyping of field-grown wheat in the UK highlights contribution of light response of photosynthesis and flag leaf longevity to grain yield. *Journal of experimental botany*, **68**, 3473–3486.
- Casson S, Gray JE (2008) Influence of environmental factors on stomatal development. *New Phytologist*, **178**, 9–23.
- Casson SA, Hetherington AM (2010) Environmental regulation of stomatal development. *Current Opinion in Plant Biology*, **13**, 90–95.
- Charmet G (2011) Wheat domestication: Lessons for the future. *Comptes Rendus - Biologies*, **334**, 212–220.
- Chater CC, Caine RS, Tomek M et al. (2016) Origin and function of stomata in the moss *Physcomitrella patens*. *Nature plants*, **2**.
- Chen ZH, Chen G, Dai F et al. (2017) Molecular Evolution of Grass Stomata. *Trends in Plant Science*, **22**, 124–139.
- Contribution of Working Groups I, II and III to the Fifth Assessment Report of the Intergovernmental Panel on Climate Change, Geneva, Switzerland I (2014) *AR5 Synthesis Report: Climate Change 2014*.
- Cotthem WRJ (1970) A classification of stomatal types. *Botanical Journal of the Linnean Society*, **63**, 235–246.
- Cowan IR (1977) Stomatal Behaviour and Environment. *Advances in Botanical Research*, **4**, 117–228.
- Cowan IR, Farquhar GD (1977) Stomatal function in relation to leaf metabolism and environment. *Soc Exp Biol*, **31**, 471–505.
- Crawford AJ, McLachlan DH, Hetherington AM, Franklin KA (2012) High temperature exposure increases plant cooling capacity. *Current Biology*, **22**, R396–R397.
- Crowley TJ, Berner RA (2001) CO₂ and climate change. *Science*, **292**, 870–872.

- Croxdale J (1998) Stomatal patterning in monocotyledons: *Tradescantia* as a model system. *Journal of Experimental Botany*, **49**, 279–292.
- Croxdale JL (2000) Stomatal patterning in angiosperms. *American journal of botany*, **87**, 1069–80.
- Daloso DM, Anjos L, Fernie AR (2016) Roles of sucrose in guard cell regulation. *New Phytologist*, **211**, 809–818.
- Darvasi A, Soller M (1995) Advanced intercross lines, an experimental population for fine genetic mapping. *Genetics*.
- Darwin C (1898) Observations on stomata. *Philosophical Transactions of the Royal Society of London. Series B, Containing Papers of a Biological Character*, **190**, 531–621.
- Dittrich P, Raschke K (1977) Malate metabolism in isolated epidermis of *Commelina communis* L. in relation to stomatal functioning. *Planta*, **134**, 77–81.
- Dixon J, Braun H-J, Kosina P, Crouch J (2009) *Wheat facts and futures 2009*.
- Doheny-Adams T, Hunt L, Franks PJ, Beerling DJ, Gray JE (2012) Genetic manipulation of stomatal density influences stomatal size, plant growth and tolerance to restricted water supply across a growth carbon dioxide gradient. *Phil. Trans. R. Soc. B*, **367**, 547–555.
- Dow GJ, Bergmann DC (2014) Patterning and processes: How stomatal development defines physiological potential. *Current Opinion in Plant Biology*.
- Dow GJ, Berry JA, Bergmann DC (2014a) The physiological importance of developmental mechanisms that enforce proper stomatal spacing in *Arabidopsis thaliana*. *New Phytologist*, **201**, 1205–1217.
- Dow GJ, Bergmann DC, Berry JA (2014b) An integrated model of stomatal development and leaf physiology. *New Phytologist*, **201**, 1218–1226.
- Drake PL, Froend RH, Franks PJ (2013) Smaller, faster stomata: scaling of stomatal size, rate of response, and stomatal conductance. *Journal of Experimental Botany*, **64**, 495–505.
- Drake PL, de Boer HJ, Schymanski SJ, Veneklaas EJ (2019) Two sides to every leaf: water and CO₂ transport in hypostomatous and amphistomatous leaves. *New Phytologist*, **222**, 1179–1187.
- Driscoll SP, Prins A, Olmos E, Kunert KJ, Foyer CH (2006) Specification of adaxial and abaxial stomata, epidermal structure and photosynthesis to CO₂ enrichment in maize leaves. *Journal of Experimental Botany*, **57**, 381–390.
- Dubcovsky J, Dvorak J (2007) Genome plasticity a key factor in the success of polyploid wheat under domestication. *Science*, **316**, 1862–1866.
- Dunn J, Hunt L, Afsharinafar M et al. (2019) Reduced stomatal density in bread wheat leads to increased water-use efficiency. *Journal of Experimental Botany*, **70**, 4737–4747.

- Dvorak J, Akhunov ED (2005) Tempos of gene locus deletions and duplications and their relationship to recombination rate during diploid and polyploid evolution in the Aegilops-Triticum alliance. *Genetics*, **171**, 323–332.
- Edwards D (1998) Stomata in early land plants: an anatomical and ecophysiological approach. *Journal of Experimental Botany*, **49**, 255–278.
- Edwards D, Abbott GD, Raven J (1996) Cuticles of early land plants: a palaeoecophysiological evaluation. *Kersteins G, Cambridge University Press. Plant cuticles: an integrated functional approach*, 1–31.
- Ehleringer JR (1989) Carbon Isotope Ratios and Physiological Processes in Aridland Plants. , pp. 41–54. Springer, New York, NY.
- Elliott-Kingston C, Haworth M, Yearsley JM, Batke SP, Lawson T, McElwain JC (2016) Does Size Matter? Atmospheric CO₂ May Be a Stronger Driver of Stomatal Closing Rate Than Stomatal Size in Taxa That Diversified under Low CO₂. *Frontiers in plant science*, **7**, 1253.
- Evans L, Rawson H (1970) Photosynthesis and Respiration by the Flag Leaf and Components of the Ear During Grain Development In Wheat. *Australian Journal of Biological Sciences*, **23**, 245.
- Evans JR, Kaldenhoff R, Genty B, Terashima I (2009) Resistances along the CO₂ diffusion pathway inside leaves. *Journal of Experimental Botany*, **60**, 2235–2248.
- Evenson RE, Gollin D (2003) Assessing the impact of the green revolution, 1960 to 2000. *Science (New York, N.Y.)*, **300**, 758–62.
- Faralli M, Lawson T (2020) Natural genetic variation in photosynthesis: an untapped resource to increase crop yield potential? **101**, 518–528.
- Faralli M, Cockram J, Ober E et al. (2019a) Genotypic, developmental and environmental effects on the rapidity of g_{s} in Wheat: Impacts on carbon gain and water-use efficiency. *Frontiers in Plant Science*, **10**.
- Faralli M, Matthews J, Lawson T (2019b) Exploiting natural variation and genetic manipulation of stomatal conductance for crop improvement. *Current Opinion in Plant Biology*, **49**, 1–7.
- Faris JD (2014) Wheat domestication: key to agricultural revolutions past and future. In: *Tuberosa R, Graner A, Frison E, eds. Genomics of plant genetic resources.*, pp. 439–464. Springer, Dordrecht, the Netherlands.
- Farquhar GD, Sharkey TD (1982) Stomatal Conductance and Photosynthesis. *Annual Review of Plant Physiology*, **33**, 317–345.
- Farquhar GD, von Caemmerer S, Berry JA (1980) A biochemical model of photosynthetic CO₂ assimilation in leaves of C₃ species. *Planta*, **149**, 78–90.
- Field KJ, Duckett JG, Cameron DD, Pressel S (2015) Stomatal density and aperture in non-vascular land plants are non-responsive to above-ambient atmospheric CO₂ concentrations. *Annals of Botany*, **115**.
- Fiorin L, Brodribb TJ, Anfodillo T (2016) Transport efficiency through uniformity: Organization of veins and stomata in angiosperm leaves. *New Phytologist*.

- Fischer RA, Rees D, Sayre KD, Lu Z-M, Condon AG, Saavedra AL (1998) Wheat Yield Progress Associated with Higher Stomatal Conductance and Photosynthetic Rate, and Cooler Canopies. *Crop Science*, **38**, 1467.
- Food and Agriculture Organization of the United Nations, IFAD, UNICEF W and W (2017) *The State of Food Security and Nutrition in the World 2017. Building resilience for peace and food security*. Rome.
- Food and Agriculture Organization of the United Nations (FOA) (2014) Wheat - the largest primary commodity. *FOASTAT*.
- Food Security Information Network (2017) *Global report on food crisis 2017*. 1–15 pp.
- Franks PJ (2004) Stomatal control and hydraulic conductance, with special reference to tall trees. *Tree physiology*, **24**, 865–78.
- Franks PJ, Beerling DJ (2009) Maximum leaf conductance driven by CO₂ effects on stomatal size and density over geologic time. *Proc. Nat. Acad. Sci.*, 10343–10347.
- Franks PJ, Casson S (2014) Connecting stomatal development and physiology. *New Phytologist*, **201**, 1079–1082.
- Franks PJ, Farquhar GD (2001) The effect of exogenous abscisic acid on stomatal development, stomatal mechanics, and leaf gas exchange in *Tradescantia virginiana*. *Plant physiology*, **125**, 935–42.
- Franks PJ, Farquhar GD (2007) The mechanical diversity of stomata and its significance in gas-exchange control. *Plant physiology*, **143**, 78–87.
- Franks PJ, Leitch IJ, Ruszala EM, Hetherington AM, Beerling DJ (2012a) Physiological framework for adaptation of stomata to CO₂ from glacial to future concentrations. *Philosophical Transactions of the Royal Society B: Biological Sciences*, **367**, 537–546.
- Franks PJ, Freckleton RP, Beaulieu JM, Leitch IJ, Beerling DJ (2012b) Megacycles of atmospheric carbon dioxide concentration correlate with fossil plant genome size. *Philosophical Transactions of the Royal Society B: Biological Sciences*, **367**, 556–564.
- Franks PJ, Doheny-Adams TW, Britton-Harper ZJ, Gray JE (2015) Increasing water-use efficiency directly through genetic manipulation of stomatal density. *New Phytologist*, **207**, 188–195.
- Fujita T, Noguchi K, Terashima I (2013) Apoplastic mesophyll signals induce rapid stomatal responses to CO₂ in *Commelina communis*. *New Phytologist*, **199**, 395–406.
- Gardner KA, Wittern LM, Mackay IJ (2016) A highly recombined, high-density, eight-founder wheat MAGIC map reveals extensive segregation distortion and genomic locations of introgression segments. *Plant Biotechnology Journal*, **14**, pp 1406-1417.
- Gay AP, Hurd RG (1975) THE INFLUENCE OF LIGHT ON STOMATAL DENSITY IN THE TOMATO. *New Phytologist*, **75**, 37–46.

- Gooding MJ, Dimmock JPRE, France J, Jones SA (2000) Green leaf area decline of wheat flag leaves: the influence of fungicides and relationships with mean grain weight and grain yield. *Annals of Applied Biology*, **136**, 77–84.
- Gray JE, Holroyd GH, van der Lee FM et al. (2000) The HIC signalling pathway links CO₂ perception to stomatal development. *Nature*, **408**, 713–6.
- Gray SB, Dermody O, Klein SP et al. (2016) Intensifying drought eliminates the expected benefits of elevated carbon dioxide for soybean. *Nature Plants*, **2**, 1–8.
- Hachez C, Milhiet T, Heinen RB, Chaumont F (2017) Roles of Aquaporins in Stomata. , pp. 167–183. Springer, Cham.
- Han S-K, Torii KU (2016) Lineage-specific stem cells, signals and asymmetries during stomatal development. *Development (Cambridge, England)*, **143**, 1259–70.
- Hancock JF (2005) Contributions of domesticated plant studies to our understanding of plant evolution. *Annals of Botany*, **96**, 953–963.
- Hannon M, Gimpel J, Tran M, Rasala B, Mayfield S (2010) Biofuels from algae: Challenges and potential. *Biofuels*, **1**, 763–784.
- Hara K, Kajita R, Torii KU, Bergmann DC, Kakimoto T (2007) The secretory peptide gene EPF1 enforces the stomatal one-cell-spacing rule. *Genes & development*, **21**, 1720–5.
- Hara K, Yokoo T, Kajita R et al. (2009) Epidermal cell density is autoregulated via a secretory peptide, EPIDERMAL PATTERNING FACTOR 2 in Arabidopsis leaves. *Plant & cell physiology*, **50**, 1019–31.
- Harrison EL, Arce Cubas L, Gray JE, Hepworth C (2020) The influence of stomatal morphology and distribution on photosynthetic gas exchange. *The Plant Journal*, **101**, 768–779.
- Hatfield JL, Dold C (2019) Water-use efficiency: Advances and challenges in a changing climate. *Frontiers in Plant Science*, **10**.
- Hatfield JL, Prueger JH (2015) Temperature extremes: Effect on plant growth and development. *Weather and Climate Extremes*, **10**, 4–10.
- Haworth M, Elliott-Kingston C, McElwain JC (2011) Stomatal control as a driver of plant evolution. *Journal of Experimental Botany*, **62**, 2419–2423.
- Hedden P (2003) The genes of the Green Revolution. *Trends in Genetics*, **19**, 5–9.
- Henry C, John GP, Pan R, Bartlett MK, Fletcher LR, Scoffoni C, Sack L (2019) A stomatal safety-efficiency trade-off constrains responses to leaf dehydration. *Nature Communications*, **10**.
- Hepworth C, Doheny-Adams T, Hunt L, Cameron DD, Gray JE (2015) Manipulating stomatal density enhances drought tolerance without deleterious effect on nutrient uptake. *New Phytologist*, **208**.
- Hetherington AM, Woodward FI (2003) The role of stomata in sensing and driving environmental change. *Nature*, **424**, 901–908.

- Heun M, Schäfer-Pregl R, Klawan D, Castagna R, Accerbi M, Borghi B, Salamini F (1997) Site of einkorn wheat domestication identified by DNA fingerprinting. *Science*, **278**, 1312–1314.
- Hill KE, Guerin GR, Hill RS, Watling JR (2014) Temperature influences stomatal density and maximum potential water loss through stomata of *Dodonaea viscosa* subsp. *angustissima* along a latitude gradient in southern Australia. 657–665.
- Hiyama A, Takemiya A, Munemasa S et al. (2017) Blue light and CO₂ signals converge to regulate light-induced stomatal opening. *Nature Communications*, **8**.
- Hoagland DR, Arnon DI (1950) The water-culture method for growing plants without soil. *Circular. California Agricultural Experiment Station*, **347**.
- Huang S, Sirikhachornkit A, Su X, Faris J, Gill B, Haselkorn R, Gornicki P (2002) Genes encoding plastid acetyl-CoA carboxylase and 3-phosphoglycerate kinase of the *Triticum/Aegilops* complex and the evolutionary history of polyploid wheat. *Proceedings of the National Academy of Sciences of the United States of America*, **99**, 8133–8138.
- Hughes J, Hepworth C, Dutton C et al. (2017) Reducing stomatal density in barley improves drought tolerance without impacting on yield. *Plant Physiology*.
- Hunt L, Gray JE (2009) The Signaling Peptide EPF2 Controls Asymmetric Cell Divisions during Stomatal Development. *Current Biology*, **19**, 864–869.
- Hunt L, Bailey KJ, Gray JE (2010) The signalling peptide EPFL9 is a positive regulator of stomatal development. *New Phytologist*, **186**, 609–614.
- Imamura S. (1943) Untersuchungen über den Mechanismus der Turgorschwankung der Spaltöffnungs- chliesszellen. *Jpn. J. Bot.*, **12**, 251–346.
- Inoue S-I, Kinoshita T (2017) Blue Light Regulation of Stomatal Opening and the Plasma Membrane H⁺-ATPase. *Plant physiology*, **174**, 531–538.
- Ishimaru K, Shiota K, Higa M, Kawamitsu Y (2001) Identification of quantitative trait loci for adaxial and abaxial stomatal frequencies in *Oryza sativa*. *Plant Physiology and Biochemistry*, **39**, 173–177.
- Janssen PJD, Lambrevia MD, Plumeré N et al. (2014) Photosynthesis at the forefront of a sustainable life. *Frontiers in chemistry*, **2**, 36.
- Johnson BL, Dhaliwal HS (1976) Reproductive Isolation of *Triticum boeoticum* and *Triticum urartu* and the Origin of the Tetraploid Wheats. *American Journal of Botany*, **63**, 1088.
- Jones HG (2014) *Plants and Microclimate*, 3rd editio edn. Cambridge University Press.
- Kellogg EA (2001) Evolutionary history of the grasses. *Plant physiology*, **125**, 1198–205.
- Kerber ER, Rowland GG (1974) Origin of the free threshing character in hexaploid wheat. *Canadian Journal of Genetics and Cytology*, **16**, 145–154.

- Khazaei H, Monneveux P, Hongbo S, Mohammady S (2010) Variation for stomatal characteristics and water use efficiency among diploid, tetraploid and hexaploid Iranian wheat landraces. *Genetic Resources and Crop Evolution*, **57**, 307–314.
- Kim TH, Böhmer M, Hu H, Nishimura N, Schroeder JI (2010) Guard cell signal transduction network: Advances in understanding abscisic acid, CO₂, and Ca²⁺ signaling. *Annual Review of Plant Biology*, **61**, 561–591.
- Kimber G, Sears ER (2015) Evolution in the Genus *Triticum* and the Origin of Cultivated Wheat. , pp. 154–164. John Wiley & Sons, Ltd.
- King J, Grewal S, Yang C et al. (2017) A step change in the transfer of interspecific variation into wheat from *Amblyopyrum muticum*. *Plant Biotechnology Journal*, **15**, 217–226.
- Knapp AK, Hamerlynck EP, Owensby CE (1993) Photosynthetic and Water Relations Responses to Elevated CO₂ in the C₄ Grass *Andropogon gerardii*. *International Journal of Plant Sciences*, **154**, 459–466.
- Kottapalli J, David-Schwartz R, Khamaisi B et al. (2018) Sucrose-induced stomatal closure is conserved across evolution. *PLoS ONE*, **13**.
- Kuhlgert S, Austic G, Zegarac R et al. (2016) MultispeQ Beta: A tool for large-scale plant phenotyping connected to the open photosynQ network. *Royal Society Open Science*, **3**.
- Laanemets K, Brandt B, Li J et al. (2013) Calcium-dependent and - independent stomatal signaling network and compensatory feedback control of stomatal opening via Ca²⁺ sensitivity priming. *Plant Physiology*, **163**, 504–513.
- Ladejobi O, Elderfield J, Gardner KA et al. (2016) Maximizing the potential of multi-parental crop populations. *Applied and Translational Genomics*, **11**, 9–17.
- Laidlaw CG., Knight RC. (1916) A description of a recording porometer and a note on stomatal behavior during wilting. *ANNUALS OF BOTANY*, **30**, 47–56.
- Lawson T (2009) Tansley review Guard cell photosynthesis and stomatal function. *New Phytologist*, **181**, 13–34.
- Lawson T, Blatt MR (2014) Stomatal size, speed, and responsiveness impact on photosynthesis and water use efficiency. *Plant Physiology*, **164**.
- Lawson T, Matthews J (2020) Guard Cell Metabolism and Stomatal Function. *Annual Review of Plant Biology*, **71**, 273–302.
- Lawson T, Morison J IL (2004) Stomatal function and physiology. *The Evolution of Plant Physiology*, 217–242.
- Lawson T, Morison J (2006) Visualising patterns of CO₂ diffusion in leaves. *New Phytologist*, **169**, 641–643.
- Lawson T, Vialet-Chabrand S (2019) Speedy stomata, photosynthesis and plant water use efficiency. *New Phytologist*, **221**, 93–98.
- Lawson T, Weyers J (1999) Spatial and temporal variation in gas exchange over the lower surface of *Phaseolus vulgaris* L. primary leaves. *Journal of Experimental Botany*, **50**, 1381–1391.

- Lawson T, Weyers J, A Brook R (1998a) The nature of heterogeneity in the stomatal behaviour of *Phaseolus vulgaris* L. primary leaves. *Journal of Experimental Botany*, **49**, 1387–1395.
- Lawson T, James W, Weyers J (1998b) A surrogate measure of stomatal aperture. *Journal of Experimental Botany*, **49**, 1397–1403.
- Lawson T, von Caemmerer S, Baroli I (2010) Photosynthesis and Stomatal Behaviour. In: *Progress in Botany*, **72**, pp. 265–304. Springer, Berlin, Heidelberg.
- Lawson T, Kramer DM, Raines CA (2012) Improving yield by exploiting mechanisms underlying natural variation of photosynthesis. *Current Opinion in Biotechnology*, **23**, 215–220.
- Lawson T, Simkin AJ, Kelly G, Granot D (2014) Mesophyll photosynthesis and guard cell metabolism impacts on stomatal behaviour. *New Phytologist*, **203**.
- Leakey ADB, Press MC, Scholes JD (2003) High-temperature inhibition of photosynthesis is greater under sunflecks than uniform irradiance in a tropical rain forest tree seedling. *Plant, Cell & Environment*, **26**, 1681–1690.
- Leakey ADB, Ainsworth EA, Bernacchi CJ, Rogers A, Long SP, Ort DR (2009) Elevated CO₂ effects on plant carbon, nitrogen, and water relations: Six important lessons from FACE. *Journal of Experimental Botany*, **60**, 2859–2876.
- Lee J, Bowling DJF (1992) Effect of the mesophyll on stomatal opening in *Commelina communis*. *Journal of Experimental Botany*, **43**, 951–957.
- Lee JS, Kuroha T, Hnilova M et al. (2012) Direct interaction of ligand-receptor pairs specifying stomatal patterning. *Genes & development*, **26**, 126–36.
- Lee JS, Hnilova M, Maes M et al. (2015) Competitive binding of antagonistic peptides fine-tunes stomatal patterning. *Nature*, **522**, 439–443.
- Lehmann P, Or D (2015) Effects of stomata clustering on leaf gas exchange. *New Phytologist*, **207**, 1015–1025.
- Lev-Yadun S, Gopher A, Abbo S (2000) The cradle of agriculture. *Science*, **288**, 1602–1603.
- Lloyd F (1908) *The physiology of stomata*. Carnegie Institution of Washington.
- Lobell DB, Schlenker W, Costa-Roberts J (2011) Climate trends and global crop production since 1980. *Science (New York, N.Y.)*, **333**, 616–20.
- Lodge RJ, Dijkstra P, Drake BG, Morison JIL (2001) Stomatal acclimation to increased CO₂ concentration in a Florida scrub oak species *Quercus myrtifolia* Willd. *Plant, Cell & Environment*, **24**, 77–88.
- Lomax BH, Woodward FIW, Leitch IJ, Knight CA, Lake JA (2008) Genome Size as a Predictor of Guard Cell Length in *Arabidopsis thaliana* Is Independent of Environmental Conditions on JSTOR. *New Phytologist*, **181**, 311–314.
- Long SP (1991) Modification of the response of photosynthetic productivity to rising temperature by atmospheric CO₂ concentrations: Has its importance been underestimated? *Plant, Cell & Environment*, **14**, 729–739.

- Long SP, Ainsworth EA, Leakey ADB, Nösberger J, Ort DR (2006) Food for thought: lower-than-expected crop yield stimulation with rising CO₂ concentrations. *Science (New York, N.Y.)*, **312**, 1918–21.
- Long SP, Marshall-Colon A, Zhu X-G (2015) Meeting the Global Food Demand of the Future by Engineering Crop Photosynthesis and Yield Potential. *Cell*, **161**, 56–66.
- Lu Z, Quinones MA, Zeiger E (1993) Abaxial and adaxial stomata from Pima cotton (*Gossypium barbadense* L.) differ in their pigment content and sensitivity to light quality. *Plant, Cell & Environment*, **16**, 851–858.
- Lu Z, Percy RG, Qualset CO, Zeiger E (1998) Stomatal conductance predicts yields in irrigated Pima cotton and bread wheat grown at high temperatures of historical series from Pima cotton and bread wheat bred for higher yields at supra. *Journal of Experimental Botany*, **49**, 453–460.
- Lundgren MR, Mathers A, Baillie AL et al. (2019) Mesophyll porosity is modulated by the presence of functional stomata. *Nature Communications*, **10**.
- Lupton FGH (1972) Further experiments on photosynthesis and translocation in wheat. *Annals of Applied Biology*, **71**, 69–79.
- Lynch M, Walsh B (1998) *Genetics and Analysis of Quantitative Traits*. Sinauer, Sunderland, UK.
- Mackay IJ, Bansept-Basler P, Barber T et al. (2014) An Eight-Parent Multiparent Advanced Generation Inter-Cross Population for Winter-Sown Wheat: Creation, Properties, and Validation. *G3: Genes, Genomes, Genetics*, **4**.
- Maestri E, Klueva N, Perrotta C, Gulli M, Nguyen HT, Marmioli N (2002) Molecular genetics of heat tolerance and heat shock proteins in cereals. *Plant Molecular Biology*, **48**, 667–681.
- Maggio A, Crieckinge T Van, Malingreau JP (2015) *JRC Science and Policy Reports - Global Food Security 2030 – Assessing trends with a view to guiding future EU policies*.
- Mansfield TA, Hetherington AM, Atkinson CJ (1990) Some Current Aspects of Stomatal Physiology. *Annual Review of Plant Physiology and Plant Molecular Biology*, **41**, 55–75.
- Marcussen T, Sandve SR, Heier L et al. (2014) Ancient hybridizations among the ancestral genomes of bread wheat. *Science (New York, N.Y.)*, **345**, 1250092.
- Matthews JSA, Lawson T (2019) Climate change and Stomatal Physiology. *Annual Plant Reviews*, **2**.
- Matthews JSA, Vialet-Chabrand S, Lawson T (2018) Acclimation to fluctuating light impacts the rapidity of response and diurnal rhythm of stomatal conductance. *Plant Physiology*, **176**.
- Matthews JSA, Vialet-Chabrand S, Lawson T (2020) Role of blue and red light in stomatal dynamic behaviour. *Journal of Experimental Botany*, **71**.
- Mcadam SAM, Brodribb TJ (2012) Stomatal innovation and the rise of seed plants. *Ecology Letters*, **15**, 1–8.

- McAdam SAM, Brodribb TJ (2014) Separating active and passive influences on stomatal control of transpiration. *Plant Physiology*, **164**, 1578–1586.
- McAusland L, Davey PA, Kanwal N, Baker NR, Lawson T (2013) A novel system for spatial and temporal imaging of intrinsic plant water use efficiency. *Journal of Experimental Botany*, **64**, 4993–5007.
- McAusland L, Vialet-Chabrand S, Davey P, Baker NR, Brendel O, Lawson T (2016) Effects of kinetics of light-induced stomatal responses on photosynthesis and water-use efficiency. *New Phytologist*, **211**, 1209–1220.
- McAusland L, Vialet-Chabrand S, Jauregui I et al. (2020) Variation in key leaf photosynthetic traits across wheat wild relatives is accession-dependent not species-dependent. *New Phytologist*, nph.16832.
- McElwain J, Chaloner WG (1995) Stomatal Density and Index of Fossil Plants Track Atmospheric Carbon Dioxide in the Palaeozoic. *Annals of Botany*, **76**, 389–395.
- McElwain JC, Yiotis C, Lawson T (2015) Using modern plant trait relationships between observed and theoretical maximum stomatal conductance and vein density to examine patterns of plant macroevolution. *New Phytologist*, **209**, 94–103.
- McElwain JC, Montañez I, White JD, Wilson JP, Yiotis C (2016) Was atmospheric CO₂ capped at 1000 ppm over the past 300 million years? *Palaeogeography, Palaeoclimatology, Palaeoecology*, **441**.
- McGuire S (2013) WHO, World Food Programme, and International Fund for Agricultural Development. 2012. The State of Food Insecurity in the World 2012. Economic growth is necessary but not sufficient to accelerate reduction of hunger and malnutrition. Rome, FAO. *Advances in Nutrition*, **4**, 126–127.
- Melis A, Zeiger E (1982) Chlorophyll a Fluorescence Transients in Mesophyll and Guard Cells. *Plant Physiology*, **69**, 642–647.
- Merilo E, Yarmolinsky D, Jalakas P et al. (2018) Stomatal VPD Response: There Is More to the Story Than ABA. *Plant physiology*, **176**, 851–864.
- Mohammady S (2002) *Inheritance of tolerance to water stress in wheat (Triticum aestivum)*. University of Newcastle, UK.
- Mohammed U, Caine RS, Atkinson JA et al. (2019) Rice plants overexpressing OsEPF1 show reduced stomatal density and increased root cortical aerenchyma formation. *Scientific Reports*, **9**, 5584.
- Monda K, Araki H, Kuhara S et al. (2016) Enhanced Stomatal Conductance by a Spontaneous Arabidopsis Tetraploid, Me-0, Results from Increased Stomatal Size and Greater Stomatal Aperture. *Plant Physiology*, **170**.
- Mooney HA, Field C, Yanes C V., Chu C (1983) Environmental controls on stomatal conductance in a shrub of the humid tropics. *Proceedings of the National Academy of Sciences*, **80**, 1295–1297.

- Morales D, Rodríguez P, Dell'Amico J, Nicolás E, Torrecillas A, Sánchez-Blanco MJ (2003) High-temperature preconditioning and thermal shock imposition affects water relations, gas exchange and root hydraulic conductivity in tomato. *Biologia Plantarum*, **47**, 203–208.
- Morison JI. (2003) Plant water use, stomatal control. *Stewart BA, Howell TA, ed. Encyclopedia of water science. New York, NY, USA: Marcel Dekker Inc.*, 680–685.
- Morison JIL, Lawson T (2007) Does lateral gas diffusion in leaves matter? *Plant, Cell and Environment*, **30**, 1072–1085.
- Morison JI., Baker N., Mullineaux P., Davies W. (2008) Improving water use in crop production. *Philosophical Transactions of the Royal Society of London B: Biological Sciences*, **363**.
- Mott KA (1988) Do Stomata Respond to CO₂ Concentrations Other than Intercellular? . *Plant Physiology*, **86**, 200–203.
- Mott KA, Buckley TN (1998) Stomatal heterogeneity. *Experimental Botany SPECIAL ISSUE*, **49**, 407–417.
- Mott KA, O'Leary JW (1984) Stomatal Behavior and CO₂ Exchange Characteristics in Amphistomatous Leaves'. *Plant Physiology*, **74**, 47–51.
- Mott KA, Parkhurst DF (1991) Stomatal responses to humidity in air and helox. *Plant, Cell & Environment*, **14**, 509–515.
- Mott KA, Peak D (2013) Testing a vapour-phase model of stomatal responses to humidity. *Plant, Cell & Environment*, **36**, 936–944.
- Mott K, Peak D (2018) Effects of the mesophyll on stomatal responses in amphistomatous leaves. *Plant, Cell & Environment*, **41**, 2835–2843.
- Mott KA, Gibson AC, O'Leary JW (1982) The adaptive significance of amphistomatic leaves. *Plant, Cell & Environment*, **5**, 455–460.
- Mott KA, Cardon ZG, Berry JA (1993) Asymmetric patchy stomatal closure for the two surfaces of *Xanthium strumarium* L. leaves at low humidity. *Plant, Cell and Environment*, **16**, 25–34.
- Mott KA, Sibbersen ED, Shope JC (2008) The role of the mesophyll in stomatal responses to light and CO₂. *Plant, Cell and Environment*, **31**, 1299–1306.
- Muir CD (2015) Making pore choices: repeated regime shifts in stomatal ratio. *Proceedings of the Royal Society B: Biological Sciences*, **282**, 20151498.
- Muir CD (2018) Light and growth form interact to shape stomatal ratio among British angiosperms. *New Phytologist*, **218**, 242–252.
- Muir C (2019) Is amphistomy an adaptation to high light? Optimality models of stomatal traits along light gradients. *bioRxiv*, 601377.
- Muir CD, Hangarter RP, Moyle LC, Davis PA (2014) Morphological and anatomical determinants of mesophyll conductance in wild relatives of tomato (*Solanum* sect. *Lycopersicon*, sect. *Lycopersicoides*; Solanaceae). *Plant, Cell and Environment*, **37**, 1415–1426.

- Murray RR, Emblow MSM, Hetherington AM, Foster GD (2016) Plant virus infections control stomatal development. *Nature Publishing Group*, **634507**.
- Nadeau JA, Sack FD (2002) Control of stomatal distribution on the Arabidopsis leaf surface. *Science (New York, N.Y.)*, **296**, 1697–700.
- Nair PKR (2014) Grand challenges in agroecology and land use systems. *Frontiers in Environmental Science*, **2**, 1.
- Negi J, Matsuda O, Nagasawa T et al. (2008) CO₂ regulator SLAC1 and its homologues are essential for anion homeostasis in plant cells. *Nature*, **452**, 483–486.
- Negi J, Hashimoto-Sugimoto M, Kusumi K, Iba K (2014) New approaches to the biology of stomatal guard cells. *Plant and Cell Physiology*, **55**, 241–250.
- NOAA (2020) Climate Change: Atmospheric Carbon Dioxide.
- Olascoaga B, Mac Arthur A, Atherton J, Porcar-Castell A (2016) A comparison of methods to estimate photosynthetic light absorption in leaves with contrasting morphology. *Tree Physiology*, **36**, 368–379.
- Ooba M, Takahashi H (2003) Effect of asymmetric stomatal response on gas-exchange dynamics. *Ecological Modelling*, **164**, 65–82.
- Outlaw WH (1983) Current concepts on the role of potassium in stomatal movements. *Physiologia Plantarum*, **59**, 302–311.
- Outlaw WH (2003) Integration of Cellular and Physiological Functions of Guard Cells. *Critical Reviews in Plant Sciences*, **22**, 503–529.
- Outlaw WH, Tarczynski MC (1984) Guard Cell Starch Biosynthesis Regulated by Effectors of ADP-Glucose Pyrophosphorylase. *Plant Physiology*, **74**, 424–429.
- Outlaw J, De Vlieghere-He X (2001) Transpiration rate. An important factor controlling the sucrose content of the guard cell apoplast of broad bean. *Plant Physiology*, **126**, 1716–1724.
- Pagani M, Freeman KH, Arthur MA (1999) Late miocene atmospheric CO₂ concentrations and the expansion of C₄ grasses. *Science*, **285**, 876–879.
- Parkhurst DF (1978) The Adaptive Significance of Stomatal Occurrence on One or Both Surfaces of Leaves. *The Journal of Ecology*, **66**, 367.
- Parkhurst DF (1994) Diffusion of CO₂ and other gases inside leaves. *New Phytologist*, **126**, 449–479.
- Parry, M., Rosenzweig, C., Iglesias, A., Fischer, G., Livermore M (1999) Climate change and world food security: a new assessment. *Global Environmental Change*, **9**, S51–S67.
- Pearcy RW (1990) Sunflecks and Photosynthesis in Plant Canopies. *Annual Review of Plant Physiology and Plant Molecular Biology*, **41**, 421–453.
- Pearson PN, Palmer MR (2000) Atmospheric carbon dioxide concentrations over the past 60 million years. *Nature*, **406**, 695–699.

- Peng JH, Dongfa •, Nevo S• E, Peng JH, Sun D, Nevo E (2011) Domestication evolution, genetics and genomics in wheat. **28**, 281–301.
- Perkins SE, Alexander L V., Nairn JR (2012) Increasing frequency, intensity and duration of observed global heatwaves and warm spells. *Geophysical Research Letters*, **39**.
- Peterhansel C, Horst I, Niessen M, Blume C, Kebeish R, Kürkcüoglu S, Kreuzaler F (2010) Photorespiration. *The Arabidopsis Book*, **8**, e0130.
- Petersen G, Seberg O, Yde M, Berthelsen K (2006) Phylogenetic relationships of Triticum and Aegilops and evidence for the origin of the A, B, and D genomes of common wheat (*Triticum aestivum*). *Molecular phylogenetics and evolution*, **39**, 70–82.
- Peterson KM, Rychel AL, Torii KU (2010) Out of the mouths of plants: the molecular basis of the evolution and diversity of stomatal development. *The Plant cell*, **22**, 296–306.
- Pillitteri LJ, Peterson KM, Horst RJ, Torii KU (2011) Molecular profiling of stomatal meristemoids reveals new component of asymmetric cell division and commonalities among stem cell populations in Arabidopsis. *The Plant cell*, **23**, 3260–75.
- Poole I, Weyers JDB, Lawson T, Raven JA (1996) Variations in stomatal density and index: implications for palaeoclimatic reconstructions. *Plant, Cell and Environment*, **19**, 705–712.
- Poole L, Lawson T, Weyers JDB, Raven JA (2000) Effect of elevated CO₂ on the stomatal distribution and leaf physiology of *Alnus glutinosa*. *New Phytologist*, **145**, 511–521.
- Pospíšilová J, Šantrůček J (1994) Stomatal patchiness. *Biologia Plantarum*, **36**, 481–510.
- Prentice I, Farquhar G, Fasham M et al. (2001) The Carbon Cycle and Atmospheric CO₂. In: *Climate change 2001: the scientific basis.*, pp. 183–239. Cambridge University Press.
- Prohens J, Gramazio P, Plazas M et al. (2017) Introgressomics: a new approach for using crop wild relatives in breeding for adaptation to climate change. *Euphytica*, **213**.
- Qu X, Peterson KM, Torii KU (2017) Stomatal development in time: the past and the future. *Current Opinion in Genetics & Development*, **45**, 1–9.
- Raissig MT, Abrash E, Bettadapur A, Vogel JP, Bergmann DC (2016) Grasses use an alternatively wired bHLH transcription factor network to establish stomatal identity. *Proceedings of the National Academy of Sciences of the United States of America*, **113**, 8326–31.
- Raissig MT, Matos JL, Anleu Gil MX et al. (2017) Mobile MUTE specifies subsidiary cells to build physiologically improved grass stomata. *Science*, **355**, 1215–1218.
- Raschke K (1975) Stomatal action. *Annu. Rev. Plant Physiol*, **26**, 309–340.

- Raven JA (1977) The Evolution of Vascular Land Plants in Relation to Supracellular Transport Processes. *Advances in Botanical Research*, **5**, 153–219.
- Raven JA (2002) Selection pressures on stomatal evolution. *New Phytologist*, **153**, 371–386.
- Raven JA (2014) Speedy small stomata? *Journal of Experimental Botany*, **65**, 1415–1424.
- Ray DK, Mueller ND, West PC, Foley JA (2013) Yield Trends Are Insufficient to Double Global Crop Production by 2050 (ed Hart JP). *PLoS ONE*, **8**, e66428.
- Reddy A, Rasineni G, Raghavendra A (2010) The impact of global elevated CO₂ concentration on photosynthesis and plant productivity on JSTOR. In: *Current Science*, pp. 46–57.
- Renny-Byfield S, Wendel JF (2014) Doubling down on genomes: Polyploidy and crop plants. *American Journal of Botany*, **101**, 1711–1725.
- Richardson F, Brodribb TJ, Jordan GJ (2017) Amphistomatic leaf surfaces independently regulate gas exchange in response to variations in evaporative demand. *Tree Physiology*, **37**, 869–878.
- Richardson F, Jordan GJ, Brodribb TJ (2020) Leaf hydraulic conductance is linked to leaf symmetry in bifacial, amphistomatic leaves of sunflower. *Journal of Experimental Botany*, **71**, 2808–2816.
- Riehl S, Zeidi M, Conard NJ (2013) Emergence of agriculture in the foothills of the Zagros mountains of Iran. *Science*, **341**, 65–67.
- Roelfsema MRG, Hedrich R (2005) In the light of stomatal opening: new insights into 'the Watergate.' *New Phytologist*, **167**, 665–691.
- Rowe MH, Bergmann DC (2010) Complex signals for simple cells: the expanding ranks of signals and receptors guiding stomatal development. *Current Opinion in Plant Biology*, **13**, 548–555.
- Royer DL (2001) Stomatal density and stomatal index as indicators of paleoatmospheric CO₂ concentration. *Review of Palaeobotany and Palynology*, **114**, 1–28.
- Rudall P (1980) Leaf anatomy of the subtribe Hyptidinae (Labiatae). *Botanical Journal of the Linnean Society*, **80**, 319–340.
- Rudall PJ, Knowles EVW (2013) Ultrastructure of stomatal development in early-divergent angiosperms reveals contrasting patterning and pre-patterning. *Annals of Botany*, **112**, 1031–1043.
- Sack L, Buckley TN (2016) The Developmental Basis of Stomatal Density and Flux. *Plant physiology*, **171**, 2358–2363.
- Salamini F, Özkan H, Brandolini A, Schäfer-Pregl R, Martin W (2002) Genetics and geography of wild cereal domestication in the near east. *Nature Reviews Genetics*, **3**, 429–441.
- Sax K (1922) Sterility in Wheat Hybrids. II. Chromosome Behavior in Partially Sterile Hybrids. *Genetics*, **7**, 513–52.

- Schlenker W, Roberts MJ (2009) Nonlinear temperature effects indicate severe damages to U.S. crop yields under climate change. *Proceedings of the National Academy of Sciences of the United States of America*, **106**, 15594–8.
- Schlenker W, Hanemann WM, Fisher AC (2006) The Impact of Global Warming on U.S. Agriculture: An Econometric Analysis of Optimal Growing Conditions. *Review of Economics and Statistics*, **88**, 113–125.
- Schnabl H, Raschke K (1980) Potassium Chloride as Stomatal Osmoticum in *Allium cepa* L., a Species Devoid of Starch in Guard Cells. *Plant Physiology*, **65**, 88–93.
- Schroeder JI, Allen GJ, Hugouvieux V, Kwak JM, Waner D (2001) Guard cell signal transduction. *Annual Review of Plant Biology*, **52**, 627–658.
- Scott MF, Ladejobi O, Amer S et al. (2020) Multi-parent populations in crops: a toolbox integrating genomics and genetic mapping with breeding. *Heredity*, 1–21.
- Semenov MA, Mitchell RAC, Whitmore AP, Hawkesford MJ, Parry MAJ, Shewry PR (2012) Shortcomings in wheat yield predictions. *Nature Climate Change*, **2**, 380–382.
- Sharkey, D. T, BERNACCHI CJ, FARQUHAR GD, SINGSAAS EL (2007) Fitting photosynthetic carbon dioxide response curves for C₃ leaves. *Plant, Cell & Environment*, **30**, 1035–1040.
- Shimazaki K, Doi M, Assmann SM, Kinoshita T (2007) Light Regulation of Stomatal Movement. *Annual Review of Plant Biology*, **58**, 219–247.
- Shiu S-H, Bleecker AB (2001) Plant Receptor-Like Kinase Gene Family: Diversity, Function, and Signaling. *Science Signaling*, **2001**, re22–re22.
- Sibbersen E, Mott KA (2010) Stomatal responses to flooding of the intercellular air spaces suggest a vapor-phase signal between the mesophyll and the guard cells. *Plant Physiology*, **153**, 1435–1442.
- Simkin AJ, Faralli M, Ramamoorthy S, Lawson T (2020) Photosynthesis in non-foliar tissues: implications for yield. *The Plant Journal*, **101**, 1001–1015.
- Smith S, Weyers JDB, Berry WG (1989a) Variation in stomatal characteristics over the lower surface of *Commelina communis* leaves. *Plant, Cell and Environment*, **12**, 653–659.
- Smith WK, Knapp AK, Reiners WA (1989b) Penumbral Effects on Sunlight Penetration in Plant Communities. *Ecology*, **70**, 1603–1609.
- Soares AS, Driscoll SP, Olmos E, Harbinson J, Arrabaça MC, Foyer CH (2008) Adaxial/abaxial specification in the regulation of photosynthesis and stomatal opening with respect to light orientation and growth with CO₂ enrichment in the C₄ species *Paspalum dilatatum*. *New Phytologist*, **177**, 186–198.
- Soh WK, Yiotis C, Murray M et al. (2019) Rising CO₂ drives divergence in water use efficiency of evergreen and deciduous plants. *SCIENCE ADVANCES*, **5**, eaax7906.

- Sreeharsha RV, Sekhar KM, Reddy AR (2015) Plant Science Delayed flowering is associated with lack of photosynthetic acclimation in Pigeon pea (*Cajanus cajan* L .) grown under elevated CO₂. *Plant Science*, **231**, 82–93.
- Stamp P, Herzog H (1976) Flag-leaf senescence and grain growth in certain German varieties of spring wheat (*Triticum aestivum* L.). *Z Pflanzenzucht.*, **77**, 330–338.
- Stevens J, Faralli M, Wall S, Stamford JD, Lawson T (2020) Stomatal Responses to Climate Change.
- Stoy V (1963) The Translocation of C¹⁴-Labelled Photosynthetic Products from the Leaf to the Ear in Wheat. *Physiologia Plantarum*, **16**, 851–866.
- Talbott LD, Zeiger E (1996) Central roles for potassium and sucrose in guard-cell osmoregulation. *Plant Physiology*, **111**, 1051–1057.
- Taylor AH (1920) The measurement of diffuse reflection factors and a new absolute reflectometer. *Journal of the Optical Society of America*, **4**, 9–23.
- Taylor SH, Franks PJ, Hulme SP et al. (2012) Photosynthetic pathway and ecological adaptation explain stomatal trait diversity amongst grasses. *New Phytologist*, **193**, 387–396.
- Teskey R, Wertin T, Bauweraerts I, Ameye M, McGuire MA, Steppe K (2015) Responses of tree species to heat waves and extreme heat events. *Plant Cell and Environment*, **38**, 1699–1712.
- Ticha I (1982) Photosynthetic characteristics during ontogenesis of leaves. 7. Stomata density and sizes.
- Tinoco-Ojanguren C, Pearcy RW (1993) Stomatal dynamics and its importance to carbon gain in two rainforest Piper species - II. Stomatal versus biochemical limitations during photosynthetic induction. *Oecologia*, **94**, 395–402.
- Tominaga J, Kawamitsu Y (2015) Tracing photosynthetic response curves with internal CO₂ measured directly. *Environmental Control in Biology*, **53**, 27–34.
- Tominaga J, Shimada H, Kawamitsu Y (2018) Direct measurement of intercellular CO₂ concentration in a gas-exchange system resolves overestimation using the standard method. *Journal of Experimental Botany*, **69**, 1981–1991.
- Trust GD (2019) Wheat: *Triticum* spp.
- Turner NC, Singh DP (1984) Responses of adaxial and abaxial stomata to light and water deficits in sunflower and sorghum. *New Phytologist*, **96**, 187–195.
- Urban J, Ingwers M, McGuire MA, Teskey RO (2017a) Stomatal conductance increases with rising temperature. *Plant Signaling and Behavior*, **12**, 1356534.
- Urban J, Ingwers MW, McGuire MA, Teskey RO (2017b) Increase in leaf temperature opens stomata and decouples net photosynthesis from stomatal conductance in *Pinus taeda* and *Populus deltoides* x *nigra*. *Journal of Experimental Botany*, **68**, 1757–1767.
- Vahisalu T, Kollist H, Wang YF et al. (2008) SLAC1 is required for plant guard cell S-type anion channel function in stomatal signalling. *Nature*, **452**, 487–491.

- Vatén A, Bergmann DC (2012) Mechanisms of stomatal development: An evolutionary view. *EvoDevo*, **3**, 11.
- Vergara-Díaz O, Chairi F, Vicente R et al. (2018) Leaf dorsoventrality as a paramount factor determining spectral performance in field-grown wheat under contrasting water regimes. *Journal of Experimental Botany*, **69**, 3081–3094.
- Violet-chabrand S, Matthews JSA, Simkin AJ, Raines CA, Lawson T (2017) Importance of Fluctuations in Light on Plant. **173**, 2163–2179.
- Violet-Chabrand S, Lawson T (2019a) Dynamic leaf energy balance: deriving stomatal conductance from thermal imaging in a dynamic environment. *Journal of Experimental Botany*.
- Violet-Chabrand S, Lawson T (2019b) Dynamic leaf energy balance: Deriving stomatal conductance from thermal imaging in a dynamic environment. *Journal of Experimental Botany*, **70**, 2839–2855.
- Violet-Chabrand S, Dreyer E, Brendel O (2013) Performance of a new dynamic model for predicting diurnal time courses of stomatal conductance at the leaf level. *Plant, Cell & Environment*, **36**, 1529–1546.
- Violet-Chabrand S, Matthews JSA, Brendel O et al. (2016) Modelling water use efficiency in a dynamic environment: An example using *Arabidopsis thaliana*. *Plant Science*, **251**, 65–74.
- Violet-Chabrand S, Matthews JSA, Simkin AJ, Raines CA, Lawson T (2017a) Importance of fluctuations in light on plant photosynthetic acclimation. *Plant Physiology*, **173**, 2163–2179.
- Violet-Chabrand SRM, Matthews JSA, McAusland L, Blatt MR, Griffiths H, Lawson T (2017b) Temporal Dynamics of Stomatal Behavior: Modeling and Implications for Photosynthesis and Water Use. *Plant Physiology*, **174**.
- Wang Y, Noguchi K, Terashima I (2008a) Distinct light responses of the adaxial and abaxial stomata in intact leaves of *Helianthus annuus* L. *Plant, Cell & Environment*, **31**, 1307–1316.
- Wang Y, Noguchi K, Terashima I (2008b) Distinct light responses of the adaxial and abaxial stomata in intact leaves of *Helianthus annuus* L. *Plant, Cell & Environment*, **31**, 1307–1316.
- Weyers JDB, Johansen LG (1985) Accurate estimation of stomatal aperture from silicone rubber impressions. *New Phytologist*, **101**, 109–115.
- Weyers JDB, Lawson T (1997) Heterogeneity in Stomatal Characteristics. *Advances in Botanical Research*, **26**, 317–352.
- Weyers JDB, Paterson NW (1987) Responses of *Commelina communis* Stomata In Vitro. *Journal of Experimental Botany*, **38**, 631–641.
- Weyers JDB, Lawson T, Peng ZY (1997) Variation in stomatal characteristics at the whole-leaf level. Scaling-up from cell to Landsc. *SEB seminar series volume: Scaling-up from cell to Landsc.*
- Wheeler T, von Braun J (2013) Climate Change Impacts on Global Food Security. *Science*, **341**.

- Wiggans RG (1921) Variations in the Osmotic Concentration of the Guard Cells During the Opening and Closing of Stomata. *American Journal of Botany*, **8**, 30.
- Willmer C, Fricker M (1996) *Stomata*. Springer Netherlands, 400 pp.
- Wolde GM, Mascher M, Schnurbusch T (2019) Genetic modification of spikelet arrangement in wheat increases grain number without significantly affecting grain weight. *Molecular Genetics and Genomics*, **294**, 457–468.
- Wong SC, Cowan IR, Farquhar GD (1979) Stomatal conductance correlates with photosynthetic capacity. *Nature*, **282**, 424–426.
- Wong S-C, Cowan IR, Farquhar GD (1985) Leaf Conductance in Relation to Rate of CO₂ Assimilation. *Plant Physiology*, **78**, 826–829.
- Woodward FI (1987) Stomatal numbers are sensitive to increases in CO₂ from pre-industrial levels. *Nature*, **327**, 617–618.
- Woodward F (1998) Do plants really need stomata? *Journal of Experimental Botany*, **49**, 471–480.
- Woodward FI, Kelly CK (1995) The influence of CO₂ concentration on stomatal density. *New Phytologist*, **131**, 311–327.
- Woodward FI, Lake JA, Quick WP (2002) Stomatal development and CO₂: Ecological consequences. *New Phytologist*, **153**, 477–484.
- Xiong D, Flexas J (2020) From one-side to two-sides: the effects of stomatal distribution on photosynthesis. *New Phytologist*.
- Xu Z, Zhou G (2008) Responses of leaf stomatal density to water status and its relationship with photosynthesis in a grass. *Journal of Experimental Botany*, **59**, 3317–3325.
- Xu Z, Jiang Y, Jia B, Zhou G (2016) Elevated-CO₂ Response of Stomata and Its Dependence on Environmental Factors. **7**.
- Yamamoto Y, Negi J, Wang C, Isogai Y, Schroeder JI, Iba K (2016) The transmembrane region of guard cell SLAC1 channels perceives CO₂ signals via an ABA-independent pathway in Arabidopsis. *Plant Cell*, **28**, 557–567.
- Yamori W, Kusumi K, Iba K, Terashima I (2020) Increased stomatal conductance induces rapid changes to photosynthetic rate in response to naturally fluctuating light conditions in rice. *Plant, Cell & Environment*, **43**, 1230–1240.
- Yera R, Davis S, Frazer J, Tallman G (1986) Responses of Adaxial and Abaxial Stomata of Normally Oriented and Inverted Leaves of *Vicia faba* L. to Light. *Plant Physiology*, **82**, 384–389.
- Zadok JC, Chang TT, Konzak CF (1974) A decimal code for the growth stages of cereals. *Weed Research*, **14**, 415–421.
- Zeiger E, Farquhar GD, Cowan IR (1987) Stomatal Function. *Stanford, California: Stanford University Press*.

- Zhang L, Niu H, Wang S, Zhu X, Luo C, Li Y, Zhao X (2012) Gene or environment? Species-specific control of stomatal density and length. *Ecology and Evolution*, **2**, 1065–1070.
- Zhang K, Wang X, Cheng F (2019) Plant Polyploidy: Origin, Evolution, and Its Influence on Crop Domestication. *Horticultural Plant Journal*, **5**, 231–239.
- Zhao C, Liu B, Piao S et al. (2017) Temperature increase reduces global yields of major crops in four independent estimates. *Proceedings of the National Academy of Sciences of the United States of America*, **114**, 9326–9331.
- Zhu X-G, Portis AR, Long SP (2004) Would transformation of C3 crop plants with foreign Rubisco increase productivity? A computational analysis extrapolating from kinetic properties to canopy photosynthesis. *Plant, Cell and Environment*, **27**, 155–165.
- Zhu X-G, Long SP, Ort DR (2010) Improving Photosynthetic Efficiency for Greater Yield. *Annual Review of Plant Biology*, **61**, 235–261.